frontiers
RESEARCH TOPICS

VOLITIONAL INHIBITION: THE GATEWAY FOR AN EFFICIENT CONTROL OF VOLUNTARY MOVEMENTS

Hosted by
Giovanni Mirabella

frontiers in
NEUROENGINEERING

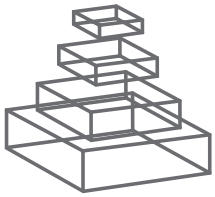

frontiers

Cover image provided by Ibbl sarl, Lausanne CH

ISSN 1664-8714
ISBN 978-2-88919-062-1
DOI 10.3389/978-2-88919-062-1

ABOUT FRONTIERS

Frontiers is more than just an open-access publisher of scholarly articles: it is a pioneering approach to the world of academia, radically improving the way scholarly research is managed. The grand vision of Frontiers is a world where all people have an equal opportunity to seek, share and generate knowledge. Frontiers provides immediate and permanent online open access to all its publications, but this alone is not enough to realize our grand goals.

FRONTIERS JOURNAL SERIES

The Frontiers Journal Series is a multi-tier and interdisciplinary set of open-access, online journals, promising a paradigm shift from the current review, selection and dissemination processes in academic publishing.
All Frontiers journals are driven by researchers for researchers; therefore, they constitute a service to the scholarly community. At the same time, the Frontiers Journal Series operates on a revolutionary invention, the tiered publishing system, initially addressing specific communities of scholars, and gradually climbing up to broader public understanding, thus serving the interests of the lay society, too.

DEDICATION TO QUALITY

Each Frontiers article is a landmark of the highest quality, thanks to genuinely collaborative interactions between authors and review editors, who include some of the world's best academicians. Research must be certified by peers before entering a stream of knowledge that may eventually reach the public - and shape society; therefore, Frontiers only applies the most rigorous and unbiased reviews.
Frontiers revolutionizes research publishing by freely delivering the most outstanding research, evaluated with no bias from both the academic and social point of view.
By applying the most advanced information technologies, Frontiers is catapulting scholarly publishing into a new generation.

WHAT ARE FRONTIERS RESEARCH TOPICS?

Frontiers Research Topics are very popular trademarks of the Frontiers Journals Series: they are collections of at least ten articles, all centered on a particular subject. With their unique mix of varied contributions from Original Research to Review Articles, Frontiers Research Topics unify the most influential researchers, the latest key findings and historical advances in a hot research area!
Find out more on how to host your own Frontiers Research Topic or contribute to one as an author by contacting the Frontiers Editorial Office: researchtopics@frontiersin.org

VOLITIONAL INHIBITION: THE GATEWAY FOR AN EFFICIENT CONTROL OF VOLUNTARY MOVEMENTS

Hosted By:
Giovanni Mirabella, University of Rome "La Sapienza", Italy

Being able to suppress a pending action is a fundamental ability for surviving in an unpredictable World. Sudden events, such as the appearance of a physical obstacle, might require a quick change of the planned motor strategy. The first step toward this goal is to suppress the pre-programmed actions. Understanding the functional characteristics and the neural underpinnings of inhibition is a primary aim, both for the treatment of such diseases as attention-deficit hyperactivity disorder, where the decision-making abilities are severely impaired, and for the development of efficient brain–machine interfaces.

Despite an incredible amount of work, witnessed by tens of articles published on Medline, both the localizations of the neural substrates of voluntary inhibition and their specific contributions to this executive function are still controversial. However, the ability of vetoing pending actions is likely to be at the basis of self control and of mental simulation of voluntary actions. In other words the veto power is a cornerstone of our will. As such the neural code underling volitional inhibition should be taken into account to feed appropriate signals into artificial devices to mimic voluntary movements.

The aim of the present Research Topic is twofold. On the one hand it will show the most innovative aspects of the current researches on the neural substrates and functional mechanisms of volitional inhibition. On the other hand it will deal with the possible applications of the acquired knowledge for building up interfaces that could collect and decode incoming neural signals in order to move artificial limbs and/or to interact with personal computers.

Table of Contents

frontiers in
NEUROENGINEERING

EDITORIAL
published: 28 August 2012
doi: 10.3389/fneng.2012.00020

Volitional inhibition and brain–machine interfaces: a mandatory wedding

Giovanni Mirabella*[1,2]

[1] *Istituiti di Ricovero e Cura a Carattere Scientifico Neuromed, Pozzilli, Italy*
[2] *Department of Physiology and Pharmacology "V. Erspamer," La Sapienza University, Rome, Italy*
**Correspondence: giovanni.mirabella@uniroma1.it*

Edited by:
Laura Ballerini, University of Trieste, Italy

Reviewed by:
Boris Burle, CNRS & Aix-Marseille Université, France

A key feature of voluntary behavior is its flexibility which, in a sense, represents the other side of self-control. We need to select and perform actions whenever they are more opportune, i.e., whenever the costs intrinsically associated with them are lower than their benefits. Given that we cannot predict with certainty the occurrence of an event and the time lag elapsing between the decision to move and the physical execution of a movement, we have developed the ability to cancel pending actions. Suppressing ongoing acts is fundamental when sudden changes in the surrounding environment take place. For instance, the sudden arrival of a car in the road we were about to cross requires us to stop our step to avoid being hit. The great importance of this executive function, named "volitional" inhibition, is witnessed by the great number of brain regions implicated in its elaboration. Here, the term volitional does not imply a conscious participation. In humans the emergence of awareness coupled with the vetoing ability gave rise to what Libet (1985) called "free would not," that is, our capacity to freely cancel those actions we do not wish to perform. However, we do not exert our free will on every choice we have to make, but just on those more controversial or salient (e.g., how to respond to the request of working over the week-end). Most of the time the fate of actions is decided by automatic processes, otherwise we could not have sufficient free capacity for other computations.

Overall volitional inhibition represents a cornerstone of voluntary behavior but, despite an incredible amount of work, both the localizations of its neural substrates and their specific contributions are still controversial. For instance, it has been suggested that inhibitory commands are generated in a right-lateralized frontal–basal ganglia–thalamic network (Aron et al., 2007), but there is scant knowledge about where they act. One paper in this Research Topic (Mattia et al., 2012) indicates that the motor cortices (both the primary motor cortex and the premotor cortex) are the targets of cancelation commands (see also Mirabella et al., 2011). In other words, it suggests that the same neural substrates involved in planning and executing an act (see also Busan et al., 2012) are also involved in its suppression. Along the same lines, Pastor-Bernier et al. (2012) show that neurons of the premotor cortex continuously update their activities during movement planning, so that their discharge reflects switches between alternative plans when a selected movement option suddenly turns out to be inappropriate.

Importantly, as described in the review by Stuphorn and Emeric (2012), the inhibitory network not only provides signals indicating the withholding of actions whenever a stop signal is presented (reactive control), but also provides signals enabling the subject to adopt a response strategy which takes into account the context in which he or she operates. This form of cognitive control over response execution, named proactive control, adjusts the response selection and preparation process in anticipation of known task demands, driven by endogenous signals. Several lines of evidence indicate the involvement of the medial frontal cortex in proactive control. Wriessnegger et al. (2012) also ascribe to these regions a role in inhibiting learned motor programs.

Despite the relevance of volitional inhibition in shaping voluntary behavior, its role has been almost completely neglected by those scientists who tried to implement brain–machine interfaces (BMIs). These interfaces are aimed at exploiting neural activity recorded from the brain, e.g., motor commands, to control the movements of external devices, e.g., prosthetic limbs. By translating brain signals into action, a BMI can enable a person suffering from paralysis to move again using artificial limbs. Notwithstanding the successes of the BMI approach there are still several limitations. Signals extracted from the brain are typically noisy, so the guidance of prosthetic limbs is still far from approximating natural behaviors. In this Research Topic, three papers report significant improvements in BMI algorithms. Wang et al. (2012) demonstrate the possibility of detecting the onset and the direction of intended movements exploiting electrocorticographic signals recorded from the surface of the cortex of pharmacoresistant epileptic patients. Lew et al. (2012) show that from the analysis of the readiness potential is possible to detect the movement intention in single trials. This is very relevant because the capability of detecting the neural correlates of self-paced movement at the single-trial level is a fundamental step toward the development of efficient BMIs. In fact, normally we perform a given movement just once rather than repeating them several times in a stereotyped fashion. As a consequence, BMI algorithms relying on brain activity averaged over a number of trials are not very naturalistic.

Finally, Ifft et al. (2012) successfully tried, for the first time, to implement a BMI that can extract response inhibition signals and thus can mimic the suppression of a motor plan and its reprogramming when required by external events. As a model they used single-unit activity of over trained monkeys so it is not obvious that this result could be applied effortlessly to humans; however, it is the first demonstration that brain signals sustaining the flexibility of human behavior can be fed into a BMI. In the same direction, Yang et al. (2012) have developed a

field-programmable gate array using dedicated real-time hardware circuitry exploiting a model built on the firing rate recorded in the frontal eye field of monkeys during a countermanding oculomotor task (a task which probes the subject's ability to stop pending saccades). Their device is able to simulate the behavioral performance during the task, showing the reliability of the inhibitory control system that can potentially be employed to build an efficient prosthetic system. Although intriguing, further studies are required to assess whether this system can be generalized to limb movements, as there is evidence showing that the saccadic and arm movements are controlled in different ways (see, e.g., Mirabella et al., 2009, 2011).

All in all I hope that the readers of this issue will be convinced of intimate and inextricable connection between volitional inhibition and voluntary behavior. From this it should naturally follow that, in order to allow prosthetic devices to mimic naturally enacted movements, it is necessary to build algorithms capable of decoding brain activity underlying the suppression of pre-programmed actions when unpredictable events require a quick change of the planned motor strategy.

ACKNOWLEDGMENTS

I should like to thank all the authors for participating as well as the chief editor, Laura Ballerini, for her constant support, advice, and encouragement during the preparation of this Research Topic. I also wish to thank the reviewers, whose contributions improved the papers composing the present issue. This research was supported by: (a) internal source: IRCCS Neuromed Hospital, Italy; (b) external sources: (i) the Italian Ministry of Work, Health, and Social Policies (Bando Giovani ricercatori 2007 to Giovanni Mirabella); (ii) Italian Ministry of University and Research (PRIN n.2008_RBFNLH_005 to Giovanni Mirabella).

REFERENCES

Aron, A. R., Behrens, T. E., Smith, S., Frank, M. J., and Poldrack, R. A. (2007). Triangulating a cognitive control network using diffusion-weighted magnetic resonance imaging (MRI) and functional MRI. *J. Neurosci.* 27, 3743–3752.

Busan, P., Zanon, M., Vinciati, F., Monti, F., Pizzolato, G., and Battaglini, P. (2012). Transcranial magnetic stimulation and preparation of visually guided reaching movements. *Front. Neuroeng.* 5:18. doi: 10.3389/fneng.2012.00018

Ifft, P. J., Lebedev, M. A., and Nicolelis, M. A. L. (2012). Reprogramming movements: extraction of motor intentions from cortical ensemble activity when movement goals change. *Front. Neuroeng.* 5:16. doi: 10.3389/fneng.2012.00016

Lew, E., Chavarriaga, R., Silvoni, S., and Millán, J. (2012). Detection of self-paced reaching movement intention from EEG signals. *Front. Neuroeng.* 5:13. doi: 10.3389/fneng.2012.00013

Libet, B. (1985). Unconscious cerebral initiative and the role of conscious will in voluntary action. *Behav. Brain Sci.* 8, 529–566.

Mattia, M., Spadacenta, S., Pavone, L., Quarato, P., Esposito, V., Sparano, A., Sebastiano, F., Di Gennaro, G., Morace, R., Cantore, G., and Mirabella, G. (2012). Stop-event-related potentials from intracranial electrodes reveal a key role of premotor and motor cortices in stopping ongoing movements. *Front. Neuroeng.* 5:12. doi: 10.3389/fneng.2012.00012

Mirabella, G., Pani, P., and Ferraina, S. (2009). The presence of visual gap affects the duration of stopping process. *Exp. Brain Res.* 192, 199–209.

Mirabella, G., Pani, P., and Ferraina, S. (2011). Neural correlates of cognitive control of reaching movements in the dorsal premotor cortex of rhesus monkeys. *J. Neurophysiol.* 106, 1454–1466.

Pastor-Bernier, A., Tremblay, E., and Cisek, P. (2012). Dorsal premotor cortex is involved in switching motor plans. *Front. Neuroeng.* 5:5. doi: 10.3389/fneng.2012.00005

Stuphorn, V., and Emeric, E. E. (2012). Proactive and reactive control by the medial frontal cortex. *Front. Neuroeng.* 5:9. doi: 10.3389/fneng.2012.00009

Wang, Z., Gunduz, A., Brunner, P., Ritaccio, A. L., Ji, Q., and Schalk, G. (2012). Decoding onset and direction of movements using electrocorticographic (ECoG) signals in humans. *Front. Neuroeng.* 5:15. doi: 10.3389/fneng.2012.00015

Wriessnegger, S. C., Bauernfeind, G., Schweitzer, K., Kober, S., Neuper, C., and Mueller-Putz, G. (2012). The interplay of prefrontal and sensorimotor cortices during inhibitory control of learned motor behaviour. *Front. Neuroeng.* 5:17. doi: 10.3389/fneng.2012.00017

Yang, S., McGinnity, T. M., and Wong-Lin, K. (2012). Adaptive proactive inhibitory control for embedded real-time applications. *Front. Neuroeng.* 5:10. doi: 10.3389/fneng.2012.00010

Received: 23 July 2012; accepted: 04 August 2012; published online: 28 August 2012.
Citation: Mirabella G (2012) Volitional inhibition and brain–machine interfaces: a mandatory wedding. Front. Neuroeng. 5:20. doi:10.3389/fneng.2012.00020

frontiers in
NEUROENGINEERING

ORIGINAL RESEARCH ARTICLE
published: 04 April 2012
doi: 10.3389/fneng.2012.00005

Dorsal premotor cortex is involved in switching motor plans

Alexandre Pastor-Bernier, Elsa Tremblay and Paul Cisek*

Département de Physiologie and Groupe de Recherche sur le Système Nerveux Central, Université de Montréal, Montréal, QC, Canada

Edited by:
Giovanni Mirabella, La Sapienza University, Italy

Reviewed by:
Hun-Kuk Park, Kyung Hee University, Korea (South)
Vassiliy Tsytsarev, University of Maryland School of Medicine, USA
Giovanni Mirabella, La Sapienza University, Italy

***Correspondence:**
Paul Cisek, Département de Physiologie, Université de Montréal, C.P. 6218 Succursale Centre-ville, Montréal, QC H3C 3J7, Canada.
e-mail: paul.cisek@umontreal.ca

Previous studies have shown that neural activity in primate dorsal premotor cortex (PMd) can simultaneously represent multiple potential movement plans, and that activity related to these movement options is modulated by their relative subjective desirability. These findings support the hypothesis that decisions about actions are made through a competition within the same circuits that guide the actions themselves. This hypothesis further predicts that the very same cells that guide initial decisions will continue to update their activities if an animal changes its mind. For example, if a previously selected movement option suddenly becomes unavailable, the correction will be performed by the same cells that selected the initial movement, as opposed to some different group of cells responsible for online guidance. We tested this prediction by recording neural activity in the PMd of a monkey performing an instructed-delay reach selection task. In the task, two targets were simultaneously presented and their border styles indicated whether each would be worth 1, 2, or 3 juice drops. In a random subset of trials (FREE), the monkey was allowed a choice while in the remaining trials (FORCED) one of the targets disappeared at the time of the GO signal. In FORCED-LOW trials the monkey was forced to move to the less valuable target and started moving either toward the new target (Direct) or toward the target that vanished and then curved to reach the remaining one (Curved). Prior to the GO signal, PMd activity clearly reflected the monkey's subjective preference, predicting his choices in FREE trials even with equally valued options. In FORCED-LOW trials, PMd activity reflected the switch of the monkey's plan as early as 100 ms after the GO signal, well before movement onset (MO). This confirms that the activity is not related to feedback from the movement itself, and suggests that PMd continues to participate in action selection even when the animal changes its mind on-line. These findings were reproduced by a computational model suggesting that switches between action plans can be explained by the same competition process responsible for initial decisions.

Keywords: decision-making, movement preparation, reach, motor planning, free choice, monkey, computational model, biased competition

INTRODUCTION

Natural behavior requires animals to make many kinds of decisions. For example, an animal is often faced with selecting between different movements that accomplish the same behavioral goal, such as different directions to run to escape a predator. At a higher level of selection, the same animal may decide between different types of activity, such as running away versus turning around to fight. Still other kinds of decisions may involve purely abstract choices, which are not (at least immediately) associated with any specific action. In human behavior, such decisions may be extremely abstract, such as choosing what kind of career to pursue in life. Because the brain was built through continuous evolutionary refinement, we expect that the neural mechanisms of decisions at different levels of abstraction share many aspects of their architecture, and that consideration of simple spatial decisions between movement options may yield insights into decision-making in general (Cisek and Kalaska, 2010).

Recent work has suggested that, at least in the case of selecting between actions, decision-making is intimately integrated with sensorimotor control (Basso and Wurtz, 1998; Platt and Glimcher, 1999; Romo et al., 2004; Cisek and Kalaska, 2005; Gold and Shadlen, 2007). This has led to the proposal that while an animal is deciding between actions, neural activity in the sensorimotor system represents several movements simultaneously and the decision is made by selecting between these parallel representations (Kim and Shadlen, 1999; Cisek, 2007; Cisek and Kalaska, 2010). For example, Cisek and Kalaska (2005) found that while a monkey is deciding between two different potential reaching movements, neural activity in dorsal premotor cortex (PMd) represents both options simultaneously and reflects the selection of one over the other when the monkey makes his choice. This is consistent with earlier proposals suggesting parallel movement preparation (Fagg and Arbib, 1998; Tipper et al., 1998; Erlhagen and Schoner, 2002), and with the hypothesis that action selection is accomplished through a biased competition within a sensorimotor map of potential actions (Cisek, 2006).

This "affordance competition" hypothesis (Cisek, 2007) stands in contrast to the classical serial model, in which decisions

are made in higher cognitive centers and the resulting choice passed down to the sensorimotor system for execution. Instead, it suggests that decisions are determined when a competition between actions is resolved *within* the sensorimotor system—e.g., for reaching, within the fronto-parietal cortex and associated corticostriatal loops. This means that although the biases that influence the decision may come from many sources, including the activity of higher cognitive regions, it is in the sensorimotor system that the final decision is taken. For selecting between actions, this makes good sense from an ecological perspective: the systems most sensitive to the spatial and dynamic attributes of the candidate actions are best qualified to make the final selection that takes all of these factors into account. For example, when choosing between actions, the spatial layout of the immediate environment directly specifies the options and is of critical importance for evaluating what is the best choice in terms of payoffs and costs. Indeed, all else being equal, humans select the action that is least demanding from a biomechanical perspective (Cos et al., 2011), suggesting that the same "forward models" (Shadmehr et al., 2010) useful for predicting the consequences of motor commands may also play a role in selecting the actions themselves by biasing activity in sensorimotor cortices.

Decision-making within a sensorimotor map is particularly useful for spatial choices, such as selecting among different ways to escape a predator through an environment filled with obstacles. If two escape routes are close together, then you should not waste time deciding but instead run between them and choose in flight. In contrast, if you are up against a wall then a clear "winner-take-all" decision is critical, even if it takes a little more time to resolve. Finally, even during ongoing escape, you must continuously evaluate and update the options presented by the environment in case what appeared as an escape route turns out to be a dead end and/or if a new and better option presents itself. If that new option is already partially represented in sensorimotor maps of potential actions, then switching to it will be very fast.

In an analogy to the above scenario, here we consider selection between reaching movements to different spatially specified targets. The affordance competition hypothesis predicts that if we present a monkey with multiple reaching options associated with different rewards, neural activity in PMd will be modulated by the *relative* value of those rewards. However, if a single option is present, then its value will not influence PMd activity because there is no competition. A recent study in our lab (Pastor-Bernier and Cisek, 2011) confirmed both of these predictions, showing relative value modulation when two targets were presented but no value modulation with one target. Furthermore, it was found that the competition between options was strongest when they were furthest apart—just as predicted in the prey escape example described above. All of these results are consistent with the idea that the competition unfolds within a sensorimotor map that respects the pragmatic issues of selecting actions in space, and all of them could be simulated with a simple model of biased competition among populations of tuned cells (Cisek, 2006).

In summary, previous studies have shown that the process of deciding between actions involves the very same brain regions that are implicated in sensorimotor guidance of actions, consistent with the affordance competition hypothesis (Cisek, 2007). However, the hypothesis also makes a complementary prediction: that the same cells involved in selecting the initial action will continue to be involved in adjusting and even switching between actions during overt behavior. In other words, if the environment changes and old opportunities are lost or new ones become available, the same integrated selection and sensorimotor guidance system should reflect the switch of the plan. Here, we investigate this issue by examining neural activity in PMd after a monkey has chosen one of two actions, but the selected option becomes unavailable. We examined the same cells whose delay period activity showed relative value modulation in our previous work (Pastor-Bernier and Cisek, 2011) but extended our analysis to the activity after the GO signal, with particular interest in trials in which the option with highest payoff becomes unavailable. Some of these results have been previously presented in abstract form (Pastor-Bernier et al., 2011).

MATERIALS AND METHODS

INSTRUMENTATION AND TECHNICAL PROCEDURES

A male monkey (*Macaca mulatta*) performed a planar center-out reaching task illustrated in **Figure 1A**. The task involved moving a cursor from a central circle (2 cm radius) to one of six possible targets (2.4 cm radius) spaced at 60° intervals around a 12.6 cm radius circle. The monkey performed movements using a cordless stylus whose position was recorded (125 Hz) by a digitizing tablet (*CalComp*). Target stimuli and continuous cursor feedback were projected onto a mirror suspended between the monkey's gaze and the tablet, creating the illusion that they are in the plane of the tablet. Oculomotor behavior was unconstrained, as eye movements do not strongly influence arm-related PMd activity (Cisek and Kalaska, 2002), but was monitored with an infrared oculometer (ASL). Neural activity was recorded with 3–4 independently moveable microelectrodes (*NAN microdrive*) and data acquisition was performed with AlphaLab (*Alpha-Omega*). On-line spike discrimination was used to estimate cell preferred directions for choosing target locations. All analog waveforms were stored on disk for offline sorting using principal components (*Plexon*). All task events, trajectory data and spike times were stored in a database (*Microsoft SQL Server 2005*) accessed through custom scripts for data analysis (*Matlab*). After completing training, the animal was implanted under general anesthesia with a titanium head post and a recording chamber placed using MRI images (*Brainsight primate*). The chamber was centered on the arm area of PMd, between the precentral dimple and the junction of the arcuate sulcus and spur (**Figure 1B**). All procedures followed university and national guidelines for animal care.

BEHAVIORAL TASK

The monkey began each trial by placing the cursor in the central circle for a 350–650 ms Center-Hold-Time (CHT). Next, one or two cyan targets appeared, with border styles indicating the amount of juice that the monkey was likely to receive for reaching to that target (See **Figure 1A**, inset). The reward was determined probabilistically to encourage the monkey to explore available options (Herrnstein, 1961). A "low-value" target (L, thick border) had a 60% chance of yielding 1 drop, 30% chance of yielding 2,

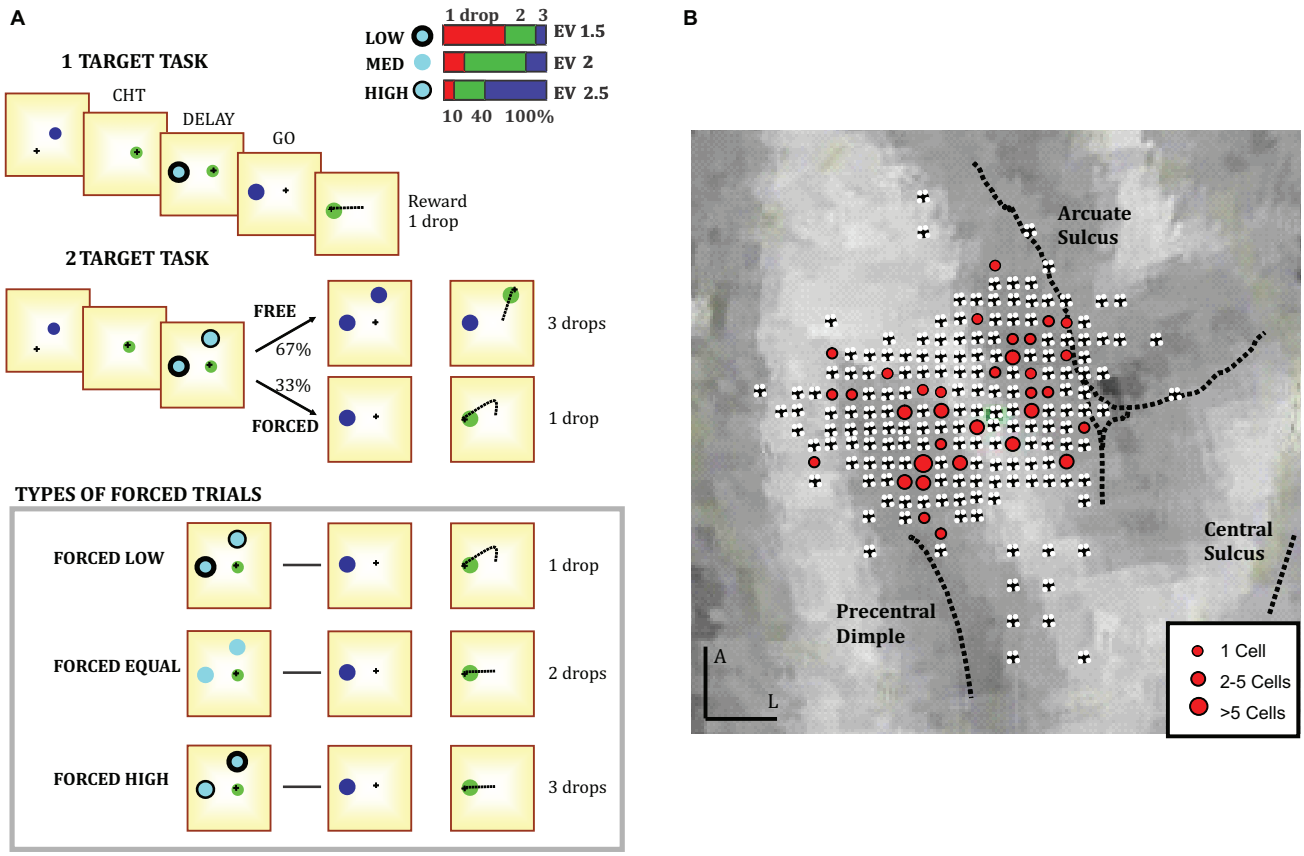

FIGURE 1 | (A) Behavioral tasks. The tasks involve moving a cursor from a central circle to one of six possible target locations. At the beginning of each trial the monkey placed the cursor in the center and two targets appeared. Each target was associated with different rewards indicated by different border styles (legend shows the probability of receiving 1 (red), 2 (green), or 3 (blue) drops of juice for each border style). The monkey had to keep the cursor in the center until the targets changed color (GO signal). Then, it moved to one of the targets and held the cursor there to get a reward. In one variant of the task, the monkey was presented with only one target (1T). In a second variant two targets were presented, and the monkey was either free to move to either of them after the GO signal (FREE trials), or one disappeared after GO leaving the monkey with only the remaining option (FORCED trials). **(B)** The recording locations in PMd. Black crosses indicate recording sites. The locations for cells modulated by relative value (RV cells) are shown with red circles ($N = 52$).

and 10% chance of yielding 3 (Expected value, EV = 1.5). A "medium-value" target (M, no border) was worth 2 (60%), 1 (20%), or 3 drops (20%) (EV = 2). A "high-value" target (H, thin border) was worth 3 (60%), 2, (30%), or 1 drop (10%) (EV = 2.5). The non-monotonic relationship between border thickness and value was used to dissociate motivational factors from physical properties of stimuli. In particular, the most visually salient cue with a thick border style is deliberately chosen to have a small payoff ("low value") to dissociate saliency from value effects. The monkey held the cursor in the center for an instructed delay period (DELAY, 700–1300 ms) until a GO signal was indicated by a change in target color and the disappearance of the central circle. After the GO signal, the monkey had to initiate the movement within a 550 ms reaction time (RT) (which had to be at least 100 ms, to discourage anticipation). To receive a reward, the monkey had to move to a target within a maximum 550 ms movement time (MT) and hold the cursor there for 500 ms (Target-Hold-Time, THT). When cells were isolated, we first ran a block of 90 trials in which only one target was presented (1T), to identify the DELAY-period preferred target (PT) of each cell. Next, we ran a block of 180 two-target trials (2T), including ones where the PT target was present and low, medium, or high-valued, while the other target (OT) appeared at 60°, 120°, or 180° away and was low, medium, or high-valued. Each block also included 30 trials in which the targets were 120° apart but neither was in the direction of the PT. In this paper we focus only on trials in which the targets are 120° apart (90 trials per 2T block) and at least one of the presented targets was the cell's PT. In 67% of 2T trials (FREE), the monkey was free to move to either target after the GO signal. In 33% of 2T trials (FORCED), one of the targets disappeared at GO and the monkey had to move to the remaining one. FREE and FORCED trials were randomly interleaved to encourage the animal to keep both options partially prepared. FORCED trials were classified according to the value of the target that disappears after the GO signal. In FORCED LOW trials the target with the higher expected

value disappears (inset in **Figure 1A** bottom), while the opposite is true in FORCED HIGH trials. In a FORCED EQUAL trial both the target that disappears and the target that remains have the same value.

KINEMATIC ANALYSIS

Movement trajectories were re-sampled at a constant rate (200 Hz) and filtered using a two-way butterworth filter [0 phase lag, 4th order, norm. cutoff 0.05 (∼20 Hz)] using Matlab functions *butter* and *filtfilt* (Mathworks). The initial direction vector (**IDV**) was calculated as the *X* and *Y* coordinate cartesian arctangent (*atan2*) between the position at movement onset (MO) and the position 100 ms later. Trials were sorted by short RT (<180 ms), medium RT (between 180 ms and 240 ms) or long RT (>240 ms). The mean trajectory profiles and mean IDVs were calculated for each RT group independently. To determine whether the **IDV** was pointing to a given target in space, we calculated the mean **IDV** in the 1T condition for each target individually. Then, 2T trials were classified as "*direct*" to the selected target if their **IDV** fell within ±60 degrees of that target's mean **IDV** in the 1T condition. Trials whose **IDV** pointed away from the ultimately acquired target were classified as "*curved*."

CELL TUNING AND RELATIVE VALUE DISCRIMINATION

We investigated only cells that had both spatial tuning and relative value discrimination (see Pastor-Bernier and Cisek, 2011) during DELAY. We calculated directional tuning preferences for the cells during each behavioral epoch (DELAY, MT, and THT) and assessed significance with a non-parametric bootstrap test (1000 shuffles, $p < 0.05$; Cisek et al., 2003). To assess whether a cell discriminated relative value during DELAY, we examined whether the cell showed statistically significant differences in firing rate between a "HIGH" value condition (value in PT was larger than OT) and a "LOW" value condition (value in OT larger than PT) for the last 300 ms prior to the GO signal (One-Way ANOVA, $p < 0.05$). This was done to verify whether the same cells that are involved in the initial decision continue to reflect plan switches after the GO signal. Cells satisfying both requirements were used for post-GO analyses. Discrimination latencies were obtained using a sliding ANOVA method adapted from Peng et al., 2008 (window: 50 ms, step: 5 ms, $p < 0.05$) to perform a statistical temporal analysis between the HIGH and LOW value conditions. We obtained latencies for relative value discrimination with respect to the GO signal by aligning the neural activity on GO and parsing each trial backwards for 700 ms (shortest variable DELAY duration). This chosen interval ensured that all trials had a similar time range for firing rate comparisons. The latency of relative-value discrimination was obtained as the last 80 ms sliding time-window for which a statistical difference could be observed. The cells that satisfied both the One-Way ANOVA and sliding-ANOVA requirements were called relative value discriminating cells (**RV cells**, *N*: 52). This population is identical to the data-set described previously (Pastor-Bernier and Cisek, 2011) in which relative-value effects were assessed for particular value combinations (PTvsOT: 3vs1, 2vs1, 3vs2) using paired ANOVA and Tukey–Kramer tests.

PLAN-SWITCH ANALYSIS

FORCED LOW trials were of particular interest for plan-switching analysis because they represent conflict situations in which the more desirable option must be replaced by the less desirable option. In these "plan-switch" cases, DELAY activity prior to GO (pre-GO plan) was compared with activity after GO (post-GO plan). We further distinguished cases where the target that disappears is located in the cell's PT or in the OT, giving rise to two different kinds of FORCED LOW trials. In FORCED LOW PT2OT trials the pre-GO DELAY activity reflects an initial plan to PT and the post-GO activity a final plan to OT. In FORCED LOW OT2PT trials the pre-GO DELAY activity reflects a movement plan to OT and the post-GO activity a final plan to PT. To obtain plan-switch latencies FORCED LOW trials were compared with trials belonging to the FREE condition in which the animal naturally chose the high valued option (FORCED-FREE comparison). To obtain the switch latency from an initial plan to PT to a final plan to OT (**SwitchPT2OT**) the activity of FORCED LOW PT2OT trials was compared with FREE trials in which PT was the plan selected (FREE HIGH PT). This type of switch is illustrated in **Figure 3A**. The plan-switch latency was obtained by parsing the neural activity for both types of trials from GO to movement offset using a sliding ANOVA method (window: 50 ms, step: 5 ms, $p < 0.05$) and calculated as the first moment in time in which they were significantly different for at least 80 ms *after* the GO signal. For the plan-switch latency to be valid we also required that there be no significant difference between the FORCED LOW PT2OT and the FREE HIGH PT types of trial for at least 300 ms *before* the GO signal (One-Way ANOVA, $p < 0.05$ ms). To calculate the switch latency from an initial OT plan to a final PT plan (**SwitchOT2PT**) the activity of FORCED LOW OT2PT trials was compared to FREE HIGH OT trials in which OT was selected. **Figure 3B** illustrates an example of this type of switch. We define as "convergence" the situation in which the pre-GO DELAY activity for two types of trials represents different movement plans, while the post-GO activity represents the same plan. The time of convergence to a plan in the PT direction (**CONV**) is found by comparing FORCED LOW OT2PT trials with FREE HIGH PT trials (**Figure 3C**). Convergence to an OT plan cannot be determined from the activity of cells because activity to OT is generally low. To obtain **CONV** latency a similar sliding ANOVA method was used, although the time of convergence was defined as the first moment after the GO signal in which the difference between the two types of trial was *not significant* ($p > 0.05$) for at least 80 ms. We also required the pre-GO DELAY activity between FORCED LOW OT2PT and FREE HIGH PT to be different for at least 300 ms (One-Way ANOVA, $p < 0.05$). In a variant of the plan-switch latency study we used FORCED HIGH trials instead of FREE HIGH trials for the calculation of plan-switch latencies (FORCED-FORCED comparison). This allowed us to address whether differences in visual input after the GO signal (the number of remaining targets) could have an effect on the plan-switching process.

The population's mean switch latencies (ms) were calculated using the sliding-ANOVA method mentioned above. The confidence intervals (CI) at 95% probability ($p < 0.05$) were obtained as $\pm Z \times \sqrt{E}$, where Z represents the critical area for

the distribution of mean switch latencies across trials. Z can be approximated to ± 1.96 assuming by the central limit theorem (Polya, 1920) that the mean distribution tends to normality with large sample sizes. The variable E represents the error variance of the mean and was calculated using the expression correcting for overlapping intervals described in Müller (1993) (Equation 3.7) and cited elsewhere (Dacorogna et al., 2001; Hansen and Lunde, 2006).

$$E = r/N^2 \times [rR - (r^2 - 1)/3]$$

where $r = \min(m,N)$, $R = \max(m,N)$ and where m is the overlap between intervals and N is the number of samples per time interval.

In our case we have a 50 ms window sliding by 5 ms bins. Therefore, $m = 45$ and $N = 10$. Because m > N, then $r = N$, and $R = m$, and the previous expression takes the form:

$$E = m - N/3 - 1/3N$$

Solving numerically with $m = 45$ and $N = 10$, we obtain $E = 41.7$ and therefore,

$$\mathrm{CI} = \pm 1.96\sqrt{41.7} = \pm 12.6 \approx \pm 13\ \mathrm{ms}$$

With no overlap $m = 0$, $r = 0$, $R = 1$, $N = 1$, and the error of overlap $E = 0$.

COMPUTATIONAL MODELING

The model (Cisek, 2006) is aimed at explaining and predicting systems-level phenomena such as response patterns over large population of neurons. It is implemented with a set of equations describing the activity of several populations of neurons that correspond to specific cortical regions. Each population is organized as a layer of neurons that are tuned to spatial directions of potential actions. Each neuron in a layer behaves according to an expression that defines how its activity changes over time as a function of four terms: passive decay, excitation toward saturation, inhibition, and noise. This expression can also be called "mean-rate leaky integrator" (Grossberg, 1973) and takes the following form:

$$dX/dt = -\alpha X + (\beta - X)\gamma \cdot E - X \cdot I + \theta, \qquad (1)$$

where X is the mean firing rate of a given neuron, dX/dt is the change in rate over time, E is the excitatory input, I is the inhibitory input, α is a decay rate, β is the maximum activity of a neuron, γ is the excitatory gain, and θ is the Gaussian noise. The connections between each layer are hardwired and organized to respect basic neuroanatomical connection patterns. Further details concerning connectivity patterns and model behavior have been described previously elsewhere (Cisek, 2006). For purposes of the present task the model's "prefrontal" activity was scaled by a signal related to the absolute value of each target (low = 0.3, medium = 0.7, high = 1.0). To simulate plan switches, we removed one of the two presented targets (high valued target in FORCED LOW trials) at the beginning of the GO epoch. All parameter settings were identical to Cisek (2006), except that we used a gradual GO signal that allows the activity in PMd to gradually spill into the M1 layer. The gradual GO signal is defined as a multiplicative factor that scales the input from PMd to M1 and is zero before the GO instruction. After the GO instruction, it grows as $2.5 \cdot t$ where t is the time since the GO instruction.

Note that the model in its present form is not intended to simulate the movement itself. Activity in the model M1 population simply indicates the initial direction of movement, computed as the preferred direction of the first M1 cell that crosses a threshold of activity equal to 1.75.

BEHAVIORAL RESULTS

In 1T trials the monkey's success rate was 98%, in 2T FREE it was 99%, and in 2T FORCED it was 96% (in all cases $N > 60{,}000$). In 2T FREE trials the monkey selected the more valuable target 90% of the time, indicating that he understood the meaning of the stimulus cues. We found that movement times (MT) were shorter to higher-valued targets in 1T trials (400 ms to high-value and 416 ms to low-value targets). Although the difference was small, it was significant (Kolmogorov–Smirnov test (KS), $p < 0.01$). RTs in 1T trials did not depend on target value (KS-test $p > 0.05$ for all comparisons).

We observed an interaction effect between RT and trajectory kinematics in 2T trials. Trajectories belonging to short RT trials were generally more curved than trajectories belonging to medium or long RT trials (**Figure 2A**). This effect was accentuated by the value of the unselected target with respect to the value of the selected target in the FORCED condition. Trajectories in the FORCED LOW condition (**Figure 2A,** rightmost panel) were generally more curved than the ones in the FORCED HIGH or FREE HIGH conditions (**Figure 2A,** left and middle panels). These curved movements have an initial launching direction toward the target that vanishes and are corrected later to the remaining target. To quantify this we obtained the mean trajectory **IDV** across all conditions (**Figure 2B**). We observed that a great deal of the curvature in FORCED LOW trials was due to movements launching to the target that becomes unavailable after GO (High value). This effect was particularly strong for short RT trials and moderate for intermediate RT trials. Long RT trials were essentially straight toward the remaining target (**Figure 2B**, rightmost panel). We didn't see this effect when the monkey was forced to move to the high value target or when the monkey was free to choose among the two targets, because in either situation the preferred and available target were the same. We further investigated the interaction between RT, relative value, and initial launching direction by comparing raw RT distributions. The mean RTs in FREE HIGH (266 ms, light-brown dashed histogram), FORCED HIGH (271 ms, dark-brown dashed histogram), and FORCED LOW (279 ms, black dashed histogram), were very similar (**Figure 2D**) with only small differences between the mean RTs in FREE HIGH and FORCED LOW distributions (KS-test, $p < 0.01$). This could be due to the contribution of a higher proportion of correct trials in FREE HIGH than in FORCED LOW trials (3% difference). Most importantly we observed that the mean RT in FORCED LOW trials with "direct" trajectories (red

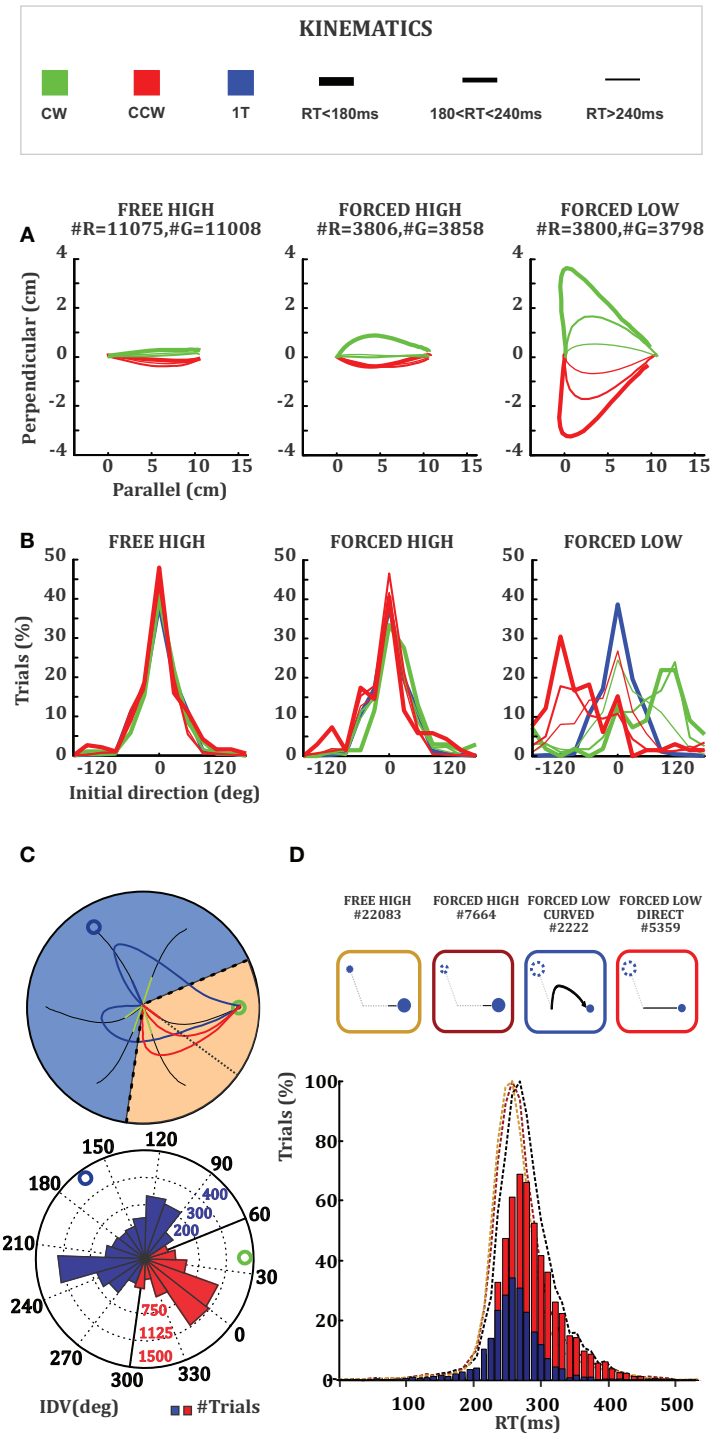

FIGURE 2 | (A) Average trajectories for 2T trials with the unselected target located 120° clockwise (red) or counterclockwise (green) to the selected target (always on the right). The three panels from left to right represent FREE, FORCED HIGH, and FORCED LOW trials. The line thickness represents trials classified by their RT. Thick lines correspond to long RT (>240 ms), medium sized lines to intermediate RT (between 180 and 240 ms) and thin lines short RT (<180 ms) (See Method sections for details). **(B)** Distribution of initial launching directions, with selected target at 0°. The color and line thickness code is the same as in **Figure 2A**. Blue histograms represent 1T trials to the selected target. **(C)** Method used to classify trials as direct (red) or curved (blue). The top panel shows individual FORCED LOW trials when the remaining target is to the right and the vanished target is to the upper left. Small arrows indicate the IDVs and the red region indicates the 120° angle around the average, within which trials were considered to be "direct." The bottom panel shows a rose plot of the distribution of individual IDVs. **(D)** The RT distributions of FORCED LOW (black dash) trials, including FORCED LOW "*direct*" (red solid) and "*curved*" (blue solid) trials along with the RT distributions of FREE HIGH (light brown dash) and FORCED HIGH (dark brown dash).

histogram, 291 ms) was significantly longer *(21 ms difference, KS-test, $p < 0.01$)* than the mean RT in FORCED LOW trials with "curved" trajectories (blue histogram, 270 ms). In comparison, FORCED LOW "curved" trials and FORCED HIGH trials did not show RT differences (KS-test, $p > 0.05$) **(Figure 2D)**.

NEURAL RESULTS

PMd ACTIVITY PREDICTS SWITCHING OF MOTOR PLANS AHEAD OF MOVEMENT ONSET

Activity was recorded from 327 cells from the arm area of PMd (**Figure 1B)** of which 226 (69%) had significant directional tuning during at least one epoch (DELAY, MT, THT) and were considered task-related. Here, we focus on cells with DELAY-period tuning (181/226, 80%), 52 of which (29%) were modulated by relative value combinations during DELAY (One-Way ANOVA, $p < 0.05$) and were considered further for the plan-switch analyses (relative value, **RV cells**). In the first variant of this analysis we compared neural activity in FORCED LOW versus FREE HIGH conditions (FORCED-FREE). **Figures 3A–C** shows three individual cells illustrating the different types of plan-switch analyses. In a **SwitchPT2OT** (**Figure 3A)** we compare trials that had a pre-GO plan to PT and a post-GO plan to OT (FORCED LOW PT2OT, green trace) with trials that had both a pre-GO and post-GO plan to PT (FREE HIGH PT, red trace). In a **SwitchOT2PT** (**Figure 3B)** we compare trials with a pre-GO plan to OT and a post-GO plan to PT (FORCED LOW OT2PT, blue trace) with trials that had both a pre-GO and post-GO plan to OT (FREE HIGH OT, pink trace). In a convergence (**CONV**) the pre-GO plan is different for two types of trials (FORCED LOW OT2PT and FREE HIGH PT) but is the same (movement plant to PT) after the GO signal (**Figure 3C**). **Figures 3D–G** show additional examples that had statistically significant plan switches at the individual cell level. Thirty-seven of the 52 (71%) **RV cells** showed statistically significant modulation (sliding ANOVA $p < 0.05$) in at least one plan-switch analysis in the FORCED-FREE latency comparison and are referred to as **Switch cells**. Switches of activity of the other cells did not reach statistical significance, often because those cells were recorded during only a few trials of each type.

To address the role of visual input (the number of targets remaining after GO) on the plan-switching process, we also compared FORCED LOW versus FORCED HIGH conditions (FORCED-FORCED comparison). **Figures 3F–G** illustrates a single cell example in which plan switches were obtained both for the FORCED-FREE comparison (**Figure 3F**) and for the FORCED-FORCED comparison (**Figure 3G**). Twenty-eight out of 52 (54%) **RV cells** showed statistically significant modulation to plan switches in the FORCED-FORCED comparison. **Table 1** summarizes the cell counts for the different types of switch in both comparisons.

To test whether the plan-switch pattern observed at the individual cell level also held at the population level, we obtained the population profile for plan-switching in **Switch Cells** and all **RV** cells separately and for both FORCED-FREE **(Figures 4A–B)** and FORCED-FORCED **(Figures 4C–D)** comparisons. We observed that the latency of SwitchPT2OT and SwitchOT2PT for **Switch Cells** was 155 ± 13 ms (95% CI) after the GO signal and, therefore, well before MO (300 ± 50 ms) in both FORCED-FREE and FORCED-FORCED comparisons (**Figures 4E–F**). Convergence to a plan occurred later, 190 ms $\pm$ 13 ms after the GO signal, but still well-ahead of MO. These results held for both the **Switch cell** or **RV cell** populations, although we observed that switch latencies in the larger **RV cell** population were later than in the **Switch cell** population by about 15–20 ms (this difference did not reach statistical significance, ANOVA $p > 0.05$), and was presumably due to the presence, in the RV population, of cells with very few trials resulting in a larger standard error. **Table 2** summarizes the latency results for each cell population and comparison.

PMd CONTRIBUTION TO KINEMATICS PRIOR TO MOVEMENT ONSET (INITIAL DIRECTION) IS OBSERVED IN SITUATIONS WHERE THERE IS NO RELATIVE VALUE BIAS

We examined the cell responses in the plan-switch paradigm taking into account the initial direction of the reach movements in each trial. By doing so we classified trajectories as initially aiming to the selected target ("direct," to PT or OT) or initially aiming to the unselected target ("curved"). We compared both direct and curved movements in the conditions that were more likely to provoke curvatures due to plan-switches, namely the FORCED LOW and FORCED EQUAL conditions. **Figures 5A–C** shows population histograms for **Switch cells** and **RV cells**, comparing FORCED LOW direct and curved trials. We observed that curvature is not predicted by DELAY activity in the FORCED LOW condition. We did not observe statistically significant differences either between activity in the FORCED LOW PT2OT direct trials and FORCED LOW PT2OT curved trials, or between FORCED LOW OT2PT direct and FORCED LOW PT2OT curved (ANOVA, $p > 0.05$ in both cases). However, DELAY activity in the FORCED EQUAL conditions does predict whether a trial will be curved or straight. During the 600 ms prior to the GO signal, we observed statistically significant differences (ANOVA, $p < 0.05$) between FORCED EQUAL direct and FORCED EQUAL curved trials, for both **Switch cell** and **RV cell** populations (**Figures 5D–F**). It is noteworthy to mention that these differences take place only during DELAY prior to the monkey's knowledge of which target will disappear (GO), and reflect pre-GO selection biases. That is, among the FORCED EQUAL trials there are some in which the pre-GO activity happens to be strongly biased toward one target, and when that target disappears, the bias is likely to cause a curved movement (green and blue traces).

Note that, as shown in **Figures 5B,E**, when we align activity on the MO we can see that the switch of the plan (computed at the population level) occurs approximately 150 ms before MO. This is interesting because in the curved trials the monkey still launches to the now non-existent target.

A BIASED COMPETITION MODEL CAN REPRODUCE THE DYNAMICS OF THE PLAN-SWITCH

Cisek (2006) described a "biased competition" model of action selection, in which populations of cells along the dorsal stream implement a distributed representation of potential actions that compete against each other through lateral inhibition (**Figure 6A**, see Methods). The model simulates relative value effects reported previously when reward-related biasing signals are introduced into PFC (Pastor-Bernier and Cisek, 2011). Here, we used the

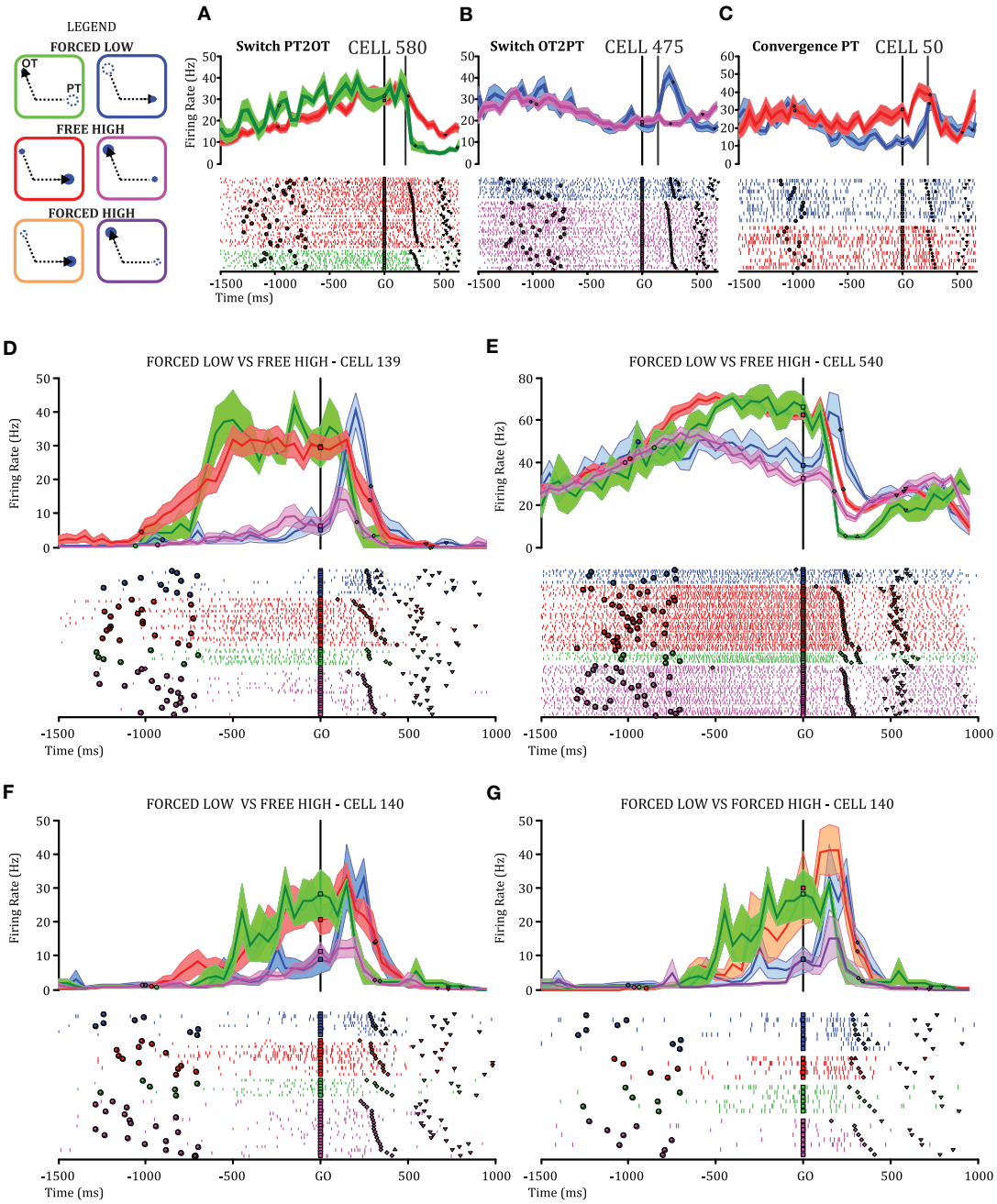

FIGURE 3 | Top-left: The different types of trials are represented in color boxes. Target position is indicated by a blue circle in PT or in OT. The target value is indicated by circle size. In a "FORCED LOW" condition the most valuable option disappears after the GO signal (dashed circles) giving rise to two possibilities: whether the target with the larger value (big circle) was the cell's PT (green box) or the other target (blue box). In both cases the monkey is forced to move to the remaining option (small circle). We compare these trials with "FREE HIGH" trials, in which the monkey is free to choose the target located either in PT or OT (red or pink) and selects the option with higher value (FORCED-FREE comparison). We also separately compare FORCED LOW trials with "FORCED HIGH" trials in which the target that disappeared after the GO signal was the less valuable one (orange and violet) (FORCED-FORCED comparison). In all panels bold black arrowheads indicate the selected option. **(A–G)** Examples of the activity of individual cells illustrating the switching of movement plans observed between the pre-GO and the post-GO period. Cell activity is depicted as firing-rate histograms, with mean ± s.t.e., and rasters in which black marks indicate cue onset, go signal, movement onset and offset, with trials sorted by RT. A switch from PT to OT (**SwitchPT2OT**) is seen by comparing trials that have a pre-GO plan to PT and a post-GO plan to OT (green) with trials that have both a pre-GO and post-GO plan to PT (red). The time of the switch is indicated by a gray vertical bar (only in **Figures 1A–C** for simplicity). The alignment of activity on the GO signal for rasters and firing rate histograms is indicated by a black vertical bar in all panels. A switch from OT to PT (**SwitchOT2PT**) is seen by comparing trials that have a pre-GO plan to OT and a post-GO plan to PT (blue) with trials that have both a pre-GO and post-GO plan to OT (pink). The time of convergence to a plan in the PT direction (**CONV**) is found by comparing trials with a pre-GO and post-GO plan to PT (red) with trials with a pre-GO plan to OT but a post-GO plan to PT (blue). Convergence to an OT plan cannot be determined from the activity of cells because activity to OT is generally low.

same model to simulate plan switches by removing one of the two presented targets at the beginning of the GO epoch and by letting the activity in PMd gradually spill into the M1 layer (see Methods). **Figure 6D** shows the activity of a simulated neuron illustrating plan switches from OT2PT, PT2OT, and convergence to PT. Note that the timing of the PT2OT and OT2PT plan switches occur simultaneously and prior to MO. This is also the case for convergence to PT. These results are compatible with the experimental data and suggest that PMd contains all the information concerning the final action plan before MO. **Figure 6B** shows RT distributions from FORCED LOW simulations for trials in which the model launched toward the target that vanished (blue) or the remaining target (red). We observe that RTs are shorter for trials initiated toward the vanishing target, in agreement with behavioral data (**Figure 2D**). **Figure 6C** shows the distribution of initial launching directions. Note that the blue distribution (which comprises the majority of early RT trials) is aimed toward the target that vanished, predicting that if the model were equipped with online feedback during the movement itself, it would produce curved trajectories as in the behavioral data. **Figure 6E** shows

Table 1 | Classification of cells.

PMd Cell counts	*N*
Cells with any delay activity	**181**
Delay activity only	77
Movement and delay activity	104
Discrimination of relative value (RV)	**52**
Delay and movement	30
Delay only	22
Switch Cells *FORCED vs. FREE	**37**
Switch OT2PT	31
Switch PT2OT	22
Convergence PT	15
Switch **FORCED vs. FORCED	**28**
Switch OT2PT	24
Switch PT2OT	17
Convergence PT	13

*FORCED LOW vs FREE HIGH

**FORCED LOW vs FORCED HIGH

Cell counts per condition and type of plan switch.

Table 2 | Population latencies obtained with sliding ANOVA.

	SwitchPT2OT	SwitchOT2PT	Convergence PT
N:37 POP ANOVA			
FORCED-FREE	155 ± 13*	155	190
FORCED-FORCED	170	155	190
N:52 POP ANOVA			
FORCED-FREE	170	170	190
FORCED-FORCED	190	160	190

*CI for all comparisons.

Plan switch latencies in PMd cells that discriminate relative values (RV cells, N = 52) and in a cell subset with individually statistically significant switches (Switch cells, N = 37). The mean activity for each individual cell was calculated prior to pooling the cells together in order to obtain a balanced contribution of each cell. Latency values were obtained by a sliding ANOVA on the population profile. CI = 95% confidence interval for latency values at p < 0.05.

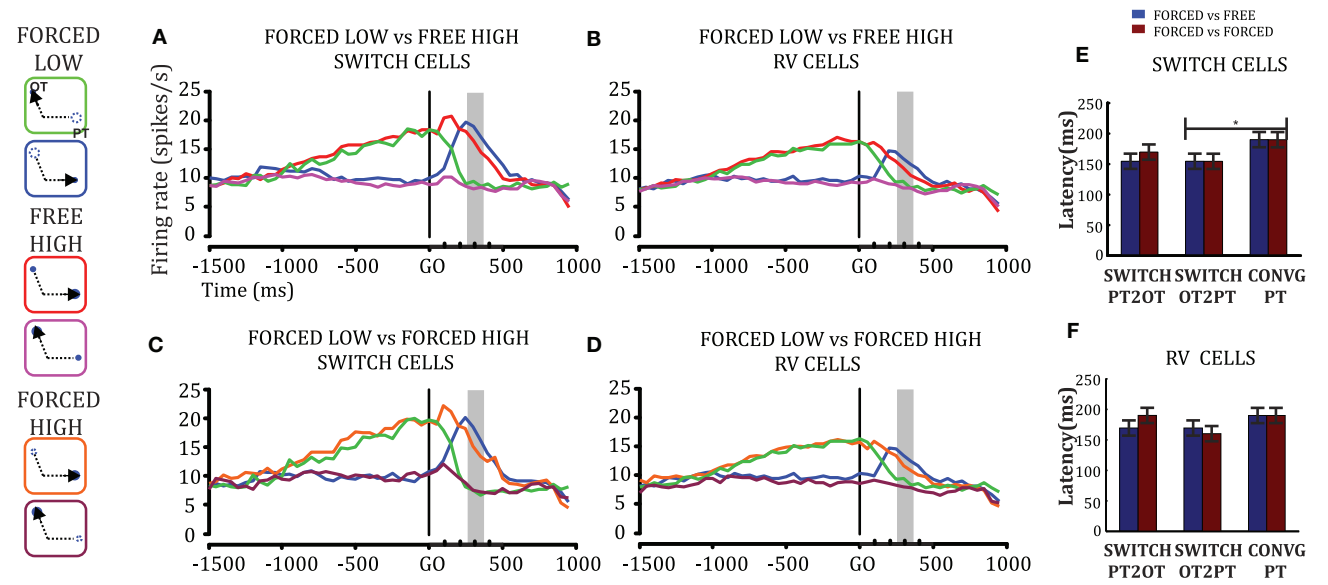

FIGURE 4 | Population activity. Cells with statistically significant plan switches (**Switch Cells**, $N = 37$) and all cells discriminating relative values (**RV Cells**, $N = 52$) were examined separately for switch latencies in the FORCED vs. FREE **(A–B)** and FORCED vs. FORCED comparisons **(C–D)**. The gray bar indicates the time range of movement onset. The legend has the same color code as in **Figures 3E–F**. Comparison of the latencies of SwitchPT2OT, SwitchOT2PT, and CONV in these two groups of cells in FORCED-FREE (blue bars) and FORCED-FORCED comparisons (brown bars). The horizontal line above the histograms represent comparisons that were statistically significant (ANOVA, $p < 0.05$).

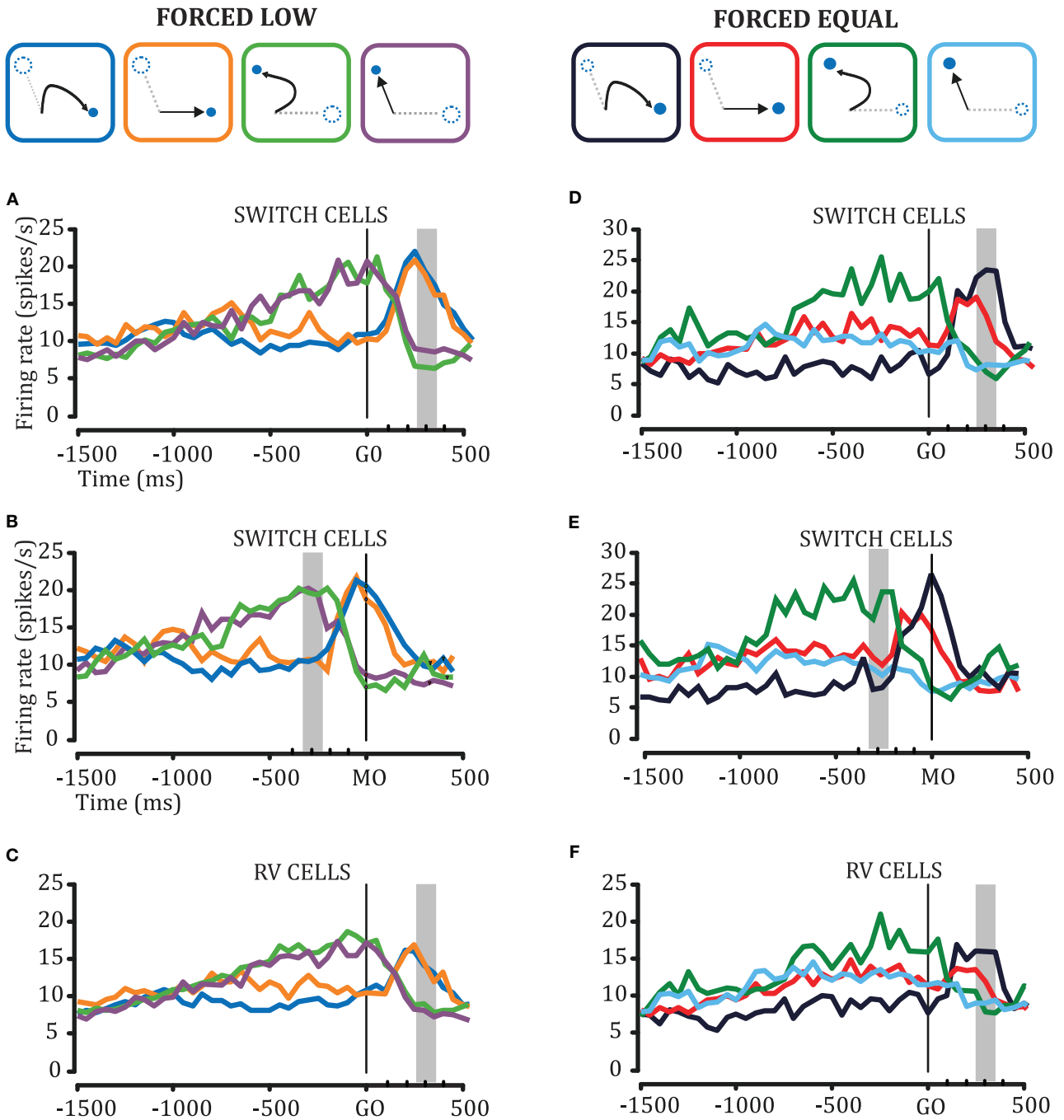

FIGURE 5 | Cell responses in the plan switch paradigm taking into account the initial direction of the reach movements in each trial. **(A–C)** Comparison of direct and curved movements in the FORCED LOW condition for **Switch Cells (A–B)** and **RV Cells (C)**. Trajectories are classified as curved to PT (blue box), curved to OT (green box), direct to PT (orange), or direct to OT (violet). **(D–F)** Comparison of straight and curved movements in the FORCED EQUAL condition for **Switch Cells (D–E)** and **RV Cells (F)**. Trajectories are classified as curved to PT (dark blue box), curved to OT (dark green box), direct to PT (magenta) or direct to OT (cyan). In panels **A, C, D,** and **F** the data is aligned on GO and the gray bar represents the time range of movement onset. Panels **B** and **E** replot the data in **A** and **D**, respectively, with alignment on movement onset (MO), and the grey bar indicates the time range of the GO signal.

the model's Parietal, PFC (rostral and caudal), PMd (rostral to caudal), and M1 population patterns of activity during a FORCED LOW trial where we observe a plan switch that is completed before MO. In contrast, in the trial shown in **Figure 6F**, the model launches the movement before the plan switch is complete. We observe that the timing of plan switches in all PMd layers is before MO, in agreement with our experimental results.

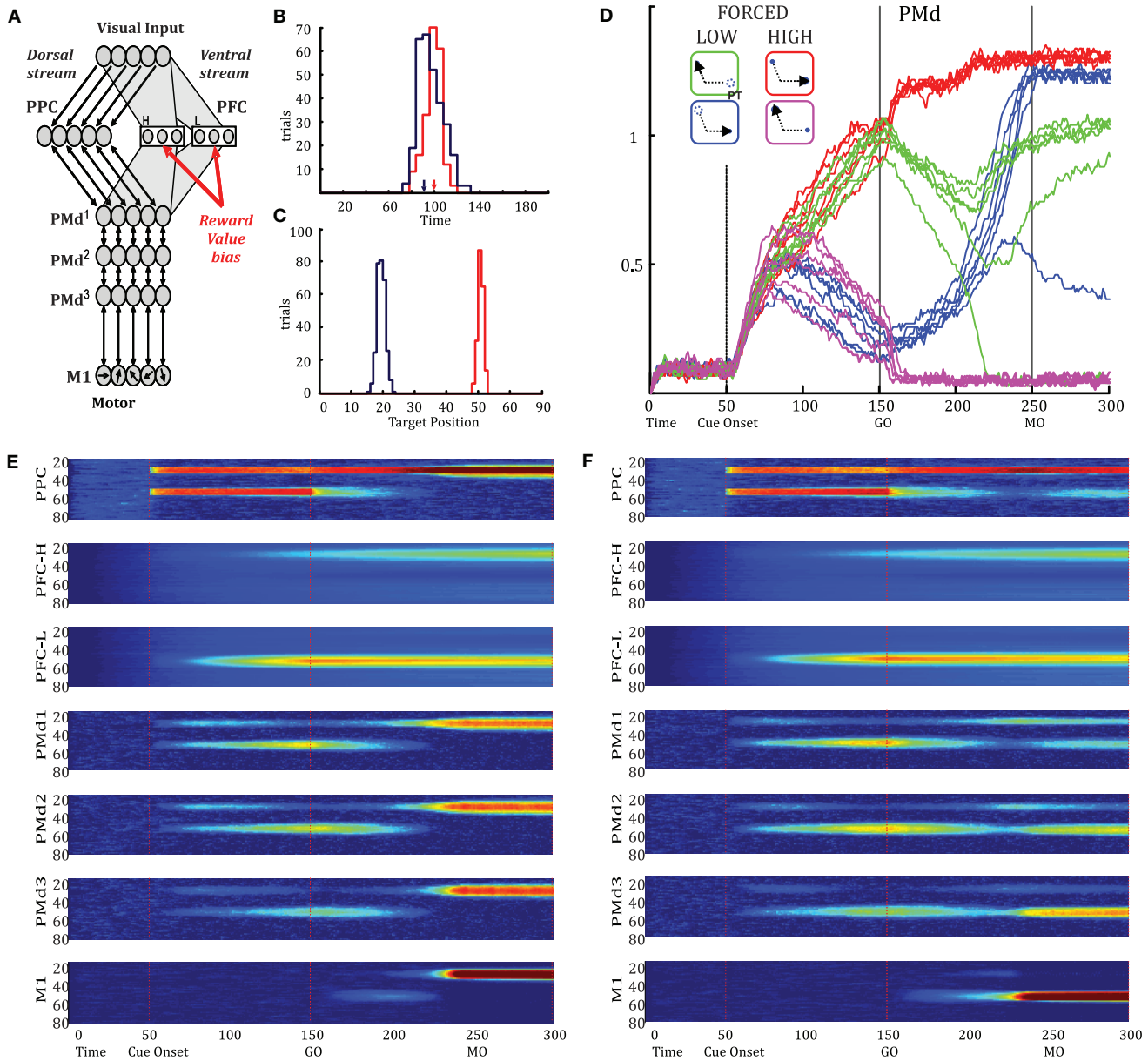

FIGURE 6 | (A) Model of action selection, in which populations of cells along the dorsal stream implement a distributed representation of potential actions that compete against each other through lateral inhibition. Each population is modeled as a set of tuned neurons with "on-center-off-surround" recurrent connectivity. The model includes posterior parietal cortex (PPC), prefrontal cortex (PFC), three regions of PMd (rostral to caudal), and primary motor cortex (M1). Biasing signals related to absolute reward value (High, H or Low, L) enter as independent inputs to particular PFC layers (PFC-H, PFC-L). **(B)** RT distributions for trials in which the model launched to the target that vanished (blue) or to the remaining target (red). **(C)** Initial launching directions toward the vanishing target (blue, at position 20) or remaining target (red, at position 50). **(D)** A simulated neuron showing activity during four compared conditions: FORCED LOW OT2PT (blue), FORCED HIGH OT (purple), FORCED LOW PT2OT (green), and FORCED HIGH PT (red). Individual lines represent individual simulated trials. **(E)** Patterns of activity in the model's Parietal, PFC, PMd (rostral to caudal) and M1 populations, during a FORCED LOW trial in which the target at position 50 was more valuable but vanished at the time of the GO signal, and the plan switch was completed prior to MO. **(F)** Patterns of activity in another FORCED LOW trial, but in which the movement was launched before the plan switch was complete, initiating to the target at position 50.

DISCUSSION

Recent studies have shown that while a monkey is deciding between two potential reaching movements, neural activity in the dorsal PMd can specify both movements simultaneously (Cisek and Kalaska, 2002, 2005; Klaes et al., 2011), and the neural representations of these movements are modulated by their relative subjective desirability (Pastor-Bernier and Cisek, 2011). These findings suggest that decisions between reaching actions are

made within the same brain regions involved in the execution of the actions themselves, in agreement with research on reaching (Cisek, 2007; Pesaran et al., 2008; Cisek and Kalaska, 2010) and oculomotor control (for reviews, see Glimcher, 2003; Gold and Shadlen, 2007). In fact, decisions about eye movements appear to involve even the superior colliculus, a brainstem structure that is just two synapses away from the motor neurons that move the eye (Basso and Wurtz, 1998; Carello and Krauzlis, 2004; Horwitz et al., 2004; Ignashchenkova et al., 2004; Thevarajah et al., 2009).

However, the finding that decision variables (such as relative value) influence neural activity in sensorimotor regions does not necessarily imply that these same cells continue to be involved in the on-line guidance of movement. It is plausible that once a decision is made and an action is launched toward a given target, the decision-related cells fall silent while a separate circuit becomes responsible for guiding movement toward the selected target. The results presented here suggest that this is not the case. We found that the very same PMd cells previously shown to reflect relative value during a delay period continue to update their activity to reflect when the monkey changes its plan during situations in which a previously selected action becomes unavailable. This argues against the distinction between regions responsible for choosing an action and those responsible for its guidance through on-line feedback, and in favor of the hypothesis that decisions emerge through a competition within the same circuit that guides movement execution (Cisek, 2007).

A number of earlier studies provide converging evidence consistent with this integrated view. For example, it has been shown that humans and monkeys can quickly and smoothly update their movement plans when the location of the reach target suddenly and unpredictably changes (Georgopoulos et al., 1981, 1983; Prablanc and Martin, 1992; Desmurget et al., 1999; Day and Lyon, 2000; Archambault et al., 2009, 2011; Gritsenko et al., 2011), even when they are not consciously aware of the change. During these "target jump" experiments, neural activity in fronto-parietal cortex smoothly transitions between the original and final motor plan (Archambault et al., 2009, 2011), without any "refractory period" for aborting the previous plan before preparing a new one. Among the regions tested, the earliest changes in neural activity were found in PMd, in which 50% of cells reflected the new plan about 140 ms after a target jump, followed by M1 at 180 ms and dorsal area 5 at 200 ms (Archambault et al., 2011). This is comparable to the latency of responses to target jumps in earlier studies by Georgopoulos et al. (1983), who observed latencies of about 130–150 ms in the rostral part of M1.

Interestingly, the neural latencies to target jumps are comparable to the latencies of plan switches observed in PMd in our study—about 155 ms for both increases (SwitchOT2PT) and decreases of activity (SwitchPT2OT). They are also comparable to the latencies reported by Wise and Mauritz (1985) in a study in which the stimulus that instructed the plan switches was presented during the delay period, well before the GO signal. In that study, it was found that PMd cells reflected the switch with a median latency of 140–150 ms. In other words, the latency with which neural activity in PMd reflects a plan change is approximately 140–150 ms after the sensory stimulus which instructs that plan change. This holds true regardless of whether that stimulus is the change of a target from one location to another during the delay period (Wise and Mauritz, 1985), the displacement of a target during RT or movement (Georgopoulos et al., 1983; Archambault et al., 2009, 2011), or the offset of a PT that leaves only a less-desirable one available (present study). Furthermore, we found that the latency at which cells became suppressed when their PT disappeared (SwitchPT2OT) was not statistically different than the latency with which their discharge increased when their PT, which was initially less desirable, suddenly became the only remaining option (SwitchOT2PT). The similarity of these neural latencies across different experimental conditions demonstrates that in all cases, neural activity in PMd remains sensitive to new information pertinent to available actions and their values. This suggests a view whereby sensory information continuously flows into the motor system (Coles et al., 1985; Cisek, 2007), as opposed to a view of separate computational stages involved in canceling one motor program and computing a new one.

The neural processes of canceling a planned movement have been studied in the frontal eye fields (Hanes et al., 1998), superior colliculus (Pare and Hanes, 2003) and for arm-reaching studies in the supplementary motor area (SMA), pre-SMA (Scangos and Stuphorn, 2010) and PMd (Mirabella et al., 2011) using the countermanding task (Logan et al., 1984). In this task, subjects are asked to make a saccade or reach to a target, but to inhibit the movement if an infrequent STOP-signal is presented after a variable delay following the GO signal. As the delay increases, it becomes increasingly difficult to successfully inhibit the movement, making it possible to estimate a given subject's "stop-signal reaction time" (SSRT). Although many cortical areas such as motor cortex (M1) and supplemental cortical areas (pre-SMA and SMA) harbor neurons with DELAY activity related to movement planning (Okano and Tanji, 1987) it is unlikely that these areas are involved in processes causally related to movement cancellation because their responses to a stop signal take place *after* the SSRT (Scangos and Stuphorn, 2010). In contrast, Mirabella et al. (2011) found that during successful STOP trials, neurons in PMd show activity changes *prior* to the SSRT, making it possible that this region is involved in inhibiting the movement. This is consistent with the findings reported here that the suppression of PMd activity tuned to the target which vanished (SwitchPT2OT) occurs well before MO.

Our behavioral results are compatible with the proposal that at the end of the DELAY period, the movement to the higher-valued target is more strongly prepared than the movement to the lower-valued target. When the higher target disappears in a FORCED LOW trial, then one of two things can happen. If the RT is short, then the movement initiates toward the location of the unavailable target and the monkey must later turn around (curved trials, **Figure 2D** blue). If the RT is long, then the monkey completes his plan switch and initiates directly to the remaining target (direct trials, **Figure 2D** red). Nevertheless, what is surprising is that in both cases, neural activity in PMd already clearly reflects the change of plan more than 150 ms before the MO. This can be seen in **Figures 5A,B**. For example, the green traces illustrate trials in which the monkey initiated the movement toward the PT of recorded cells, which was the more valuable of the targets present during the DELAY. However, that target vanished

and so the monkey curved its movement trajectory and arrived at the remaining target. Although the neural activity becomes suppressed within 200 ms of the GO signal, reflecting the change of plan away from the PT, the initial movement some 100 ms later is still launched in the direction of the original plan. This happens most often during trials with short RTs (**Figures 2B,D**) suggesting that the motor system has a certain "inertia" that cannot be easily overcome. That is, movement initiation and muscle contraction could be starting to take place shortly after the GO signal despite the possibility that the more desirable choice will become unavailable. In this sense, the short-RT curved movements would be a natural consequence of the monkey's impulsivity and a strategy of reaching quickly and correcting the trajectory when necessary. In FORCED LOW trials, we found no significant difference in PMd activity between curved versus direct trials (**Figures 5A–C**), suggesting that other regions (presumably M1) may be more strongly responsible for determining whether the movement launches toward the initially selected or not. In FORCED EQUAL trials, we did observe differences in PMd activity when comparing curved versus direct movements (**Figures 5D–F**), but we believe this is simply due to selection bias: Curved movements (dark blue and green traces) are more likely to occur when the monkey happens to be strongly biased during DELAY toward the target that vanished, while direct movements could result equally from trials in which DELAY activity is biased to the PT, the OT, or neither, and the average DELAY activity of these three groups of trials will lie somewhere in the middle (red and cyan traces).

Cisek (2006) described a model of biased competition between action plans, which was originally designed to capture neural data on the simultaneous specification of multiple movements (Cisek and Kalaska, 2005) and behavioral data on the distributions of initial directions in short-RT pointing tasks (Favilla, 1997; Ghez et al., 1997). That same model, without any changes in parameters, was able to simulate more recent data on the modulation of PMd activity by relative subjective desirability (Pastor-Bernier and Cisek, 2011). In the model, potential actions are encoded as hills of activity in populations of directionally tuned neurons with short-range mutual excitation between similarly tuned cells and long-range lateral inhibition among cells with different tuning. The distance dependence of these lateral interactions is responsible for producing both the distance-dependent distributions of initial reach directions (Favilla, 1997; Ghez et al., 1997) and the distance-dependent influence of the value of one target on the PMd activity related to another (Pastor-Bernier and Cisek, 2011). That same model, only slightly modified with a gradual GO signal, is also able to reproduce our current results on plan switches (**Figure 6D**) and the distributions and timing of initial launching directions (**Figures 6B,C**). Note, however, that the model makes no attempt whatsoever to explain activity after MO—it includes no dynamics for producing or guiding movement, and its M1 activity should only be interpreted as capturing the initial pattern around the time of MO. Nevertheless, despite the absence of any movement production mechanisms in the present form of the model, it is consistent with models in which the movement trajectory is generated through continuous feedback via proprioceptive and visual signals (Bullock and Grossberg, 1988; Bullock et al., 1998; McIntyre and Bizzi, 1993; Burnod et al., 1999; Shadmehr and Wise, 2005) and through internal forward models (Bullock et al., 1993; Miall and Wolpert, 1996; Shadmehr et al., 2010). The model is compatible with general theories proposing that movements unfold as a dynamical system that is guided by the continuously updated pattern of activity within a distributed sensorimotor map. These patterns of activity can be shaped by a variety of processes, including attention (Tipper et al., 1998; Baldauf and Deubel, 2010), decision-variables (Cisek, 2007), and continuous spatial information from the dorsal visual stream (Goodale and Milner, 1992; Milner and Goodale, 1995; Desmurget et al., 1999; Day and Lyon, 2000).

That a relatively simple "biased competition" model can explain this fairly large set of data is particularly interesting given that the same mechanism is often used to explain the neural mechanisms of spatial attention (Desimone and Duncan, 1995; Boynton, 2005). This supports the conjecture (Allport, 1987; Rizzolatti et al., 1987; Neumann, 1990; Duncan, 2006; Cisek, 2007) that both attention and decision-making are related aspects of a general process of selection necessary to arbitrate between the many demands and opportunities for action that animals are continuously faced with in their natural environment. In this view, sensory information is continuously winnowed along the dorsal stream as it is converted into information specifying potential actions and ultimately guiding their execution. In all cases, this winnowing process involves a biased competition, but the specific dynamics of the process may be somewhat different in different brain regions.

For example, Louie et al. (2011) showed that activity in LIP was best described as

$$R = R_{\max}\frac{V_{\text{in}} + \beta}{\sigma + V_{\text{in}} + V_{\text{out}}}, \tag{2}$$

where R is the firing rate, $R_{\max}$ is the maximum firing rate, V_{in} is the value of targets in the receptive field, V_{out} is the total value of targets outside the receptive field, and β and σ are the baseline activity and semi-saturation terms, respectively, (see Reynolds and Heeger, 2009). Note that, as shown by Grossberg (1973), the normalization computation described by Equation (2) can be produced by the steady-state solution of Equation (1) if the excitation term E is equal to V_{in} and the inhibition term I is equal to V_{out} (see Cohen and Grossberg, 1983, for a proof of Lyapunov stability for a general class of such networks). In other words, divisive normalization may result from the competitive interactions within neural populations.

Louie et al. (2011) found that to explain their LIP data, the parameter σ had to be large, implying incomplete normalization such that LIP cells exhibited value-related modulation even with a single target. In contrast, our results suggest that PMd exhibits complete or nearly complete divisive normalization, because in the 1T task we found no value-related modulation whatsoever (Pastor-Bernier and Cisek, 2011), as if the σ parameter is zero. This raises the intriguing question of whether partial divisive normalization is the trend in parietal cortex, which is still far from overt execution, while activity is more fully normalized in regions closer to motor output, such as PMd. This would make good sense if PMd is most closely related to the process of final arbitration

between potential actions, but a deeper understanding of these differences between LIP and PMd requires further investigation.

To summarize, we found evidence that PMd neurons, which appear to be involved in the competition determining the initial selection of action, continue to take part in action selection after MO, reflecting a change of plan when a selected target becomes unavailable. This finding is compatible with previous studies of plan changes during the delay period (Wise and Mauritz, 1985) and during target jump paradigms (Georgopoulos et al., 1983; Archambault et al., 2009, 2011), as well as with the suggestion that PMd activity may be causally involved in the voluntary inhibition of movement (Mirabella et al., 2011). Taken together, these results provide support for the general hypothesis that the brain mechanisms for selecting between actions involve the same circuits that guide the execution of the actions during overt behavior.

ACKNOWLEDGMENTS

We thank Marie-Claude Labonté for technical support and Pascal Poisson-Fortier for valuable comments regarding the manuscript and analyses. This work was supported by research grants from the Canadian Institutes of Health Research and the EJLB Foundation, a GRSNC doctoral fellowship to Alexandre Pastor-Bernier, and an infrastructure grant from the Fonds de la recherche en Santé du Québec.

REFERENCES

Allport, D. A. (1987). "Selection for action: some behavioral and neurophysiological considerations of attention and action," in *Perspectives on Perception and Action*, eds H. Heuer and A. F. Sanders (Hillsdale, NJ: Lawrence Erlbaum Associates), 395–419.

Archambault, P. S., Caminiti, R., and Battaglia-Mayer, A. (2009). Cortical mechanisms for online control of hand movement trajectory: the role of the posterior parietal cortex. *Cereb. Cortex* 19, 2848–2864.

Archambault, P. S., Ferrari-Toniolo, S., and Battaglia-Mayer, A. (2011). Online control of hand trajectory and evolution of motor intention in the parietofrontal system. *J. Neurosci.* 31, 742–752.

Baldauf, D., and Deubel, H. (2010). Attentional landscapes in reaching and grasping. *Vision Res.* 50, 999–1013.

Basso, M. A., and Wurtz, R. H. (1998). Modulation of neuronal activity in superior colliculus by changes in target probability. *J. Neurosci.* 18, 7519–7534.

Boynton, G. M. (2005). Attention and visual perception. *Curr. Opin. Neurobiol.* 15, 465–469.

Bracewell, R. M., Mazzoni, P., Barash, S., and Andersen, R. A. (1996). Motor intention activity in the macaque's lateral intraparietal area. II. Changes of motor plan. *J. Neurophysiol.* 76, 1457–1464.

Bullock, D., Cisek, P., and Grossberg, S. (1998). Cortical networks for control of voluntary arm movements under variable force conditions. *Cereb. Cortex* 8, 48–62.

Bullock, D., and Grossberg, S. (1988). Neural dynamics of planned arm movements: emergent invariants and speed-accuracy properties during trajectory formation. *Psychol. Rev.* 95, 49–90.

Bullock, D., Grossberg, S., and Guenther, F. H. (1993). A self-organizing neural model of motor equivalent reaching and tool use by a multijoint arm. *J. Cogn. Neurosci.* 5, 408–435.

Burnod, Y., Baraduc, P., Battaglia-Mayer, A., Guigon, E., Koechlin, E., Ferraina, S., Lacquaniti, F., and Caminiti, R. (1999). Parieto-frontal coding of reaching: an integrated framework. *Exp. Brain Res.* 129, 325–346.

Carello, C. D., and Krauzlis, R. J. (2004). Manipulating intent: evidence for a causal role of the superior colliculus in target selection. *Neuron* 43, 575–583.

Cisek, P. (2006). Integrated neural processes for defining potential actions and deciding between them: a computational model. *J. Neurosci.* 26, 9761–9770.

Cisek, P. (2007). Cortical mechanisms of action selection: the affordance competition hypothesis. *Philos. Trans. R. Soc. Lond. B Biol. Sci.* 362, 1585–1599.

Cisek, P., Crammond, D. J., and Kalaska, J. F. (2003). Neural activity in primary motor and dorsal premotor cortex in reaching tasks with the contralateral versus ipsilateral arm. *J. Neurophysiol.* 89, 922–942.

Cisek, P., and Kalaska, J. F. (2002). Simultaneous encoding of multiple potential reach directions in dorsal premotor cortex. *J. Neurophysiol.* 87, 1149–1154.

Cisek, P., and Kalaska, J. F. (2005). Neural correlates of reaching decisions in dorsal premotor cortex: specification of multiple direction choices and final selection of action. *Neuron* 45, 801–814.

Cisek, P., and Kalaska, J. F. (2010). Neural mechanisms for interacting with a world full of action choices. *Annu. Rev. Neurosci.* 33, 269–298.

Cohen, M. A., and Grossberg, S. (1983). Absolute stability of global pattern formation and parallel memory storage by competitive neural networks. *IEEE Trans. Syst. Man Cybern.* SMC-13, 815–826.

Coles, M. G., Gratton, G., Bashore, T. R., Eriksen, C. W., and Donchin, E. (1985). A psychophysiological investigation of the continuous flow model of human information processing. *J. Exp. Psychol. Hum. Percept. Perform.* 11, 529–553.

Cos, I., Belanger, N., and Cisek, P. (2011). The influence of predicted arm biomechanics on decision making. *J. Neurophysiol.* 105, 3022–3033.

Dacorogna, M., Gençay, R., Müller, U., and Pictet, O. (2001). Effective return, risk aversion and drawdowns. *Physica A Stat. Mech. Appl.* 289, 229–248.

Day, B. L., and Lyon, I. N. (2000). Voluntary modification of automatic arm movements evoked by motion of a visual target. *Exp. Brain Res.* 130, 159–168.

Desimone, R., and Duncan, J. (1995). Neural mechanisms of selective visual attention. *Annu. Rev. Neurosci.* 18, 193–222.

Desmurget, M., Epstein, C. M., Turner, R. S., Prablanc, C., Alexander, G. E., and Grafton, S. T. (1999). Role of the posterior parietal cortex in updating reaching movements to a visual target. *Nat. Neurosci.* 2, 563–567.

Duncan, J. (2006). EPS mid-career award 2004: brain mechanisms of attention. *Q. J Exp. Psychol. (Colchester.)* 59, 2–27.

Erlhagen, W., and Schoner, G. (2002). Dynamic field theory of movement preparation. *Psychol. Rev.* 109, 545–572.

Fagg, A. H., and Arbib, M. A. (1998). Modeling parietal-premotor interactions in primate control of grasping. *Neural Netw.* 11, 1277–1303.

Favilla, M. (1997). Reaching movements: concurrency of continuous and discrete programming. *Neuroreport* 8, 3973–3977.

Georgopoulos, A. P., Kalaska, J. F., Caminiti, R., and Massey, J. T. (1983). Interruption of motor cortical discharge subserving aimed arm movements. *Exp. Brain Res.* 49, 327–340.

Georgopoulos, A. P., Kalaska, J. F., and Massey, J. T. (1981). Spatial trajectories and reaction times of aimed movements: effects of practice, uncertainty, and change in target location. *J. Neurophysiol.* 46, 725–743.

Ghez, C., Favilla, M., Ghilardi, M. F., Gordon, J., Bermejo, R., and Pullman, S. (1997). Discrete and continuous planning of hand movements and isometric force trajectories. *Exp. Brain Res.* 115, 217–233.

Glimcher, P. W. (2003). The neurobiology of visual-saccadic decision making. *Annu. Rev. Neurosci.* 26, 133–179.

Gold, J. I., and Shadlen, M. N. (2007). The neural basis of decision making. *Annu. Rev. Neurosci.* 30, 535–574.

Goodale, M. A., and Milner, A. D. (1992). Separate visual pathways for perception and action. *Trends Neurosci.* 15, 20–25.

Gritsenko, V., Kalaska, J. F., and Cisek, P. (2011). Descending corticospinal control of intersegmental dynamics. *J. Neurosci.* 31, 11968–11979.

Grossberg, S. (1973). Contour enhancement, short term memory, and constancies in reverberating neural networks. *Stud. Appl. Math.* 52, 213–257.

Hanes, D. P., Patterson, W. F. 2nd, and Schall, J. D. (1998). Role of frontal eye fields in countermanding saccades: visual, movement, and fixation activity. *J. Neurophysiol.* 79, 817–834.

Hansen, P. R., and Lunde, A. (2006). Realized variance and market microstructure noise. *J. Bus. Econ. Stat.* 24, 127–161.

Herrnstein, R. J. (1961). Relative and absolute strength of response as a function of frequency of reinforcement. *J. Exp. Anal. Behav.* 4, 267–272.

Horwitz, G. D., Batista, A. P., and Newsome, W. T. (2004). Representation of an abstract

perceptual decision in macaque superior colliculus. *J. Neurophysiol.* 91, 2281–2296.

Ignashchenkova, A., Dicke, P. W., Haarmeier, T., and Thier, P. (2004). Neuron-specific contribution of the superior colliculus to overt and covert shifts of attention. *Nat. Neurosci.* 7, 56–64.

Kim, J. N., and Shadlen, M. N. (1999). Neural correlates of a decision in the dorsolateral prefrontal cortex of the macaque. *Nat. Neurosci.* 2, 176–185.

Klaes, C., Westendorff, S., Chakrabarti, S., and Gail, A. (2011). Choosing goals, not rules: deciding among rule-based action plans. *Neuron* 70, 536–548.

Logan, G. D., Cowan, W. B., and Davis, K. A. (1984). On the ability to inhibit simple and choice reaction time responses: a model and a method. *J. Exp. Psychol. Hum. Percept. Perform.* 10, 276–291.

Louie, K., Grattan, L. E., and Glimcher, P. W. (2011). Reward value-based gain control: divisive normalization in parietal cortex. *J. Neurosci.* 31, 10627–10639.

McIntyre, J., and Bizzi, E. (1993). Servo hypotheses for the biological control of movement. *J. Mot. Behav.* 25, 193–202.

Miall, R. C., and Wolpert, D. M. (1996). Forward models for physiological motor control. *Neural Netw.* 9, 1265–1279.

Milner, A. D., and Goodale, M. A. (1995). *The Visual Brain in Action*. Oxford: Oxford University Press.

Mirabella, G., Pani, P., and Ferraina, S. (2011). Neural correlates of cognitive control of reaching movements in the dorsal premotor cortex of rhesus monkeys. *J. Neurophysiol.* 106, 1454–1466.

Müller, U. (1993). *Statistics of Variables Observed Over Overlapping Intervals Internal Document UAM*. 1993-06-18. Olsen and Associates. Available at http://citeseer.ist.psu.edu/muller93statistics.html

Neumann, O. (1990). "Visual attention and action," in *Relationships Between Perception and Action: Current Approaches*, eds O. Neumann and W. Prinz (Berlin: Springer-Verlag), 227–267.

Okano, K., and Tanji, J. (1987). Neuronal activities in the primate motor fields of the agranular frontal cortex preceding visually triggered and self-paced movement. *Exp. Brain Res.* 66, 155–166.

Pare, M., and Hanes, D. P. (2003). Controlled movement processing: superior colliculus activity associated with countermanded saccades. *J. Neurosci.* 23, 6480–6489.

Pastor-Bernier, A., and Cisek, P. (2011). Neural correlates of biased competition in premotor cortex. *J. Neurosci.* 31, 7083–7088.

Pastor-Bernier, A., Tremblay, E., and Cisek, P. (2011). "Dorsal premotor cortex is involved in switching motor plans," *Program No. 405.05. 2011, Neuroscience Meeting Planner.* (Washington, DC: Society for Neuroscience). [Online].

Pesaran, B., Nelson, M. J., and Andersen, R. A. (2008). Free choice activates a decision circuit between frontal and parietal cortex. *Nature* 453, 406–409.

Peng, X., Sereno, M. E., Silva, A. K., Lehky, S. R., and Sereno, A. B. (2008). Shape selectivity in primate frontal eye field. *J. Neurophysiol.* 100, 796–814.

Platt, M. L., and Glimcher, P. W. (1999). Neural correlates of decision variables in parietal cortex. *Nature* 400, 233–238.

Polya, G. (1920). Über den zentralen Grenzwertsatz der Wahrscheinlichkeitsrechnung und das Momentenproblem. *Math. Z.* 8, 171–181.

Prablanc, C., and Martin, O. (1992). Automatic control during hand reaching at undetected two-dimensional target displacements. *J. Neurophysiol.* 67, 455–469.

Reynolds, J. H., and Heeger, D. J. (2009). The normalization model of attention. *Neuron* 61, 168–185.

Rizzolatti, G., Riggio, L., Dascola, I., and Umilta, C. (1987). Reorienting attention across the horizontal and vertical meridians: evidence in favor of a premotor theory of attention. *Neuropsychologia* 25, 31–40.

Romo, R., Hernandez, A., and Zainos, A. (2004). Neuronal correlates of a perceptual decision in ventral premotor cortex. *Neuron* 41, 165–173.

Scangos, K. W., and Stuphorn, V. (2010). Medial frontal cortex motivates but does not control movement initiation in the countermanding task. *J. Neurosci.* 30, 1968–1982.

Shadmehr, R., Smith, M. A., and Krakauer, J. W. (2010). Error correction, sensory prediction, and adaptation in motor control. *Annu. Rev. Neurosci.* 33, 89–108.

Shadmehr, R., and Wise, S. P. (2005). *The Computational Neurobiology of Reaching and Pointing: A Foundation for Motor Learning*. Cambridge, MA: MIT Press.

Thevarajah, D., Mikulic, A., and Dorris, M. C. (2009). Role of the superior colliculus in choosing mixed-strategy saccades. *J. Neurosci.* 29, 1998–2008.

Tipper, S. P., Howard, L. A., and Houghton, G. (1998). Action-based mechanisms of attention. *Philos. Trans. R. Soc. Lond. B Biol. Sci.* 353, 1385–1393.

Wise, S. P., and Mauritz, K. H. (1985). Set-related neuronal activity in the premotor cortex of rhesus monkeys: effects of changes in motor set. *Proc. R. Soc. Lond. B Biol. Sci.* 223, 331–354.

Conflict of Interest Statement: The authors declare that the research was conducted in the absence of any commercial or financial relationships that could be construed as a potential conflict of interest.

Received: 24 January 2012; paper pending published: 23 February 2012; accepted: 11 March 2012; published online: 04 April 2012.

*Citation: Pastor-Bernier A, Tremblay E and Cisek P (2012) Dorsal premotor cortex is involved in switching motor plans. Front. Neuroeng. **5**:5. doi: 10.3389/fneng.2012.00005*

frontiers in
NEUROENGINEERING

ORIGINAL RESEARCH ARTICLE
published: 08 August 2012
doi: 10.3389/fneng.2012.00018

Transcranial magnetic stimulation and preparation of visually-guided reaching movements

Pierpaolo Busan[1]*, Marco Zanon[2], Federica Vinciati[1], Fabrizio Monti[3], Gilberto Pizzolato[3] and Piero P. Battaglini[1]

[1] *BRAIN, Center for Neuroscience, Department of Life Sciences, University of Trieste, Trieste, Italy*
[2] *Department of Medical and Biological Sciences, University of Udine, Udine, Italy*
[3] *Department of Medical, Surgical and Health Sciences, University of Trieste, Trieste, Italy*

Edited by:
Giovanni Mirabella, University of La Sapienza, Italy

Reviewed by:
Hun-Kuk Park, Kyung Hee University, South Korea
Patrizia Fattori, University of Bologna, Italy
Giovanni Mirabella, University of La Sapienza, Italy

****Correspondence:***
Pierpaolo Busan, BRAIN, Center for Neuroscience, Department of Life Sciences, University of Trieste, Via Fleming 22, Trieste 34127, Italy.
e-mail: pbusan@units.it

To better define the neural networks related to preparation of reaching, we applied transcranial magnetic stimulation (TMS) to the lateral parietal and frontal cortex. TMS did not evoke effects closely related to preparation of reaching, suggesting that neural networks already identified by our group are not larger than previously thought. We also replicated previous TMS/EEG data by applying TMS to the parietal cortex: new analyses were performed to better support reliability of already reported findings (Zanon et al., 2010; *Brain Topography* 22, 307–317). We showed the existence of neural circuits ranging from posterior to frontal regions of the brain after the stimulation of parietal cortex, supporting the idea of strong connections among these areas and suggesting their possible temporal dynamic. Connection with ventral stream was confirmed. The present work helps to define those areas which are involved in preparation of natural reaching in humans. They correspond to parieto-occipital, parietal and premotor medial regions of the left hemisphere, i.e., the contralateral one with respect to the moving hand, as suggested by previous studies. Behavioral data support the existence of a discrete stream involved in reaching. Besides the serial flow of activation from posterior to anterior direction, a parallel elaboration of information among parietal and premotor areas seems also to exist. Present cortico-cortical interactions (TMS/EEG experiment) show propagation of activity to frontal, temporal, parietal and more posterior regions, exhibiting distributed communication among various areas in the brain. The neural system highlighted by TMS/EEG experiments is wider with respect to the one disclosed by the TMS behavioral approach. Further studies are needed to unravel this paucity of overlap. Moreover, the understanding of these mechanisms is crucial for the comprehension of response inhibition and changes in prepared actions, which are common behaviors in everyday life.

Keywords: movement execution, parietal cortex, premotor cortex, reaching, transcranial magnetic stimulation, TMS/EEG co-registration

INTRODUCTION

Several works have tapped on neural underpinnings of reaching movement preparation, focusing on parieto-frontal circuits (e.g., Andersen and Buneo, 2002; Andersen and Cui, 2009; Cisek and Kalaska, 2010). In particular, reaching movements under visual guidance are prepared using different information which is elaborated in different frames of reference. These are, for example, eye-, limb-, body- or head-centered (Cohen and Andersen, 2002; Beurze et al., 2010) using visual as well as proprioceptive information (Buneo et al., 2002; Filimon et al., 2009; Jackson et al., 2009). Since preparation of reaching movements involves the activation of a fronto-parietal network (Tannè et al., 1995; Johnson et al., 1996; Galletti et al., 2001; Marconi et al., 2001; Gamberini et al., 2009; Bakola et al., 2010; Passarelli et al., 2011), it has been hypothesized that it integrates information about physical properties and location of a target into the motor plan of a reaching movement (Buneo et al., 2002; Cohen and Andersen, 2002). In fact, Milner and Goodale (2006) suggested the existence of a dorsal stream that mediates sensory-motor transformations for visually-guided movements overlapping with the above mentioned anatomic regions. They also suggested the existence of a ventral stream, which would be more involved in the elaboration of object's features primarily involving occipito-temporal regions.

An unsolved issue regarding implementation of reaching movements is related to the possible dominance of one hemisphere, preferably the left one (Goodale, 1988), usually viewed as the dominant hemisphere in right-handed people (e.g., Iacoboni, 2006; Vingerhoets et al., 2011). Thus, the left hemisphere likely plays a special role in organizing movements during visually-guided reaching (Goodale, 1988). The contralateral limb may be more represented during planning of reaching, activating a wide series of neural networks (e.g., Kertzman et al., 1997; Medendorp et al., 2003, 2005). The activation of both hemispheres in similar tasks (Calton et al., 2002; Connolly et al., 2003; Prado et al., 2005)

or of structures modulated by ipsilateral reaching has also been reported (Chang et al., 2008; Busan et al., 2009b). However, in our previous and present investigations, we mainly concentrated on the left hemisphere of subjects using their right hand, considering that this should allow to individuate the better representation of neural circuits for reaching (see above).

By stimulating medial parieto-occipital, parietal and premotor regions with TMS, we have previously identified a discrete network of regions that were involved in the preparation of reaching movements (Busan et al., 2009a,c). Specifically, at the start of preparation, we induced a facilitation in reaction time (RT) in a medial parieto-occipital region near the parieto-occipital sulcus, independently of the use of foveal or peripheral vision, and independently of the target position (however, strongest effects were observed for foveal vision and central reaching). Moreover, the stimulation of a region close to the posterior parietal cortex resulted in slower RT when TMS was delivered at about half of the preparatory process, affecting only central reaching. This same region was facilitated (showing faster reaction times) when stimulating at the start of reaching preparation. This was explained by the state-dependent theory of TMS (Silvanto and Muggleton, 2008): the TMS effect may strongly depend on the excitability of the stimulated region. Referring to our data, TMS could "pre-activate" cortical regions at the start of the preparatory process before their effective involvement in the stream, facilitating their intervention. In contrast, when cortical regions are already involved in the task, the adjunction of "neural noise" (Miniussi et al., 2010) may interfere with their correct functioning and, consequently, a slower elaboration of information may result.

When stimulating at about half of the mean RT in a more anterior left parietal region (around the intraparietal sulcus), we were able to induce an additional shortening of RT, facilitating the preparation of reaching (Busan et al., 2009a). Moreover, we were able to evoke a similar effect stimulating the left premotor dorsal cortex, in the same time window, suggesting a parallel processing of information in these cortical regions (Busan et al., 2009a).

We have now extended the mapping of cortical areas possibly involved in preparing visually-guided reaching movements. We tested whether the application of TMS to regions more laterally located in comparison to previous ones will affect the reaching movement preparation. Occipital, parietal and premotor cortices were stimulated. Negative results would have implied that the preparation of natural reaching is strictly related to structures in the superior parietal lobule (SPL). This should support the hypotheses of a "dorso-medial" stream that is preferentially involved in reaching movements, classically opposed to a "dorso-lateral" stream, possibly more devoted to grasping and/or reach-to-grasp movements (Jeannerod et al., 1995; Davare et al., 2006, 2010; Koch et al., 2010). On the contrary, if TMS would have elicited any effect, this would suggest a wider extent of the stream and a role for some of its more lateral regions in the preparation of reaching (Koch et al., 2008; Vesia et al., 2008, 2010; Reichenbach et al., 2011).

We also were interested in understanding the relations among cortical regions possibly involved in the preparation of reaching. Using a TMS/Electroencephalography (EEG) co-registration approach, we individuated an ensemble of areas recruited by stimulation of the left parietal cortex (putatively around the intraparietal sulcus) that comprises areas of the temporo-occipital regions (i.e., the ventral stream; Zanon et al., 2010). This confirms an interchange of information between dorsal and ventral streams, and that they are not segregated systems (e.g., Schenk and Milner, 2006; Borra et al., 2008), adding information about the temporal dynamics of this activity.

We also wished to further characterize the temporal dynamics of activation elicited by stimulation of the previously investigated region (Zanon et al., 2010), thus we used a TMS/EEG co-registration approach replicating that experiment, but adopting different analyses. Slightly different, but compatible findings were expected that would strengthen the previous conclusions.

A better understanding of the circuitry involved in the preparation of reaching is important for practical purposes such as, for example, the implementation of rehabilitative protocols or prosthetic devices. Moreover, the understanding of the organization and physiology of response inhibition could be helped by the knowledge of the physiology and organization of unrestrained reaching movements.

MATERIALS AND METHODS

BEHAVIORAL TMS STUDY

Subjects

A total of 58 healthy subjects underwent TMS over different cortical regions, as reported in **Table 1**. Subjects were right-handed (Edinburgh Inventory; Oldfield, 1971). Participants gave written informed consent after receiving information about TMS, in compliance with the Declaration of Helsinki and the Ethics Committee of the University of Trieste. Participants could leave the study at any time, although all completed the experiments. These statements apply also to TMS/EEG procedures.

Cortical stimulation

TMS was delivered over three brain regions of the left hemisphere: five scalp locations were in parietal cortex, four in premotor cortex, and one in parieto-occipital cortex. For each location, TMS was delivered at three different times during preparation of reaching: 25% of mean reaction time (m-RT), 50% of m-RT, and 75% of m-RT (**Table 1**).

TMS (Medtronic MagPro R30) was delivered through a figure-of-eight coil (diameter of each wing about 7 cm), oriented tangentially to the scalp (single pulse stimulation; biphasic waves; pulse duration: 280 μs). The coil was secured on the scalp by hand and position was checked and readjusted if necessary. The coil was maintained with a 45° orientation with respect to the inter-hemispheric fissure with the handle pointing downward and backward.

Subject's heads were not restrained, although participants were asked to maintain a stable position for the entire experiment. The stimulation coil was maintained in position even when no TMS was delivered.

Stimulated scalp positions, were determined according to an adapted EEG coordinate system (e.g., Herwig et al., 2003; Jurcak et al., 2007) and using a probabilistic method (Steinsträter et al., 2002; http://www.neuro03.uni-muenster.de/ger/t2tconv/). Points of stimulation were marked on a cap. Stimulated points with the

Table 1 | Stimulated areas and subjects recruited for the behavioral experiments.

Stimulated cortical region (left hemisphere)	Time of stimulation (% of m-RT)	Subjects			
		N	males/females	Age range	Mean age/standard deviation
Lateral parieto-occipital cortex	25	13	8/5	20–29	23.4/3.0
Lateral parieto-occipital cortex and lateral premotor cortex	50 and 75	10	6/4	20–27	24.8/3.1
Inferior parietal lobule	25	9	5/4	20–30	23.9/2.8
Inferior parietal lobule	50	10	3/7	22–31	25.5/3.1
Inferior parietal lobule	75	16	9/7	22–46	25.5/3.5
Lateral premotor cortex	25	10	6/4	20–27	24.8/3.1

The time of stimulation with respect to the onset of movements is also reported. The same 10 subjects participated in premotor cortex and parieto-occipital (with TMS at 50% and 75% of m-RT) experiments.

underlying main sulci are shown in **Figure 1**. In each experiment, scalp locations were randomly stimulated in blocks.

Pre-experimental procedures

Before each experiment, the best point activating the right hand first dorsal interosseous muscle (FDI) was determined and the resting motor threshold (RMT) was the stimulus intensity triggering at least a 50 μV response on electromyography (EMG; band pass filtering 20–2000 Hz) in half of stimulations. Surface Ag/AgCl electrodes were used (tendon-belly montage). Intensity of TMS was then set at 120% RMT. When stimulating premotor areas, the intensity of TMS was 110% RMT to limit current diffusion to primary motor cortex. Before the experiment, stimulation points in premotor cortex were evaluated for the possibility that stimulation led to muscular responses on hand/tongue muscles by EMG. When a muscular response was evident, the point of stimulation was slightly moved anteriorly until muscular response was no longer evident. Clearly, these procedures could make the individuation of premotor cortex uncertain, but we preferred to minimize contamination from neighboring neural structures, such as the motor cortex.

Experimental setting

During experiments, each subject was seated at a table. He/she was asked to place his/her right hand on a sensor light placed 5 cm away from his/her chest. The sensor light was connected to an impedance detector allowing measurements of the RT (the time elapsed from the go-signal to movement onset). A metallic grid was placed over the table, covering three light emitting diodes (LEDs) positioned at the center, right, and left at about 35 cm from subjects. LEDs were covered by a white sheet and were visible when illuminated only. LEDs to the right and left of subjects were positioned at 40° from the central one. LED lighting was the go-signal and the subject was asked to move the hand from the sensor, toward the grid to reach the LED. A cross drawn along the midline of the grid was used to maintain steady fixation during the experiment. Subject reached targets on the left and the right using peripheral vision, while the central target was reached using foveal vision. This requirement forced the inhibition of saccadic movements toward the target when it was lateral. However, this was necessary to investigate the effect of peripheral vision in the preparation of reaching. Arm and eye movements were recorded with a digital video camera (Sony DCR-SR30E) to discard incorrect trials. Timing of TMS delivery and all events were controlled by a PCMCIA acquisition board (NI-DAQ 6024E, National Instruments, Texas, USA) allowing RT recording. Before experiments, subjects performed about 20 reaching trials with targets distributed to the center, right, and left to measure their m-RT.

At the beginning of each trial, subjects focused their attention on the cross. They maintained their right hand on the light sensor before the LED was lit. This signaled the subject to move as soon as possible, maintaining steady central fixation. Subjects performed 42 randomized trials for each stimulated point: 21 trials with and 21 without TMS (TMS and NO-TMS conditions; 14 trials for every target location, 7 with and 7 without TMS) for each point and for each TMS condition (25%, 50%, 75% of m-RT). If, after the execution of a block, the m-RT was reduced more than 20% (due to implicit learning or familiarization with apparatus), a new m-RT was measured considering the last NO-TMS trials.

Data treatment and statistical analysis

TV recordings were analyzed off-line, excluding trials where eyes did not remain on the central cross for the entire trial duration. To avoid the influence of inadequate attention, trials with an RT longer than 700 msec or shorter than 100 msec were excluded. Trials were discarded when trajectory corrections were made. Data that were beyond two standard deviations with respect to the mean of the condition were discarded. Statistical analysis on RT was conducted with repeated measures ANOVA (see the "Results" section). A $p < 0.05$ was considered as the significant threshold. When interactions among main effects were significant, further analyses were conducted to explore these effects (see the "Results" section). The normality of data was also checked.

Control experiments

Past and present experiments detected different effects due to methodological issues, also in relation to the TMS state-dependent theory (Silvanto and Muggleton, 2008). Thus, we replicated part of previous experiments (see Busan et al., 2009c)

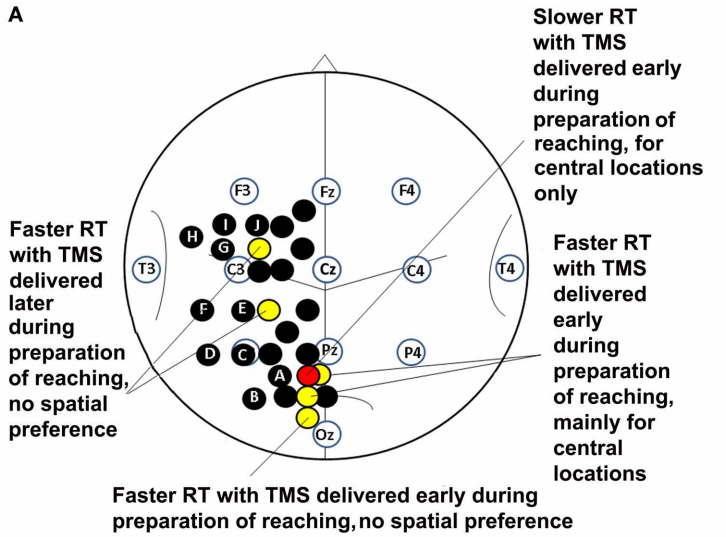

B

POINTS	LOCATIONS ON THE SCALP
A	8.75% of the nasion-inion distance below Pz and 13.75% of the bi-auricolar distance to the left from the midline
B	20% of the bi-auricolar distance to the left of POz
C	Corresponds to P3
D	Corresponds to P5
E	Corresponds to CP3
F	Corresponds to CP5
G	5% of the bi-auricolar distance to the left of C3 and 5% of the nasion-inion distance ahead of C3
H	10% of the bi-auricolar distance to the left of C3 and 7.5% of the nasion-inion distance ahead of C3
I	5% of the bi-auricolar distance to the left of FC3
J	5% of the bi-auricolar distance to the right of FC3

FIGURE 1 | Location of points of stimulation on the scalp and previous results. (A) Schematic drawing of the scalp showing points of stimulation in previous investigations (black, yellow and red circles; Busan et al., 2009a,c) and the present work (black circles with letters). Positions of selected scalp EEG electrodes are also reported together with an outline of main sulci. Point A corresponds to a parieto-occipital lateral position, points B-F are positioned over the putative inferior parietal lobule, while points G-J are positioned over the putative premotor cortex. (**B**) Table of stimulated points and related locations on the scalp.

in which a slightly different setting was used. In those experiments, subjects reached a solid target: the go-signal was given with eyes closed, so as not to see the positioning of the target itself. Thus, a "double" RT was registered, composed of the time needed to open the eyes and that required to start movements. The stimulation of a region over medial SPL (5% of the nasion-inion distance below Pz and 5% of the bi-auricular distance to the left) was effective in increasing RT at 75% of the (double) m-RT.

In eight right-handed, healthy subjects (three males, five females; age range 20–25, mean age 22.4, standard deviation – SD- 1.5), we performed the same experiment as the previous by applying TMS at 75% of m-RT of the (double) RT over medial SPL.

Results were compared to those collected in a second control experiment, where six right-handed, healthy subjects (two males, four females; age range 22–29; mean age 23.7, SD 2.7) performed the same task, but with open eyes and using LEDs instead of the solid target. TMS was applied at 50% of m-RT, a time considered as equivalent to the 75% of the (double) m-RT in previous experiments. Statistical comparisons were made using Student's *t*-test. The results obtained from these settings have been qualitatively compared to evaluate the possibility that different effects could be observed with respect to slightly different experimental requests, possibly sustaining the TMS state-dependent theory (Silvanto and Muggleton, 2008).

TMS/EEG study

A TMS/EEG experiment was carried out to confirm and extend previous findings (Zanon et al., 2010). Nine right-handed healthy subjects (five males and four females, age range 20–26 years, mean age 23.9 years, SD 2.1) participated in these experiments. Subjects were seated with closed eyes for the duration of blocks to reduce ocular artifacts.

TMS apparatus, coil orientation, protocols, instrumentations and data acquisition procedures were the same as those described in Zanon et al. (2010). Stimuli were delivered on the left parietal

cortex on the same scalp location stimulated previously (Zanon et al., 2010). It corresponded to a region putatively involved in reaching preparation (Busan et al., 2009a).

EEG and data analysis

EEG traces were recorded and treated as in Zanon et al. (2010). For data analysis, an average of 95.7 (SD 15.3) epochs was considered for real TMS and 89.7 (SD 15.3) for sham. Part of the TMS artifact as well as all the other remaining artifacts were eliminated as much as possible using EEGLAB (Delorme and Makeig, 2004). The first 20 msec prior to the delivery of stimulations and 35 msec after them were deleted. Independent component analysis (Jung et al., 2000) allowed for elimination of artifacts (e.g., those related to the slow decay/recovery after TMS).

Epochs were then averaged to obtain real and sham TMS evoked potentials (TEPs). Considering the remaining TMS artifact that could influence the analyses, a "linear detrend" function was applied when needed, generally in a time between 35 and 300 msec after the delivery of stimuli. Finally, averaged real and sham TEPs were re-referenced (average reference).

sLORETA (standardized low resolution brain electromagnetic tomography; Pascual-Marqui, 2002) was used to compute the cortical three-dimensional distribution of neuronal activity comparing real and sham TEPs. sLORETA is a standardized discrete, three-dimensional distributed, linear, minimum norm inverse solution (Pascual-Marqui, 2002). Computations were made in a realistic head model (Fuchs et al., 2002) using the MNI152 template (Mazziotta et al., 2001), with three-dimensional space solution restricted to cortical gray matter, as determined by the probabilistic Talairach atlas (Lancaster et al., 2000), and with electrode positions superimposed on the MNI152 scalp (Oostenveld and Praamstra, 2001; Jurcak et al., 2007). The intracerebral volume is partitioned in 6239 voxels at 5 mm spatial resolution. Anatomical labels such as Brodmann areas are also reported using MNI space, with corrections to Talairach space (Brett et al., 2002).

In the present work, sLORETA was used to perform a voxel-by-voxel within-subjects comparison of real vs. sham TMS induced current density distribution in the brain. Significant differences in EEG source maps were assessed with non-parametric statistical analysis (Statistical non-Parametric Mapping: SnPM; Nichols and Holmes, 2002), as previously described (Zanon et al., 2010).

We reduced the localization error by applying regularization in the source reconstruction. We considered the mean signal-to-noise ratio of averaged ERPs, for each subject in every condition, from 35 to 300 msec after delivery of the stimulus with respect to baseline.

After reconstructing the EEG cortical sources distribution for both real and sham TMS conditions, analyses were conducted considering single time frames in a time ranging from 35 to 300 msec after stimulation. Statistics were implemented also considering the mean neural activity in time windows individuated by visual inspection of TEPs. The following comparisons were implemented: from 35 to 60 msec, from 60 to 130 msec, from 130 to 245 msec, and from 245 to 300 msec. Significance was set at $p < 0.05$, correcting for multiple comparisons. SnPM in sLORETA allowed for correction of multiple comparisons even with respect to all voxels and all time samples.

RESULTS

BEHAVIORAL TMS STUDY

We considered the main effects and interactions among TMS (yes/no), location of stimulation on the scalp (one, four, or five positions), target position in space (central, left, and right) with repeated measures ANOVA. We conducted analyses for each timing of TMS delivery. Student's *t*-test (Bonferroni corrected) was used to characterize significant findings. When a three-way interaction was significant, the statistical model was investigated by two-way interactions and then with a Student's t-test (Bonferroni corrected). Results obtained for all conditions (**Figure 1**) are summarized in **Table 2**. We observed that an effect related to target position was always evident (parieto-occipital cortex: 25% m-RT: $p = 0.043$; 50% m-RT: $p = 0.012$; 75% m-RT: $p = 0.013$; parietal cortex: always $p < 0.009$; premotor cortex: always $p < 0.009$), mainly indicating that subjects had longer RTs for movements toward the left targets. Moreover, TMS always resulted in faster RT when stimulating at 25% of m-RT (TMS main factor, independently of target position, always $p < 0.009$).

When considering the premotor cortex, we observed an interaction of TMS vs. location of stimulation at 25% of m-RT ($p = 0.004$). However, subsequent analyses showed the presence of significant effects on all stimulated points (point G: $p < 0.009$; point H: $p < 0.009$; point I: $p < 0.009$; point J: $p < 0.009$ in **Figure 1**). Due to the wide distribution of effective points of stimulation, we considered these results as unspecific effects, likely confirming that the facilitating effect caused by TMS when stimulating at 25% of m-RT was not related to a genuine effect (e.g., Sawaki et al., 1999). All remaining comparisons never reached significance.

CONTROL EXPERIMENTS

Two control experiments were performed. In the first, we replicated the original result of slowed RT (TMS mean reaction time: 690.25, SD 101.5; no-TMS mean reaction time: 652.8, SD 109.2; $p = 0.04$) when stimulating medial left posterior parietal cortex using the original experimental setting (Busan et al., 2009c), reaching toward the center. We performed a second experiment where subjects were required to keep their eyes open. In this instance we did not replicate findings of the previous experiment, and no significant differences were evident between TMS and no-TMS when reaching toward the center with foveal observation (TMS mean reaction time: 309.0, SD 33.8; no-TMS mean reaction time: 312.1, SD 30.0; $p = 0.60$).

TMS/EEG STUDY

ERP description and sLORETA

Real and sham TEPs showed positive and negative deflections (see, for example, Paus et al., 2001; Bonato et al., 2006). Specifically, when Cz electrode was considered, we observed four peaks (**Figure 2**) during real TMS: (i) a negative component (N45; mean amplitude −4.2 microvolts, SD 3.0; mean latency 44.8 msec, SD 2.4), (ii) a positive one (P65; mean amplitude 1.7 microvolts, SD 1.5; mean latency 63.2 msec, SD 5.2), followed by (iii) a negative one (N95; mean amplitude −6.6 microvolts, SD 2.1; mean latency 95.5 msec, SD 11.7), and, finally, (iv) a positive one (P165; mean amplitude 7.2 microvolts, SD 2.3; mean

Table 2 | Reaction times observed in behavioral experiments.

Points	Target location	25% of m-RT		50% of m-RT		75% of m-RT	
		TMS	NO-TMS	TMS	NO-TMS	TMS	NO-TMS
A	Central	287.6 (39.6)	301.1 (39.6)	286.6 (24.9)	293.2 (25.9)	296.0 (32.6)	290.3 (29.3)
	Left	292.9 (47.9)	318.6 (43.0)	298.8 (25.0)	305.2 (30.3)	303.1 (22.2)	309.5 (27.6)
	Right	284.5 (34.1)	301.7 (39.8)	288.1 (31.5)	287.2 (30.4)	292.2 (23.8)	290.7 (22.8)
B	Central	290.2 (39.5)	304.3 (40.7)	348.4 (64.3)	345.0 (79.8)	309.6 (35.9)	310.8 (34.9)
	Left	327.0 (56.6)	341.4 (59.1)	382.2 (69.7)	391.1 (68.3)	333.5 (51.4)	336.6 (49.4)
	Right	284.8 (38.7)	296.4 (41.3)	328.9 (58.2)	339.2 (67.9)	299.9 (39.4)	302.9 (38.9)
C	Central	298.2 (46.4)	309.2 (49.2)	338.1 (54.1)	342.4 (58.4)	308.9 (40.6)	308.0 (39.6)
	Left	314.4 (62.2)	346.6 (66.1)	380.7 (61.7)	374.1 (63.3)	338.1 (60.6)	334.4 (60.4)
	Right	279.8 (36.5)	294.7 (42.1)	323.9 (40.4)	330.1 (49.5)	306.4 (40.9)	302.7 (43.5)
D	Central	290.9 (42.0)	308.7 (43.5)	349.0 (56.6)	351.4 (52.6)	314.7 (45.2)	311.7 (46.7)
	Left	308.5 (66.6)	333.5 (68.9)	389.0 (71.6)	387.7 (65.2)	340.4 (58.5)	343.7 (62.3)
	Right	287.9 (44.5)	299.5 (37.3)	329.4 (53.5)	339.3 (52.7)	311.2 (44.5)	312.9 (40.3)
E	Central	292.4 (42.3)	305.5 (43.7)	348.2 (49.9)	342.2 (57.0)	316.5 (45.9)	324.7 (52.4)
	Left	323.4 (72.7)	346.5 (63.8)	389.2 (61.1)	383.6 (64.0)	344.4 (62.9)	350.3 (62.6)
	Right	277.0 (38.2)	298.2 (40.3)	327.5 (44.7)	329.9 (49.3)	308.4 (43.5)	307.7 (41.3)
F	Central	292.3 (46.9)	305.8 (42.6)	359.9 (61.7)	369.1 (58.8)	312.2 (44.2)	313.0 (40.7)
	Left	321.3 (62.7)	338.8 (65.2)	395.6 (72.2)	400.2 (81.6)	347.3 (59.6)	341.7 (62.0)
	Right	287.3 (39.8)	294.7 (38.4)	340.7 (56.9)	352.2 (59.3)	300.1 (36.8)	305.7 (37.5)
G	Central	267.3 (22.4)	293.8 (21.7)	289.3 (22.6)	291.5 (23.0)	292.5 (27.7)	291.6 (35.6)
	Left	273.7 (12.4)	305.6 (26.2)	305.2 (21.1)	307.4 (28.9)	310.0 (25.6)	303.4 (34.4)
	Right	267.8 (21.9)	297.4 (20.1)	282.5 (20.2)	292.3 (29.9)	292.7 (22.1)	287.9 (29.7)
H	Central	270.8 (21.1)	285.7 (24.5)	296.7 (17.4)	289.6 (21.1)	283.4 (21.2)	286.8 (31.1)
	Left	288.7 (27.1)	303.1 (27.8)	301.9 (15.8)	313.8 (27.8)	297.9 (22.7)	300.6 (26.1)
	Right	275.8 (25.5)	286.0 (27.2)	278.7 (23.6)	286.2 (23.5)	283.8 (20.4)	285.9 (24.7)
I	Central	278.9 (16.7)	297.1 (18.2)	292.2 (27.4)	293.7 (25.9)	290.8 (20.2)	288.5 (26.4)
	Left	287.1 (22.1)	304.3 (25.9)	296.4 (29.8)	306.8 (32.7)	300.3 (30.5)	303.7 (26.7)
	Right	278.9 (25.8)	299.5 (26.5)	289.6 (27.8)	287.1 (25.2)	290.9 (22.4)	290.5 (29.1)
J	Central	272.2 (22.3)	294.5 (21.3)	288.7 (18.7)	292.1 (21.4)	288.3 (25.7)	286.3 (33.0)
	Left	285.7 (30.6)	313.6 (25.7)	309.8 (30.1)	312.8 (23.0)	309.0 (28.4)	301.1 (27.0)
	Right	267.9 (21.4)	293.1 (30.4)	287.3 (27.0)	293.4 (26.8)	292.9 (26.4)	284.2 (24.6)

Mean of reaction times (SD in brackets) obtained for parieto-occipital (point A), parietal (points B–F), and premotor (points G–J) cortices.

latency 161.9 msec, SD 15.3). Sham TEPs showed similar deflections with reduced amplitudes compared to real TMS (**Figure 2**). The acoustic contamination was evident (Nikouline et al., 1999) in both conditions.

Time frame by time frame comparison of the entire time window showed a significant ($p < 0.05$) difference between the real and sham TMS in the time ranges between 116–126 msec, 134–146 msec, and at about 190 msec after the delivery of stimuli.

In the first time range (116–126 msec), we observed significant voxels in the left postcentral gyrus, left inferior parietal lobule (IPL), and right motor regions. In the same interval, but with a slight delay, further significant voxels were also evident in the right cuneus, right middle occipital gyrus, right lingual gyrus, right precuneus, right SPL, right IPL, as well as in the right angular gyrus. The cingulate gyrus and the posterior cingulate also showed significant voxels in this time window.

In the second time range (134–146 msec) we observed significant voxels in the right SPL, right IPL, right supramarginal gyrus, right postcentral gyrus, precuneus and sub-gyral. Finally, at 190 msec after TMS we observed significant voxels in the left superior temporal gyrus and supramarginal gyrus.

Maximal peaks of activation and number of voxels activated for each significant time frame are reported in **Table 3**. The main patterns of activations are shown in **Figure 3**.

We also took into consideration the mean activation across the overall four time-windows of interest (**Figure 4**). In this case, significance was $p < 0.0125$. The first time window (from 35 to 60 msec) did not reach the threshold for significance, while it was reached in the second time window (60–130 msec): we observed significant voxels in the contralateral posterior regions (mainly in the cuneus and precuneus –bilaterally-, IPL and SPL, the middle occipital gyrus, the lingual gyrus –bilaterally-, the cingulate gyrus, and posterior cingulate –bilaterally). Significant voxels were also evident in the right inferior, middle, and superior temporal gyrus. Finally, we observed significant voxels in the left and right superior, middle and medial frontal gyrus, right inferior frontal gyrus, left and right precentral gyrus, right postcentral gyrus, and left sub-gyral.

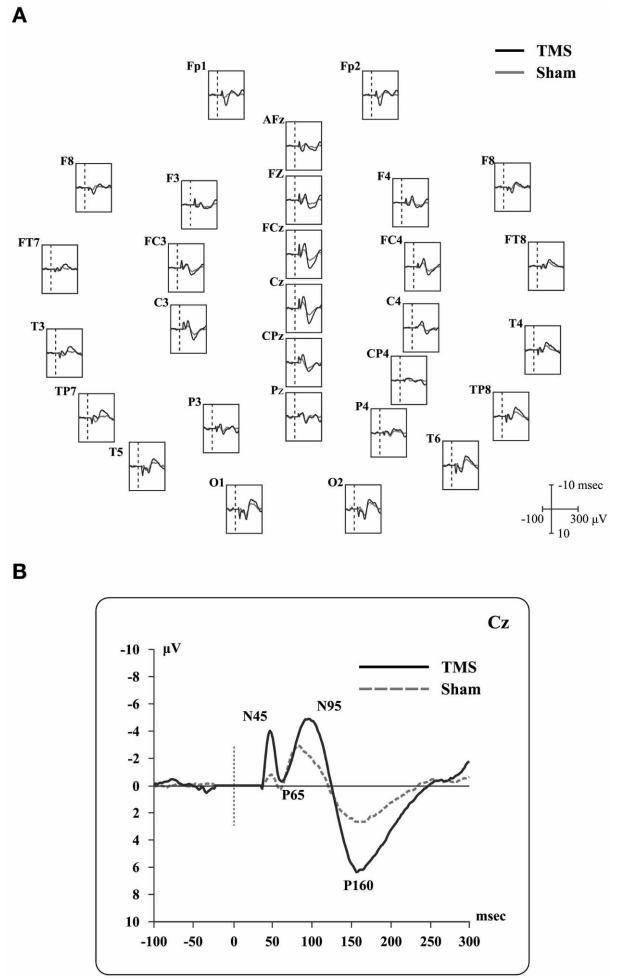

FIGURE 2 | Real TMS and sham TMS evoked potentials in 9 healthy subjects. (**A**) Grand-average of real TMS evoked potentials ranging from 100 msec before to 300 msec after the stimulation, showing all recorded electrodes. Real TMS evoked potentials are superimposed on sham-evoked potentials. Site of stimulation over the parietal cortex is also shown. (**B**) Grand-average of evoked potentials recorded at the Cz electrode, showing the main deflections described in the text.

The third time window (130–245 msec) showed a pattern of significant voxels that comprised the right precentral and postcentral gyrus, right inferior frontal gyrus, and the left medial frontal gyrus. Posteriorly, we observed significant voxels in the right and left fusiform gyrus, left uncus, left and right parahippocampal gyrus, right cuneus and precuneus, right posterior cingulate, right lingual gyrus and right IPL. Finally, significant propagation was seen also in the left and right inferior temporal gyrus and the right insula.

The last window, ranging from 245 to 300 msec, showed activations in the right postcentral gyrus and left superior temporal gyrus. Results are summarized in **Table 4** and **Figure 4**.

DISCUSSION

In the present investigation, we report findings obtained by stimulating cortical areas along a "dorso-lateral" stream in the left hemisphere in healthy right-handed people during the preparation of visually-guided reaching movements performed with the dominant hand. Lateral parietal and premotor regions resulted not to be strictly involved in the preparation of visually-guided reaching as measured by the present protocol. This confirms that the neural network for preparation of reaching is quite localized, as already suggested by our previous works (Busan et al., 2009a,c).

The following discussion will focus on the parietal cortex, considering that our previous results on dorsal premotor cortex (Busan et al., 2009a) could be related to non-specific effects, even if we are well aware that the premotor cortex plays a role in the preparation of motor responses and in reaching (e.g., Prado et al., 2005; Pesaran et al., 2006; Batista et al., 2007; Hoshi and Tanji, 2007; Beurze et al., 2010).

SEGREGATED SYSTEMS FOR THE PREPARATION OF REACHING MOVEMENTS?

The present findings suggest that the neural network herein stimulated is not strongly involved in visually-guided reaching movements. Our previous studies (Busan et al., 2009a,c) showed the presence of a discrete dorsal neural circuit starting from the medial parieto-occipital cortex, involving the SPL near the intraparietal sulcus and the dorsal premotor cortex. However it should be kept in mind that the effect of TMS could be due to the modulation of regions simply linked to the stimulated area.

The left hemisphere was chosen for its dominance for praxis (e.g., Goodale, 1988; Haaland and Harrington, 1989), and the left parietal cortex involvement in arm movement planning (Rushworth et al., 2003; Wheaton et al., 2009). SPL lesions in the left hemisphere can result in misreaching throughout the workspace (Perenin and Vighetto, 1988), while a right hemisphere lesion may be more related with lateralized visual field effects (Perenin and Vighetto, 1988; Battaglia-Mayer et al., 2006). However, left parietal lesions may have effects only in the contralateral visual field (Riddoch, 1935). Thus, the posterior parietal cortex plays a pivotal role in the preparation of actions (Goodale and Milner, 1992; Jeannerod et al., 1995; Andersen et al., 1997) with a contralateral limb bias in more anterior parietal regions and less evident in the parieto-occipital cortex (Busan et al., 2009b; Vesia et al., 2010).

Our previous and present results are in agreement with literature (e.g., Kastner et al., 1998; Fattori et al., 2001, 2005; Andersen and Buneo, 2002; Calton et al., 2002; Snyder et al., 2006; Trillenberg et al., 2007; Ciavarro and Ambrosini, 2011; Striemer et al., 2011) supporting a role for SPL in preparation of reaching (Goodale and Milner, 2004; Buneo and Andersen, 2006). In particular, Beurze et al. (2010) found parieto-occipital activations related with foveal vision comparable with our results.

Striemer et al. (2011) suggested that SPL is preferentially related to programming of actions and on-line control, while IPL should not. The latter should be more related with selecting the goal and/or target of the action. They found an effect on endpoint accuracy when using a triple pulse TMS over SPL during the preparation of movement, while this was not observed when stimulating IPL. They also observed a significant reduction in RT, which might be related to unspecific effects but it might also be a genuine result. In fact, this finding is congruent with

Table 3 | Results from time frame by time frame sLORETA analysis.

Time of activation (msec)	Maximal peak of activation			Other significant voxels (BA)	Number of activated voxels
	x, y, z (MNI coordinates)	BA	Anatomical landmark		
116	−50, −30, 55	2	Left postcentral gyrus	40 L, 1 L, 4 R	15
118	−45, 25, 50	2	Left postcentral gyrus	1 L, 3 L, 19 R	10
120	40, −75, 40	19	Right Precuneus	2 L, 3 L, 7 R, 18 R, 30 R, 31 R, 39 R, 40 L/R	57
122	40, −75, 45	7	Right superior parietal lobule	18 R, 19 R, 23 L/R, 31 R, 39 R	45
124	−5, −15, 30	23	Left cingulate gyrus	17 R, 18 R, 19 R, 23 R, 24 L, 29 R, 30 R, 31 L/R	111
126	10, −75, 15	18	Right cuneus	7 R, 17 R, 23 R, 30 R, 31 R	109
134	20, −60, 55	7	Right precuneus	/	11
136	25, −60, 60	7	Right superior parietal lobule	5 R	42
138	30, −60, 60	7	Right superior parietal lobule	5 R, 40 R	27
140	30, −55, 60	7	Right superior parietal lobule	2 R, 5 R, 40 R	44
142	30, −60, 60	7	Right superior parietal lobule	2 R, 5 R, 40 R	66
144	35, −60, 55	7	Right superior parietal lobule	5 R, 40 R	52
146	50, −45, 45	40	Right inferior parietal lobule	/	23
190	−60, −60, 20	22	Left superior temporal gyrus	40 L	2

Time of activation and location of maximal peaks which were significant with analysis made on the entire window of interest (35–300 msec). The remaining significant voxels are also reported. BA: Brodmann Areas; L = left; R = right.

our previous results (Busan et al., 2009a,c). Striemer et al. (2011) suggested that those results might be correlated to attentional or intentional processes rather than to motor planning. Along these lines, we already controlled the possibility that unspecific attention processes biased our results (Busan et al., 2009a,c), but the possibility that they were also related to attention processes specifically related to reaching movements cannot be ruled out. However, these processes should be more likely related with IPL than with SPL involvement (Rushworth et al., 2001; Desmurget and Sirigu, 2009). Striemer et al. (2011) also suggested that an influence of TMS on motor programming should have an impact on motor performance in terms of movement accuracy, while an influence on motor attention or intention (Desmurget and Sirigu, 2009) should affect RT (Striemer et al., 2009). However, Snyder et al. (2006) demonstrated in nonhuman primates that RT could be affected when interfering with SPL. Other studies suggested that IPL may also have a role in programming goal directed reaching, whereas the SPL and intraparietal sulcus may be more related to on-line control of movement (Glover, 2004; Pisella et al., 2006).

Thus, our present and previous data (Busan et al., 2009a,c) support the existence of different and partially segregated neural circuits for the implementation of different motor tasks (Jeannerod et al., 1995). They are consistent with the suggestion of a "dorso-medial" stream preferentially involved in reaching movements, classically opposed to a "dorso-lateral" stream that preferably manages reach-to-grasp and/or grasping movements (e.g., Jeannerod et al., 1995; Burnod et al., 1999; Randerath et al., 2010). This suggestion is supported by results obtained with different paradigms and settings (Desmurget et al., 2005; Prado et al., 2005; Fernandez-Ruiz et al., 2007; Filimon et al., 2009; for a review see Vesia et al., 2010).

However, evidence against this possibility has also been advanced (Desmurget et al., 1996; Smeets and Brenner, 1999; Mon-Williams and McIntosh, 2000), showing that the implementation of reaching is not so much segregated, and that wider circuits can participate. In fact, circuits for preparation of reaching may overlap with the neural requests needed for grasping or reach-to-grasp implementation, with still more integrated mechanisms needed for prehension (Binkofski et al., 1998; Smeets and Brenner, 1999; Ulloa and Bullock, 2003; Tunik et al., 2005; Rice et al., 2006). Moreover, it should be noted that regions of the IPL, as for example the angular or the supramarginal gyrus, have been associated with preparation and/or on-line control of visually guided reaching (Koch et al., 2008; Vesia et al., 2008, 2010; Reichenbach et al., 2011).

In the brain, information can be processed serially as well as along parallel pathways (e.g., Burnod et al., 1999; Naranjo et al., 2007; Buneo et al., 2008). Serial organization fits well with the concept that information travels from peripheral to complex "association" areas and then to output channels for action. Similarly, parallel organization of cognitive processes (Cisek and Kalaska, 2010) is supported by a series of studies suggesting that tasks such as visuo-motor integration rely on a network that provides concomitant activation of different cortical regions (Battaglia-Mayer et al., 2006; Naranjo et al., 2007). Our previous data (Busan et al., 2009a,c) support the vision of a mainly serial elaboration of information in this type of task, but also offer a suggestion toward the concept of a parallel elaboration.

TMS/EEG results are in relation with state-dependent activity of the brain, since they were obtained in a resting condition and closed eyes. Brain dynamics were evaluated in a basic condition, usually defined as a "default mode brain state" (Raichle et al., 2001; Raichle and Snyder, 2007; Greicius et al., 2009) where the brain is however active. This reduced the possibility of EEG contamination by movements or other processes.

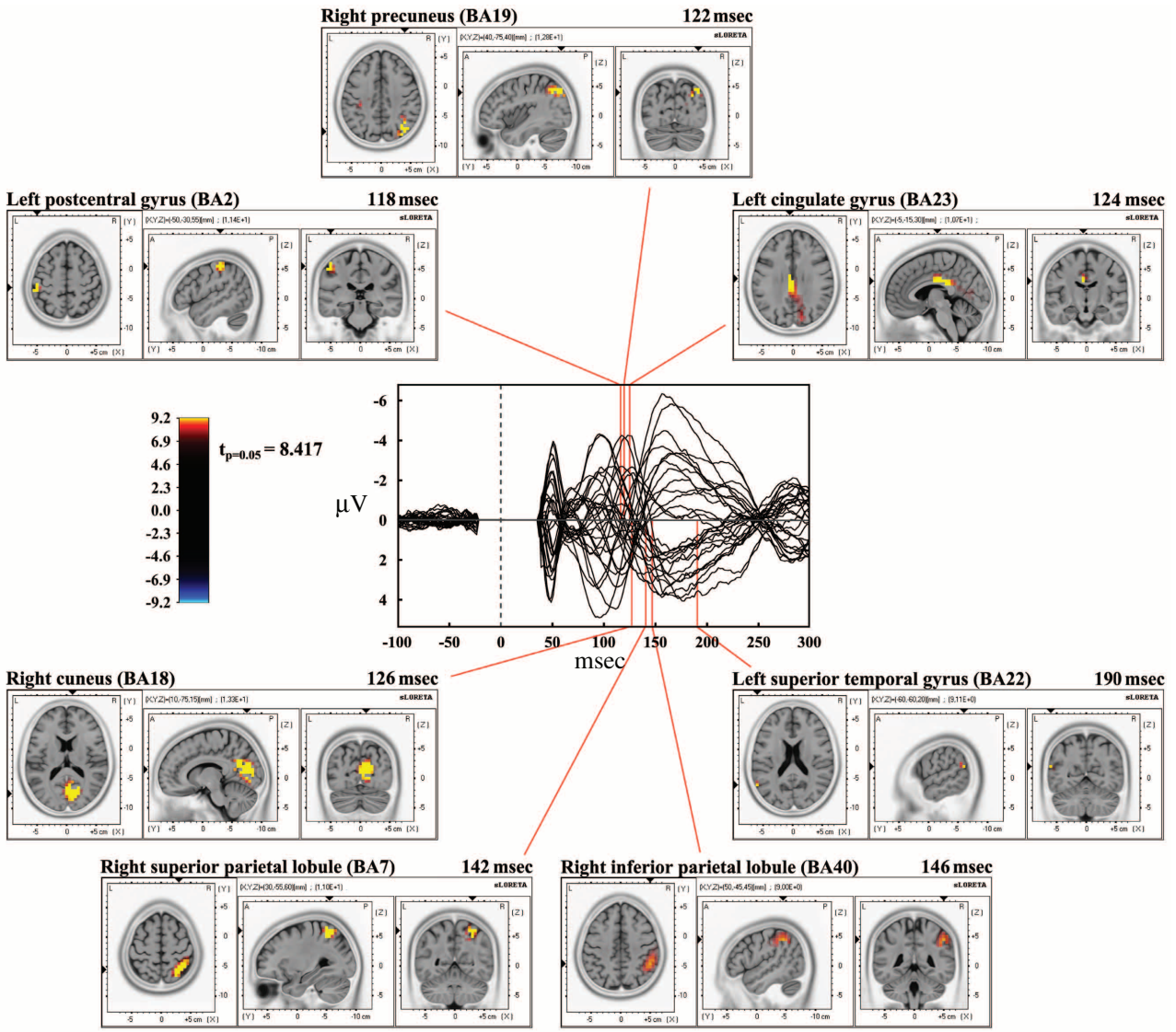

FIGURE 3 | Results from time frame by time frame sLORETA analysis. Representation of the main patterns of activation obtained in time frame by time frame analysis compared to a butterfly plot showing the grand-averaged (for all subjects) evoked potentials (real TMS) for each electrode.

Concurrent TMS/EEG offers insights into how brain areas interact during information processing (Ilmoniemi and Kicić, 2010). The present work shows propagation of activity ranged mainly from the left somatosensory and parietal structures to right parietal, somatosensory, motor, and more posterior activations. Deep regions of the brain, such as cingulate regions, had significant voxels in late and discrete time windows. Finally, activity in the left temporal and parietal cortices was evident around 190 msec from the delivery of TMS. Instead, when considering the mean neural activity in discrete time of interest, interactions were found among the parietal cortex and, mainly, the posterior regions of the brain. Moreover, significant propagations were found in the left and right frontal regions and in post-central areas, as well as in occipito-temporal regions, and in the right insula.

Our previous studies (Zanon et al., 2010) suggested the presence of an interchange of information between parietal cortex and occipito-temporal cortex at about 170 msec after TMS. An interaction between dorsal and ventral streams has already been proposed (e.g., Himmelbach and Karnath, 2005; Borra et al., 2008; Makuuchi et al., 2012). Valyear and Culham (2010) showed that tool-selective activity was related with parietal and ventral stream activations.

Interestingly, in the present findings, we observed the activation of a neural source around 190 msec from TMS (stimulating the left parietal cortex) in a ventral region in left temporo-parietal cortex. This gives further support to previous results regarding the possibility of an interchange of information between the dorsal and ventral streams: this region has been reported to have a supportive role in the elaboration, for

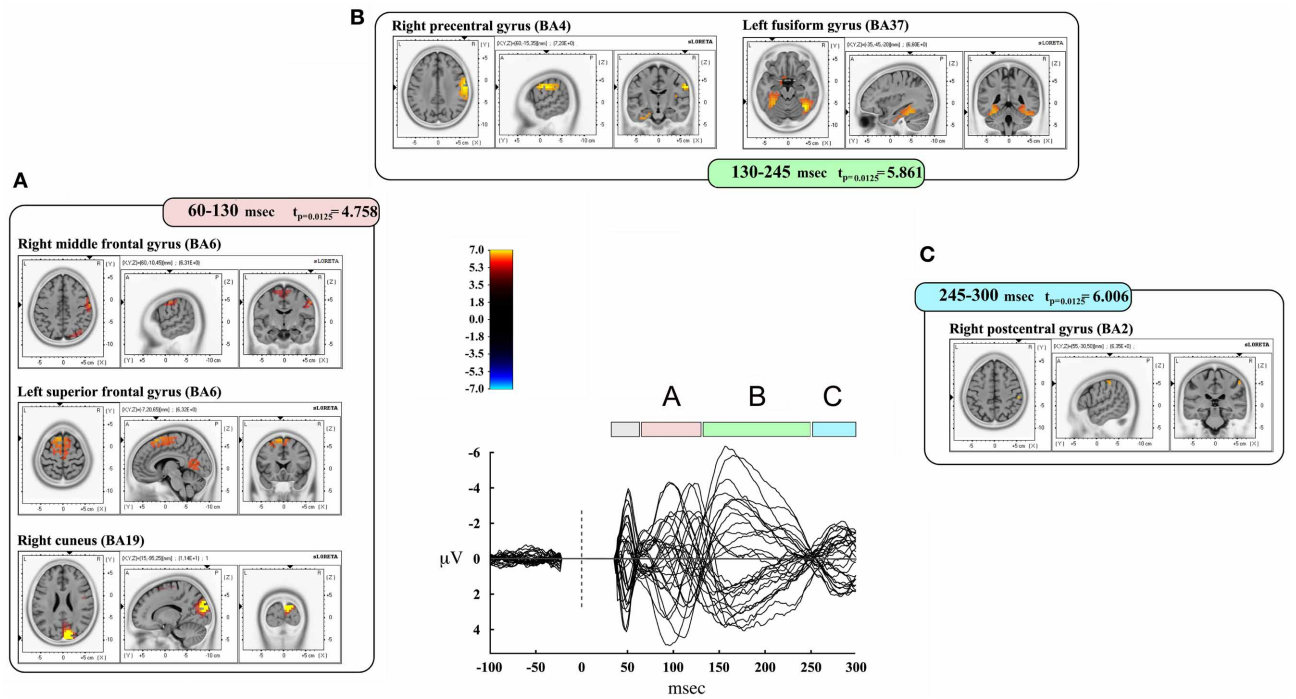

FIGURE 4 | Results from discrete time window sLORETA analysis. Representation of some of the main results obtained when considering the mean neural activity in discrete time windows. Results are plotted compared to the different time ranges considered, as evident from the butterfly plot showing the grand-averaged (for all subjects) evoked potentials (real TMS) for each electrode. Colors and letters are plotted in correspondence to the different time windows of interest. **(A)** Time window from 60 to 130 msec. **(B)** Time window from 130 to 245 msec. **(C)** Time window from 245 to 300 msec.

Table 4 | Results from discrete time windows sLORETA analysis.

Window of activation (msec)	Maximal peak of activation			Other significant voxels (BA)	Number of voxels activated
	x, y, z (MNI coordinates)	BA	Anatomical landmark		
35–60	N.S.	N.S	N.S.	N.S.	N.S.
60–130	15, −95, 25	19	Right cuneus	1 R, 2 R, 3 R, 4 R, 6 L/R, 7 R, 8 L/R, 9 R, 17 R, 18 L/R, 20 R, 21 R, 23 L/R, 29 L/R, 30 L/R, 31 L/R, 32 L, 38 R, 39 R, 40 R	513
130–245	60, −15, 35	4	Right precentral gyrus	1 R, 2 R, 3 R, 6 R, 9 R, 13 R, 17 R, 18 R, 19 L/R, 20 L/R, 23 R, 25 L, 28 L, 30 R, 31 R, 34 L, 35 L, 36 L/R, 37 L/R, 40 R	280
245–300	55, −30, 50	2	Right postcentral gyrus	22 L	4

Time of activation and location of maximal peaks which were significant are reported. The remaining significant voxels are also reported. BA: Brodmann Areas; L, left; R, right; N.S. = Not Significant.

example, of object features in a cross-modal integration (Taylor et al., 2009). Moreover, the analysis of mean neural activity confirmed the presence of neural activations in occipito-temporal regions of the brain in a time window comprised between 130–245 msec, again suggesting interactions between the two systems.

The present findings are in general agreement with previous TMS/EEG studies that assessed the temporal dynamics underlying different tasks. For example, Massimini et al. (2005) investigated how the activation of cortical areas was transmitted to the rest of the brain during wakefulness or sleep. In the case of aware subjects, activation in the parietal cortex was observed about 120 msec after TMS onset. An inverse propagation from the parietal cortex to premotor regions in comparable times was also observed. Another study showed that stimulation of left posterior regions of the brain could elicit activations of frontal areas bilaterally in the first 80 msec from the delivery of the stimulus, depending on a series of variables such as, for

example, stimulation intensity or stimulation angle (Casali et al., 2010).

The present findings integrate and extend previous results (Zanon et al., 2010), suggesting the possibility of the existence of wide links between the parietal cortex and other brain regions, ranging from frontal to more posterior parietal, temporal and occipital areas (e.g., Hagmann et al., 2008; Borra and Rockland, 2011). These findings are the result of a series of possible direct and/or indirect links among the highlighted cortical regions. The ones discussed are only the main aspects related to the present pattern of cortico-cortical interactions centered on the parietal cortex, in order to guide the interpretation of behavioral results. Further information about this topic can be found by referring to more specific publications (e.g., Hagmann et al., 2008; Mars et al., 2011).

PREPARATION AND INHIBITION OF MOVEMENTS

This study shed light on the neural underpinnings of visually-guided reaching movements. The knowledge of regions involved in reaching movement preparation is relevant also to understand the way in which the suppression of reaches is implemented. To this respect it has been proposed that a network composed by the inferior frontal cortex, the subthalamic nucleus and pre-SMA (supplementary motor area) is responsible of inhibitory control (Aron et al., 2007a). In fact, neural substrates of suppression have been found in SMA, pre-SMA, basal ganglia and frontal regions (e.g., Matsuzaka and Tanji, 1996; Aron and Poldrack, 2006; Chen et al., 2010; Mirabella et al., 2012; Swann et al., 2012), as well as in cingulate cortex, insula, prefrontal, fronto-parietal and temporal regions (e.g., Kalaska and Crammond, 1995; Aron et al., 2007b; Chikazoe et al., 2009; Coxon et al., 2009; Stinear et al., 2009; Swick et al., 2011). However, evidence suggests that the motor cortex should be the final target of inhibitory commands that could be elaborated elsewhere (Coxon et al., 2006; Mirabella et al., 2011). Furthermore it has been shown that the parietal cortex can play a role in response stopping or inhibition (e.g., Watanabe et al., 2002; Coxon et al., 2009; Wheaton et al., 2009) and in movement decision-related tasks (Karch et al., 2009). Again these are structures that might also be involved in movement control (e.g., Battaglia-Mayer et al., 2006, 2007; Lindner et al., 2010; Ciavarro and Ambrosini, 2011). Some overlap between inhibition and execution of reaching is witnessed by the fact that strategic changes in movement programming for the very same movements under different cognitive contexts have been shown, requiring different degrees of control during movement (Mirabella et al., 2008). However, Mirabella et al. (2006) showed that the Stop/Go processes interacting in a countermanding task are independent, but likely influenced by a common factor when they are under the control of the same hemisphere.

LIMITATIONS OF THE STUDY

The present study has a few limitations. The use of slightly different experimental settings could lead to poorly comparable results. However, the lack of significant effects cannot be entirely attributed to the differences adopted. Particular time windows of stimulation or the state-dependent excitability of the cortex could be also critical. Finally, the possibility that different regions could intervene in different manner compared to task requests should be kept in mind.

One of the changes we adopted in the present experiments was to make the subject work with open rather than closed eyes. The rationale for using a "double" RT paradigm in the previous experiments (putatively, a first one from the go signal to the opening of the eyes and a second one from the opening of the eyes to the start of movement; Busan et al., 2009a,b,c) was in relation with the possibility to study a real-time preparation of reaching movements, avoiding that the subject knew in advance positioning of the target. However, it is evident that the presence of a "double" RT represents a complication. On the other hand, in the present experimental setting, a possible effect related to the visual feedback of the arm cannot be completely ruled out. However, in our previous study (Busan et al., 2009c), the evidence of a slower RT only toward the central reaching position could make this point less critical (e.g., Ferraina et al., 1997; Graziano et al., 2000; Buneo and Andersen, 2006; Khan et al., 2007; Filimon et al., 2009; Beurze et al., 2010; Bosco et al., 2010). We should also consider the possibility that different preparations of movement could be present at the same moment in the brain (Cisek and Kalaska, 2010; Cui and Andersen, 2011) before the go-signal, and that subjects simply selected the movement when requested (Cisek and Kalaska, 2010).

We might have not been able to apply TMS at the right time and the possibility that some effects were undetected in present and previous investigations remains, also in relation to the state-dependent theory (Silvanto and Muggleton, 2008). In this sense, the facilitating effects induced by TMS could be also explained as a possible disruption of inhibitory/controlling/competitive processes, which allowed the controlled areas to enhance their functioning (Walsh and Pascual-Leone, 2003).

Specific limitations in the TMS/EEG experiment may also be present. For example, TMS evokes not only responses related to TMS, but also potentials due to acoustic and somatic stimulation. Sham stimulation was implemented to obtain a control for acoustic stimulation, but an optimal control for somatic stimulation is difficult to be obtained. Even if we tried to eliminate the majority of artifacts with ICA (Jung et al., 2000), the possibility remains that these and some other hidden artifacts were still present in the collected data.

CONCLUDING REMARKS

The data herein reported contribute to further understand the organization of movements. They are in agreement with the suggestion that SPL is more involved in the preparation of natural reaching compared to more lateral structures. However, TMS/EEG findings showed that parietal cortex stimulation propagates toward a wide system of areas. This suggests that segregation among neural systems is not restrictive, and favors alternative hypotheses suggesting that overlap between different neural structures is needed for the implementation of different movements.

This evidence also represents a complementary point of view with respect to neural organization of movement and response

inhibition or stopping, suppression of pending actions, or the quick change of prepared actions. In fact, the organization of reaching and its neural machinery should be highlighted in order to relate them to situations such as inhibition or stopping of action.

ACKNOWLEDGMENTS

This work received partial financial support from the Italian Ministry for Education, University, and Research (MIUR; Grant PRIN-2008RBFNLH_004 to Piero P. Battaglini; http://prin.miur.it/).

REFERENCES

Andersen, R. A., and Buneo, C. A. (2002). Intentional maps in posterior parietal cortex. *Annu. Rev. Neurosci.* 25, 189–220.

Andersen, R. A., and Cui, H. (2009). Intention, action planning and decision making in parietal-frontal circuits. *Neuron* 63, 568–583.

Andersen, R. A., Snyder, L. H., Bradley, D. C., and Xing, J. (1997). Multimodal representation of space in the posterior parietal cortex and its use in planning movements. *Ann. Rev. Neurosci.* 20, 303–330.

Aron, A. R., Behrens, T. E., Smith, S., Frank, M. J., and Poldrack, R. A. (2007a). Triangulating a cognitive control network using diffusion-weighted magnetic resonance imaging (MRI) and functional MRI. *J. Neurosci.* 27, 3743–3752.

Aron, A. R., Durston, S., Eagle, D. M., Logan, G. D., Stinear, C. M., and Stuphorn, V. (2007b). Converging evidence for a fronto-basal-ganglia network for inhibitory control of action and cognition. *J. Neurosci.* 27, 11860–11864.

Aron, A. R., and Poldrack, R. A. (2006). Cortical and subcortical contributions to stop signal response inhibition: role of the subthalamic nucleus. *J. Neurosci.* 26, 2424–2433.

Bakola, S., Gamberini, M., Passarelli, L., Fattori, P., and Galletti, C. (2010). Cortical connections of parietal field PEc in the macaque: linking vision and somatic sensation for the control of limb action. *Cereb. Cortex* 20, 2592–2604.

Batista, A. P., Santhanam, G., Yu, B. M., Ryu, S. I., Afsheen, A., and Shenoy, K. V. (2007). Reference frames for reach planning in macaque dorsal premotor cortex. *J. Neurophysiol.* 98, 966–983.

Battaglia-Mayer, A., Archambault, P. S., and Caminiti, R. (2006). The cortical network for eye-hand coordination and its relevance to understanding motor disorders of parietal patients. *Neuropsychologia* 47, 2607–2620.

Battaglia-Mayer, A., Mascaro, M., and Caminiti, R. (2007). Temporal evolution and strenght of neural activity in parietal cortex during eye and hand movements. *Cereb. Cortex* 17, 1350–1363.

Beurze, S. M., Toni, I., Pisella, L., and Medendorp, W. P. (2010). Parietofrontal cortex reference frames for reach planning in human. *J. Neurophysiol.* 104, 1736–1745.

Binkofski, F., Dohle, C., Posse, S., Stephan, K. M., Hefter, H., Seitz, R. J., and Freund, H. J. (1998). Human anterior intraparietal area subserves prehension: a combined lesion and functional MRI activation study. *Neurology* 50, 1253–1259.

Bonato, C., Miniussi, C., and Rossini, P. M. (2006). Transcranial magnetic stimulation and cortical evoked potentials: a TMS/EEG co-registration study. *Clin. Neurophysiol.* 117, 1699–1707.

Borra, E., Belmalih, A., Calzavara, R., Gerbella, M., Murata, A., Rozzi, S., and Luppino, G. (2008). Cortical connections of the macaque anterior intraparietal (AIP) area. *Cereb. Cortex* 18, 1094–1111.

Borra, E., and Rockland, K. S. (2011). Projections to early visual areas V1 and V2 in the calcarine fissure from parietal association areas in the macaque. *Front. Neuroanat.* 5:35. doi: 10.3389/fnana.2011.00035

Bosco, A., Breveglieri, R., Chinellato, E., Galletti, C., and Fattori, P. (2010). Reaching activity in the medial posterior parietal cortex of monkeys is modulated by visual feedback. *J. Neurosci.* 30, 14773–14785.

Brett, M., Johnsrude, I. S., and Owen, A. M. (2002). The problem of functional localization in the human brain. *Nat. Rev. Neurosci.* 3, 243–249.

Buneo, C. A., and Andersen, R. A. (2006). The posterior parietal cortex: sensorimotor interface for the planning and online control of visually guided movements. *Neuropsychologia* 44, 2594–2606.

Buneo, C. A., Batista, A. P., Jarvis, M. R., and Andersen, R. A. (2008). Time-invariant reference frames for parietal reach activity. *Exp. Brain Res.* 188, 77–89.

Buneo, C. A., Jarvis, M. R., Batista, A. P., and Andersen, R. A. (2002). Direct visuomotor transformations for reaching. *Nature* 416, 632–636.

Burnod, Y., Baraduc, P., Battaglia-Mayer, A., Guigon, E., Koechlin, E., Ferraina, S., Lacquaniti, F., and Caminiti, R. (1999). Parieto-frontal coding of reaching: an integrated framework. *Exp. Brain Res.* 129, 325–346.

Busan, P., Barbera, C., Semenic, M., Monti, F., Pizzolato, G., Pelamatti, G., and Battaglini, P. P. (2009a). Effect of transcranial magnetic stimulation (TMS) on parietal and premotor cortex during planning of reaching movements. *PLoS ONE* 4:e4621. doi: 10.1371/journal.pone.0004621

Busan, P., Jarmolowska, J., Semenic, M., Monti, F., Pelamatti, G., Pizzolato, G., and Battaglini, P. P. (2009b). Involvement of ipsilateral parieto-occipital cortex in the planning of reaching movements: evidence by TMS. *Neurosci. Lett.* 460, 112–116.

Busan, P., Monti, F., Semenic, M., Pizzolato, G., and Battaglini, P. P. (2009c). Parieto-occipital cortex and planning of reaching movements: a transcranial magnetic stimulation study. *Behav. Brain Res.* 201, 112–119.

Calton, J. L., Dickinson, A. R., and Snyder, L. H. (2002). Non-spatial, motor-specific activation in posterior parietal cortex. *Nat. Neurosci.* 5, 580–588.

Casali, A. G., Casarotto, S., Rosanova, M., Mariotti, M., and Massimini, M. (2010). General indices to characterize the electrical response of the cerebral cortex to TMS. *Neuroimage* 49, 1459–1468.

Chang, S. W. C., Dickinson, A. R., and Snyder, L. H. (2008). Limb-specific representation for reaching in the posterior parietal cortex. *J. Neurosci.* 28, 6128–6140.

Chen, X., Scangos, K. W., and Stuphorn, V. (2010). Supplementary motor area exerts proactive and reactive control of arm movements. *J. Neurosci.* 30, 14657–14675.

Chikazoe, J., Jimura, K., Hirose, S., Yamashita, K., Miyashita, Y., and Konishi, S. (2009). Preparation to inhibit a response complement response inhibition during performance of a stop-signal task. *J. Neurosci.* 29, 15870–15877.

Ciavarro, M., and Ambrosini, E. (2011). Specificity for reach planning in the human PPC. *J. Neurosci.* 31, 2719–2720.

Cisek, P., and Kalaska, J. F. (2010). Neural mechanisms for interacting with a world full of action choices. *Annu. Rev. Neurosci.* 33, 269–298.

Cohen, Y. E., and Andersen, R. A. (2002). A common reference frame for movement plans in the posterior parietal cortex. *Nat. Rev. Neurosci.* 3, 553–562.

Connolly, J. D., Andersen, R. A., and Goodale, M. A. (2003). FMRI evidence for a "parietal reach region" in the human brain. *Exp. Brain Res.* 153, 140–145.

Coxon, J. P., Stinear, C. M., and Byblow, W. D. (2006). Intracortical inhibition during volitional inhibition of prepared action. *J. Neurophysiol.* 95, 3371–3383.

Coxon, J. P., Stinear, C. M., and Byblow, W. D. (2009). Stop and go: the neural basis of selective movement prevention. *J. Cogn. Neurosci.* 21, 1193–1203.

Cui, H., and Andersen, R. A. (2011). Different representations of potential and selected motor plans by distinct parietal areas. *J. Neurosci.* 31, 18130–18136.

Davare, M., Andrei, M., Cosnard, G., Thonnard, J. L., and Olivier, E. (2006). Dissociating the role of ventral and dorsal premotor cortex in precision grasping. *J. Neurosci.* 26, 2260–2268.

Davare, M., Rothwell, J. C., and Lemon, R. N. (2010). Causal connectivity between the human anterior intraparietal area and premotor cortex during grasp. *Curr. Biol.* 20, 176–181.

Delorme, A., and Makeig, S. (2004). EEGLAB: an open source toolbox for analysis of single-trial EEG dynamics including independent component analysis. *J. Neurosci. Methods* 134, 9–21.

Desmurget, M., Prablanc, C., Arzi, M., Rossetti, Y., Paulignan, Y., and Urquizar, C. (1996). Integrated control of hand transport and orientation during prehension movements. *Exp. Brain Res.* 110, 265–278.

Desmurget, M., and Sirigu, A. (2009). A parietal-premotor network for movement intention and motor awareness. *Trends Cogn. Sci.* 13, 411–419.

Desmurget, M., Turner, R. S., Prablanc, C., Russo, G. S., Alexander, G. E., and Grafton, S. T. (2005). Updating target location at the end of an orienting saccade affects

the characteristics of simple point-to-point movements. *J. Exp. Psychol. Hum. Percept. Perform.* 31, 1510–1536.

Fattori, P., Gamberini, M., Kutz, D. F., and Galletti, C. (2001). 'Arm-reaching' neurons in the parietal area V6A of the macaque monkey. *Eur. J. Neurosci.* 13, 2309–2313.

Fattori, P., Kutz, D. F., Breveglieri, R., Marzocchi, N., and Galletti, C. (2005). Spatial tuning of reaching activity in the medial parieto-occipital cortex (area V6A) of macaque monkey. *Eur. J. Neurosci.* 22, 956–972.

Fernandez-Ruiz, J., Goltz, H. C., DeSouza, J. F. X., Vilis, T., and Crawford, J. D. (2007). Human parietal "reach region" primarily encodes intrinsic visual direction, not extrinsic movement direction, in a visual-motor dissociation task. *Cereb. Cortex* 17, 2283–2292.

Ferraina, S., Garasto, M. R., Battaglia-Mayer, A., Ferraresi, P., Johnson, P. B., Lacquaniti, F., and Caminiti, R. (1997). Visual control of hand reaching movement: activity in parietal area 7 m. *Eur. J. Neurosci.* 9, 1090–1095.

Filimon, F., Nelson, J. D., Huang, R. S., and Sereno, M. I. (2009). Multiple parietal reach regions in humans: cortical representations for visual and proprioceptive feedback during on-line reaching. *J. Neurosci.* 29, 2961–2971.

Fuchs, M., Kastner, J., Wagner, M., Hawes, S., and Ebersole, J. S. (2002). A standardized boundary element method volume conductor model. *Clin. Neurophysiol.* 113, 702–712.

Galletti, C., Gamberini, M., Kutz, D. F., Fattori, P., Luppino, G., and Matelli, M. (2001). The cortical connections of area V6, an occipito-parietal network processing visual information. *Eur. J. Neurosci.* 13, 1572–1588.

Gamberini, M., Passarelli, L., Fattori, P., Zucchelli, M., Bakola, S., Luppino, G., and Galletti, C. (2009). Cortical connections of the visuomotor parietooccipital area V6Ad of the macaque monkey. *J. Comp. Neurol.* 513, 622–642.

Glover, S. (2004). Separate visual representations in the planning and control of action. *Behav. Brain Sci.* 27, 3–24.

Goodale, M. A. (1988). Hemispheric differences in motor control. *Behav. Brain Res.* 30, 203–214.

Goodale, M. A., and Milner, A. D. (1992). Separate visual pathways for perception and action. *Trends Neurosci.* 15, 20–25.

Goodale, M. A., and Milner, A. D. (2004). Plans for action. *Behav. Brain Sci.* 27, 37–41.

Graziano, M. S. A., Cooke, D. F., and Taylor, C. S. R. (2000). Coding the location of the arm by sight. *Science* 290, 1782–1786.

Greicius, M. D., Supekar, K., Menon, V., and Dougherty, R. F. (2009). Resting-state functional connectivity reflects structural connectivity in the default mode network. *Cereb. Cortex* 19, 72–78.

Haaland, K. Y., and Harrington, D. L. (1989). Hemispheric control of the initial and corrective components of aiming movements. *Neuropsychologia* 27, 961–969.

Hagmann, P., Cammoun, L., Gigandet, X., Meuli, R., Honey, C. J., and Wedeen, V. J. (2008). Mapping the structural core of human cerebral cortex. *PLoS Biol.* 6:1479–1493. doi: 10.1371/journal.pbio.0060159

Herwig, U., Satrapi, P., and Schönfeldt-Lecuona, C. (2003). Using the international 10-20 EEG system for positioning of transcranial magnetic stimulation. *Brain Topogr.* 16, 95–99.

Himmelbach, M., and Karnath, H. O. (2005). Dorsal and ventral stream interaction: contributions from optic ataxia. *J. Cogn. Neurosci.* 17, 632–640.

Hoshi, E., and Tanji, J. (2007). Distinctions between dorsal and ventral premotor areas: anatomical connectivity and functional properties. *Curr. Opin. Neurobiol.* 17, 234–242.

Iacoboni, M. (2006). Visuo-motor integration and control in the human posterior parietal cortex: evidence from TMS and fMRI. *Neuropsychologia* 44, 2691–2699.

Ilmoniemi, R. J., and Kičić, D. (2010). Methodology for combined TMS and EEG. *Brain Topogr.* 22, 233–248.

Jackson, S. R., Newport, R., Husain, M., Fowlie, J. E., O'Donoghue, M., and Bajaj, N. (2009). There may be more to reaching than meets the eye: re-thinking optic ataxia. *Neuropsychologia* 47, 1397–1408.

Jeannerod, M., Arbib, M. A., Rizzolatti, G., and Sakata, H. (1995). Grasping objects: the cortical mechanisms of visuomotor transformation. *Trends Neurosci.*18, 314–320.

Johnson, P. B., Ferraina, S., Bianchi, L., and Caminiti, R. (1996). Cortical networks for visual reaching. Physiological and anatomical organization of frontal and parietal lobe arm regions. *Cereb. Cortex* 6, 102–119.

Jung, T. P., Makeig, S., Humphries, C., Lee, T. W., McKeown, M. J., Iragui, V., and Sejnowski, T. J. (2000). Removing electroencephalographic artifacts by blind source separation. *Psychophysiology* 37, 163–178.

Jurcak, V., Tsuzuki, D., and Dan, I. (2007). 10/20, 10/10, and 10/5 systems revisited: their validity as relative head-surface-based positioning systems. *Neuroimage* 34, 1600–1611.

Kalaska, J. F., and Crammond, D. J. (1995). Deciding not to go: neuronal correlates of response selection in a go/nogo task in primate premotor and parietal cortex. *Cerebr. Cortex* 5, 410–428.

Karch, S., Mulert, C., Thalmeier, T., Lutz, J., Leicht, G., Meindl, T., Möller, H. J., Jäger, L., and Pogarell, O. (2009). The free choice whether or not to respond after stimulus presentation. *Hum. Brain Mapp.* 30, 2971–2985.

Kastner, S., Demmer, I., and Ziemann, U. (1998). Transient visual field defect induced by transcranial magnetic stimulation over human occipital lobe. *Exp. Brain Res.* 118, 19–26.

Kertzman, C., Schwarz, U., Zeffiro, T. A., and Hallett, M. (1997). The role of posterior parietal cortex in visually guided reaching movements in humans. *Exp. Brain Res.* 114, 170–183.

Khan, A. Z., Crawford, J. D., Blohm, G., Urquizar, C., Rossetti, Y., and Pisella, L. (2007). Influence of initial hand and target position on reach errors in optic ataxia and normal subjects. *J. Vis.* 7, 1–16.

Koch, G., Cercignani, M., Pecchioli, C., Versace, V., Oliveri, M., Caltagirone, C., Rothwell, J., and Bozzali, M. (2010). *In vivo* definition of parieto-motor connections involved in planning of grasping movements. *Neuroimage* 51, 300–312.

Koch, G., Del Olmo, M. F., Cheeran, B., Schippling, S., Caltagirone, C., Driver, J., and Rothwell, J. C. (2008). Functional interplay between posterior parietal and ipsilateral motor cortex revealed by twin-coil transcranial magnetic stimulation during reach planning toward contralateral space. *J. Neurosci.* 28, 5944–5953.

Lancaster, J. L., Woldorff, M. G., Parsons, L. M., Liotti, M., Freitas, C. S., Rainey, L., Kochunov, P. V., Nickerson, D., Mikiten, S. A., and Fox, P. T. (2000). Automated Talairach Atlas labels for functional brain mapping. *Hum. Brain Mapp.* 10, 120–131.

Lindner, A., Iyer, A., Kagan, I., and Andersen, R. A. (2010). Human posterior parietal cortex plans where to reach and what to avoid. *J. Neurosci.* 30, 11715–11725.

Makuuchi, M., Someya, Y., Ogawa, S., and Takayam, Y. (2012). Hand shape selection in pantomimed grasping: interaction between the dorsal and the ventral visual streams and convergence on the ventral premotor area. *Hum. Brain Mapp.* 33, 1821–1833.

Marconi, B., Genovesio, A., Battaglia-Mayer, A., Ferraina, S., Squatrito, S., Molinari, M., Lacquaniti, F., and Caminiti, R. (2001). Eye-hand coordination during reaching. I Anatomical relationship between parietal and frontal cortex. *Cereb. Cortex* 11, 513–527.

Mars, R. B., Jbabdi, S., Sallet, J., O'Reilly, J. X., Croxson, P. L., Olivier, E., Noonan, M. A. P., Bergmann, C., Mitchell, A. S., Baxter, M. G., Behrens, T. E., Johansen-Berg, H., Tomassini, V., Miller, K. L., and Rushworth, M. F. S. (2011). Diffusion-weighted imaging tractography-based parcellation of the human parietal cortex and comparison with human and macaque resting-state functional connectivity. *J. Neurosci.* 31, 4087–4100.

Massimini, M., Ferrarelli, F., Huber, R., Esser, S. K., Singh, H., and Tononi, G. (2005). Breakdown of cortical effective connectivity during sleep. *Science* 309, 2228–2232.

Matsuzaka, Y., and Tanji, J. (1996). Changing directions of forthcoming arm movements: neuronal activity in the presupplementary and supplementary motor area of monkey cerebral cortex. *J. Neurophysiol.* 76, 2327–2342.

Mazziotta, J., Toga, A., Evans, A., Fox, P., Lancaster, J., Zilles, K., Woods, R., Paus, T., Simpson, G., Pike, B., Holmes, C., Collins, L., Thompson, P., MacDonald, D., Iacoboni, M., Schormann, T., Amunts, K., Palomero-Gallagher, N., Geyer, S., Parsons, L., Narr, K., Kabani, N., Le Goualher, G., Boomsma, D., Cannon, T., Kawashima, R., and Mazoyer, B. (2001). A probabilistic atlas and reference system for the human brain: International Consortium for Brain Mapping (ICBM). *Philos. Trans. R. Soc. Lond. B Biol. Sci.* 356, 1293–1322.

Medendorp, W. P., Goltz, H. C., Crawford, J. D., and Vilis, T. (2005). Integration of target and effector information in human posterior parietal cortex for the planning of action. *J. Neurophysiol.* 93, 954–962.

Medendorp, W. P., Goltz, H. C., Vilis, T., and Crawford, J. D. (2003).

Gaze-centered updating of visual space in human parietal cortex. *J. Neurosci.* 23, 6209–6214.

Milner, D., and Goodale, M. (2006). *The Visual Brain in Action.* Oxford, USA: Oxford University Press.

Miniussi, C., Ruzzoli, M., and Walsh, V. (2010). The mechanism of transcranial magnetic stimulation in cognition. *Cortex* 46, 128–130.

Mirabella, G., Iaconelli, S., Romanelli, P., Modugno, N., Lena, F., Manfredi, M., and Cantore, G. (2012). Deep brain stimulation of subthalamic nuclei affects arm response inhibition in Parkinson's patients. *Cereb. Cortex* 22, 1124–1132.

Mirabella, G., Pani, P., and Ferraina, S. (2008). Influence of context on reaction and movement times. *Cogn. Neuropsychol.* 25, 996–1010.

Mirabella, G., Pani, P., and Ferraina, S. (2011). Neural correlates of cognitive control of reaching movements in the dorsal premotor cortex of rhesus monkeys. *J. Neurophysiol.* 106, 1454–1466.

Mirabella, G., Pani, P., Parè, M., and Ferraina, S. (2006). Inhibitory control of reaching movements in humans. *Exp. Brain Res.* 174, 240–255.

Mon-Williams, M., and McIntosh, R. D. (2000). A test between two hypotheses and a possible third way for the control of prehension. *Exp. Brain Res.* 134, 268–273.

Naranjo, J. R., Brovelli, A., Longo, R., Budai, R., Kristeva, R., and Battaglini, P. P. (2007). EEG dynamics of the frontoparietal network during reaching preparation in humans. *Neuroimage* 34, 1673–1682.

Nichols, T. E., and Holmes, P. A. (2002). Nonparametric permutation tests for functional neuroimaging; a primer with examples. *Hum. Brain Mapp.* 15, 1–25.

Nikouline, V., Ruohonen, J., and Ilmoniemi, R. J. (1999). The role of the coil click in TMS assessed with simultaneous EEG. *Clin. Neurophysiol.* 110, 1325–1328.

Oldfield, R. C. (1971). The assessment and analysis of handedness: the Edinburgh inventory. *Neuropsychologia* 9, 97–113.

Oostenveld, R., and Praamstra, P. (2001). The five percent electrode system for high-resolution EEG and ERP measurements. *Clin. Neurophysiol.* 112, 713–719.

Pascual-Marqui, R. D. (2002). Standardized low resolution brain electromagnetic tomography: a new method for localizing electrical activity in the brain. *Int. J. Psychophysiol.* 18, 49–65.

Passarelli, L., Rosa, M. G., Gamberini, M., Bakola, S., Burman, K. J., Fattori, P., and Galletti, C. (2011). Cortical connections of area V6Av in the macaque: a visual-input node to the eye/hand coordination system. *J. Neurosci.* 31, 1790–1801.

Paus, T., Sipila, P. K., and Strafella, A. P. (2001). Synchronization of neuronal activity in the human primary motor cortex by transcranial magnetic stimulation: an EEG study. *J. Neurophysiol.* 86, 1983–1990.

Perenin, M. T., and Vighetto, A. (1988). Optic ataxia: a specific disruption in visuomotor mechanisms. I. Different aspects of the deficit in reaching for objects. *Brain* 111, 643–674.

Pesaran, B., Nelson, M. J., and Andersen, R. A. (2006). Dorsal premotor neurons encode the relative position of the hand, eye and goal during reach planning. *Neuron* 51, 125–134.

Pisella, L., Binkofski, F., Lasek, K., Toni, I., and Rossetti, Y. (2006). No double-dissociation between optic ataxia and visual agnosia: multiple sub-streams for multiple visuo-manual integrations. *Neuropsychologia* 44, 2734–2748.

Prado, J., Clavagnier, S., Otzenberger, H., Scheiber, C., Kennedy, H., and Perenin, M. T. (2005). Two cortical systems for reaching in central and peripheral vision. *Neuron* 48, 849–858.

Raichle, M. E., MacLeod, A. M., Snyder, A. Z., Powers, W. J., Gusnard, D. A., and Shulman, G. L. (2001). A default mode of brain function. *Proc. Natl. Acad. Sci. U.S.A.* 98, 676–682.

Raichle, M. E., and Snyder, A. Z. (2007). A default mode of brain function: a brief history of an evolving idea. *Neuroimage* 237, 1083–1090.

Randerath, J., Goldenberg, G., Spijkers, W., Li, Y., and Hermsdörfer, J. (2010). Different left brain regions are essential for grasping a tool compared with its subsequent use. *Neuroimage* 53, 171–180.

Reichenbach, A., Bresciani, J. P., Peer, A., Bülthoff, H. H., and Thielscher, A. (2011). Contributions of the PPC to online control of visually guided reaching movements assessed with fMRI-guided TMS. *Cereb. Cortex* 21, 1602–1612.

Rice, N. J., Tunik, E., and Grafton, S. T. (2006). The anterior intraparietal sulcus mediates grasp execution, independent of requirement to update: new insights from transcranial magnetic stimulation. *J. Neurosci.* 26, 8176–8182.

Riddoch, G. (1935). Visual disorientation in homonymous half-fields. *Brain* 58, 376–382.

Rushworth, M. F. S., Johansen-Berg, H., Göbel, S. M., and Devlin, J. T. (2003). The left parietal and premotor cortices: motor attention and selection. *Neuroimage* 20, S89–S100.

Rushworth, M. F. S., Krams, M., and Passingham, R. E. (2001). The attentional role of the parietal cortex: the distinct lateralization and localization of motor attention in the human brain. *J. Cogn. Neurosci.* 13, 698–710.

Sawaki, L., Okita, T., Fukiwara, M., and Mizumo, K. (1999). Specific and non-specific effects of transcranial magnetic stimulation upon simple and go/no-go reaction time. *Exp. Brain Res.* 127, 402–408.

Schenk, T., and Milner, A. D. (2006). Concurrent visuomotor behavior improves form discrimination in a patient with visual form agnosia. *Eur. J. Neurosci.* 24, 1495–1503.

Silvanto, J., and Muggleton, N. G. (2008). New light through old windows: moving beyond the "virtual lesion" approach to transcranial magnetic stimulation. *Neuroimage* 39, 549–552.

Smeets, J. B., and Brenner, E. (1999). A new view on grasping. *Mot. Control* 3, 237–271.

Snyder, L. H., Dickinson, A. R., and Calton, J. L. (2006). Preparatory delay activity in the monkey parietal reach region predicts reach reaction times. *J. Neurosci.* 26, 10091–10099.

Steinsträter, O., Sommer, J., Deppe, M., and Knecht, S. (2002). The Münster T2T-Converter. http://www.neuro03.uni-muenster.de/ger/t2tconv/

Stinear, C. M., Coxon, J. P., and Byblow, W. D. (2009). Primary motor cortex and movement prevention: where stop meets go. *Neurosci. Biobehav. Rev.* 33, 662–673.

Striemer, C., Locklin, J., Blangero, A., Rossetti, Y., Pisella, L., and Danckert, J. (2009). Attention for action? Examining the link between attention and visuomotor control deficits in a patient with optic ataxia. *Neuropsychologia* 47, 1491–1499.

Striemer, C. L., Chouinard, P. A., and Goodale, M. A. (2011). Programs for action in superior parietal cortex: a triple-pulse TMS investigation. *Neuropsychologia* 49, 2391–2399.

Swann, N. C., Cai, W., Conner, C. R., Pieters, T. A., Claffey, M. P., George, J. S., Aron, A. R., and Tandon, N. (2012). Roles for the pre-supplementary motor area and the right inferior frontal gyrus in stopping action: electrophysiological responses and functional and structural connectivity. *Neuroimage* 59, 2860–2870.

Swick, D., Ashley, V., and Turken, U. (2011). Are the neural correlates of stopping and not going identical? Quantitative meta-analysis of two response inhibition tasks. *Neuroimage* 56, 1655–1665.

Tannè, J., Boussaud, D., Boyer-Zeller, N., and Rouiller, E. M. (1995). Direct visual pathways for reaching movements in the macaque monkey. *Neuroreport* 29, 267–272.

Taylor, K. I., Stamatakis, E. A., and Tyler, L. K. (2009). Crossmodal integration of object features: voxel-based correlations in brain-damaged patients. *Brain* 132, 671–683.

Trillenberg, P., Sprenger, A., Petersen, D., Kömpf, D., Heide, W., and Helmchen, C. (2007). Functional dissociation of saccade and hand reaching control with bilateral lesions of the medial wall of the intraparietal sulcus: implication for optic ataxia. *Neuroimage* 36, T69–T76.

Tunik, E., Frey, S. H., and Grafton, S. T. (2005). Virtual lesions of the anterior intraparietal area disrupt goal-dependent on-line adjustments of grasp. *Nat. Neurosci.* 8, 505–511.

Ulloa, A., and Bullock, D. (2003). A neural network simulating human reach-grasp coordination by continuous updating of vector positioning commands. *Neural Netw.* 16, 1141–1160.

Valyear, K. F., and Culham, J. C. (2010). Observing learned object-specific functional grasps preferentially activates the ventral stream. *J. Cogn. Neurosci.* 22, 970–984.

Vesia, M., Prime, S. L., Yan, X., Sergio, L. E., and Crawford, J. D. (2010). Specificity of human parietal saccade and reach regions during transcranial magnetic stimulation. *J. Neurosci.* 30, 13052–13065.

Vesia, M., Yan, X., Henriques, D. Y., Sergio, L. E., and Crawford, J. D. (2008). Transcranial magnetic stimulation over human dorsal-lateral posterior parietal cortex disrupts integration of hand position signals into the reach plan. *J. Neurophysiol.* 100, 2005–2014.

Vingerhoets, G., Alderweireldt, A. S., Vandemaele, P., Cai, Q., Van der Haegen, L., Brysbaert, M.,

and Achten, E. (2011). Praxis and language are linked: evidence from co-lateralization in individuals with atypical language dominance. *Cortex*. doi: 10.1016/j.cortex.2011.11.003. [Epub ahead of print].

Walsh, V., and Pascual-Leone, A. (2003). *A Neurochronometrics of Mind*. Cambridge, MA: The MIT Press.

Watanabe, J., Sugiura, M., Sato, K., Sato, Y., Maeda, Y., Matsue, Y., Fukuda, H., and Kawashima, R. (2002). The human prefrontal and parietal association cortices are involved in NO-GO performances: an event-related fMRI study. *Neuroimage* 17, 1207–1216.

Wheaton, L., Fridman, E., Bohlhalter, S., Vorbach, S., and Hallett, M. (2009). Left parietal activation related to planning, executing and suppressing praxis hand movements. *Clin. Neurophysiol.* 120, 980–986.

Zanon, M., Busan, P., Monti, F., Pizzolato, G., and Battaglini, P. P. (2010). Cortical connections between dorsal and ventral visual streams in humans: evidence by TMS/EEG co-registration. *Brain Topogr.* 22, 307–317.

Conflict of Interest Statement: The authors declare that the research was conducted in the absence of any commercial or financial relationships that could be construed as a potential conflict of interest.

Received: 18 February 2012; accepted: 19 July 2012; published online: 08 August 2012.

*Citation: Busan P, Zanon M, Vinciati F, Monti F, Pizzolato G and Battaglini PP (2012) Transcranial magnetic stimulation and preparation of visually-guided reaching movements. Front. Neuroeng. **5**:18. doi: 10.3389/fneng.2012.00018*

frontiers in
NEUROENGINEERING

ORIGINAL RESEARCH ARTICLE
published: 29 June 2012
doi: 10.3389/fneng.2012.00012

Stop-event-related potentials from intracranial electrodes reveal a key role of premotor and motor cortices in stopping ongoing movements

M. Mattia[1], S. Spadacenta[2,3], L. Pavone[2], P. Quarato[2], V. Esposito[2], A. Sparano[2], F. Sebastiano[2], G. Di Gennaro[2], R. Morace[2], G. Cantore[2] and G. Mirabella[2,4]*

[1] *Department of Technologies and Health, Istituto Superiore di Sanità, Viale Regina Elena, Rome, Italy*
[2] *IRCCS Neuromed, Via Atinense, Pozzilli (IS), Italy*
[3] *PhD Program in Neurophysiology, Department of Physiology and Pharmacology, University of Rome La Sapienza Piazzale Aldo Moro, Rome, Italy*
[4] *Department of Physiology and Pharmacology, University of Rome La Sapienza, Piazzale Aldo Moro, Rome, Italy*

Edited by:
Laura Ballerini, University of Trieste, Italy

Reviewed by:
Hari S. Sharma, Uppsala University, Sweden
Liang Guo, Massachusetts Institute of Technology, USA

****Correspondence:***
G. Mirabella, Department of Physiology and Pharmacology "V. Erspamer", La Sapienza University, Piazzale Aldo Moro 5, 00185 Rome, Italy.
e-mail: giovanni.mirabella@uniroma1.it

In humans, the ability to withhold manual motor responses seems to rely on a right-lateralized frontal–basal ganglia–thalamic network, including the pre-supplementary motor area and the inferior frontal gyrus (IFG). These areas should drive subthalamic nuclei to implement movement inhibition via the hyperdirect pathway. The output of this network is expected to influence those cortical areas underlying limb movement preparation and initiation, i.e., premotor (PMA) and primary motor (M1) cortices. Electroencephalographic (EEG) studies have shown an enhancement of the N200/P300 complex in the event-related potentials (ERPs) when a planned reaching movement is successfully stopped after the presentation of an infrequent stop-signal. PMA and M1 have been suggested as possible neural sources of this ERP complex but, due to the limited spatial resolution of scalp EEG, it is not yet clear which cortical areas contribute to its generation. To elucidate the role of motor cortices, we recorded epicortical ERPs from the lateral surface of the fronto-temporal lobes of five pharmacoresistant epileptic patients performing a reaching version of the countermanding task while undergoing presurgical monitoring. We consistently found a stereotyped ERP complex on a single-trial level when a movement was successfully cancelled. These ERPs were selectively expressed in M1, PMA, and Brodmann's area (BA) 9 and their onsets preceded the end of the stop process, suggesting a causal involvement in this executive function. Such ERPs also occurred in unsuccessful-stop (US) trials, that is, when subjects moved despite the occurrence of a stop-signal, mostly when they had long reaction times (RTs). These findings support the hypothesis that motor cortices are the final target of the inhibitory command elaborated by the frontal–basal ganglia–thalamic network.

Keywords: volitional inhibition, stop signal task, countermanding task, voluntary movements, electrocorticography (ECoG), reaching movements, event-related potentials (ERP)

INTRODUCTION

Our survival depends on our ability to maximize the chances of achieving desired goals. Given that in the real-world events cannot be predicted with certainty, the opportunity of executing an action needs to be continuously evaluated during the entire period, from the instant when the initial decision whether to act is taken to the time when motor output is generated. In fact, during this temporal gap the environmental conditions might have changed and thus the cost of the selected action might turn out to be high or to be inappropriate for achieving the selected goal (Haggard, 2008). This check might be achieved by comparing the output of a predictive forward model with a goal description (Wolpert and Miall, 1996) and might lead to the suppression of the pending movement when the mismatch between the two becomes too large, i.e., in those situations in which a radical change of the planned motor strategy is required. Thus, voluntary inhibition is a hinge of our behavioral flexibility. This form of inhibitory control has often been studied by exploiting the countermanding paradigm (Logan, 1994). This paradigm probes a subject's ability to withhold a planned movement triggered by a go signal when an infrequent stop signal is presented after a variable delay. Starting from the behavioral performance during the countermanding task it is possible to yield an estimate of the duration of the suppression process (stop-signal reaction time, SSRT; Logan and Cowan, 1984; Band et al., 2003; Boucher et al., 2007). The SSRT is a key behavioral parameter for uncovering the neural substrates of inhibition. In fact, those brain regions showing a change in activity when a movement is produced with respect to when it is suppressed, and where the onset of this shift precedes the end of the SSRT, can be assumed to be causally related to the suppression process.

Several studies in humans have ascribed the inhibitory control of manual motor actions to a network of regions, belonging to the right hemisphere, which comprises two areas of the frontal cortex, the inferior frontal gyrus (IFG; Aron et al., 2003, 2007; Chambers et al., 2006) and the pre-supplementary motor area (Floden and Stuss, 2006; Aron et al., 2007; Nachev et al., 2007). Both areas are thought to modulate the cortical neural processes for movement initiation via the hyperdirect route, passing through the right subthalamic nucleus (STN) (Aron and Poldrack, 2006; Aron et al., 2007). However, the picture is far from complete. Some recent studies have suggested that both subthalamic nuclei contribute to voluntary inhibition (van den Wildenberg et al., 2006; Mirabella et al., 2012). Li et al. (2008) demonstrated that the head of the caudate nucleus of both hemispheres have a role in movement suppression, while activity of the STN would be related to attentional monitoring of the stop signal. In addition, Brass and Haggard (2007) showed that the left dorsal fronto-median cortex (dFMC; BA 9) is specifically associated with endogenous inhibition of intentional action. In this case a possible explanation for this divergence comes from the fact that previous studies focused on inhibition triggered by external stimuli rather than inner volition (see also Mirabella, 2007).

Even though both the neural substrates of voluntary inhibition and their specific role in this executive function are still hotly debated, it is very likely that commands generated by these brain regions have to influence in a top-down manner those cortical areas critically involved in limb movement preparation and initiation, i.e., M1 and PMA (Evarts, 1968; Tanji and Evarts, 1976; Cheney and Fetz, 1980; Weinrich and Wise, 1982; Crammond and Kalaska, 2000; Churchland et al., 2010). In fact, Coxon et al. (2006), by applying the transcranial magnetic stimulation on M1 during the execution of a countermanding task, demonstrated that this area is involved in movement suppression. Furthermore, a recent study by Mirabella et al. (2011) demonstrated the existence of neurons in the dorsal PMA which exhibit a pattern of activity compatible with the control of reaching arm movement initiation and suppression.

Scalp EEG studies exploiting the countermanding task have shown that successfully stopped trials are associated with an enhancement of the N200/P300 complex in the ERPs with respect either to unsuccessful-stop (US) trials or no-stop trials (Kok et al., 2004; Ramautar et al., 2006; Schmajuk et al., 2006; Liotti et al., 2007; Dimoska and Johnstone, 2008). Even though few studies have indicated PMA and M1 as the neural source of a component of this complex, because the spatial resolution of scalp EEG is limited it is not yet clear which brain regions contribute to its generation.

Swann et al. (2009) tried to overcome this limitation by recording directly from the cortical surface of pharmaco-resistant epileptic patients undergoing presurgical monitoring. In this study results were provided for only two electrodes for each patient, one located over the right IFG and the other located over M1. Swann et al. (2009) found that responses in the beta frequency band (13–18 Hz) at the two sites were differently modulated for successful-stop (SS) versus US trials. Thus, they concluded that the stopping command is implemented in a right IFG-basal ganglia circuit via synchronized activity in the beta band, and finally acts upon M1. This study left a number of unanswered questions. First of all, ERPs were not computed and thus it was not possible to assess whether an ERP complex associated with inhibitory control was expressed. Second, and more importantly, as just two out of many more electrodes were selected an overall picture of the activity changes recorded from the sampled regions of the brain could not be drawn. In order to provide answers to these questions we recorded the electrocorticogram (ECoG) of five epileptic patients with a grid placed over fronto-temporal regions. Thanks to the high spatiotemporal resolution of ECoG, we aimed to identify the cortical areas involved in inhibitory control and the timing of their activation. We found that a stereotyped ERP complex was selectively expressed in M1, PMA, and BA 9 on a single-trial level whenever a movement was successfully suppressed. As the ERP onset preceded the end of the SSRT, we concluded that motor cortices are causally involved in inhibitory control, and likely they might represent the final target on which inhibitory commands exert their action.

MATERIALS AND METHODS

PARTICIPANTS

Five right-handed subjects with intractable epilepsy, who underwent temporary implantation of subdural electrode grids for the localization of seizure foci prior to surgical resection, participated in the present study. All subjects gave their informed consent and were free to withdraw from the study at any time. The general procedures were approved by the local Institutional Ethics Committee (IRCCS Neuromed, Pozzilli, Italy) and were performed in accordance with the ethical standards laid down in the Declaration of Helsinki of 1964.

Apart from the chronic epilepsy, none of the subjects showed major overt cognitive deficits and were functionally independent. Thus, all patients fully understood experimenters' instructions and performed the task easily. Their relevant demographic, clinical, neuropsychological, and neuroradiological data are reported in **Table 1**.

ELECTRODES AND ECoG ACQUISITION

The implanted electrode grids (Ad-Tech Medical Corp., Racine, WI, USA) consisted of circular (1 mm height, 4 mm diameter) platinum–iridium contacts embedded in a thin (0.5 mm) flexible transparent silastic plate and evenly spaced at 10 mm centers. All patients but one had 64-contact grids; one (RO) had a 48-contact grid. The number and placement of electrodes were determined solely by clinical considerations.

Data acquisition relied on a 128-AC-channel Beehive Millenium monitoring system (Grass Telefactor, West Warwick, RI, USA), with sampling rate of 400 Hz and a bandpass filter between 0.1 and 70 Hz. All recording contacts were referenced to an electrode placed outside the skull (either at Fpz or on the mastoid bones).

Exploiting the same apparatus we also recorded the electromyogram (EMG) of the flexor digitorum superficialis, the electrocardiogram (ECG), and both eye movements and blinking via an electro-oculogram (EOG) derived from electrodes placed over the lateral canthus of the left eye.

Table 1 | Clinical data of patients affected by refractory epilepsy participating in the experiment.

	Age	Sex	Years since diagnosis	Education (years)	Total IQ	Sizure focus	Grid location	MRI findings
RO	43	M	25	13	69	Left fronto-mesial	Left frontal	No pathological findings
BR	39	F	11	8	95	Left temporo-mesial	Left fronto-temporal	Focal cortical dysplasia of the left temporal pole
RN	25	M	20	17	103	Right temporo-mesial	Right fronto-temporal	No pathological findings
PF	30	M	19	13	76	Left temporo-mesial	Left fronto-temporal	Left mesial temporal lobe sclerosis
DA	34	F	27	8	86	Unclear	Right fronto-temporal	No pathological findings

For each patient sex, age, years since diagnosis, years of education, total intelligence quotient (IQ), location of the seizure focus, positioning of the grid, and clinical findings revealed by magnetic resonance imaging (MRI) are given.

ELECTRODE LOCALIZATIONS

Subdural electrodes were localized exploiting a 3-D high-resolution computed tomography (CT; General Electric Light Speed Multi Slice, Milwaukee, WI, USA), made one day after grid placement. The CT scans of the electrode array were projected onto a brain template using the "Location on Cortex" package (Miller et al., 2007), which returns the location of each electrode in Tailarach coordinates. Finally, Tailarach coordinates were converted in the corresponding MNI (Montreal Neurological Insitute) coordinates using the Tailarach-Client application (Lancaster et al., 2000).

APPARATUS

Patients were lying on their beds, in front of a PC monitor (17 inch, LCD, refresh rate 75 Hz, 640 × 480 resolution) on which visual stimuli, consisting of red circles (2.4 cd/m^2) with a diameter of 2.8 cm against a dark background of uniform luminance (<0.01cd/m^2), were presented. The PC monitor was equipped with a touch screen (MicroTouch; sampling rate 200 Hz) for touch-position monitoring. A non-commercial software package, CORTEX, was used to control stimulus presentation and collect behavioral responses. The temporal arrangements of stimulus presentation were synchronized with the monitor refresh rate. Salient behavioral events (start of the trial, go-signal onset, stop-signal onset, finger detach, end of trial) were sent to the ECoG data system acquisition via TTL pulses reduced in amplitude by a voltage divider and decoupled through an optoisolator chip.

BEHAVIORAL TASKS

Patients performed a reaching version of the countermanding task previously described (Mirabella et al., 2006, 2008, 2009). The countermanding task consisted of a random mix of 67% no-stop trials and 33% stop trials (**Figure 1A**). All trials began with the appearance of a central cue which the subjects had to touch with their right index finger, holding that position for a variable period (500–800 ms). Then, in no-stop trials the central cue disappeared and, simultaneously, a peripheral target appeared (go-signal) 15 cm to the right or to the left of the center of the screen. Subjects had to perform a speeded reaching movement toward the peripheral target. In contrast, in stop trials the central cue re-appeared (stop-signal) at a variable delay (stop-signal delay; SSD) following the go-signal. In this instance subjects were instructed to inhibit their movements, holding the central cue for a period of 400–600 ms. SS trials were those in which subjects withheld the movement, while US trials were those in which they moved. Auditory feedback was given for correct responses.

The SSD is the critical dependent variable in this paradigm because stopping becomes increasingly difficult as it lengthens. To allow the participants to succeed in cancelling the response in about 50% of the stop trials, SSDs were changed using a staircase procedure (Levitt, 1971; Osman et al., 1990). In each stop trial, SSD increased by three display refresh intervals (or 39.9 ms) if in the previous stop-trial the patient succeeded in cancelling the response. SSD decreased by the same amount of time if patients failed. The staircase started from an SSD of 119.7 ms (9 refresh rates), an appropriate delay suggested by pilot experiments to quickly achieves the desired failure rate for stop trials.

We verbally informed patients about the staircase procedure and thus we made them aware that the probability of stopping would approximate to 50%, irrespective of whether they were postponing their response or not. In addition we set an upper reaction time (RT) limit for no-stop trials; whenever the RTs were longer than 800 ms, no-stop trials were aborted.

Patients were required to complete four (three patients) or six (two patients) blocks of 60 trials (240 or 360 trials). Resting periods were allowed between blocks whenever requested. Before starting the task, about 50 practice trials were given for familiarizing subjects with the apparatus.

BEHAVIORAL DATA ANALYSIS

For each experimental condition the corresponding SSRT was estimated, according to the procedure described in detail in Mirabella et al. (2009). Briefly, we exploited the so-called integration method, relying on the hypothesis of a stop process modeled by a constantly growing state variable, the SSRT, which is the time needed to cross a threshold value (Logan and Cowan, 1984; Logan, 1994; Band et al., 2003). Using the so-called mid-run estimate method (Wetherill and Levitt, 1965; Levitt, 1971), we computed the "representative SSD" as the delay that best allows the subject to withhold a response half of the times. This value was calculated as follows. In each session, the sequence of SSDs displayed ramps of either increasing or decreasing values according to the performance of the subject; the "representative SSD" was estimated by averaging the values corresponding to the midpoint

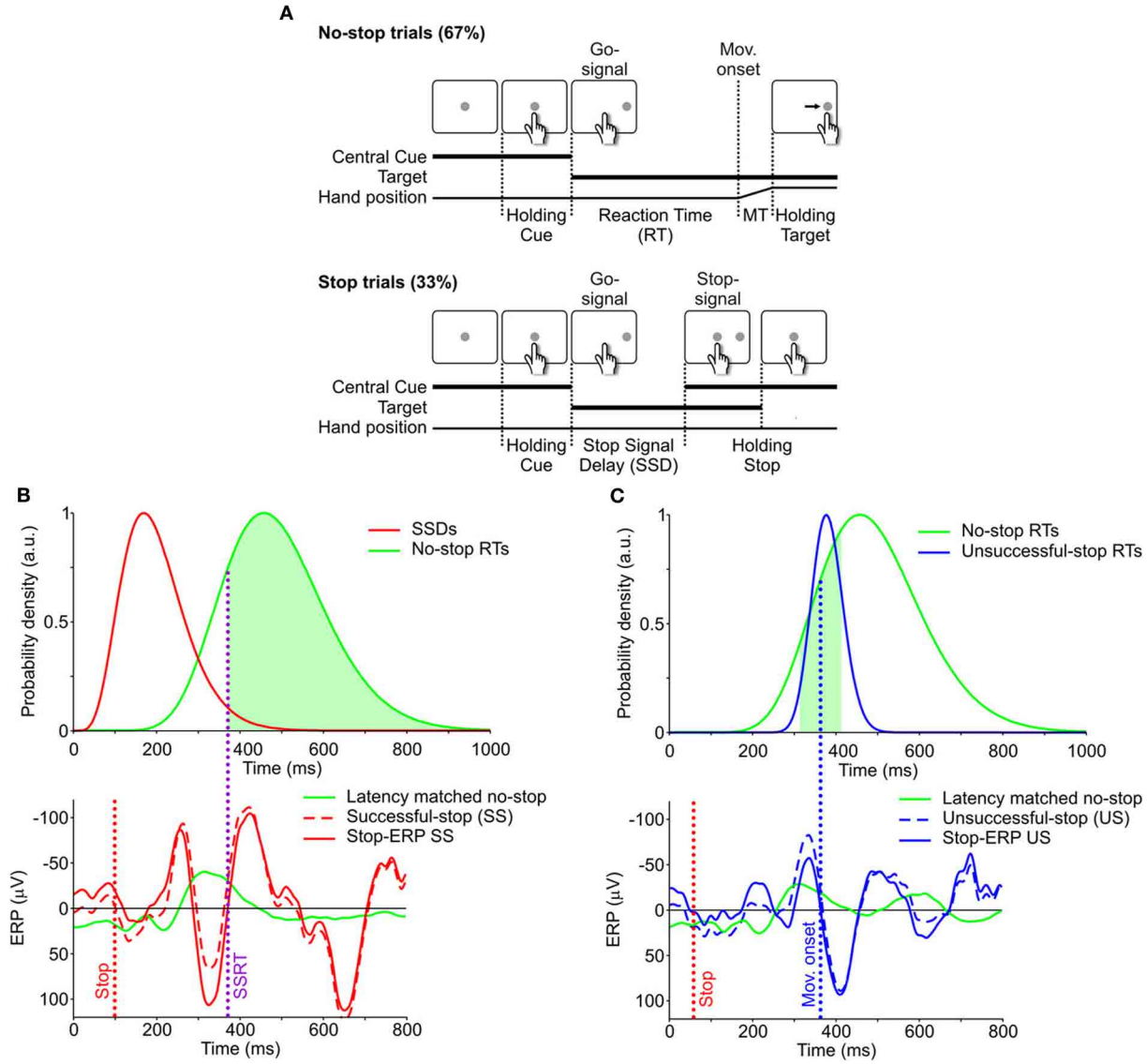

FIGURE 1 | Behavioral task and single-trial estimate of stop-ERPs. **(A)** Sequence of screen displays (white boxes) and subject responses (hand positions) during no-stop (top) and successful-stop (SS, bottom) trials of the countermanding task. No-stop trials were randomly interspersed with stop trials, which were 33% of the total trials. MT, movement time. See "Materials and Methods" for further details. **(B)** Top: distributions of SSDs in stop trials (red) and of RTs in no-stop trials (green). Bottom: event-related potentials (ERPs) aligned to the go-signal. Green curve: average ERP of "latency-matched" no-stop trials (green area in top panel), i.e., trials having RT longer than the stop signal reaction time (SSRT, vertical purple dotted line). Dashed red curve: ERP of a single SS trial. Solid red curve: stop-ERP for the same SS trial resulting from the difference between dashed-red and solid-green curves. Red vertical dotted line: stop-signal presentation. **(C)** Top panel. Distributions of RTs in unsuccessful-stop (US) trials (blue) and in no-stop trials (green, same as in panel **B**). Bottom panel: solid green curve: average ERP of no-stop trial latencies matched with US trials (green area in top panel), i.e., trials having RTs in the 100 ms interval centered around movement onset (blue vertical dotted line) of the given US trial. Blue dashed curve: ERP of a single US trial. Blue solid curve: stop-ERP resulting from the difference between dashed-blue and solid-green curves.

of every second ramp. The ending time of the stop process was calculated by integrating the RT distribution of no-stop trials from the onset of the go-signal until the integral equaled the corresponding observed proportion of US trials (Logan, 1994; see **Figure 1C**). Finally, the SSRT estimate was computed as the difference between the ending time of the stop process and the "representative SSD."

ELECTROPHYSIOLOGICAL DATA POST-PROCESSING

Electrode recordings from all patients were post-processed in order to improve the signal-to-noise ratio and to remove possible artifacts. A cross-correlation analysis showed a significant and non-specific correlation between acquired electrical potentials from electrodes of the grid and the EOG. No correlation was found with other "external" signals such as EMG, ECG, and

trigger channels used to synchronize timing of the ECoG data with behavioral events (see section "Apparatus").

To remove ocular electrical artifacts, for each subject we performed an independent component analysis (ICA) on a time interval of 400 s using the FastICA toolbox for Matlab (Natick, MA, USA; Hyvärinen and Oja, 1997; Hyvärinen, 1999). The independent component (IC) most closely correlated with every ECoG channel was the one best representing the EOG. Hence, we "cleaned" ECoG by subtracting this IC from the originally acquired signals.

Artifact-free ECoG potentials were smoothed in time by low-pass filtering time series with a moving average on a sliding window of 50 ms. This window size was a good compromise between improvements in signal-to-noise ratio and lack of temporal resolution.

Finally, we performed spatial filtering to remove possible non-specific global fluctuations in electrical potentials across nearby electrodes. We applied a variant of the surface Laplacian proposed by Hjorth (1975), recently adapted to high-density EEG data processing (Cimenser et al., 2011). Following this procedure we computed, as local reference for each ECoG electrode of the grid, the average voltage of the closest neighboring ECoG channels. Electric potential $V_i(t)$ at location i and time t was detrended as follows:

$$J_i(t) = V_i(t) - \frac{1}{M}\sum_{m=1}^{M} V_i^m(t)$$

where the sum was over the four nearest neighbors of the given electrode. On the grid border, where fewer than four neighbors were present, only the two symmetric nearby electrodes were taken into account. The following ERP analysis relied only on filtered voltages $J_i(t)$, to which we simply referred as electrical potentials or electrode voltages.

ESTIMATE OF STOP-ERPs

In this paper we adopted a novel approach to isolate the electrophysiological activity related to movement suppression, i.e., we tried to extract it at the single-trial level exploiting the following approach. In each SS trial the inhibitory activity overlaps with two other processes, (1) the perceptual elaboration of the go-signal and (2) movement planning. In order to subtract these two components and to detect the countermanding-related activity, we contrasted the neural responses during a single SS trial with that recorded in the so-called "*latency-matched*" no-stop trials, i.e., those trials whose RTs were longer than the sum of SSD and SSRT calculated from the same data (see Hanes et al., 1998 and Mirabella et al., 2011). These are the trials in which, given the length of the SSRT, the movement would have been canceled if the stop signal had been presented at the given SSD (represented by the subset of trials under the green area in the top panel of **Figure 1B**). We first computed the average ERPs of latency-matched no-stop trials (**Figure 1B**, bottom panel), centered on the go-signal, and we obtained a "stop-ERP" (dashed line) by subtracting it from the ERP measured during a single SS trial (continuous line).

Using the same method we also computed the US ERPs by subtracting the ERP in a given US trials from the average ERP computed from the subset of no-stop trials corresponding to a 100 ms RT interval centered around the time of movement onset of the US trial (**Figure 1C**, green area of the top panel). These are the trials in which the movement would not have been canceled if the stop-signal had been presented. This comparison reveals whether a stop-ERP was present even though the subject made a mistake.

RESULTS

BEHAVIORAL RESULTS

Behavioral data relevant to the performance of the countermanding task are reported in **Table 2**. The average SSRT was compatible with that measured in epileptic patients tested in similar conditions (Swann et al., 2009). Some subjects (PF and BR) showed a lower stopping rate than desired; however, they performed the task sufficiently well. Furthermore, for each subject we found that in all occurrences the distributions of the RTs of US trials were significantly shorter than those of no-stop trials (Kolmogorov–Smirnov test, $P < 0.05$), as required by the race model (Logan and Cowan, 1984; Logan, 1994; see also Boucher et al., 2007) in order to obtain a reliable estimate of the SSRT.

SINGLE-TRIAL DETECTION OF STOP-ERP IN SS TRIALS

Neural activity correlated with inhibition processes might be effectively coupled with a machine decoder or an automated controller only if it fulfills a minimum requirement: it has to be

Table 2 | Behavioral data describing the performance in the countermanding task.

	SSRT (ms)	Representative SSD (ms)	*P*(failure)	Mean RTs (ms) of no-stop trials (±SEM)	Mean RTs (ms) of US trials (±SEM)
RO	258.9	256	0.45	580.7 (±19.7)	445.9 (±19.4)
BR	260	119.8	0.40	614.0 (±25.8)	436.8 (±34.3)
RN	241.2	483.6	0.54	390.6 (±9.7)	336.9 (±7.65)
PF	195.38	483.6	0.39	741.3 (±23)	518.0 (±39.9)
DA	271.8	185.2	0.48	511.2 (±16.4)	380.3 (±7.1)
Mean	245.5 ± 13.4	309.7 ± 78.3	0.45 ± 0.03	567.6 (±57.9)	423.6 (±30.8)

For each patient the duration of the suppression process (the stop-signal reaction time, SSRT), the representative stop signal delay (SSD), the probability of cancelling a response [P(failure)], the mean reaction times (RTs) of no-stop and unsuccessful-stop trials are reported. The average values (±SEM) are shown in the bottom row.

detectable at the single-trial level with high enough time resolution. From a visual inspection of average ERPs in stop trials aligned to the stop-signal appearance, we found evidence of a characteristic pattern of delayed deflections of electrode voltages. To find out whether such average ERP complexes were observable in single trials we performed a correlation analysis comparing the ERPs from each couple of SS trials (see **Figure 2A**). As stop-ERPs are likely to occur at different times in different trials, we measured the Pearson correlation coefficient ρ between ERPs artificially shifted in time (**Figure 2A**, **right**). Exploiting this procedure we aimed to identify the time shift which would give the maximum ρ (**Figure 2A**, **left**). We considered only ERPs in a time interval between 100 and 350 ms following stop-signals. For each grid electrode we computed the correlation between all possible couples of SS trials. The matrix of maximum ρ values between couples of SS trials from the same example channels (**Figure 2B**) clearly shows that in most instances a high value of ρ (reddish pixels) was found. This indicates that the same,

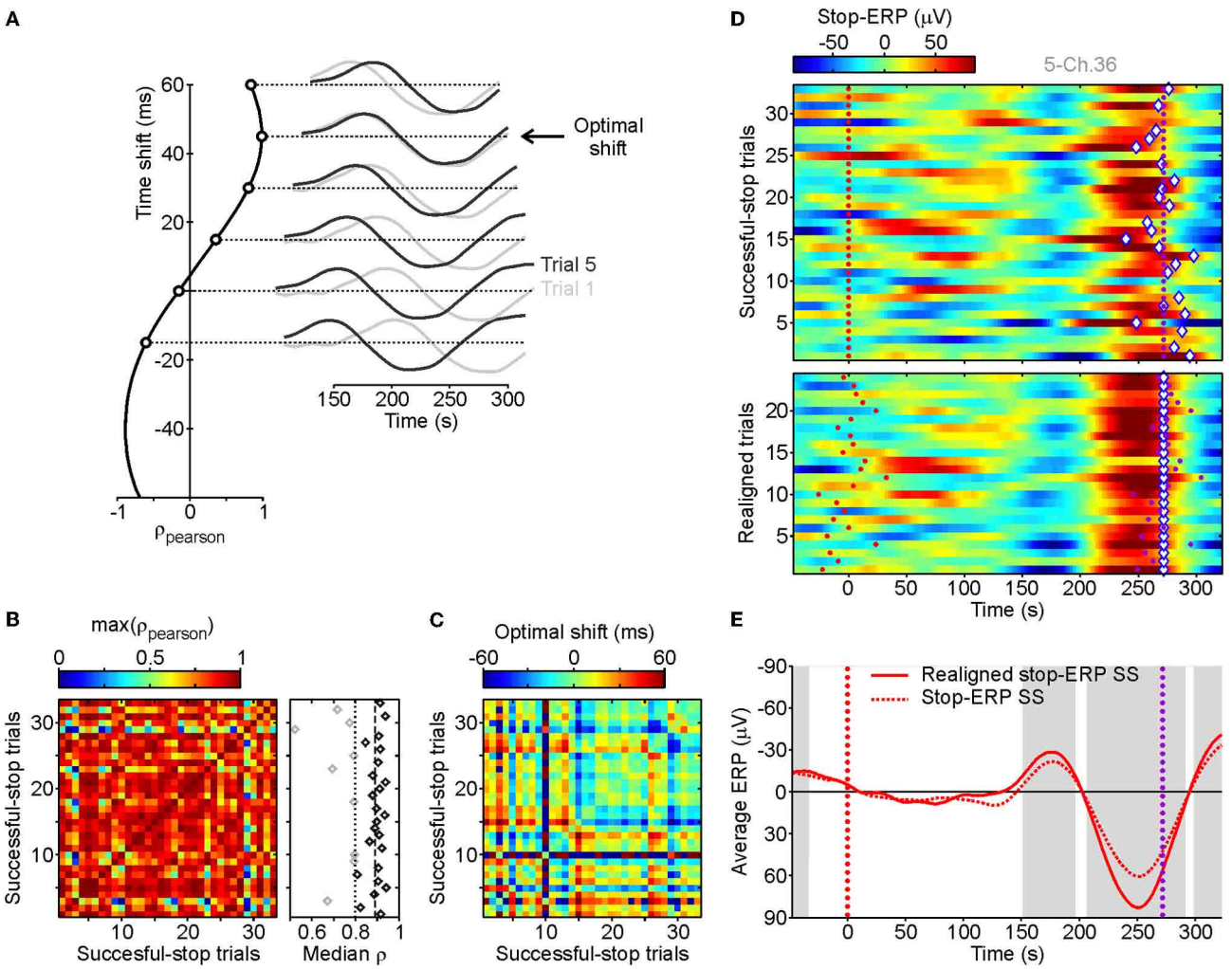

FIGURE 2 | Stop-ERP detection at single-trial level for successful-stop (SS) trials. (A) Pearson correlation (ρ, leftmost panel) between two stop-ERPs derived from the two example SS trials, represented in the rightmost panel (dark and light gray curves), obtained when they are artificially and progressively shifted in time. The optimal shift is the time shift for obtaining the maximum positive correlation (45 ms). **(B)** Matrix of maximal ρs obtained at the optimal shifts between all SS trials for one grid contact. Rightmost panel, medians of the maximal ρs for each SS trial (represented in a row of the left matrix). Vertical dashed line, median of the median ρs across SS trials. Vertical dotted line, lower threshold for selected SS trials (black diamonds represent SS trials with median correlation above threshold, gray diamonds represent those below threshold; see Result section for details). **(C)** Matrix of optimal shifts between SS trials leading to the maximal correlation. Optimal shifts ranged from −60 to +60 ms. **(D)** Top panel: raster plot of stop-ERPs in SS trials from the same example recording. Red dotted line, stop-signal occurrence. Purple dotted line, end of the SSRT. Diamonds, absolute time shift related to the SSRT for each SS trial estimated from the time shift matrix of panel **C**. Bottom panel: realignment of stop-ERPs with respect to the absolute time shift of SS trials with a median correlation above the threshold ($n = 24$ of 33). **(E)** Average stop-ERP obtained from trials of top and bottom raster plots of panel **D**. Gray areas, time intervals at which the realigned stop-ERP was significantly different from 0 (Wilcoxon signed-rank test, $P < 0.01$).

or a very similar, ERP complex was present in most SS trials. In order to detect in which trials the stop-ERPs emerged more neatly, we computed the median of the maximum ρ for each SS trial (**Figure 2B**, **right**). We discarded those trials with median values lower than a threshold (dotted vertical line) as they did not show the typical stop-ERP complex (gray diamonds). The threshold value was computed as the median of the medians (dashed vertical line) minus three times the standard deviation (SD) of the 50% larger medians (black diamonds on the right of dashed line). **Figure 2C** represents the matrix of the "optimal" time shifts producing the maximum ρ matrix. From this matrix we extracted the "absolute" time shift for each trial, that is, the amount of time shift needed to realign the voltage trace in order to obtain the maximum ρ. The array of absolute time shifts X was carried out by inverting the linear equation $A\ X = B$, where values of B were the optimal shifts shown in **Figure 2C** and A was a matrix of 0, 1, and -1 to express optimal shifts as differences between absolute time shifts. Because such a linear system is over-determined (A was not a square matrix) its solution is the best one in the least-squares sense.

In the top panel of **Figure 2D**, voltage changes with time for each SS trial are reported with respect to the end of the SSRT in a raster plot. In each trial the absolute time shift is indicated by a diamond. Stop-ERP complexes have a recognizable negative–positive peak sequence. To make it clearer we realigned the selected SS trials with respect to the absolute time shift (**Figure 2D**, **bottom**). The realignment gave an improvement in the signal-to-noise ratio in the average ERPs, as shown in **Figure 2E** where the original and realigned stop-ERPs are superimposed. Interestingly, this ERP complex started to emerge within the SSRT, that is, voltage deflection was significantly different from 0 before the end of the SSRT (first gray area). This suggests a causal relationship between the average stop-ERPs and the ongoing inhibition process.

DISTRIBUTION OF AVERAGE STOP-ERPs ACROSS THE CORTEX

Subdural grids give the opportunity of simultaneously sampling wide regions of the cortex with a relatively high spatial resolution, so this technique makes it possible to investigate the cortical regions where the stop-ERPs originate and which areas are involved in the suppression process.

As a preliminary step we selected those recording channels with no pathological EEG activity throughout the investigation (e.g., pathological interictal activity) and those located outside the seizure onset area (identified by expert neurologists PQ and GD). To be as objective as possible, for each electrode contact we computed the trial-by-trial SD of ERPs in the 100 ms following the go-signal in SS trials (see **Figure 3A** for an example patient). To discard noisy channels we computed a threshold value as follows. We calculated the median of the SDs across all the grid contacts, selected the 50% of channels with the lowest SDs and then calculated the standard deviation of their SDs; we then added three times this SD to the median to give the threshold value. Those electrodes with SDs larger than the threshold value were excluded. For the remaining channels we computed the realigned stop-ERPs, as previously described. As can be seen from **Figure 3B**, the average stop-ERP was selectively expressed in only a few areas (mainly BA4, BA6, BA9), where it occurred well before the end of SSRT (purple dotted lines). The selective occurrence of average stop-ERPs in this example patient can be better appreciated from the contour map of **Figure 3C** where the largest peaks of each ERP are plotted. A hot spot in BA6 (PMA) is apparent, together with smaller peaks located at other contacts of the same area and in the nearby regions BA4 (M1) and BA9 (dFMC) (the same dashed regions as in **Figure 3B**).

To identify grid contacts showing the largest average stop-ERPs, we measured the stop-ERP size by computing the integral of the absolute voltage within those time intervals where the ERPs were significantly different from 0 (gray intervals) during the SSRTs (**Figure 3D**). Then we selected those channels whose ERP size was larger than the median plus three times the SD of the ERP sizes of the 50% of contacts with the smallest sizes. In the example patient, **Figure 3D**, 14 out of 47 channels passed the selection.

The same analysis was performed across all other patients, and overall we retained a population of 39 electrodes. The distribution of these contacts (**Figure 4A**) clearly showed that most of them were located either in M1, in PMA or in dFMC. Other BAs never had more than two channels with large enough average stop-ERPs (blue bar). Importantly, in the overwhelming majority of contacts the onset time of average stop-ERPs always preceded the end of SSRT (**Figure 4B**, **right**, average time lag: -82.7 ± 7.3 ms), suggesting a causal relationship between these ERPs and successful movement inhibition. Furthermore, average stop-ERP complexes seemed to emerge first in motor cortices (M1, PMA, BA9) and later in other areas (t-test, $\mathrm{df} = 37$; $P < 0.05$).

We also evaluated the similarity between average stop-ERPs across all selected channels, computing the time lag between the negative and positive (N-P) peak of the complex. As shown in **Figure 4C**, we found that the distribution of this time interval was fairly narrow, the SD being only 21% of the mean (92.1 ± 19.4 ms; SE 3.1 ms); this supports the idea of the existence of a stereotyped stop-ERP complex across cortical areas and subjects.

SINGLE-TRIAL DETECTION OF STOP-ERP IN US TRIALS

We have interpreted the emergence of stop-ERP at the single-trial level as a footprint of the inhibitory process of pending reaching arm movements. Clearly it could not be linked to either eye movements or blinking as ocular artifacts were removed (see Materials and Methods). The ERP could not even be related to the sensory processing of the go-signal given that we subtracted neural responses during SS trials from those recorded during no-stop trials (see Materials and Methods). However, it could be argued that the countermanding-related modulation during SS trials could be driven by the visual presentation of the stop-signal. In fact, only in stop trials did the stop-signal appear after the SSD.

To rule out this possibility we compared the neural activity in SS and US trials as the stop-signal is presented in both type of trials and therefore possible differences cannot be ascribed merely to its appearance.

In top panel of **Figure 5A**, the raster plots of ERPs computed from US trials were shown for the same contact as illustrated

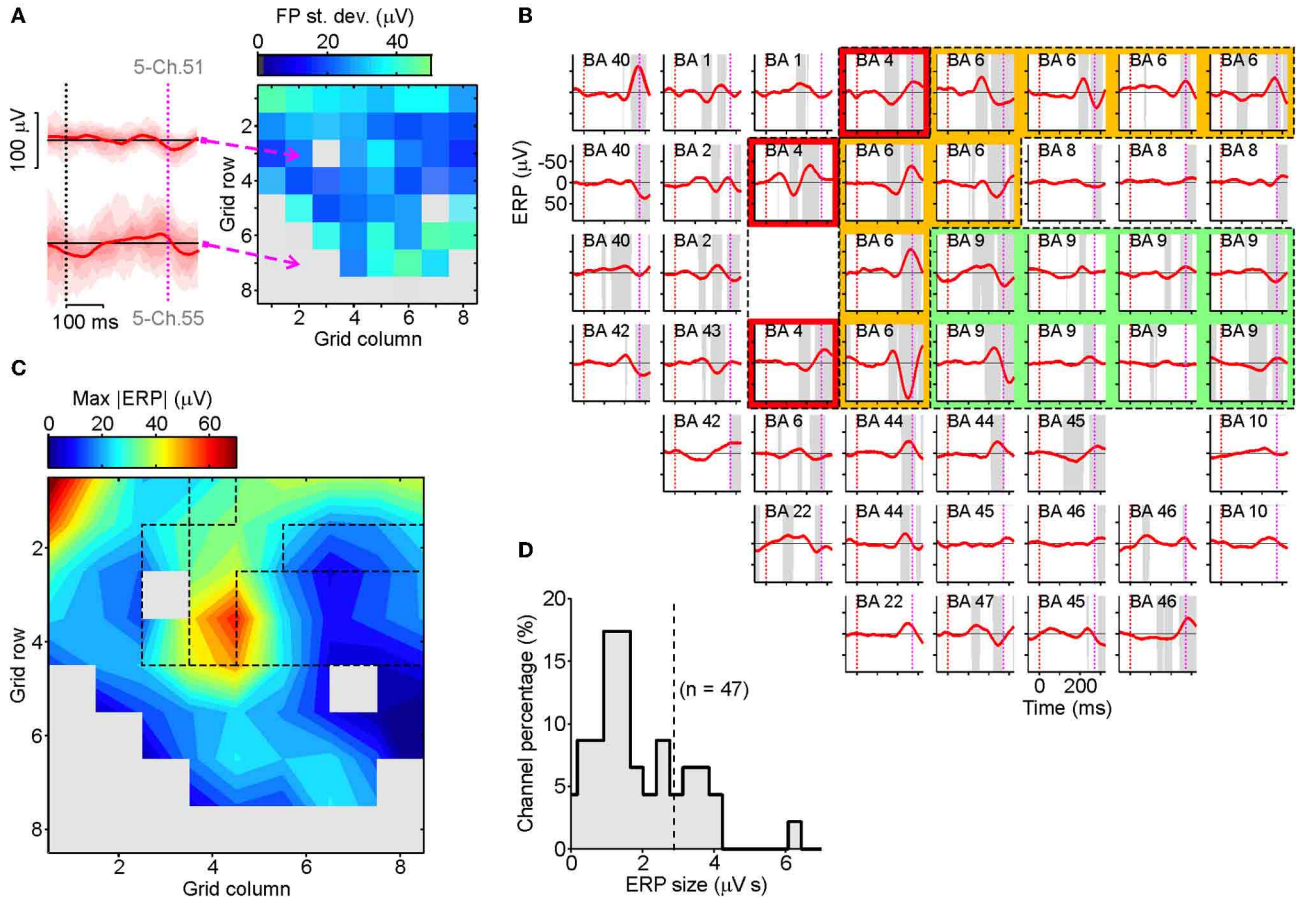

FIGURE 3 | Spatiotemporal distribution of stop-ERPs in successful-stop (SS) trials. (A) Map of the standard deviations (SDs) of field potentials (FPs) in SS trials at each contact of the grid for an example patient (right). SDs of FPs were evaluated in a time window of 100 ms following the go-signal onset. Gray elements were excluded from further analyses because they had SDs greater than a threshold value (see Results section for further details). Left, ERPs for two example channels with low (top) and high (bottom) voltage variability. Solid curves, average ERPs. Reddish areas represent time course of ERP distribution across trials: different shadings mark percentiles multiples of 10. **(B)** Average realigned stop-ERPs (solid red curves) of SS trials centered on stop-signal appearance corresponding to the selected channels. Other conventions as in **Figure 2E**. Subplot labels: Broadmann's areas (BAs) over which electrodes were positioned. Colored areas: electrodes placed over the primary motor cortex (red, BA4), the premotor cortex (yellow, BA6) and the dorsal fronto-median cortex (green, BA9). **(C)** Smoothed contour map of the maximum absolute stop-ERP amplitudes (ERP) shown in panel **B**. Dashed areas correspond to the colored area of panel **B**. **(D)** Histogram of the stop-ERP sizes of panel **B**. Stop-ERP sizes were computed as the integral of absolute values of stop-ERP voltage deflections in the interval periods marked by gray areas within SSRT. Dashed line: threshold value for selecting the subset of channels with large enough stop-ERPs used for population analyses (see text for details).

in **Figure 2D.** Interestingly, using the same procedure described in section "Behavioral Results," we found in several US trials stop-ERPs closely matched with those detected in SS trials. They occurred sparsely across trials, mainly when the RTs were longer (top trials in **Figure 5A**, **top**). The realignment of stop-ERPs according to the optimal time shift (**Figure 5A**, **bottom**) evidently displayed the similarity with ERP complexes of SS trials. The average ERP of US trials (**Figure 5B**, solid blue curve) showed that, although the shape of stop-ERPs was preserved, voltage deflections in SS trials (red curve) occurred earlier than in US trials. The presence and the timing of stop-ERPs in US trials ruled out the possibility that such ERPs could be merely a visually-evoked reaction to the stop-signal. In fact, if this were the case then ERPs should have occurred in both SS and US trials with the same frequency and average latency from the stop-signal appearance.

We tested the robustness of this result across our population by probing whether the 39 contacts at which we previously detected stop-ERPs in SS trials also showed them in US trials. We found that a large subset of electrodes ($n = 32$ of 39; 82%) showed stop-ERPs in both types of trial. To assess the latency between the two average stop-ERPs, we computed the time lag between the midpoint of the negative and the positive peaks of the complex and the stop-signal presentation. Then we calculated the difference between such time lags for US and SS trials. As shown in **Figure 5C**, average stop-ERPs in US trials occurred mainly later than those of SS trials (mean delay: 6.9 ± 2.1 ms, Wilcoxon signed-rank test, $P < 0.01$).

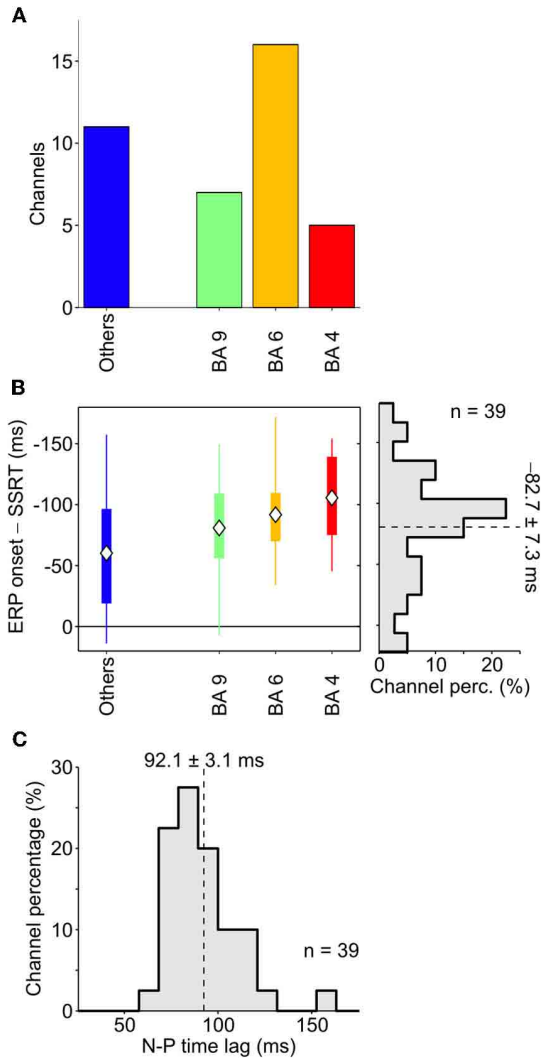

FIGURE 4 | Onset of stop-ERPs in successful-stop trials. (A) Number of channels showing large enough average stop-ERPs ($n = 39$) grouped by Brodmann area (BA; see text for details). Blue bar (others) represents those areas where channels were not selected more than twice across all patients **(B)** Box plot of stop-ERP onsets measured with respect to the end of SSRT across all selected channels in all patients. Stop-ERP onset was defined as the first time that an electrode voltage was significantly different from 0. Diamonds indicate average onset times. Thick bars indicate the first and the third quartile. Vertical lines indicate the extreme time lags in the channel group. Right, distribution of stop-ERP onset times. Dashed line, average stop-ERP onset (± SEM) across all selected channels. **(C)** Distribution of time lags between negative and positive (N-P) peaks across stop-ERPs. Dashed line, average peak distance (± SEM).

Finally, we worked out a detection index D to quantify how many times a stop-ERP was detected in US trials with short versus long RTs as follows:

$$D = (F_{\text{late}} - F_{\text{early}})/(F_{\text{late}} + F_{\text{early}})$$

where F_{early} and F_{late} are, respectively, the fraction of stop-ERPs detected in the first and in the last 33% of US trials sorted by RTs, as in **Figure 5A**. The index can be negative down to minus

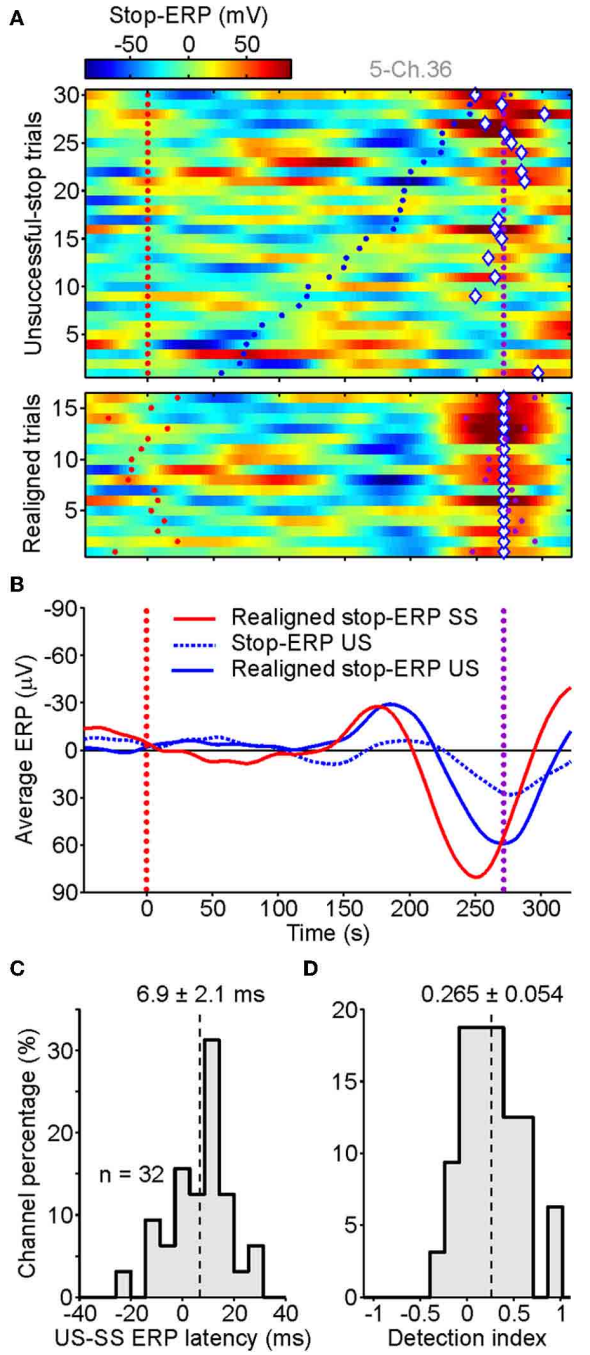

FIGURE 5 | Stop-ERPs in unsuccessful-stop (US) trials. (A) Raster plots of stop-ERPs in US trials from the same channel illustrated in **Figure 2**. Top panel. Red dotted line, stop-signal occurrence. Purple dotted line, end of the SSRT. Blue dots: movement onset time. Diamonds, optimal shift with respect to SSRT (purple dots; see text for futher details). Bottom panels: stop-ERP of US trials realigned to the optimal shift. **(B)** Average of realigned stop-ERPs of SS trials (solid red, the same as in **Figure 2E**) and US trials (solid blue). Dotted blue curve, average across not-shifted US trials. **(C)** Distribution of latency differences between realigned stop-ERPs of US and SS trials (see text for details). **(D)** Histogram of detection index values indicating how many stop-ERPs were found for late movement onset times (last third of US trials in panel **A-top**) versus early detaches (first third of US trials).

one, when stop-ERPs are not present in the late fraction of US trials, or up to plus one, when stop-ERPs are present only in the fraction of US trials with long RTs. The result of this analysis (**Figure 5D**) shows a distribution of D significantly shifted above 0 (mean: 0.265 ± 0.054; Wilcoxon signed-rank test, $P < 0.001$), confirming that most stop-ERPs occur for those US trials with the longest RTs.

DISCUSSION

ROLE OF MOTOR CORTICES IN INHIBITING REACHING ARM MOVEMENTS

The main goal of the present study was to investigate the neural activity associated with arm movement suppression across several brain regions, mostly located over the lateral surface of the frontal lobe. Among these areas motor cortices (e.g., PMA, Coxon et al., 2006; M1, Mirabella et al., 2011), as well as IFG (Aron et al., 2003) have been shown to be involved in preventing planned arm movements. However, to date none have been recorded simultaneously from all these regions exploiting the high spatiotemporal resolution allowed by the ECoG. To this aim we did not select *a priori* any electrode but, after discarding those contacts with a high noise level, we analyzed the activity of all the remaining ones.

In addition, taking advantage of the larger amplitude of EEG signals recorded from subdural electrodes with respect to scalp EEG signals, we extracted neural activity at the single-trial level (stop-ERP) related to the inhibitory process of reaching movements and excluding other confounding factors (e.g., the appearance of the go-signal, eye movement or movement planning). We found that a characteristic signature of the cancellation process occurs in the great majority of SS trials. Because, as expected, there was a trial-by-trial variability in the timing of stop-ERP emergence, we improved the signal-to-noise ratio by realigning the trials with respect to the end of the SSRT (see section "Single-trial detection of stop-ERP in SS trials" for further details). Then we computed the average stop-ERP across realigned trials at each contact and we selected those contacts that had the largest voltage amplitudes. At the end of this "blind" procedure we found that the selected recording channels were mainly located in M1, PMA, and dFMC. Crucially, the analysis of the stop-ERP onset revealed that the change in the electrical activity took place well before the behavioral estimate of the end of the cancellation process. This finding indicates that these areas are causally involved in stopping ongoing movements and that they are probably the source of the N200/P300 complex found in scalp EEG studies.

Clearly, these are not the only neural substrates of the cancellation process. In fact, it is very well known that ERPs are generated by fixed-latency phase-locked responses, especially at low frequencies (Heinze et al., 1994). At the same time brain dynamics also entail non-phase-locked oscillations (Tallon-Baudry and Bertrand, 1999; Bernat et al., 2007), as those occurring when multiple task conditions and/or many stimulus types are processed (Jung et al., 2001). Therefore, there is no contradiction between our results and those obtained by Swann et al. (2009) showing an increase in the beta frequency band in the right IFG for SS versus US trials. In fact it is known that the IFG is implicated in several cognitive functions such as stimulus-driven attention (Corbetta and Shulman, 2002), response selection (Mostofsky and Simmonds, 2008), working memory (Mars et al., 2008) and inhibitory control (Aron et al., 2003).

Interestingly, Swann et al. (2009) demonstrated that, in agreement with our data, M1 is involved in inhibitory processes because US trials induce a larger desynchronization in the alpha/beta band than do SS trials. Even though they did not explore PMA activity, the study by Mirabella et al. (2011) identified in the dorsal part of PMA of monkeys a population of neurons showing a pattern of activity which correlates with the suppression of programmed arm movements. Overall our findings are fully congruent with the existing literature, but for the first time they offer a clearer picture of the involvement of motor cortices in the countermanding task, strongly suggesting that inhibition occurs at relatively low levels in the motor hierarchy (see also Stinear et al., 2009). We also found that the dFMC has a role in voluntarily inhibiting actions based on external stimuli, extending previous findings indicating a role for this area just in the suppression of self-generated movements (Brass and Haggard, 2007). Classically this is considered a high hierarchy motor area; however, at least in this context it seems to behave similarly to lower lever motor regions.

Motor cortices are probably the final target on which the inhibitory command generated by the frontal–basal ganglia–thalamic network acts. The components of this network and the precise way it works are still hotly debated. However, on the basis of the available anatomical and physiological data, we can put forward the following hypothesis of network functioning. Whenever we are about to move, the motor cortices (M1 and PMA) send an efferent copy of their descending output to the input components of the basal ganglia, the striatum, and the STN. These projections are somatotopically organized (Mink, 1996) and influence the activity in the thalamocortical pathway, projecting back to M1 and PMA. Both the STN (Aron and Poldrack, 2006; van den Wildenberg et al., 2006; Mirabella et al., 2011) and the striatum (Li et al., 2008; Zandbelt and Vink, 2010) are involved in inhibitory control, but possibly they have different roles (see Mirabella et al., 2011). STN should have a direct role in the suppression of the movement, while the striatum should play a role in proactive control during countermanding. Whenever the stop signal is presented its appearance would be detected by some of the frontal areas of the network, probably by the right IFG, given that it monitors unexpected changes in the external environment (Corbetta and Shulman, 2002). In its turn the IFG would activate the STN through the hyperdirect pathway (Nambu et al., 2002), allowing for quick braking of the motor output from motor cortices (Aron and Poldrack, 2006; Aron et al., 2007). Therefore, according to this schema PMA and M1 would represent the final target of the inhibitory command elaborated by the frontal–basal ganglia–thalamic network.

It has to be stressed that in the present study we could not assess whether the inhibitory network is right-lateralized (Aron et al., 2007). Among our patients, three had a grid placed over the surface of the fronto-temporal lobes of the right hemisphere and two had a grid over the same regions of the left hemisphere. Qualitatively, data were not different even though subjects were right-handed and all used the dominant hand.

This might be explained by the fact that we mainly found inhibitory signals in PMA and M1. These regions are known to be bilaterally activated during the production of reaching movements (Kawashima et al., 1998; Donchin et al., 2002; Cisek et al., 2003) and thus it is likely that, to suppress a reaching movement, inhibitory commands have to be sent bilaterally to both motor cortices. This topic definitely deserves further studies.

Finally, it is noteworthy to underline that the present findings can be affected to some extent by the coarse spatial sampling of our clinical grids. Indeed the optimal inter-electrode distance of 1.25 mm (Srinivasan et al., 1998; Freeman et al., 2003) is much smaller than the 1 cm spacing of the grids we employed. Thus, neural activity might be more localized than that we have detected. Furthermore, our procedure for electrode localization, based on the projection of electrode contacts onto a brain template (see section "Electrode localizations"), is less precise than the estimates relying on the projection of the electrode position on the subjects' own brain maps. In particular, as all the selected electrodes in BA 9 where just on the border with PMA we suspect they actually might be located in PMA.

STOP-ERP IN US TRIALS AND THE HORSE RACE MODEL

In its original formulation the race model assumed that the go process (the process initiated by the go-signal leading to the execution of the movement) and the stop process (the one initiated by the stop-signal leading to the inhibition of the movement) were stochastically independent, i.e., their ending times were uncorrelated (Logan and Cowan, 1984). However, complete independence between the go and stop process is unlikely. In fact, Boucher et al. (2007) revised the model, proposing that the go and stop processes are independent for most of their duration but they interact briefly and strongly near the end of the race (interactive race model). However, even in this interactive race model, the length of the SSRT primarily reflects the period during which stop and go processes are independent, so its predictions correspond to those of the original race model.

One prediction of the race model testing the independence assumption between go and stop processes is that the mean RT of US trials should be shorter than the mean RT of no-stop trials (Logan and Cowan, 1984). That is because reaching movements were produced in both the no-stop trials and the US, but the latter were initiated because the go process finished before the stop process. Therefore, considering the distribution of the RTs of the no-stop trials, the responses that escape inhibition should be those corresponding to reaching movements that had RTs shorter than the SSD plus the estimated SSRT. We found that this prediction was satisfied for all patients.

Nonetheless we also found that stop-ERPs occurred not only when subjects successfully stopped their movement but also when they wrongly moved their arm despite the occurrence of a stop-signal. Crucially, stop-ERP in US trials are mainly present in the fraction of US trials with long RTs (see **Figure 5A**). This finding is compatible with a late modulation of neural activity determined by an ineffective stop process, namely by a stop processes which is incapable of suppressing an arm movement. In conclusion, stop-ERPs in US trials might represent the effect of the interaction between the stop and the go process taking place around the end of the race (Boucher et al., 2007), when the stop process loses.

DECODING OF RESPONSE INHIBITION: BRAIN-COMPUTER INTERFACE AND REHABILITATION

Decoding cortical signals underpinning motor decisions is the backbone of brain-computer interfaces (BCI) to recover or improve motor functions (Nicolelis, 2003; Schwartz, 2004). In particular, ECoG signals, although more invasive, have been proven to allow a more effective decoding of motor intentions and to outperform EEG-based BCI (Leuthardt et al., 2004; Schalk et al., 2008; Schalk, 2010).

Effective BCIs have to read not only detailed information about overt movements to perform but also their volitional control (Fetz, 2007; Moritz et al., 2008). In other words, to drive external devices, automated decoders have to access not only motor program features but also those signals indicating the intention to move. From this perspective, it is rather surprising that the wide literature on BCIs has paid no attention to neural correlates of cognitive and behavioral inhibition. The capability of detecting a neural correlate of response inhibition at the single-trial level from ECoG signals might represent a first step in the direction of taking into account all the features of voluntary movement. BCI could rely on the stop-ERPs we have detected to take into account a sudden need to suppress planned movements, especially because on average they appear early, i.e., about 100 ms before the SSRT.

Developments in BCI have also provided robust evidence that closed-loop approaches, in which decoding performances are fed back, allow subjects to adapt their brain activity to BCI capabilities and constraints, and hence to improve motor control (Nicolelis, 2003; Schwartz, 2004). Recently, closed-loop BCIs have been suggested as a way to selectively enhance brain plasticity, envisaging more effective rehabilitative approaches to recovering from motor and cognitive impairments such as those due to strokes (Dobkin, 2007; Daly and Wolpaw, 2008). Such improvements can be driven by a closer monitoring of how brain activity changes with exercise well before any behavioral output. Another possibility is to induce subjects to perform suited mental practice, such as motor imagery, capable of speeding up an activity-dependent plasticity for proper rewiring of compromised cortical circuits (Millán et al., 2010; Wang et al., 2010). Accessing in real time the cortical fingerprints of the suppression process extends the possible clinical applications of such neurofeedback. In fact, rehabilitation strategies for cognitive deficits characterized by inefficient inhibitory control (Chamberlain et al., 2005; Chamberlain and Sahakian, 2007), such as obsessive–compulsive disorder or attention-deficit hyperactivity disorder, might benefit from closed-loop BCIs relying on stop-ERP detection.

ACKNOWLEDGMENTS

We thank all patients participating in the study, the nurses and technicians assisting us and the patients during the experiments, and Sara Iaconelli for the help provided with data collection. This research was supported by the Italian Ministry of Work, Health and Social Policies (Bando Giovani Ricercatori 2007 to G. Mirabella) and by the Italian Ministry of University and Research (PRIN n.2008_RBFNLH_005 to G. Mirabella).

REFERENCES

Aron, A. R., Behrens, T. E., Smith, S., Frank, M. J., and Poldrack, R. A. (2007). Triangulating a cognitive control network using diffusion-weighted magnetic resonance imaging (MRI) and functional MRI. *J. Neurosci.* 27, 3743–3752.

Aron, A. R., Fletcher, P. C., Bullmore, E. T., Sahakian, B. J., and Robbins, T. W. (2003). Stop-signal inhibition disrupted by damage to right inferior frontal gyrus in humans. *Nat. Neurosci.* 6, 115–116.

Aron, A. R., and Poldrack, R. A. (2006). Cortical and subcortical contributions to Stop signal response inhibition: role of the subthalamic nucleus. *J. Neurosci.* 26, 2424–2433.

Band, G. P., van der Molen, M. W., and Logan, G. D. (2003). Horse-race model simulations of the stop-signal procedure. *Acta Psychol. (Amst.)* 112, 105–142.

Bernat, E. M., Malone, S. M., Williams, W. J., Patrick, C. J., and Iacono, W. G. (2007). Decomposing delta, theta, and alpha time–frequency ERP activity from a visual oddball task using PCA. *Int. J. Psychophysiol.* 64, 62–74.

Boucher, L., Palmeri, T. J., Logan, G. D., and Schall, J. D. (2007). Inhibitory control in mind and brain: an interactive race model of countermanding saccades. *Psychol. Rev.* 114, 376–397.

Brass, M., and Haggard, P. (2007). To do or not to do: the neural signature of self-control. *J. Neurosci.* 27, 9141–9145.

Chamberlain, S. R., Blackwell, A. D., Fineberg, N. A., Robbins, T. W., and Sahakian, B. J. (2005). The neuropsychology of obsessive compulsive disorder: the importance of failures in cognitive and behavioral inhibition as candidate endophenotypic markers. *Neurosci. Biobehav. Rev.* 29, 399–419.

Chamberlain, S. R., and Sahakian, B. J. (2007). The neuropsychiatry of impulsivity. *Curr. Opin. Psychiatry* 20, 255–261.

Chambers, C. D., Bellgrove, M. A., Stokes, M. G., Henderson, T. R., Garavan, H., Robertson, I. H., Morris, A. P., and Mattingley, J. B. (2006). Executive "brake failure" following deactivation of human frontal lobe. *J. Cogn. Neurosci.* 18, 444–455.

Cheney, P. D., and Fetz, E. E. (1980). Functional classes of primate corticomotoneuronal cells and their relation to active force. *J. Neurophysiol.* 44, 773–791.

Churchland, M. M., Cunningham, J. P., Kaufman, M. T., Ryu, S. I., and Shenoy, K. V. (2010). Cortical preparatory activity: representation of movement or first cog in a dynamical machine? *Neuron* 68, 387–400.

Cimenser, A., Purdon, P. L., Pierce, E. T., Walsh, J. L., Salazar-Gomez, A. F., Harrell, P. G., Tavares-Stoeckel, C., Habeeb, K., and Brown, E. N. (2011). Tracking brain states under general anesthesia by using global coherence analysis. *Proc. Natl. Acad. Sci. U.S.A.* 108, 8832–8837.

Cisek, P., Crammond, D. J., and Kalaska, J. F. (2003). Neural activity in primary motor and dorsal premotor cortex in reaching tasks with the contralateral versus ipsilateral arm. *J. Neurophysiol.* 89, 922–942.

Corbetta, M., and Shulman, G. L. (2002). Control of goal-directed and stimulus driven attention in the brain. *Nat. Rev. Neurosci.* 3, 201–215.

Coxon, J. P., Stinear, C. M., and Byblow, W. D. (2006). Intracortical inhibition during volitional inhibition of prepared action. *J. Neurophysiol.* 95, 3371–3383.

Crammond, D. J., and Kalaska, J. F. (2000). Prior information in motor and premotor cortex: activity during the delay period and effect on pre-movement activity. *J. Neurophysiol.* 84, 986–1005.

Daly, J. J., and Wolpaw, J. R. (2008). Brain-computer interfaces in neurological rehabilitation. *Lancet Neurol.* 7, 1032–1043.

Dimoska, A., and Johnstone, S. J. (2008). Effects of varying stop-signal probability on ERPs in the stop-signal task: do they reflect variations in inhibitory processing or simply novelty effects? *Biol. Psychol.* 77, 324–336.

Dobkin, B. H. (2007). Brain-computer interface technology as a tool to augment plasticity and outcomes for neurological rehabilitation. *J. Physiol.* 579, 637–642.

Donchin, O., Gribova, A., Steinberg, O., Mitz, A. R., Bergman, H., and Vaadia, E. (2002). Single-unit activity related to bimanual arm movements in the primary and supplementary motor cortices. *J. Neurophysiol.* 88, 3498–3517.

Evarts, E. V. (1968). Relation of pyramidal tract activity to force exerted during voluntary movement. *J. Neurophysiol.* 31, 14–27.

Fetz, E. E. (2007). Volitional control of neural activity: implications for brain-computer interfaces. *J. Physiol.* 579, 571–579.

Floden, D., and Stuss, D. T. (2006). Inhibitory control is slowed in patients with right superior medial frontal damage. *J. Cogn. Neurosci.* 18, 1843–1849.

Freeman, W. J., Holmes, M. D., Burke, B. C., and Vanhatalo, S. (2003). Spatial spectra of scalp EEG and EMG from awake humans. *Clin. Neurophysiol.* 114, 1053–1068.

Haggard, P. (2008). Human volition: towards a neuroscience of will. *Nat. Rev. Neurosci.* 9, 934–946.

Hanes, D. P., Patterson, W. F., and Schall, J. D. (1998). Role of frontal eye fields in countermanding saccades: visual, movement, and fixation activity. *J. Neurophysiol.* 79, 817–834.

Heinze, H. J., Münte, T. F., and Mangun, G. R. (1994). *Cognitive Electrophysiology*. Boston, MA: Birkhäuser.

Hjorth, B. (1975). An on-line transformation of EEG scalp potentials into orthogonal source derivations. *Electroencephalogr. Clin. Neurophysiol.* 39, 526–530.

Hyvärinen, A. (1999). Fast and robust fixed-point algorithms for independent component analysis. *IEEE Trans. Neural Netw.* 10, 626–634.

Hyvärinen, A., and Oja, E. (1997). A Fast Fixed-Point Algorithm for Independent Component Analysis. *Neural Comput.* 9, 1483–1492.

Jung, T. P., Makeig, S., McKeown, M. J., Bell, A. J., Lee, T. W., and Sejnowski, T. J. (2001). Imaging brain dynamics using independent component analysis. *Proc. IEEE Inst. Electr. Electron. Eng.* 89, 1107–1122.

Kawashima, R., Matsumura, M., Sadato, N., Naito, E., Waki, A., Nakamura, S., Matsunami, K., Fukuda, H., and Yonekura, Y. (1998). Regional cerebral blood flow changes in human brain related to ipsilateral and contralateral complex hand movements – a PET study. *Eur. J. Neurosci.* 10, 2254–2260.

Kok, A., Ramautar, J. R., De Ruiter, M. B., Band, G. P., and Ridderinkhof, K. R. (2004). ERP components associated with successful and unsuccessful stopping in a stop-signal task. *Psychophysiology* 41, 9–20.

Lancaster, J. L., Woldorff, M. G., Parsons, L. M., Liotti, M., Freitas, C. S., Rainey, L., Kochunov, P. V., Nickerson, D., Mikiten, S. A., and Fox, P. T. (2000). Automated Talairach Atlas labels for functional brain mapping. *Hum. Brain Mapp.* 10, 120–131.

Leuthardt, E. C., Schalk, G., Wolpaw, J. R., Ojemann, J. G., and Moran, D. W. (2004). A brain-computer interface using electrocorticographic signals in humans. *J. Neural Eng.* 1, 63–71.

Levitt, H. (1971). Transformed up-down method in psychoacoustics. *J. Acoust. Soc. Am.* 49, 467–477.

Li, C. S., Yan, P., Sinha, R., and Lee, T. W. (2008). Subcortical processes of motor response inhibition during a stop signal task. *Neuroimage* 41, 1352–1363.

Liotti, M., Pliszka, S. R., Perez, R. 3rd, Luus, B., Glahn, D., and Semrud-Clikeman, M. (2007). Electrophysiological correlates of response inhibition in children and adolescents with ADHD: influence of gender, age, and previous treatment history. *Psychophysiology* 44, 936–948.

Logan, G. D. (1994). "On the ability to inhibit thought and action: a users' guide to the stop signal paradigm," in *Inhibitory Processes in Attention, Memory and Language*, eds D. Dagenbach and T. H. Carr (San Diego, CA: Academic Press), 189–239.

Logan, G. D., and Cowan, W. B. (1984). On the ability to inhibit thought and action: a theory of an act of control. *Psychol. Rev.* 91, 295–327.

Mars, R. B., Coles, M. G., Hulstijn, W., and Toni, I. (2008). Delay-related cerebral activity and motor preparation. *Cortex* 44, 507–520.

Millán, J. D. R., Rupp, R., Müller-Putz, G. R., Murray-Smith, R., Giugliemma, C., Tangermann, M., Vidaurre, C., Cincotti, F., Kübler, A., Leeb, R., Neuper, C., Müller, K.-R., and Mattia, D. (2010). Combining brain–computer interfaces and assistive technologies: state-of-the-art and challenges. *Front. Neurosci.* 4:161. doi: 10.3389/fnins.2010.00161

Miller, K. J., Makeig, S., Hebb, A. O., Rao, R. P., denNijs, M., and Ojemann, J. G. (2007). Cortical electrode localization from X-rays and simple mapping for electrocorticographic research: the "Location on Cortex" (LOC) package for MATLAB. *J. Neurosci. Methods* 162, 303–308.

Mink, J. W. (1996). The basal ganglia: focused selection and inhibition of competing motor programs. *Prog. Neurobiol.* 50, 381–425.

Mirabella, G. (2007). Endogenous inhibition and the neural basis of "free won't." *J. Neurosci.* 27, 13919–13920.

Mirabella, G., Iaconelli, S., Romanelli, P., Modugno, N., Lena, F., Manfredi, M., and Cantore, G. (2012). Deep brain stimulation of subthalamic nuclei affects arm response inhibition in Parkinson's patients. *Cereb. Cortex* 22, 1124–1132.

Mirabella, G., Pani, P., and Ferraina, S. (2008). Context influences on the preparation and execution of reaching movements. *Cogn. Neuropsychol.* 25, 996–1010.

Mirabella, G., Pani, P., and Ferraina, S. (2009). The presence of visual gap affects the duration of stopping process. *Exp. Brain Res.* 192, 199–209.

Mirabella, G., Pani, P., and Ferraina, S. (2011). Neural correlates of cognitive control of reaching movements in the dorsal premotor cortex of rhesus monkeys. *J. Neurophysiol.* 106, 1454–1466.

Mirabella, G., Pani, P., Paré, M., and Ferraina, S. (2006). Inhibitory control of reaching movements in humans. *Exp. Brain Res.* 174, 240–255.

Moritz, C. T., Perlmutter, S. I., and Fetz, E. E. (2008). Direct control of paralysed muscles by cortical neurons. *Nature* 456, 639–642.

Mostofsky, S. H., and Simmonds, D. J. (2008). Response inhibition and response selection: two sides of the same coin. *J. Cogn. Neurosci.* 20, 751–761.

Nachev, P., Wydell, H., O'Neill, K., Husain, M., and Kennard, C. (2007). The role of the pre-supplementary motor area in the control of action. *Neuroimage* 36(Suppl. 2), T155–T163.

Nambu, A., Tokuno, H., and Takada, M. (2002). Functional significance of the cortico-subthalamo-pallidal 'hyperdirect' pathway. *Neurosci. Res.* 43, 111–117.

Nicolelis, M. A. (2003). Brain-machine interfaces to restore motor function and probe neural circuits. *Nat. Rev. Neurosci.* 4, 417–422.

Osman, A., Kornblum, S., and Meyer, D. E. (1990). Does motor programming necessitate response execution? *J. Exp. Psychol. Hum. Percept. Perform.* 16, 183–198.

Ramautar, J. R., Kok, A., and Ridderinkhof, K. R. (2006). Effects of stop-signal modality on the N2/P3 complex elicited in the stop-signal paradigm. *Biol. Psychol.* 72, 96–109.

Schalk, G. (2010). Can electrocorticography (ECoG) support robust and powerful brain-computer interfaces? *Front. Neuroeng.* 3:9. doi: 10.3389/fneng.2010.00009

Schalk, G., Miller, K. J., Anderson, N. R., Wilson, J. A., Smyth, M. D., Ojemann, J. G., Moran, D. W., Wolpaw, J. R., and Leuthardt, E. C. (2008). Two-dimensional movement control using electrocorticographic signals in humans. *J. Neural Eng.* 5, 75–84.

Schmajuk, N. A., Larrauri, J. A., Hagenbuch, N., Levin, E. D., Feldon, J., and Yee, B. K. (2006). Startle and prepulse inhibition as a function of background noise: a computational and experimental analysis. *Behav. Brain Res.* 170, 182–196.

Schwartz, A. B. (2004). Cortical neural prosthetics. *Annu. Rev. Neurosci.* 27, 487–507.

Srinivasan, R., Nunez, P. L., and Silberstein, R. B. (1998). Spatial filtering and neocortical dynamics: estimates of EEG coherence. *IEEE Trans. Biomed. Eng.* 45, 814–826.

Stinear, C. M., Coxon, J. P., and Byblow, W. D. (2009). Primary motor cortex and movement prevention: where Stop meets Go. *Neurosci. Biobehav. Rev.* 33, 662–673.

Swann, N., Tandon, N., Canolty, R., Ellmore, T. M., McEvoy, L. K., Dreyer, S., DiSano, M., and Aron, A. R. (2009). Intracranial EEG reveals a time- and frequency-specific role for the right inferior frontal gyrus and primary motor cortex in stopping initiated responses. *J. Neurosci.* 29, 12675–12685.

Tallon-Baudry, C., and Bertrand, O. (1999). Oscillatory gamma activity in humans and its role in object representation. *Trends Cogn. Sci.* 3, 151–162.

Tanji, J., and Evarts, E. V. (1976). Anticipatory activity of motor cortex neurons in relation to direction of an intended movement. *J. Neurophysiol.* 39, 1062–1068.

van den Wildenberg, W. P., van Boxtel, G. J., van der Molen, M. W., Bosch, D. A., Speelman, J. D., and Brunia, C. H. (2006). Stimulation of the subthalamic region facilitates the selection and inhibition of motor responses in Parkinson's disease. *J. Cogn. Neurosci.* 18, 626–636.

Wang, W., Collinger, J. L., Perez, M. A., Tyler-Kabara, E. C., Cohen, L. G., Birbaumer, N., Brose, S. W., Schwartz, A. B., Boninger, M. L., and Weber, D. J. (2010). Neural interface technology for rehabilitation: exploiting and promoting neuroplasticity. *Phys. Med. Rehabil. Clin. N. Am.* 21, 157–178.

Weinrich, M., and Wise, S. P. (1982). The premotor cortex of the monkey. *J. Neurosci.* 2, 1329–1345.

Wetherill, G. B., and Levitt, H. (1965). Sequential estimation of points on a psychometric function. *Br. J. Math. Stat. Psychol.* 18, 1–10.

Wolpert, D. M., and Miall, R. C. (1996). Forward models for physiological motor control. *Neural Netw.* 9, 1265–1279.

Zandbelt, B. B., and Vink, M. (2010). On the role of the striatum in response inhibition. *PLoS ONE* 5:e13848. doi: 10.1371/journal.pone.0013848

Conflict of Interest Statement: The authors declare that the research was conducted in the absence of any commercial or financial relationships that could be construed as a potential conflict of interest.

Received: 11 April 2012; paper pending published: 28 May 2012; accepted: 15 June 2012; published online: 29 June 2012.

Citation: Mattia M, Spadacenta S, Pavone L, Quarato P, Esposito V, Sparano A, Sebastiano F, Di Gennaro G, Morace R, Cantore G and Mirabella G (2012) Stop-event-related potentials from intracranial electrodes reveal a key role of premotor and motor cortices in stopping ongoing movements. Front. Neuroeng. ***5****:12. doi: 10.3389/fneng.2012.00012*

frontiers in
NEUROENGINEERING

ORIGINAL RESEARCH ARTICLE
published: 25 July 2012
doi: 10.3389/fneng.2012.00017

The interplay of prefrontal and sensorimotor cortices during inhibitory control of learned motor behavior

Selina C. Wriessnegger[1]*†, Günther Bauernfeind[1†], Kerstin Schweitzer[2], Silvia Kober[2], Christa Neuper[2] and Gernot R. Müller-Putz[1]

[1] *Laboratory of Brain-Computer Interfaces, Institute for Knowledge Discovery, Graz University of Technology, A-8010 Graz, Steiermark, Austria*
[2] *Department of Psychology, University of Graz, A-8010 Graz, Steiermark, Austria*

Edited by:
Giovanni Mirabella, University of La Sapienza, Italy

Reviewed by:
Hari S. Sharma, Uppsala University, Sweden
Giuseppe D'Avenio, Istituto Superiore di Sanità, Italy
Sara Jahfari, University of Amsterdam, Netherlands
Bram B. Zandbelt, Vanderbilt University, USA

****Correspondence:***
Selina C. Wriessnegger, Laboratory of Brain-Computer Interfaces, Institute for Knowledge Discovery, Graz University of Technology, Krenngasse 37, A-8010 Graz, Steiermark, Austria.
e-mail: s.wriessnegger@tugraz.at

† *These authors contributed equally to this work.*

In the present study inhibitory cortical mechanisms have been investigated during execution and inhibition of learned motor programs by means of multi-channel functional near infrared spectroscopy (fNIRS). fNIRS is an emerging non-invasive optical technique for the *in vivo* assessment of cerebral oxygenation, concretely changes of oxygenated [oxy-Hb], and deoxygenated [deoxy-Hb] hemoglobin. Eleven healthy subjects executed or inhibited previous learned finger and foot movements indicated by a visual cue. The execution of finger/foot movements caused a typical activation pattern namely an increase of [oxy-Hb] and a decrease of [deoxy-Hb] whereas the inhibition of finger/foot movements caused a decrease of [oxy-Hb] and an increase of [deoxy-Hb] in the hand or foot representation area (left or medial somatosensory and primary motor cortex). Additionally an increase of [oxy-Hb] and a decrease of [deoxy-Hb] in the medial area of the anterior prefrontal cortex (APFC) during the inhibition of finger/foot movements were found. The results showed, that inhibition/execution of learned motor programs depends on an interplay of focal increases and decreases of neural activity in prefrontal and sensorimotor areas regardless of the effector. As far as we know, this is the first study investigating inhibitory processes of finger/foot movements by means of multi-channel fNIRS.

Keywords: motor learning, response inhibition, anterior prefrontal cortex (APFC), PFC, motor cortex, fNIRS

INTRODUCTION

In daily life successful human behavior strongly depends on learning and inhibition of inappropriate behavior. Specifically inhibitory control is an essential function to provide appropriate preparation and online control of required motor programs. Furthermore a fine balance between activation and inhibition is necessary for preparation of movement, initiation, motor control, and timely inhibition of the act. There are a lot of studies focusing on the question about the neural correlate of effective inhibition or suppression of behavior. Most of them used experimental paradigms like GO/NOGO (Rubia et al., 2003; Herrmann et al., 2005; Simmonds et al., 2008) tasks or STOP-Signal (Boecker et al., 2007; Tabu et al., 2011, 2012) paradigms to investigate inhibition processes. The differences between the tasks are that the GO/NOGO paradigm requires a response selection process, namely execute or inhibit a motor response, triggered by a go or a no-go-stimulus. On the other hand, in the stop task the stop signal requires withholding or stopping an already triggered motor response. For example, the results of a meta-analysis using 11 studies of event-related functional magnetic resonance imaging (fMRI) during GO/NOGO task have shown that the pre-supplementary motor area (pre-SMA) and the prefrontal-parietal circuits are crucial for response inhibition (Simmonds et al., 2008). More evidence for the involvement of the prefrontal cortex (PFC) in response inhibition came from Rubia et al. (2000, 2001, 2003) who found predominantly right hemispheric PFC activations. For example in a stop-signal study (Rubia et al., 2003) they found different activation patterns for successful and failed stopping. The right inferior PFC was correlated with successful inhibition and bilateral inferior parietal cortices were associated with failed inhibition. Whereas most fMRI studies investigated only manual response inhibition the recent study of Tabu et al. (2012) investigated also the brain representation of foot stop-signal task for the first time. They found common activation patterns of prefrontal areas (pre-SMA and bilateral ventrolateral PFC) for hand and foot stop signal tasks.

Beside a lot of fMRI studies there are also some fNIRS studies focusing on the role of PFC activation during cortical inhibition (Boecker et al., 2007; Kono et al., 2007). Functional near infrared spectroscopy (fNIRS) is a non-invasive optical imaging technique to quantify cortical activity. fNIRS allows measuring the oxygenation (haemoglobin concentration) in the cerebral cortex, which is strongly correlated to the fMRI Blood-Oxygen-Level-Dependent (BOLD) signal (Strangman et al., 2002; Steinbrink et al., 2006). Even though fNIRS has lower spatial resolution than fMRI, it has the advantage of providing information about two parameters, namely oxygenated- (oxy-Hb) and deoxygenated (deoxy-Hb) hemoglobin. As fNIRS measures changes in oxy-Hb and deoxy-Hb and consequential total hemoglobin (tot-Hb) concentration, this approach allows also

to draw conclusions about changes in neurovascular parameters like cerebral metabolic rate of oxygen (CMRO2), cerebral blood flow (CBF), and cerebral blood volume (CBV) (Malonek and Grinvald, 1996; Malonek et al., 1997; Wolf et al., 2002). Furthermore it is not sensitive to motion artifacts, is portable and can be easily used with children and patients (Strangman et al., 2002; Wolf et al., 2002).

For example Herrmann et al. (2005) replicated previous findings from fMRI-studies using fNIRS in a GO/NOGO paradigm. He found significantly higher increases of oxy-Hb and decreases of deoxy-Hb concentration during inhibition phases in the inferior part of the PFC.

It is known that successful behavior also requires appropriate retrieval of acquired motor programs or inhibition of learned actions. That is, activation and deactivation or inhibition of brain regions representing these actions. Another paradigm investigating cortical inhibition used by Hummel et al. (2002, 2004) is similar to common GO/NOGO tasks but has no time pressure and is additionally based on previous learning processes. Hummel et al. (2002) showed that acquired motor behavior is a context-dependent interaction of execution and inhibition of learned motor programs. Inhibition was associated with a decrease in motor cortical excitability below the resting state and was additionally correlated with a task-related increase of 11–13 Hz oscillatory activity on the electroencephalogram (EEG). In a later study they used fMRI to investigate inhibition of learned motor programs (Hummel et al., 2004). They found that the inhibitory changes were characterized by negative BOLD responses in an extended cerebro-cerebellar network of sensorimotor structures with a predominant role of the PFC. Such PFC activation was also found in the fNIRS study by Boecker et al. (2007) reporting a substantial activation increase in the right PFC during inhibition of already initiated responses.

In the present study we applied fNIRS to healthy subjects performing a paradigm comparable to that used by Hummel et al. (2004). We investigated bidirectional inhibition-activation processes during execution/inhibition of learned motor programs executed by hand and foot. The aim of the present study was twofold: first we wanted to replicate the findings of Hummel et al. (2004) using fMRI with multichannel fNIRS. Secondly, we investigated hemodynamic changes of response inhibition during foot movements. To our knowledge the inhibition of learned motor programs executed by hand and foot has never been investigated with multichannel fNIRS.

MATERIALS AND METHODS

PARTICIPANTS

Investigations were carried out on a group of 11 voluntary healthy subjects (four males, seven females) aged from 22 to 37 years (27.3 ± 3.9, mean $\pm$ SD). All subjects were right-handed and had normal or corrected to normal vision. Hand performance was assessed with the "Hand Dominance Test" (HDT) by Steingrüber and Lienert (1971). This test comprises three dexterity tasks, each to be performed with maximal speed and precision over 15 s, separately for the right and left-hand (tracing lines, dotting circles, and dotting squares). In this regard, dominance refers to the performance advantage of one hand relative to the other. All experiments were in compliance with the World Medical Association Declaration of Helsinki. The protocol was approved by the Ethics committee of the Medical University of Graz and the subjects gave informed written consent before the experiment.

EXPERIMENTAL PARADIGM

Three weeks prior to the experiment, subjects were instructed to train themselves on six sequences of right hand finger and right foot movements of two different task complexities at home. In **Table 1** the three experimental blocks are described in detail, divided by type of limb (finger or foot), presentation modality (activation, inhibition), sequence type (easy/difficult), number of trials and total duration of each block (**Table 1**). The necessary resources, a keyboard for finger movements and a template to train foot movements, were provided to the participants. Prior the experimental session the success of the training was tested. Only subjects, who successfully completed the test, meaning that they executed the requested finger/foot movements without errors, performed the experiment.

During the experimental sessions all subjects were seated in a comfortable arm-chair in front of a TFT monitor. The distance between the participants and the screen was about 120 cm. To avoid artifacts, the participants were instructed to relax as much as possible during the measurement. The study consisted of three sessions (**Table 1**): a finger movement session (indicated by a picture of a hand), a foot movement session (indicated by a picture of a foot), and a session with randomized finger and foot movements. Sessions were presented blockwise in the described order (**Table 1**). Within each block 50% of trials required inhibition and 50% execution. The sequences in the blocks were randomly presented.

During the finger movement session subjects had to execute or inhibit 48 sequences of right hand finger movements presented on the monitor. In order to indicate if execution or an inhibition task was required a green (execution) or a red (inhibition) frame was

Table 1 | Experimental blocks.

Block	Limb	Presentation modality	#Trials	Duration
1	finger	execution: 12 easy[a], 12 difficult[b] inhibition: 12 easy, 12 difficult 2 new	50	13 min
2	foot	execution: 12 easy, 12 difficult inhibition: 12 easy, 12 difficult 2 new	50	13 min
3	finger	execution: 6 easy, 6 difficult inhibition: 6 easy, 6 difficult 2 new	52	13 min
	foot	execution: 6 easy, 6 difficult inhibition: 6 easy, 6 difficult 2 new		

[a] *easy sequences: 1-2-3-4-1-2-3-4, 1-1-2-2-3-3-4-4, 1-3-2-4-1-3-2-4*
[b] *difficult sequences: 4-1-3-2-1-2-3-1, 3-2-1-4-3-4-1-3, 4-2-1-4-3-1-4-2*

shown around the picture of the hand one second after sequence presentation. One sequence consisted of eight movements [presented on the screen as a sequence of eight numbers (digits 1–4)] and lasted 10 s. The fingers were labeled corresponding to these digits as follows: the index finger "1," the middle finger "2," the ring finger "3," the little finger "4." During the execution task the subjects were instructed to perform the requested sequence (e.g., 4-1-3-2-1-2-3-1) on a modified keyboard until the screen turns black. The average frequency of finger (**Figure 2B**) tapping was about 25.03, resulting in about three sequences. During the inhibition task they should avoid any button press. After one trial a pause of 5 s followed. Additionally to the well trained sequences, two new sequences (1 execution, 1 inhibition) were presented in order to maintain the subject's attention. So the finger movement session consisted of 50 trials. A detailed description of the timing of one trial is given in **Figure 1**.

During the foot movement session subjects had to execute or inhibit foot movement sequences on a custom made console (**Figure 2A**). The average frequency of foot tapping was 21.18, resulting in nearly three full sequences. Apart from that, the timing and number of trials were the same as in the finger movement block. Again, in order to indicate if execution or inhibition was required a green (execution) or a red (inhibition) frame was shown around the picture of the foot.

Finally, in the session with randomized finger and foot movements the subjects had to execute or inhibit 24 fingers and foot movement sequences in random order. In contrast to the finger and foot block, four new sequences occurred, so the block consisted of 52 trials. Between the blocks the subjects had short breaks of about 5 min (see **Figure 1**).

DATA ACQUISITION AND PROCESSING

To record brain oxygenation a multichannel commercial fNIRS system (ETG-4000, Hitachi Medical Co., Japan), which is based on the continuous wave principle was used. The sampling rate was set to 10 Hz. The multi-channel system measures the change of [oxy-Hb] and [deoxy-Hb][1] in the unit of m(mol/l) × mm (further denoted as mM mm) and consisted of 15 photo-detectors and 18 light emitters, resulting in a total of 46 channels. Two 3 × 3 optode probe sets (each containing four photo-detectors and five light emitters) were used to cover the frontal and frontocentral regions as well as the parietal and occipital regions. Additionally a 3 × 5 optode probe set (containing seven photo-detectors and eight light emitters) was used to cover the central, temporal, and partially the parietal regions (**Figure 2C**). The probe sets were interconnected and mounted on a custom-made cap (**Figure 2D**). The cap was arranged in such a way that channel 40, which was used as the reference marker, was placed exactly over Cz position, according to the International 10–20 system for EEG recordings. The distance between source and detector was 3 cm, which resulted in measuring approximately 3 cm beneath the scalp. To allow a probabilistic reference to the underlying cortical areas we calculated the projections of the fNIRS channels on the cortical surface. Therefore, we used a procedure which projects topographical data based on skull landmarks into a 3D reference frame (MNI-space, Montreal Neurological Institute) optimized for fNIRS analysis (Singh et al., 2005). So for each fNIRS channel position, a set of MNI coordinates (x, y, and z) with an

[1]Subsequent the concentration of oxy-Hb and deoxy-Hb is denoted as [oxy-Hb] and [deoxy-Hb].

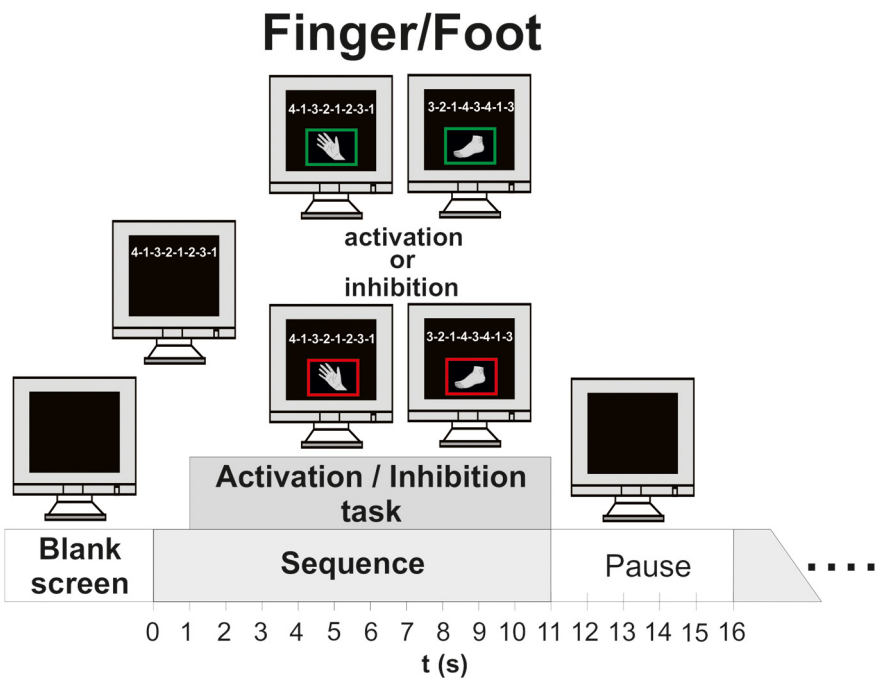

FIGURE 1 | Time course of one experimental trial (finger/foot, execution/inhibition). Left side: timing of finger movement execution/inhibition; **Right side**: timing of foot movement execution/inhibition.

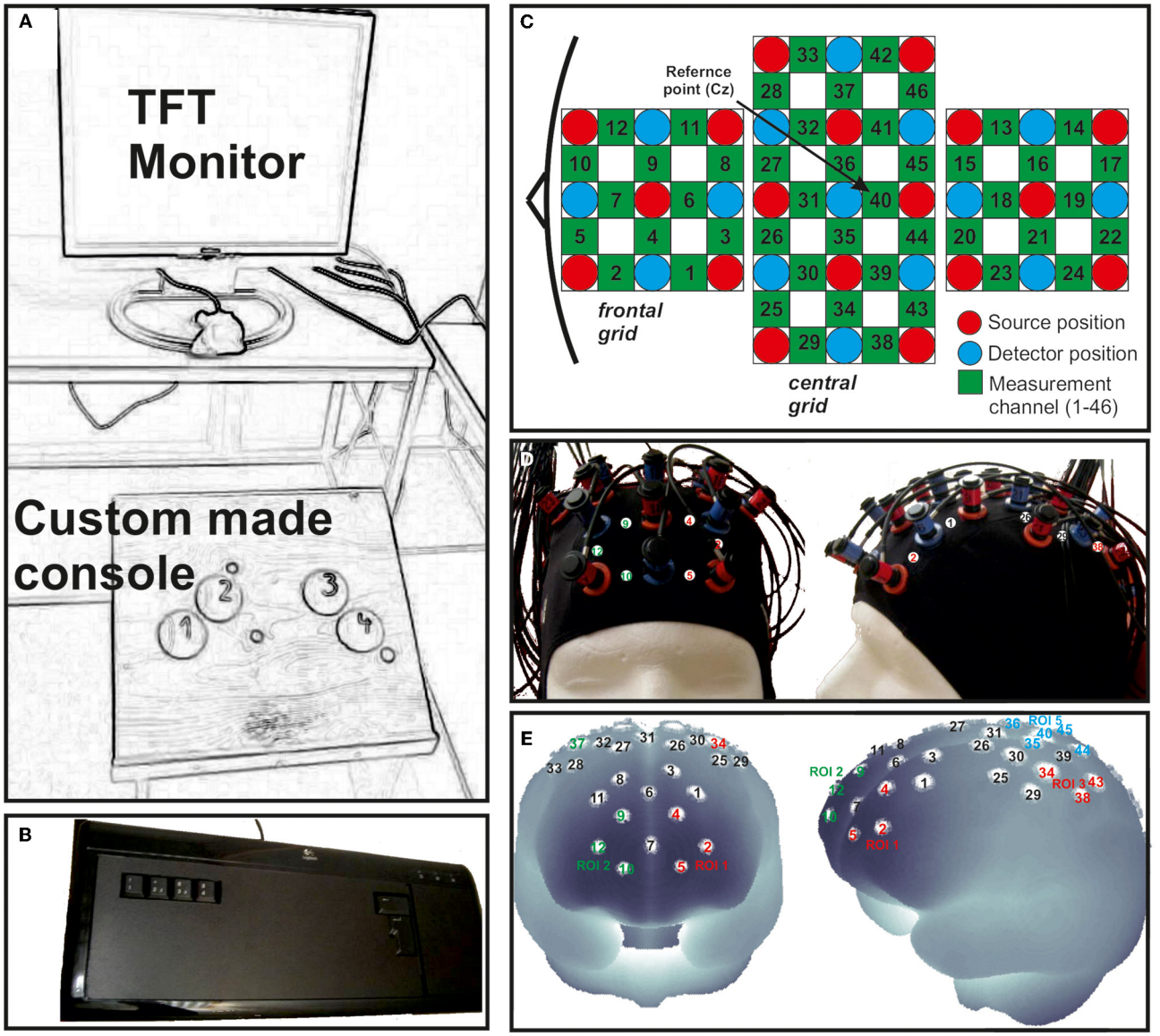

FIGURE 2 | (A) Custom made console used for foot movement responses positioned in front of a TFT monitor. **(B)** Modified keyboard for finger movement responses. **(C)** Schematic illustration of the multi-channel arrays (46 channels, two 3 × 3 grids and one 3 × 5 grid) covering frontal, central and parietal regions. **(D)** fNIRS cap with mounted optodes. **(E)** Projections of the fNIRS channel positions on the cortical surface. Positions are overlaid on a MNI-152 compatible canonical brain which is optimized for fNIRS analysis.

error estimated (SD) was calculated (see **Figure 2E** and **Table 2**). **Table 2** shows five different regions of interest (ROI) with the according channel numbers, MNI-space correspondence (x, y, z with SD) and brodmann areas (BA). For further details on the corresponding anatomical structures see (Okamoto et al., 2004; Singh et al., 2005).

After a visual inspection of the raw fNIRS data by a trained expert, trials containing motion artifacts were removed manually. Additionally, channels with poor signal quality, e.g. containing noise (on average less than 7% of the channels), were excluded. Baseline drifts were reduced by using a 0.01 Hz Butterworth high pass filter of order 6 with 30 dB attenuation in the stop band. Afterwards a common average reference (CAR) spatial filter was used to remove global influences like respiratory or blood pressure rhythms. As a result, for every time point, the mean of all non-excluded channels was calculated and subtracted from each channel (Pfurtscheller et al., 2010).

CALCULATION OF TASK RELATED CHANGES AND TOPOGRAPHIC DISTRIBUTION

The mean task related changes of [oxy-Hb] and [deoxy-Hb] referred to a 5-s baseline interval prior the task (seconds −5 to 0) were calculated. For the excluded channels (at the maximum 6 out of 46 channels) the changes were recalculated by interpolation

Table 2 | Definition and coordinates of ROIs.

ROI	Channel	MNI space correspondence				Cortical areas	
		x	*y*	*z*	SD	BA	
FPI	2	−29	67	11	5	10	MFG
	4	−13	65	28	5	10	SFG
	5	−15	73	1	4	10	MeFG
FP2	9	16	67	27	5	10	SFG
	10	15	73	0	4	10	MeFG
	12	28	69	11	5	10	SFG
C3	34	−34	−7	68	8	6	PreG
	38	−47	−24	65	5	3	PosG
	43	−36	−32	72	6	4	PreG
C4	37	39	−8	68	7	6	PreG
	42	50	−24	65	5	1	PosG
	46	39	−32	71	6	4	PreG
CZ	35	−12	−4	76	7	6	SFG
	36	15	−3	76	6	6	SFG
	40	4	−18	76	8	6	MeFG
	44	−12	−32	80	6	4	PreG
	45	15	−35	80	5	4	PreG

The projections of the fNIRS channels on the cortical surface were calculated by projecting topographical data based on skull landmarks into a 3D reference frame (MNI space, Montreal Neurological Institute). The table shows five different regions of interest (ROI) with the according channel numbers, MNI space correspondence (x, y, z with SD) and brodmann areas (BA).

BA, Brodmann area; MeFG, medial frontal gyrus; MFG, middle frontal gyrus; PreG, precentral gyrus; SFG, superior frontal gyrus; PosG, postcentral gyrus.

of the surrounding channels. In all subjects not more than one channel was interpolated in each ROI. Furthermore no interpolation was performed in frontal ROIs (FP1 and FP2). As the fNIRS data was checked for artifacts, such interpolation of channels will only cause a spatiotemporal smoothing of the hemodynamic pattern. The topographic distributions during the tasks are further visualized by plotting the [oxy-Hb] and [deoxy-Hb] values at their corresponding spatial position. A 2-D interpolation on a fine Cartesian grid was used to generate a scalp distribution. The average over two different time windows are calculated. The first time window between 0 and 4 s corresponds to the cue presentation and start of the task. The second time window between 10 and 12 s corresponds to the end of the task. The mean concentration changes of oxy-Hb and deoxy-Hb are visualized in different plots with the same scale. Increases are plotted in blue and decreases in red (according to the toolbox "EEG-Lab" from Matlab). Only well trained sequences run into analyses, concretely the mean task related concentration changes of 48 trials for each condition are plotted. The new sequences during the experimental trials were only used to keep attention.

STATISTICAL ANALYSES

Before running statistical analyses the following pre-processing steps were performed:

First, five regions of interest (ROIs: FP1, FP2, C3, Cz, C4) covering the frontal and motor cortex of both hemispheres were defined: Frontal cortex: FP1 (CH: 2, 4, 5); FP2 (CH: 9, 10, 12); Motor cortex: C3 (CH: 34, 38, 43); Cz (CH: 35, 36, 40, 44, 45); C4 (CH.: 37, 42, 46). The MNI coordinates and anatomical locations of the included channels are given in **Table 2** and **Figure 2E**. Second, the mean concentration changes were calculated in a time window of 4 s, 2 s prior and 2 s after the end of the task. Again, only the well trained sequences (48 each condition) were considered since the novel sequences were used for attentional purposes only. For statistical analyses a $2 \times 2 \times 2$ univariate repeated measures analyses of variance (ANOVA) with the within-subject factors EXEC/INHIB (execution vs. motor inhibition), FRONTAL/CENTRAL (ROI FP1/FP2 vs. ROI C3/Cz/C4), and HEMI (left vs. right hemisphere) were applied, separately for the dependent variable oxy-Hb and deoxy-Hb and for the finger and foot movement condition.

RESULTS

In general all subjects showed strong changes of [oxy-Hb][2] and [deoxy-Hb] during execution/inhibition of finger/foot movements in frontal and central cortical regions [left or medial SMA, primary motor (M1) and primary somatosensory (S1) cortex; **Figures 3**, **4**]. During finger movement execution an [oxy-Hb] increase was found central (ROI C3) compared to the inhibition condition, where frontal regions (ROI FP1 and FP2) showed [oxy-Hb] increase and [deoxy-Hb] decrease. This effect is clearly visible in the topographic maps of **Figures 5A** (foot) and **B** (finger). **Figure 5A** shows oxy-Hb and deoxy-Hb concentration changes for foot movement execution (left side) and inhibition (right side) at two different points in time (0–4 s and 8–12 s). At time point 2 (8–12 s) a clear [oxy-Hb] decrease was found at central sites during execution of finger and foot movements, whereas during movement inhibition both conditions showed a [oxy-Hb] decrease at central sites and an increase at frontal sites.

In the following paragraphs significant results of the $2 \times 2 \times 2$ univariate ANOVA are reported for finger and foot condition separately. **Table 3** shows a summary of significant *F*-values for [oxy-Hb] and [deoxy-Hb]. *F*-values at 5% level are marked with one asterisk (*), at 1% level with two asterisks (**). All repeated measures tests are Huynh–Feldt corrected.

FINGER CONDITION

For [oxy-Hb], the ANOVA revealed a significant two-way interaction effect of EXEC/INHIB * FRONTAL/CENTRAL [$F_{(1,\ 10)} = 19.20$, $p < 0.01$; $\eta^2 = 0.66$]. This interaction indicated that the type of task leads to different hemodynamic responses at frontal and central brain regions. *Post hoc*-tests (Bonferroni) showed a stronger increase in [oxy-Hb] during motor inhibition compared to active movement at frontal brain regions (FP1, FP2). At central sites (C3, Cz, C4) no significant difference in [oxy-Hb] between motor inhibition and active movement was found. Additionally [oxy-Hb] increased over central compared to frontal sites in the active movement condition. Furthermore the three-way interaction effect EXEC/INHIB * FRONTAL/CENTRAL * HEMI [$F_{(1,\ 10)} = 6.24$, $p < 0.05$; $\eta^2 = 0.38$] was significant.

[2]Subsequent the concentration of oxy-Hb and deoxy-Hb is denoted as [oxy-Hb] and [deoxy-Hb].

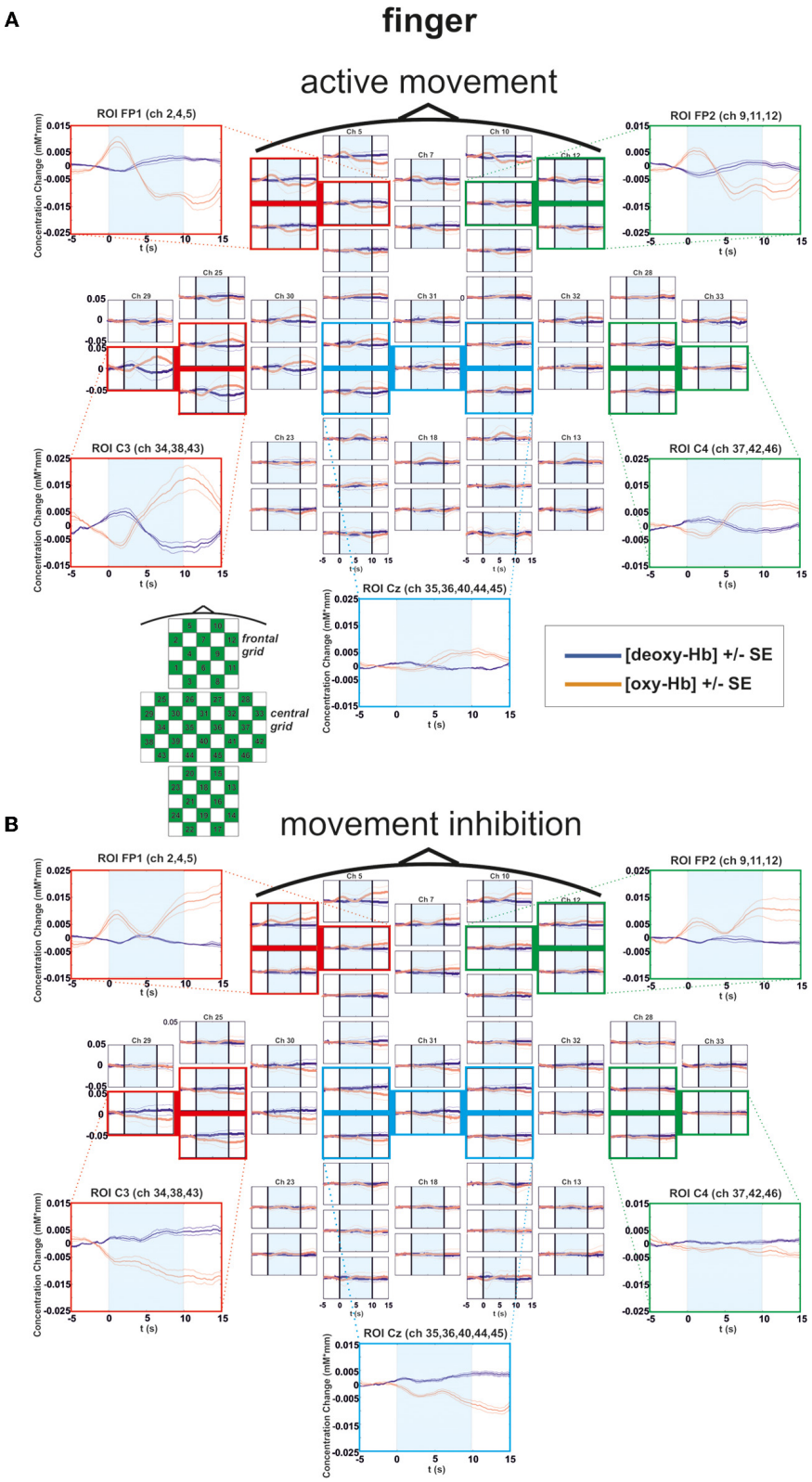

FIGURE 3 | Multichannel map illustrating oxygenation levels of ROIs of finger movement execution (A) and inhibition (B). In the middle the mean concentration changes of [oxy-Hb] and [deoxy-Hb] for each channel are illustrated. The shaded bars indicate the activation time of 10 s. Around the channel map the defined ROIs are zoomed.

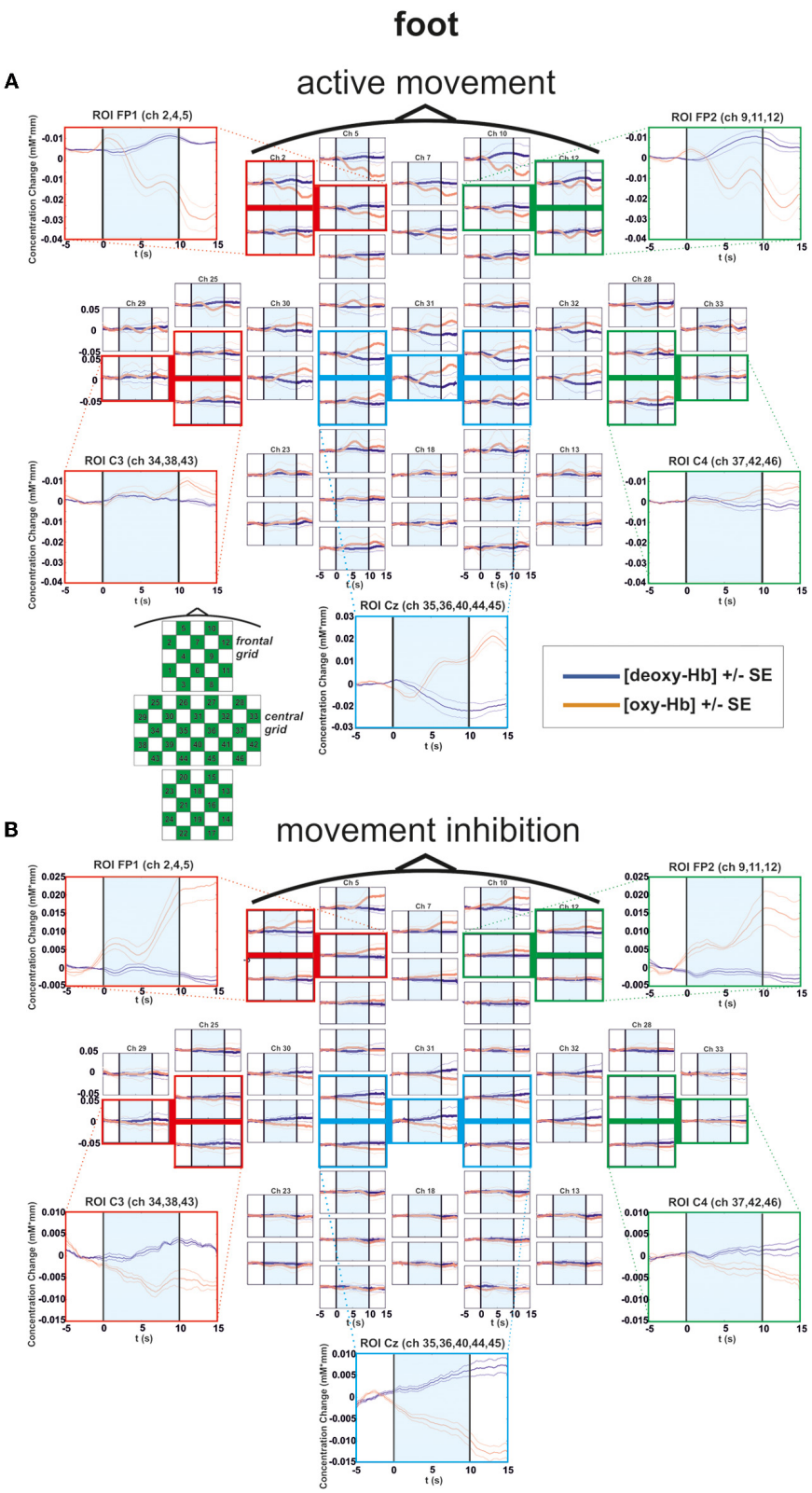

FIGURE 4 | Multichannel map illustrating oxygenation levels of ROIs of foot movement execution (A) and inhibition (B). In the middle the mean concentration changes of [oxy-Hb] and [deoxy-Hb] for each channel are illustrated. The shaded bars indicate the activation time of 10 s. Around the channel map the defined ROIs are zoomed.

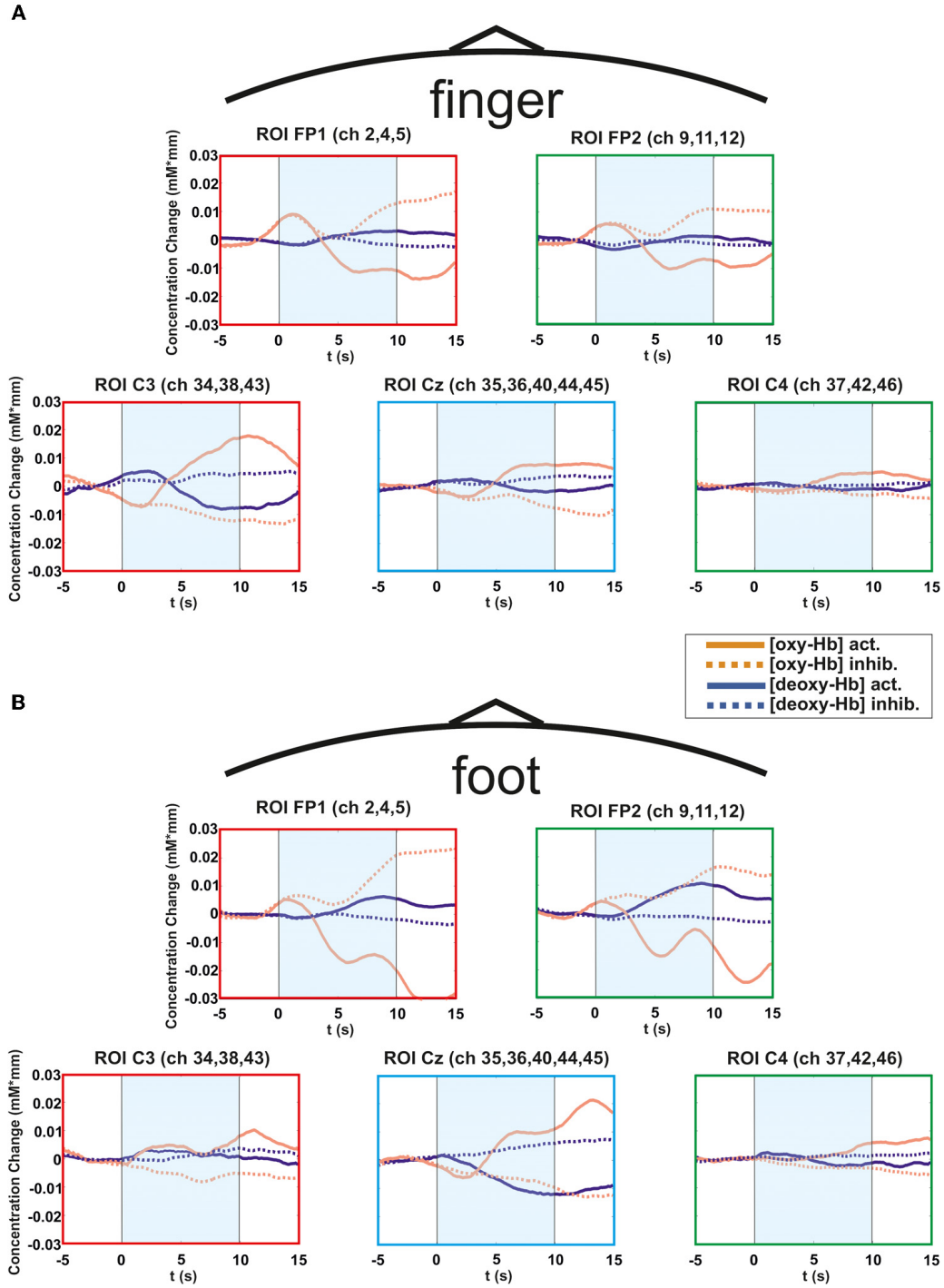

FIGURE 5 | Multichannel ROI map illustrating the mean concentration changes of [oxy-Hb] and [deoxy-Hb] for execution (thick lines) and inhibition (thin lines) together. (A) execution/inhibition of finger movement. **(B)** execution/inhibition of foot movement. The shaded bars indicate the activation time of 10 s.

Post hoc-tests (Bonferroni) showed stronger increases in [oxy-Hb] during motor inhibition compared to active movement at frontal left brain regions (FP1) and no significant difference at frontal right areas (FP2). At central left areas (C3) [oxy-Hb] was higher during active movement than during motor inhibition. Like at frontal right sites, these two conditions showed no significant difference in [oxy-Hb] at central right sites (C4). In the inhibition condition, [oxy-Hb] was significantly increased at

Table 3 | Summary of significant *F*-values for [oxy-Hb] and [deoxy-Hb].

ANOVA effects ($N = 11$)	EXEC/INHIB (2) × FRONTAL/CENTRAL (2) × HEMI (2) [oxy-Hb]	EXEC/INHIB (2) × FRONTAL/CENTRAL (2) × HEMI (2) [deoxy-Hb]
FINGER CONDITION		
EXEC/INHIB × FRONTAL/CENTRAL	$F_{(1, 10)} = 19.20^{**}$	
EXEC/INHIB × FRONTAL/CENTRAL × HEMI	$F_{(1, 10)} = 6.24^{*}$	$F_{(1, 10)} = 6.16^{*}$
FOOT CONDITION		
EXEC/INHIB	$F_{(1, 10)} = 10.79^{**}$	
EXEC/INHIB × FRONTAL/CENTRAL	$F_{(1, 10)} = 29.82^{**}$	$F_{(1, 10)} = 6.52^{*}$
FRONTAL/CENTRAL × HEMI		$F_{(1, 10)} = 5.73^{*}$
EXEC/INHIB × FRONTAL/CENTRAL × HEMI	$F_{(1, 10)} = 7.42^{*}$	

F-values at 5% level are marked with one asterisk (*), at 1% level with two asterisks (**). All repeated measures tests are Huynh–Feldt corrected.

frontal left and right compared to central left sites. In the active movement condition, [oxy-Hb] was significantly higher at central left sites than at frontal left and right sites. Summarizing, the results showed significant differences in oxy-Hb concentration changes between execution and inhibition at central and frontal sites. There is no difference in [oxy-Hb] between left and right hemisphere in the inhibition condition, leading to a more bilateral activation. The mulit-channel maps in **Figure 3** showed the mean concentration changes of [oxy-Hb] and [deoxy-Hb] described above for each ROI and for execution (**Figure 3A**) and inhibition (**Figure 3B**) separately.

For [deoxy-Hb] in the finger condition, the three-way interaction effect of EXEC/INHIB * FRONTAL/CENTRAL * HEMI [$F_{(1, 10)} = 6.16$, $p < 0.05$; $\eta^2 = 0.38$] was significant. *Post hoc*-tests (Bonferroni) indicated a stronger decrease of [deoxy-Hb] during active movement than during motor inhibition at central left brain regions (C3).

FOOT CONDITION

In the foot condition, [oxy-Hb] was higher in the motor inhibition than in the active movement condition, which gave rise to a significant main effect of EXEC/INHIB [$F_{(1, 10)} = 10.79$, $p < 0.01$; $\eta^2 = 0.52$]. The significant interaction effect of EXEC/INHIB * FRONTAL/CENTRAL [$F_{(1, 10)} = 29.82$, $p < 0.01$; $\eta^2 = 0.75$] confirmed a substantial frontal increase of [oxy-Hb] during motor inhibition compared to active movement. Additionally, [oxy-Hb] was higher at frontal sites (FP1, FP2) than at central sites (Cz) in the motor inhibition condition, whereas in the active movement condition [oxy-Hb] was higher at central sites (Cz) compared to frontal areas (FP1, FP2). This effect is clearly visible in the following multi-channel map of foot movement execution (**Figure 4A**) and inhibition (**Figure 4B**). In the middle of both figures activation changes of all 52 channels are plotted. The ROI positions are illustrated in the zoomed figures around.

Furthermore, the three-way interaction effect EXEC/INHIB * FRONTAL/CENTRAL * HEMI [$F_{(1, 10)} = 7.42$, $p < 0.05$; $\eta^2 = 0.43$] was significant, too. At central sites (Cz) no significant differences in [oxy-Hb] between active movement and motor inhibition could be found. At frontal sites (FP1, FP2), [oxy-Hb] was higher in the inhibition condition than during active movement in both hemispheres. During inhibition [oxy-Hb] was lower at central sites (left and right) compared to frontal sites (left and right). During active movement [oxy-Hb] was higher at central sites (left and right) compared to frontal sites (left and right). No significant differences in [oxy-Hb] between frontal left and right sites during inhibition were found. Again during inhibition, activation was bilateral at frontal sites like in the finger movement condition.

For [deoxy-Hb] the ANOVA revealed a significant interaction effect of EXEC/INHIB * FRONTAL/CENTRAL [$F_{(1, 10)} = 6.52$, $p < 0.05$; $\eta^2 = 0.39$]. Like for [oxy-Hb] the type of task evokes different hemodynamic responses at frontal and central sites. Additionally, the interaction effect of FRONTAL/CENTRAL * HEMI [$F_{(1, 10)} = 5.73$, $p < 0.05$; $\eta^2 = 0.36$] was significant, due to a stronger decrease in [deoxy-Hb] over central right sites compared to frontal right sites.

The overall results clearly show differences in the frontal and central brain regions depending on the type of task. In **Figure 5** the hemodynamic responses of execution and inhibition are plotted in one graph to compare the neuronal modulations more easily. In **Figure 5A** the execution/inhibition responses for finger movements and in **Figure 5B** for foot movements are plotted together.

Particularly during the finger movement execution an [oxy-Hb] increase was found centrally compared to the inhibition condition, where frontal regions showed [oxy-Hb] increase and [deoxy-Hb] decrease. This effect is clearly visible in the topographic maps of **Figures 6A** (foot) and **B** (finger). At time point 2 (8–12 s) a clear [oxy-Hb] decrease was found at central sites during execution of finger and foot movements, whereas during movement inhibition both conditions showed a [oxy-Hb] decrease at central sites and an increase at frontal sites.

DISCUSSION

The grand average hemodynamic response during finger movement execution showed a typical activation pattern, namely an increase in the [oxy-Hb] and a decrease of [deoxy-Hb] in the hand representation area (left sensorimotor cortex). In parallel with this activation pattern an [oxy-Hb] decrease and an increase of [deoxy-Hb] in the medial area of the anterior prefrontal cortex (APFC; approximately BA 10) was also observed. Furthermore, the responses during finger movement inhibition showed a decrease in the [oxy-Hb] and an increase of [deoxy-Hb] in the

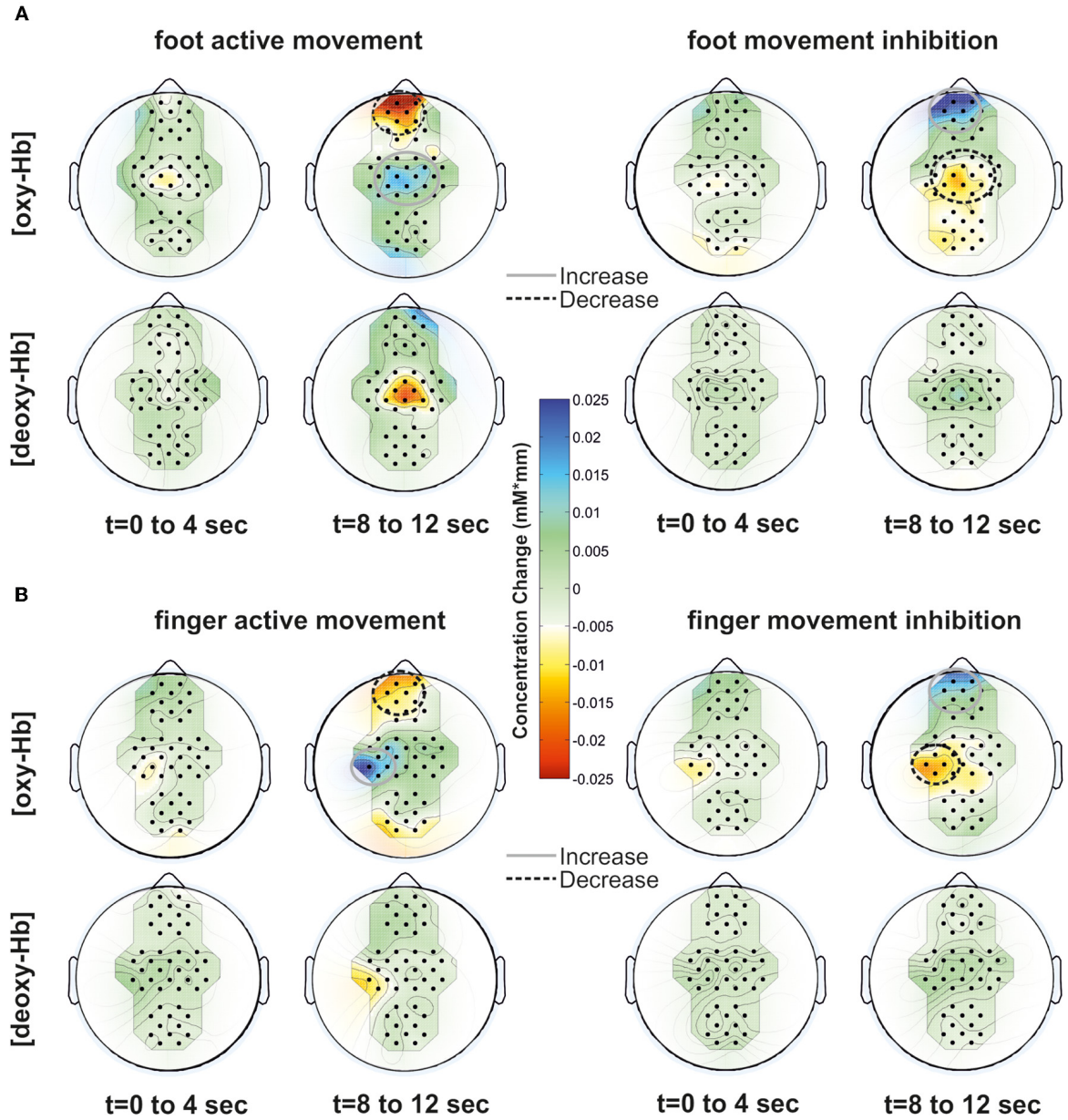

FIGURE 6 | Topographic distribution of foot (A) and finger (B) movement activation (left side) and inhibition (right side) at two time points (0–4 and 8–12 s) for [oxy-Hb] and [deoxy-Hb]. An increase of oxy/deoxy-Hb is indicated by cold colors and a decrease by warm colors.

hand representation area (left sensorimotor cortex) whereas in the medial area of the APFC [oxy-Hb] increased and [deoxy-Hb] decreased. These findings are in line with previous fMRI studies (Rubia et al., 2001, 2003; Hummel et al., 2004; Nakata et al., 2008) and fNIRS studies (Boecker et al., 2007) investigating the role of the PFC during response inhibition. For example, also Rubia and colleagues (2001) found increased BOLD signals in left hemispheric dorsolateral prefrontal, medial, and parietal cortices during a go/no-go task. In a later fMRI study investigating inhibition of learned motor programs, performed by Hummel et al. (2004) was shown that the inhibitory changes are reflected by negative BOLD responses in an extended cerebro-cerebellar network of sensorimotor structures with a predominant role of the PFC.

A lot of studies identified a neural network during response inhibition consisting of ventrolateral prefrontal cortex (VLPFC), insula, basal ganglia, pre-SMA, and dorsolateral prefrontal cortex (DLPFC) (Wager et al., 2005; Aron and Poldrack, 2006; Li et al., 2008; Nakata et al., 2008; Cai and Leung, 2009; Chikazoe et al., 2009; Chen et al., 2010; Hampshire et al., 2010; Sharp et al., 2010; Tabu et al., 2011; Mirabella et al., 2012). We additionally showed

that the APFC and sensorimotor regions (see also Coxon et al., 2006; Mirabella et al., 2011) are also involved. Whereas most of these studies only investigated cortical responses during execution/inhibition of hand movements, we are the first who additionally investigated metabolic changes of execution/inhibition during foot movements with fNIRS. Like the activation changes during finger movements we found the same pattern during foot movements, namely an increase of [oxy-Hb] during execution of foot movements over the corresponding representation of the sensorimotor areas regions and a further increase of [oxy-Hb] during inhibition of the same over APFC. This might be due to the interconnections of the PFC to motor areas, such as premotor, cingulate, and SMA, and to parietal areas (somatosensory areas). Another recent fMRI study performed by Tabu et al. (2012) also investigated response inhibition during hand and foot movements. They compared hand and foot inhibition mechanisms during a stop signal task. They found common inhibitory mechanisms in the pre-SMA and VLPFC regardless of modalities between hand and foot which is in line with our results.

For finger movements the same PFC activation was found in the fNIRS study by Boecker et al. (2007) using a stop-change paradigm. They compared successful as well as failed inhibition and they found PFC activation during both tasks, with pronounced activation increase in the right PFC during successful inhibition. In contrast to this study, where a two-channel fNIRS apparatus was used, we could also report activation changes over motor cortical regions additionally to PFC activity by using a multi-channel fNIRS system (46 channels). These results further support the idea that PFC activation is likely to reflect the implementation of inhibitory control of motor behavior. Covering sensorimotor areas we were able to provide evidence that appropriate contextual control of learned motor acts is represented in the brain by an extended network of sensorimotor structures in which metabolic activity is bidirectional modulated as suggested by Hummel et al. (2004). Concretely the stronger increase of [oxy-Hb] during execution compared to inhibition over sensorimotor areas and the stronger increase of [oxy-Hb] during inhibition of activation over prefrontal and SMA will support the theory of a distributed cortical network controlled by prefrontal top-down processes. The term "bidirectionality" as introduced by Hummel et al. (2004) does not stringently include causality, but rather the fact of reverse hemodynamic responses during inhibition and execution of movements. Whereas the study by Boecker et al. (2007) already showed that fNIRS is a suitable technique measuring prefrontal activation during the inhibition of initiated responses and the contribution of the PFC to response inhibition we could extend that knowledge by additionally showing a similar cortical activation pattern for execution/inhibition of foot movements with multichannel fNIRS.

The finding that inhibition/execution of learned motor programs depends on increases and decreases of neural activity in prefrontal and sensorimotor areas regardless of the effector is linked to the absence of a somatotopic organization of the PFC (see Tabu et al., 2012). Our study provides further evidence for a common neural network for finger and foot response inhibition.

All mentioned fMRI and fNIRS studies emphasize the role of the PFC during response inhibition, but in contrast to our results they primarily found activation in the right PFC. For example Boecker et al. (2007) found a substantial increase of [oxy-Hb] in the right PFC during successful inhibition of already initiated responses. For failed inhibition activation changes were observed bilaterally. Also Rubia et al. (2003) found in their event-related stop-signal study different activation patterns for successful and failed stopping. The results of the present study showed an increase of [oxy-Hb] in the APFC bilaterally for inhibition which might be due to the fact that we did not differentiate between successful and failed inhibition and both types run into analyses.

LIMITATIONS OF THE STUDY

The missing documentation of the type of inhibition is one limitation of the study which should be improved in future studies. A further limitation of the study is the lack of recording behavioral data at all. Whereas the typing frequencies of all movements have been recorded, the exact events (e.g., number of correct sequences) were missing.

CONCLUSION

During finger movement execution of right handed subiects, we found an increase of [oxy-Hb] and a decrease of [deoxy-Hb] in the hand representation area (left sensorimotor cortex). Additionally a [oxy-Hb] decrease and an increase of [deoxy-Hb] in the medial area of the APFC were observed, more prominently in the left hemisphere. During finger movement inhibition a decrease in the [oxy-Hb] and an increase of [deoxy-Hb] in the hand representation area was found. Furthermore, an [oxy-Hb] increase and a [deoxy-Hb] decrease in the medial area of the APFC bilaterally and the supplementary sensorimotor regions was observed. These bidirectional neuronal control which is represented by increase/decrease of oxy-Hb and deoxy-Hb concentration are in line with the results by Hummel et al. (2004) suggesting the importance of considering not only increases but also decreases of neuronal activity in the sensorimotor network and the importance of the PFC in top-down control.

Furthermore the same interpretation is valid for foot movements, where we found an increase of [oxy-Hb] over APFC during the inhibition condition. This novel finding reinforces the claim that the PFC plays an important role during inhibitory control of motor responses (Hummel et al., 2004; Boecker et al., 2007). Clearly, inhibitory control is not a unitary process mediated by a distinct brain region, instead several neural structures contribute to different components of inhibitory control of movements. This knowledge will help to understand disorders which are closely related to inhibition, for example ADHD (Aron, 2009), bipolar disorders (Rubia et al., 2001) or Parkinson's disease (Van den Wildenberg et al., 2006; Mirabella et al., 2012).

ACKNOWLEDGMENTS

This work is supported by the European ICT Program Project TOBI (FP7-224631) and by the "Land Steiermark" (project A3-22. N-13/2009-8). This paper only reflects the authors' views and funding agencies are not liable for any use that may be made of the information contained herein.

REFERENCES

Aron, A. R. (2009). Introducing a special issue on stopping action and cognition. *Neurosci. Biobehav. Rev.* 33, 611–612.

Aron, A. R., and Poldrack, R. A. (2006). Cortical and subcortical contributions to stop signal response inhibition: role of the subthalamic nucleus. *J. Neurosci.* 26, 2424–2433.

Boecker, M., Buecheler, M. M., Schroeter, M. L., and Gauggel, S. (2007). Prefrontal brain activation during stop-signal response inhibition: an event-related functional near-infrared spectroscopy study. *Behav. Brain Res.* 176, 259–266.

Cai, W., and Leung, H. C. (2009). Cotical activity during manual response inhibition guided by color and orientation cues. *Brain Res.* 1261, 20–28.

Chen, X., Scangos, K. W., and Stuphorn, V. (2010). Supplementary motor area exerts proactive and reactive control of arm movements. *J. Neurosci.* 30, 14657–14675.

Chikazoe, J., Jimura, K., Hirose, S., Yamashita, K., Miyashita, Y., and Konishi, S. (2009). Preparation to inhibit a response complements response inhibition during performance of a Stop-signal task. *J. Neurosci.* 29, 15870–15877.

Coxon, J. P., Stinear, C. M., and Byblow, W. D. (2006). Intracortical inhibition during volitional inhibition of prepared action. *J. Neurophysiol.* 95, 3371–3383.

Hampshire, A., Chamberlain, S. R., Monti, M. M., Duncan, J., and Owen, A. M. (2010). The role of the right inferior frontal gyrus: inhibition and attentional control. *Neuroimage* 50, 1313–1319.

Herrmann, M. J., Plichta, M. M., Ehlis, A. C., and Fallgatter, A. J. (2005). Optical topography during a go–no-go task assessed with multi-channel near-infrared spectroscopy. *Behav. Brain Res.* 160, 135–140.

Hummel, F., Andres, F., Altenmüller, E., Dichgans, J., and Gerloff, C. (2002). Inhibitory control of acquired motor programs in the human brain. *Brain* 125, 404–420.

Hummel, F., Saur, R., Lasogga, S., Plewnia, C., Erb, M., Wildgruber, D., Grodd, W., and Gerloff, C. (2004). To act or not to act. Neural correlates of executive control of learned motor behavior. *Neuroimage* 23, 1391–1401.

Kono, T., Matsuo, K., Tsunashima, K., Kasai, K., and Takizawa, R. (2007). Multiple-time replicability of near-infrared spectroscopy recording during prefrontal activation task in healthy men. *Neurosci. Res.* 57, 504–512.

Li, C. S., Yan, P., Sinha, R., and Lee, T. W. (2008). Subcortical processes of motor response inhibition during a stop signal task. *Neuroimage* 41, 1352–1363.

Malonek, D., Dirnagl, U., Lindauer, U., Yamada, K., Kanno, I., and Grinvald, A. (1997). Vascular imprints of neuronal activity: relationships between the dynamics of cortical blood ow, oxygenation, and volume changes following sensory stimulation. *Proc. Natl. Acad. Sci. U.S.A.* 94, 14826–14831.

Malonek, D., and Grinvald, A. (1996). Interactions between electrical activity and cortical microcirculation revealed by imaging spectroscopy: implications for functional brain mapping. *Science* 272, 551–554.

Mirabella, G., Pani, P., and Ferraina, S. (2011). Neural correlates of cognitive control of reaching movements in the dorsal premotor cortex of rhesus monkeys. *J. Neurophysiol.* 106, 1454–1466.

Mirabella, G., Iaconelli, S., Romanelli, P., Modugno, N., Lena, F., Manfredi, M., and Cantore, G. (2012). Deep brain stimulation of subthalamic nuclei affects arm response inhibition in Parkinson's patients. *Cereb. Cortex* 22, 1124–1132.

Nakata, H., Sakamoto, K., Ferretti, A., Gianni Perrucci, M., Del Gratta, C., Kakigi, R., and Luca Romani, G. (2008). Som ato-motor inhibitory processing in humans: an event-related functional MRI study. *Neuroimage* 39, 1858–1866.

Okamoto, M., Dan, H., Sakamoto, K., Takeo, K., Shimizu, K., Kohno, S., Oda, I., Isobe, S., Suzuki, T., Kohyama, K., and Dan, I. (2004). Three-dimensional probabilistic anatomical cranio-cerebral correlation via the international 10–20 system oriented for transcranial functional brain mapping. *Neuroimage* 21, 99–111.

Pfurtscheller, G., Bauernfeind, G., Wriessnegger, S. C., and Neuper, C. (2010). Focal frontal (de)oxyhemoglobin responses during simple arithmetic. *Int. J. Psychophysiol.* 76, 186–192.

Rubia, K., Overmeyer, S., Taylor, E., Brammer, M. J., Williams, S. C. R., and Simmons, A. (2000). Functional frontalisation with age: mapping neurodevelopmental trajectories with fMRI. *Neurosci. Biobehav. Rev.* 24, 13–19.

Rubia, K., Russell, T., Overmeyer, S., Brammer, M. J., Bullmore, E. T., and Sharma, T. (2001). Mapping motor inhibition: conjunctive brain activations across different versions of go/no-go and stop tasks. *Neuroimage* 13, 250–261.

Rubia, K., Smith, A. B., Brammer, M. J., and Taylor, E. (2003). Right inferior prefrontal cortex mediates response inhibition while mesial prefrontal cortex is responsible for error detection. *Neuroimage* 20, 351–358.

Sharp, D. J., Bonnelle, V., De Boissezon, X., Beckmann, C. F., James, S. G., Patel, M. C., and Mehta, M. A. (2010). Distinct frontal systems for response inhibition attentional capture and error processing. *Proc. Natl. Acad. Sci. U.S.A.* 107, 6106–6111.

Simmonds, D. J., Pekar, J. J., and Stewart, H. M. (2008). Meta-analysis of Go/No-go tasks demonstrating that fMRI activation associated with response inhibition is task-dependent. *Neuropsychologia* 46, 224–232.

Singh, A. K., Okamoto, M., Dan, H., Jurcak, V., and Dan, I. (2005). Spatial registration of multichannelmulti-subject fNIRS data to MNI space without MRI. *Neuroimage* 27, 842–851.

Steinbrink, J., Villringer, A., Kempf, F., Haux, D., Boden, S., and Obrig, H. (2006). Illuminating the BOLD signal: combined fMRI-fNIRS studies. *Magn. Reson. Imaging* 24, 495–505.

Steingrüber, H., and Lienert, G. (1971). *Hand-Dominanz-Test*. Göttingen: Hogrefe.

Strangman, G., Culver, J. P., Thompson, J. H., and Boas, D. A. (2002). A quantitative comparison of simultaneous BOLD fMRI and NIRS recordings during functional brain activation. *Neuroimage* 17, 719–731.

Tabu, H., Mima, T., Aso, T., Takahashi, R., and Fukuyama, H. (2011). Functional relevance of pre-supplementary motor areas for the choice to stop during Stop signal task. *Neurosci. Res.* 70, 277–284.

Tabu, H., Mima, T., Aso, T., Takahashi, R., and Fukuyama, H. (2012). Common inhibitory prefrontal activation during inhibition of hand and foot responses. *Neuroimage* 59, 3373–3378.

Van den Wildenberg, W. P., van Boxtel, G. J., van der Molen, M. W., Bosch, D. A., Speelman, J. D., and Brunia, C. H. (2006). Stimulation of the subthalamic region facilitates the selection and response inhibition of motor responses in Parkinson's disease. *J. Cogn. Neurosci.* 18, 626–636.

Wager, T. D., Sylvester, C. Y., Lacey, S. C., Nee, D. E., Franklin, M., and Jonides, J. (2005). Common and unique components of response inhibition revealed by fMRI. *Neuroimage* 27, 323–340.

Wolf, M., Wolf, U., Toronov, V., Michalos, A., Paunescu, L. A., Choi, J., and Gratton, E. (2002). Different time evoluion of oxyhemoglobin and deoxyhemoglobin concentration changes in visual and motor cortices during functional stimulation: a near-infrared spectroscopy study. *Neuroimage* 16(3 Pt 1), 704–712.

Conflict of Interest Statement: The authors declare that the research was conducted in the absence of any commercial or financial relationships that could be construed as a potential conflict of interest.

Received: 31 January 2012; accepted: 06 July 2012; published online: 25 July 2012. Citation: Wriessnegger SC, Bauernfeind G, Schweitzer K, Kober S, Neuper C and Müller-Putz GR (2012) The interplay of prefrontal and sensorimotor cortices during inhibitory control of learned motor behavior. Front. Neuroeng. 5:17. doi: 10.3389/fneng.2012.00017

frontiers in
NEUROENGINEERING

REVIEW ARTICLE
published: 19 June 2012
doi: 10.3389/fneng.2012.00009

Proactive and reactive control by the medial frontal cortex

***Veit Stuphorn*[1,2]* *and Erik E. Emeric*[2]**

[1] *Psychological and Brain Sciences, The Zanvyl Krieger Mind/Brain Institute, Johns Hopkins University, Baltimore, MD, USA*
[2] *Neuroscience, The Zanvyl Krieger Mind/Brain Institute, Johns Hopkins University, Baltimore, MD, USA*

Edited by:
Giovanni Mirabella, University of La Sapienza, Italy

Reviewed by:
Birte U. Forstmann, Max Planck Institute for Human Cognitive and Brain Sciences, Germany
Vassiliy Tsytsarev, University of Maryland School of Medicine, USA

***Correspondence:**
Veit Stuphorn, The Zanvyl Krieger Mind/Brain Institute, The Johns Hopkins University, 3400 N. Charles Street, 338 Krieger Hall, Baltimore, MD 21218, USA.
e-mail: veit@jhu.edu

Adaptive behavior requires the ability to flexibly control actions. This can occur either proactively to anticipate task requirements, or reactively in response to sudden changes. Recent work in humans has identified a network of cortical and subcortical brain region that might have an important role in proactive and reactive control. However, due to technical limitations, such as the spatial and temporal resolution of the BOLD signal, human imaging experiments are not able to disambiguate the specific function(s) of these brain regions. These limitations can be overcome through single-unit recordings in non-human primates. In this article, we describe the behavioral and physiological evidence for dual mechanisms of control in response inhibition in the medial frontal cortex of monkeys performing the stop signal or countermanding task.

Keywords: primate, stop signal task, inhibition, supplementary motor area, control

INTRODUCTION

Adaptive behavior requires the ability to flexibly control actions. This can occur either proactively to anticipate task requirements, or reactively in response to sudden changes. The stop-signal, or countermanding, task is a commonly used behavioral task that requires both forms of behavioral control. It is, therefore, uniquely suited to study the neuronal mechanism of proactive and reactive control.

Recent neuroimaging studies of humans in the stop signal task using manual and eye movements show activation centered on the medial and lateral frontal cortex and subthalamic nucleus (STN; Curtis et al., 2005; Aron and Poldrack, 2006; Li et al., 2006; Aron et al., 2007a). These human imaging results have emphasized critical roles of the supplementary motor cortex (preSMA/SMA), right inferior frontal cortex (IFC), and the STN in response inhibition during a manual stop signal task (reviewed by Aron, 2011). Reactive stopping depends on a fronto-basal ganglia network which includes the preSMA, the IFC, the basal ganglia, and M1. Specifically, it has been suggested that the fast inhibition of a prepared response requires activity of the IFC (Aron et al., 2003). The exact role of the IFC within the proactive inhibition process is debated and may involve the attentional detection of the stop signal and/or a direct role in inhibitory control. Furthermore, it has been suggested that the inhibitory control may be instantiated via hyperdirect input to the basal ganglia via the STN (Aron and Poldrack, 2006). Proactive control also depends on a fronto-basal ganglia network which includes premotor cortex (e.g., preSMA), dorsolateral prefrontal cortex, striatum, and palladium. In this context, inhibitory control may be instantiated via the indirect pathway.

This recent work in humans has identified a network of cortical and subcortical brain region that might have an important role in proactive and reactive control. However, due to technical limitations, such as the spatial and temporal resolution of the BOLD signal, fMRI experiments are not able to disambiguate the specific function(s) of these brain regions. In an ongoing research project we and other labs have, therefore, investigated the role of these frontal areas in behavioral control using single-unit and local field potential recordings in awake, behaving primates performing a countermanding task. In the following we will review some of the insights into the neuronal mechanisms underlying proactive and reactive control that this research has provided.

PROACTIVE AND REACTIVE CONTROL

Braver (2007, 2012) proposed the dual mechanisms of control framework which states that cognitive control operates via two distinct operating modes: proactive control and reactive control. Proactive control is a form of early selection in which goal-relevant information is actively maintained in a sustained manner, before the occurrence of cognitively demanding events, to optimally bias attention, perception, and action systems in a goal-driven manner (Miller and Cohen, 2001). Reactive control is recruited as a late correction mechanism that is mobilized only as needed, in a just-in-time manner, such as after a high interference event is detected (Jacoby et al., 1999). Thus, proactive control relies upon the anticipation and prevention of interference before it occurs, whereas reactive control relies upon the detection and resolution of interference after its onset. Although substantial theoretical and experimental progress toward elucidating the mechanisms underlying reactive inhibitory control has been made (see for example reviews by Stuphorn and Schall, 2002; Schall and Boucher, 2007), the mechanisms underlying proactive control have remained less clear.

THE STOP SIGNAL TASK

The stop signal or countermanding paradigm (**Figure 1**) has been used to investigate the neural control of movement initiation and

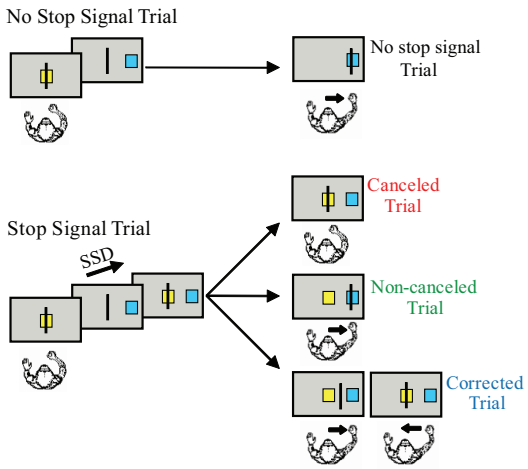

FIGURE 1 | The arm countermanding task. Each trial begins when the cursor is positioned inside the center box. After a delay, the target box appears to one side of the screen and the center box disappears, instructing the monkey to move the cursor into the target box. On stop signal trials, the center box reappears after the SSD signaling that the monkey should cancel the planned movement. On the variable-reward version of the paradigm, the color of the center box indicates whether the trial will result in a high or low reward if performed correctly.

inhibition in rats, awake behaving monkeys, and human subjects (reviewed by Schall and Boucher, 2007). The stop signal paradigm, which includes both a task design and a theoretical construct, was developed to investigate the control of action (reviewed by Logan, 1994). The stop signal paradigm has also been used to examine inhibitory control in a variety of other contexts (reviewed by Verbruggen and Logan, 2008). The stop signal task has also been used to examine patients with ADHD (reviewed by Alderson et al., 2007) and, recently, has been selected for translation for use in clinical trials (Carter et al., 2009).

Although many variations in the stimuli and effectors have been used in the stop signal task, the requirements of the task are quite simple. The stop-signal task probes the ability to control action by requiring subjects to inhibit a planned movement in response to an infrequent stop signal which they do with variable success depending on the delay of the stop signal. Stop signal task performance can be accounted by a race between a process that initiates the movement (GO process) and by one that inhibits the movement (STOP process). This race model provides an estimate of the stop signal reaction time (SSRT), which is the time required to inhibit the planned movement. The SSRT can be estimated using various methods (reviewed by Logan, 1994; Band et al., 2003). T measured in the saccade SSRT average is approximately 100 ms in monkeys and 130 ms in humans (e.g., Hanes and Schall, 1995; Hanes and Carpenter, 1999). In the manual stop signal task, the SSRT is an average of 150 ms in monkeys and 250 ms in humans (e.g., Boucher et al., 2007; Scangos and Stuphorn, 2010).

The rationale and approach for the race model analysis of the neural stop signal data has been described previously (Logan et al., 1984; Hanes et al., 1998; Hanes and Schall, 1995). Briefly, the chief virtue of the stop signal paradigm is that one can determine whether a neural or motor related signal [e.g., single-units, local field potentials (LFPs), evoked-potentials (ERPs), electromyograms (EMGs)] is sufficient to control the initiation of movements. The race model imposes two criteria that a signal must meet to play a direct role in the control of movement. First, the signal must be different when a movement is initiated versus when it is inhibited. Second and most important, this difference in activity must evolve before the SSRT elapses. Signals sufficient to control movement initiation are reactive control signals that are exerted in response to the sudden occurrence of a stop signal.

The race model assumes that the GO and STOP processes are stationary stochastic processes with independence between trials. In other words, the response time on the current trial is independent of the preceding trial. However, response times are often non-stationary and non-independent (e.g., Gilden, 2001; Wagenmakers et al., 2004). For example, it is commonly observed across experimental conditions and response modalities that subjects'response times tend to increase in the context of the stop signal task relative to that in simple response time tasks (e.g., Logan, 1981; Logan and Burkell, 1986; van den Wildenberg et al., 2003; Mirabella et al., 2006). Specifically, both short-term and long-term changes in stop-signal frequency lead to behavioral adjustments (Emeric et al., 2007; Nelson et al., 2010). For example, response times decrease after no stop signal trials and increases after stop signal trials. Furthermore, subjects' response times increase and the probability of a cancelled response increases with increasing global proportion of stop signal trials. It seems clear that when stop signal trials occur, subjects proactively adopt a more cautious strategy by slowing responses on subsequent trials.

Importantly, the stop signal task evokes both reactive and proactive forms of control. Although the Braver et al. (2007), Braver (2012) account of control is couched in terms of attentional processes, it can be used as a working hypothesis for investigating the proactive and reactive control processes involved in inhibition. The dual mechanisms of control account provide strong predictions about the temporal dynamics of brain activity related to proactive versus reactive control. Proactive control should be associated with sustained and/or anticipatory activation, which reflects the active maintenance of task goals. This activity may serve as a source of top-down bias that can facilitate processing of expected upcoming events. By contrast, reactive control should be reflected in transient activation subsequent to unexpected events.

NEURAL NETWORK UNDERLYING BEHAVIORAL CONTROL

A network of brain areas in the frontal cortex and the basal ganglia have been implicated in playing a key role in behavioral control (Floden and Stuss, 2006; Aron et al., 2007b; Picton et al., 2007) and specifically during the stop signal paradigm (Curtis et al., 2005; Aron and Poldrack, 2006; Li et al., 2006; Aron et al., 2007a). A critical component of this network is the medial frontal cortex, in particular the supplementary eye field (SEF), pre-supplementary motor area (pre-SMA), and adjacent

supplementary motor area (SMA). The SEF is involved in the control of eye movements and provides input to ocular motor structures in the striatum, SC, and brainstem (Huerta and Kaas, 1990). In contrast, the SMA is more important for the control of skeletomotor movements, such as movements of the arm and the hand (Fujii et al., 2002). The role of the pre-SMA is more debated, but seems to be more cognitive than the one of the other two and less clearly related to only one major motor system (Sumner et al., 2007). The pre-SMA and SMA, which are reciprocally connected, differ in their connectivity, with pre-SMA connected to prefrontal cortex but not motor regions, and SMA to motor regions but not prefrontal cortex (Luppino et al., 1991; Tanji, 1996; Johansen-Berg et al., 2004). The SEF, pre-SMA, and SMA also provide input to the striatum and STN (Alexander and Crutcher, 1990; Alexander et al., 1990; Nambu et al., 1996). The physiology of the medial frontal areas, as well as the one of other cortical and subcortical regions has been examined for signals sufficient to control movements in monkeys performing the saccade stop signal task (Hanes et al., 1998; Stuphorn et al., 2000, 2010; Paré and Hanes, 2003; Emeric et al., 2008, 2010; Godlove et al., 2011) and skeletomotor (Chen et al., 2010; Scangos and Stuphorn, 2010) stop signal tasks.

REACTIVE CONTROL AND PRIMARY MOTOR AREAS

In the context of the stop signal task, reactive control is recruited as a late correction mechanism that is mobilized only as needed, in a just-in-time manner, such as the instant a stop signal is perceived. Because this control mechanism is engaged only at short notice, it requires the ability to generate control signals at high speed that are capable of influencing ongoing motor activity even at a late stage of the movement preparation. This form of behavioral control is therefore, likely to be found within and interacting with the primary motor systems that directly control the relevant effectors. Most of the neurophysiological work that has investigated reactive control in monkeys has been concentrated on the oculomotor system, due to the fact that this is the currently best understood motor system (Hanes et al., 1998; Stuphorn et al., 2000; Ito et al., 2003; Paré and Hanes, 2003; but see Scangos and Stuphorn, 2010; Mirabella et al., 2012).

The FEF, located in the rostral bank of the arcuate sulcus in macaque monkeys, participates in the transformation of visual signals into saccade motor commands (reviewed by Schall, 1997). Two of the functional subpopulations of neurons that have been observed in the FEF during gaze shifts are movement and fixation neurons. Movement neurons in the FEF exhibit increased discharge before and during saccades (Goldberg, 1985; Schall, 1991a; Hanes and Schall, 1996) while fixation neurons are active during fixation and exhibit decreased discharge preceding saccades (Hanes et al., 1998; Sommer and Wurtz, 2000). FEF neurons innervate the superior colliculus (Segraves and Goldberg, 1987; Sommer and Wurtz, 2000) and the neural circuit in the brainstem that generates saccades (Segraves, 1992).

Hanes et al. (1998), the first study to apply the race model to single-unit activity during the saccade stop signal task, examined the sufficiency of FEF neurons to control the initiation of saccadic eye movements. Applying the race model to neuronal activity acquired in the context of the stop signal task, provided clear evidence that movement and fixation neurons in FEF generate signals sufficient to control the production of gaze shifts. Saccades were initiated if and only if the activity of FEF movement neurons reach a specific and constant threshold activation level which is independent to the response time (Hanes and Schall, 1996; Brown et al., 2008). Movement neurons, whose activity increased as saccades were prepared, decayed in response to the stop signal before the SSRT elapsed. Fixation cells that decreased firing before saccades exhibited elevated activity in response to the stop signal before the SSRT elapsed. The majority of visual neurons, on the other hand, did not discharge differently when saccades were initiated versus inhibited. The visual neurons that did discharge differentially when saccades were initiated versus inhibited, did so well after the SSRT had elapsed. Paré and Hanes (2003) observed parallel results for visual, movement, and fixation neurons in the superior colliculus (SC).

REACTIVE CONTROL AND MEDIAL FRONTAL CORTEX

Thus, at least one form of reactive control signals in the oculomotor system is the reactivation of fixation neurons in the FEF and SC. What is driving the onset of these neurons? At least one source is an external event, the onset of the stop signal. Its potency in the oculomotor stop signal task was probably due to the fact that it was a flash of a light in the fovea, which directly activated the gaze fixation system (Everling et al., 1998). However, there are likely to be other, more complex, driving factors. For example, the monkeys initially did not respond to reappearance of the fixation light, or at least not necessarily by inhibition of saccade preparation. This response, and presumably the sensitivity of fixation cells to specific sensory stimuli, was acquired during training. Likewise, even after training, the monkeys did not show saccade inhibition, when outside of the task setting or at the end of the recording session, when their motivation was low. Thus, there is clearly a task set that the monkeys learn during training and that guides their behavior in the stop signal task, when they know that there is a relationship between receiving reward and following certain behavioral rules, i.e., the task set. The representation of task set is a primary function of frontal cortex (Sakai, 2008). We decided, therefore, to study neurons in frontal regions that were hierarchically higher than the primary motor areas and provided input into FEF and SC. The first of the candidate regions that was tested was SEF.

The SEF is an area on the dorsomedial convexivity of the frontal cortex that seems to parallel the FEF in many ways. The activity of neurons in the SEF are modulated by visual or auditory stimuli, while other SEF neurons are modulated preceding and during saccades (e.g., Schall, 1991b; Schlag and Schlag-Rey, 1987. Stuphorn et al. (2000, 2010) examined single-unit activity during the saccade stop signal task to determine the sufficiency of SEF neurons to control the initiation of saccadic eye movements. Like the FEF movement neurons, the activity of SEF movement neurons increased as saccades were prepared. However, unlike their counterparts in the FEF, these neurons do not exhibit a reliable threshold and vanishingly few neurons in the SEF generate signals that are sufficient to control gaze (Stuphorn et al., 2000, 2010). Emeric et al. (2010) observed parallel results in the

event related local field potentials. Importantly, in the current context, no neurons were observed that showed enhanced activity on trial were the monkey successfully cancelled the saccade generation. Thus, SEF does not seem to carry reactive control signals.

Recently, we used the stop signal task to investigate the control of arm movements (Chen et al., 2010; Scangos and Stuphorn, 2010). There are important differences between these two motor systems. For example, unlike saccades, arm movements can be stopped at any point along their path (De Jong et al., 1990). This non-ballistic nature of the arm movements result in differences in the nature of the control signals required compared to the oculomotor system.

Another reason to study SMA and pre-SMA is that they are widely considered to play a completely different role in motor control, than behavioral control. Specifically, it is hypothesized that SMA and pre-SMA are primarily responsible for voluntary movement initiation (Eccles, 1982; Goldberg, 1985; Sumner et al., 2007; Haggard, 2008). This hypothesis was first formulated after the discovery of the readiness potential (RP), a slow negative scalp potential that precedes self-initiated movements in humans (Kornhuber and Deecke, 1965) and whose source has been localized to the pre-SMA (Lang et al., 1991; Ikeda et al., 1999; Yazawa et al., 2000). Single-unit recordings in monkeys have shown that the pre-SMA and SMA contain long-lead neurons that become active up to 2 s before the initiation of self-paced movements (Okano and Tanji, 1987) and that pre-SMA neurons signal the initiation of action in a time-selective manner (Mita et al., 2009). In addition, lesion studies indicate an important role of SMA in inhibition, as well (Sumner et al., 2007). Thus, there are at least two different hypotheses in the literature concerning the role of pre-SMA and SMA in motor control. The experiments mentioned above have demonstrated that the earliest activity related to movements arises in the pre-SMA and SMA, but does this activity play a causal role in movement initiation or is this activity related to reactive or proactive control?

Scangos and Stuphorn (2010) probed SMA and pre-SMA movement related neurons with a manual version of the stop signal paradigm and vanishingly few neurons provided signals sufficient to control movement initiation according to the logic of the stop signal paradigm (**Figure 2A**). However, a second group of neurons, similar to the FEF/SC fixation neurons, were more active during successful response inhibition. A minority of these cells responded early enough to be able to influence the inhibition of the movement (**Figure 2B**). Thus, a minority of SMA/pre-SMA neurons may play a role in movement inhibition but do not appear to control movement initiation.

Chen et al. (2010) examined the local field potentials that were acquired simultaneously with the SMA single-units for signals sufficient to control the initiation of arm movements. Unlike the single-units, there were significant differences in LFP power in a number of frequency bands, which correlated with the successful inhibition of the arm movement. In the beta band (5–20 Hz) there was an increase in power evoked by the stop signal which persisted long after the SSRT elapsed. Within the high gamma band (130–140 Hz), especially for planned contralateral movements, there was an increase of power immediately after the stop signal and before the SSRT. Importantly, the modulation of LFP power in both recordings clearly started before the SSRT. This indicates that the neuronal processes that underlie the changes in LFP power in the respective parts of pre-SMA and SMA were sufficient to reactively control the inhibition of arm movements.

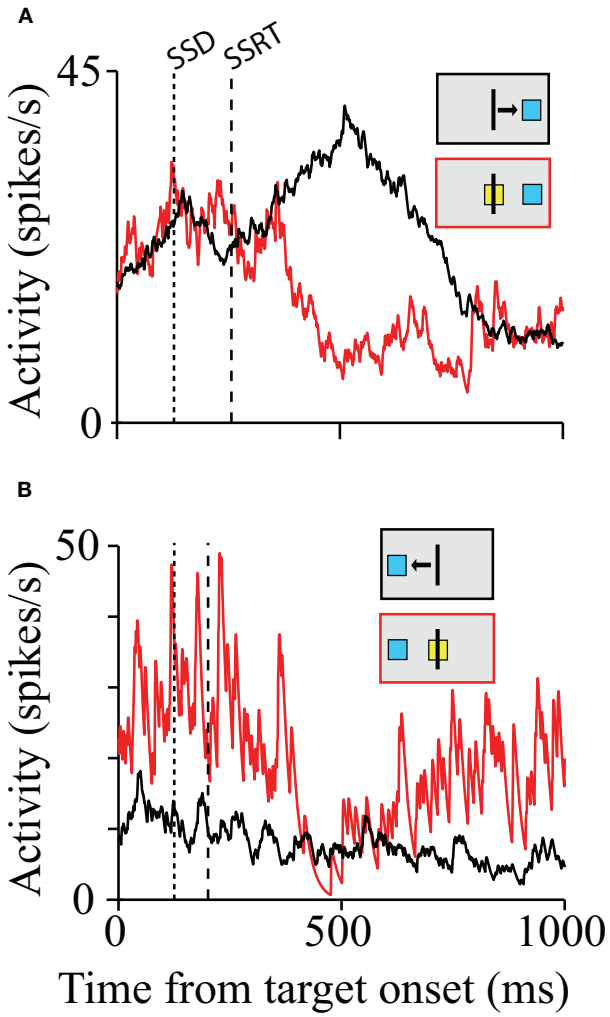

FIGURE 2 | Movement and inhibition related activity on canceled trials. The first dotted line represents the SSD. The second dashed line represents the SSRT. **(A)** Activity from a pre-SMA cell showing a difference in activity on latency-matched no-stop signal and canceled trials for the first SSD for movements to the right and left. Inhibition time occurs after the SSRT boundary for both plots. **(B)** SMA cell with a possible role in stopping movement. The arrowheads mark the average time of movement start and end. The range is indicated by the gray bar. The red and black boxes above each plot indicate the type of trial, the target location, and the movement direction (for no-stop signal trials).

The evidence we have discussed thus far suggests that, of all the brain areas probed with the stop signal paradigm, only the neurons in the FEF, SC, and pre-SMA/SMA carry signals sufficient to control movement initiation and thus provide signals consistent with reactive control. These findings show a potential functional difference between the control of the oculomotor

system (through SEF) and control of the skeletomotor system (through pre-SMA/SMA). In the oculomotor system reactive control signals are found on the level of the primary motor areas, but not in medial frontal cortex. In contrast, in the skeletomotor system the medial frontal cortex participates in reactive control. There is a number of considerations and possible interpretations of these findings.

First, it is possible that the reactive control signals exist in the SEF, but were simply overlooked in past recording experiments. That is always possible, but the fact that the negative finding in SEF is based on results in four monkeys, while the positive finding in pre-SMA/SMA is based on results in only two monkeys, makes this possibility less likely.

Second, it is possible that this finding reflects a real difference in the structure and organization of behavioral control. The number of cortical areas dedicated to the control of skeletomotor movements and their relative size is much larger than the ones of cortical areas dedicated to oculomotor control (e.g., Geyer et al., 2000). This likely reflects the fact that the dynamics and kinematic of skeletomotor movements are far more complex than saccadic eye movements. Therefore, it might not be surprising, that primary motor regions, such as FEF and SC, are sufficient for the reactive control of saccades, while in the case of skeletomotor movements it is necessary to recruit or involve medial frontal cortex as well.

Finally, one should keep in mind that the investigation and comparison of the oculo- and skeletomotor system is still incomplete. Mirabella et al. (2011) tested dorsal premotor cortex (PMd) using a variant stop signal task where the monkeys responded to visual targets by touch with a speeded reaching movement. The study found that among neurons with a movement-preparatory activity, about one-third exhibit a modulation before the behavioral estimate of the time it takes to cancel a planned movement. Hence these neurons exhibit a pattern of activity suggesting that PMd plays a critical role in the control of arm movement initiation and suppression. Some PMd neurons in the study were specifically active, when the monkeys were cancelling the arm movement. This is an intriguing finding, but a number of technical difficulties, such as the absence of EMG recordings limit the interpretation of neural activity as clear evidence of reactive control signals. Furthermore, there is currently no single-unit study of M1 using the stop signal task.

The location of the final decision as to whether or not a planned arm movement is carried out is, therefore, still not known. One possibility is that it takes place in the premotor or in the primary motor cortex (M1). A recent countermanding study in humans found that in M1, corticomotor excitability was reduced and intracortical inhibition was significantly greater on Stop trials compared with No stop signal trials at a time that preceded the onset of muscle activity (Coxon et al., 2006). These results indicate that inhibitory networks within M1 might contribute to volitional inhibition of prepared action. Another possible location for the final decision could be the basal ganglia (Mink, 1996). The internal segment of the globus pallidus (GPi) inhibits thalamic and cortical neurons, and thus serves as a block on the initiation of any action. The direct pathway through the striatum releases an action by inhibiting a specific set of GPi neurons. Both the hyperdirect pathway through the STN and the indirect pathway from the striatum through the external segment of the globus pallidus suppress actions by more wide-spread excitation of GPi (Mink, 1996; Nambu, 2004). A recent human neuroimaging study provided evidence for a role of the STN and the hyperdirect pathway in countermanding (Aron and Poldrack, 2006). Furthermore, deep brain stimulation of STN affects response inhibition in Parkinson's patients (Mirabella et al., 2012).

THE STOP SIGNAL TASK: PROACTIVE CONTROL

Proactive control adjusts the response selection and preparation process in anticipation of known task demands. Proactive control is guided by endogenous signals, instead of external triggers, and is constantly present throughout response selection and preparation. It can reflect a variety of factors such as the incentives for choosing different responses, and the frequency of task-relevant events. In the context of the stop signal task, proactive control is mostly related to a regulation of the level of excitability of the motor system. By adjusting the level of excitation and inhibition of the motor system, the proactive control system sets the threshold for initiating a response. In making these adjustments the proactive system has to negotiate the tradeoff between speed (reaction time) and accuracy (cancelation likelihood) (Bogacz et al., 2010).

Task performance in the stop signal task is clearly influenced by factors that are independent of the presence of an actual stop signal (Verbruggen and Logan, 2009). Behavioral studies in monkeys and humans show that the mean response time during no stop signal trials is delayed relative to a situation when no stop signal is expected (Verbruggen et al., 2004; Stuphorn and Schall, 2006; Verbruggen et al., 2006). Short-term changes in stop signal frequency lead to behavioral adjustments (Emeric et al., 2007; Mirabella et al., 2008; Chen et al., 2010; Nelson et al., 2010). These systematic modulations in the mean reaction time indicate the presence of proactive control.

While the experimental evidence in favor of a role of the medial frontal cortex in reactive control was mixed, there is very clear evidence for such a role in the case of proactive control. Very few neurons carried signals sufficient for saccade initiation (Stuphorn et al., 2010). However, there exists a more subtle relationship between SEF activation and saccade production. The activity of some SEF neurons was correlated with response time and varied with sequential adjustments in response latency. Trials in which monkeys inhibited or produced a saccade in a stop signal trial were distinguished by a modest difference in discharge rate of these SEF neurons before stop signal or target presentation. Parallel results were observed in the SMA (Chen et al., 2010). Furthermore, the analysis of LFP in the SMA showed that longer response times following stop signal trials (**Figure 3A**) were accompanied by an increased power in the very low-frequency (1–20 Hz) and the beta band (25–40 Hz) starting approximately 120 ms before target onset (**Figure 3B**). These findings indicate that neurons in the SEF and pre-SMA/SMA, in contrast to FEF/SC movement and fixation cells, do not contribute directly and immediately to the initiation of visually guided saccades. However the SEF, pre-SMA, and SMA may

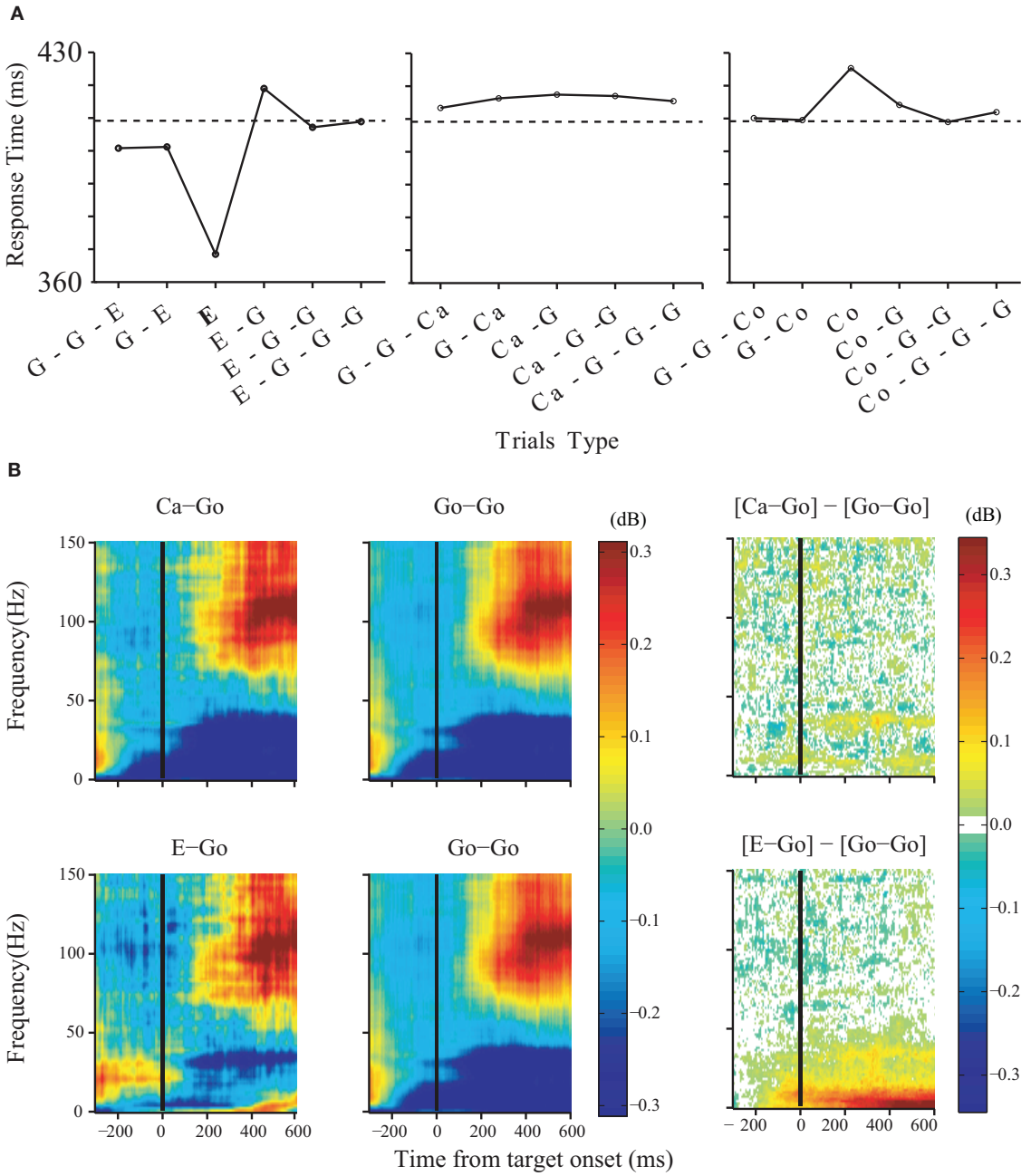

FIGURE 3 | Changes in LFP power predict arm movement inhibition. Effects of trial history on response time. **(A)** Response times for no-stop-signal and stop trials surrounding noncanceled trials (left), trials surrounding canceled trials (middle), and trials surrounding corrected trials (right). The type of trials to which the response time corresponds to is shown in bold (G: no stop signal; E: noncanceled; Ca: canceled; Co: corrected). The dotted line indicates the average response time on no-stop-signal trials. **(B)** Effects of trial history on LFP power in the SMA. Comparison was performed between three groups of no-stop-signal trials: those that followed another canceled trial (Ca-Go), those that followed a noncanceled error trial (E-Go), and those that followed a go trial (Go-Go). The time-frequency maps are aligned on target onset. The significant differences between them are shown in the right panel.

proactively regulate movement initiation by adjusting the level of excitation and inhibition of the occulomotor and skeletomotor systems based on prior performance and anticipated task requirements.

REGULATION OF SPEED-ACCURACY TRADEOFF BY MEDIAL FRONTAL CORTEX

In terms of computational reaction time models, a change in the responsiveness of the motor system translates into a shift of the

distance to the threshold at which a response is initiated (Ratcliff, 1978; Luce, 1986; Reddi and Carpenter, 2000). A decrease of the threshold is equivalent to an increase of the baseline, and vice versa (Stuphorn and Schall, 2002; Bogacz et al., 2010). Such shifts can explain speed-accuracy tradeoffs (Uchida et al., 2006). The results of neurophysiological experiments fit such reaction time models very well. The firing rate of neurons in the oculomotor (Hanes and Schall, 1996) and skeletomotor system (Lecas et al., 1986) indeed exceeds a fixed threshold, when movements are initiated. There is also some evidence for changes in baseline activity in the oculomotor system. In the superior colliculus, neurons with visual and saccade-related activity increase their baseline firing rate with increasing probability that a saccade in their motor field is required (Basso and Wurtz, 1998; Dorris and Munoz, 1998) or is more rewarding (Isoda and Hikosaka, 2008a,b).

We propose here that the dorsomedial frontal cortex, including the SMA, is the source of the proactive control signal that modulates the baseline motor activity. This hypothesis is supported by the fact that activity levels in and around the pre-SMA increased when response speed is emphasized during speed-accuracy tradeoff experiments (Forstmann et al., 2008; Ivanoff et al., 2008; van Veen et al., 2008).

The hypothesis that movement-related neurons in SEF, pre-SMA, and SMA influence reaction time by controlling excitability in the oculomotor and skeletomotor system, respectively, might be seen as contradicting the finding that these same neurons do not carry signals sufficient to control movement initiation (Scangos and Stuphorn, 2010; Stuphorn et al., 2010). However, this is not the case. We propose that SMA activity determines the response threshold, i.e., the amount of rise in motor activity that is necessary to initiate a movement. While the distance to the threshold clearly influences the average time at which it is exceeded, it is not sufficient to fully determine whether and when the threshold is actually exceeded. We propose that this process takes place in M1 and FEF, while SMA and SEF modulates this process by setting the urgency with which a movement is chosen and executed.

MOTIVATION FOR SPECIFIC ACTIONS AND ITS RELATIONSHIP TO PROACTIVE CONTROL

While our findings make it unlikely that pre-SMA and SMA play a causal role in initiating movements, lesions in these areas do have a profound influence on behavior. We found that the activity of most movement-related neurons in SMA and SEF was very strongly influenced by the reward contingency of the action (Scangos and Stuphorn, 2010; So and Stuphorn, 2010). Thus, SEF, pre-SMA, and SMA might represent the urge to act in a specific way rather than the commitment to do so. According to this interpretation the neurons in the medial frontal cortex represent a map of action values.

This interpretation of medial frontal cortex activity as a motivation signal fits with a large number of lesion and recording studies in humans and monkeys that indicate that the medial frontal cortex, in particularly pre-SMA, is responsible for self-generated, voluntary actions (Papa et al., 1991; Romo and Schultz, 1992; Deiber et al., 1999), and reflects the reward obtained by these actions (Stuphorn et al., 2000; Ito et al., 2003; Roesch and Olson, 2003, 2004; Campos et al., 2005; Sohn and Lee, 2007). Voluntary behavior is characterized by the motivation to act in order to obtain a particular goal. Lesions of the pre-SMA and SMA may lead to apathy, because the motivational drive that normally links reward expectation with specific actions is absent. However, since the motor system is still functional, external stimuli may still trigger automatic or habitual movements. This is, in fact, what is observed for SMA lesions in monkeys (Thaler et al., 1988, 1995) and humans (Levy and Dubois, 2006; Schmidt et al., 2008).

There exists a close relationship between this interpretation of medial frontal cortex activity as a motivational signal to the earlier discussed interpretation that the activity might represent proactive control signals. From an motivational point of view, there are two mutually exclusive motivations that compete with each other in the stop signal task. First, there is a motivation to GO resulting from the very frequent link between movement exceution and reward delivery. Secondly, there is a motivation to WAIT (not to stop *per se*) generated by the awareness that on any given trial a stop signal might be given. These two motivations (or action values for GO and WAIT) vary in strength according to the most recent reward and trial history. The relative strength of these motivations determines the level of excitability and the momentary speed-accuracy tradeoff of the subject at any moment in the task. However, this changing modulation of the level of excitability of the motor system was exactly what was discussed as a proactive control system earlier.

Our behavioral data showed strong sequential effects of errors and successful cancelations on the reaction time of arm movements in the stop signal task. Errors or an increased frequency of stop signal trials lead to longer reaction times on subsequent trials. Fewer stop signal trials lead to shorter reaction times. The reaction time reflects the level of responsiveness in the motor system. A less excitable state leads to longer reaction times, while a more excitable state leads to shorter reaction times. The sequential effects show that the state of responsiveness of the motor system is constantly adjusted by control signals that reset the balance of excitation and inhibition within the motor system.

We observe motivational signals in SEF, pre-SMA, and SMA during movement generation. In contrast, activity in the orbitofrontal cortex appears earlier, immediately after a cue indicating potential reward is revealed (Tremblay and Schultz, 1999; Roesch and Olson, 2003, 2004; Padoa-Schioppa and Assad, 2006), but it does not encode the action necessary to obtain the reward (Wallis and Miller, 2003; Padoa-Schioppa and Assad, 2006). Lateral prefrontal cortex activity reflects reward size and preference in the delay period before a response is made (Kobayashi et al., 2006; Sakagami and Watanabe, 2007). Striatal activity arises after a cue is presented and remains high until reward is delivered (Hikosaka et al., 1989; Hollerman et al., 1998). Thus, early reward related signals from other brain areas might feed into the SMA and pre-SMA where they are transformed into incentive signals for specific actions (So and Stuphorn, 2010).

COMPARISON OF HUMAN AND MONKEY DATA

Taken as a whole, electrophysiological data from humans and monkeys during stopping point to comparable proactive and

reactive control mechanisms. The preSMA and STN become more active when a prepotent response must be reactively inhibited (Isoda and Hikosaka, 2007, 2008a,b), while the preSMA and SMA activity is correlated with subsequent proactive changes in response time (Chen et al., 2010; Stuphorn et al., 2010). These findings fit well with the results of human studies (Aron and Poldrack, 2006; Sharp et al., 2010).

In addition, Aron and Poldrack (2006) have used human imaging results to emphasize the role of the right IFC and the STN in response inhibition during a manual stop signal task. Area 45, the cortex anterior to the inferior spur of the arcuate sulcus and lateral to the principal sulcus, is the most likely monkey homolog of the rIFG (Petrides and Pandya, 1999). Unfortunately, only very few electrophysiological recording studies in monkeys have examined neurons in area 45 in tasks requiring inhibition. These studies have used a go/nogo task and have reported neurons in BA45 that responded to behaviorally relevant cues and identified them as nogo signals (Sakagami et al., 2001). However, no activity was reported during the time period when the response to the target needed to be suppressed. Clearly, neurophysiological studies in monkeys are necessary to validate the role of IFC in stopping.

Aron et al. (2007a) used diffusion-weighted imaging tractography to show that the IFC and the STN region are connected via a white matter tract, which could underlie a hyperdirect pathway for basal ganglia control. Although, the corticocortical and thalamocortical connections of area 45 have been identified in the monkey (Contini et al., 2010; Gerbella et al., 2010), there have been no anatomical studies describing a hyperdirect projection from area 45 to the STN (e.g., Monakow et al., 1978). The existence of a hyperdirect connection between IFC/area 45 and STN is critical for the role of ICF in reactive stopping (Aron, 2011). It is therefore, of great priority to verify the existence of such a projection in monkeys.

CONCLUSION

Converging evidence from human imaging and monkey electrophysiology during stopping point to comparable proactive and reactive control mechanisms. However the exact function al role of IFC, basal ganglia, and thalamus in stopping is still unclear and will require further investigations using neurophysiological in awake behaving monkeys.

REFERENCES

Alexander, G. E., and Crutcher, M. D. (1990). Functional architecture of basal ganglia circuits: neural substrates of parallel processing. *Trends Neurosci.* 13, 266–271.

Alexander, G. E., Crutcher, M. D., and DeLong, M. R. (1990). Basal ganglia-thalamocortical circuits: parallel substrates for motor, oculomotor, "prefrontal" and "limbic" functions. *Prog. Brain Res.* 85, 119–146.

Alderson, R. M., Rapport, M. D., and Koer, M. J. (2007). Attention-deficit/hyperactivity disorder and behavioral inhibition: a meta-analytic review of the stop-signal paradigm. *J. Abnorm. Child Psychol.* 35, 745–758.

Aron, A. R., Fletcher, P. C., Bullmore, E. T., Sahakian, B. J., and Robbins, T. W. (2003). Stop-signal inhibition disrupted by damage to right inferior frontal gyrus in humans. *Nat. Neurosci.* 6, 115–116.

Aron, A. R. (2011). From reactive to proactive and selective control: developing a richer model for stopping inappropriate responses. *Biol. Psychiatry* 69, e55–e68.

Aron, A. R., and Poldrack, R. A. (2006). Cortical and subcortical contributions to stop signal response inhibition: role of the subthalamic nucleus. *J. Neurosci.* 26, 2424–2433.

Aron, A. R., Behrens, T. E., Smith, S., Frank, M. J., and Poldrack, R. A. (2007a). Triangulating a cognitive control network using diffusion-weighted magnetic resonance imaging (mri) and functional mri. *J. Neurosci.* 27, 3743–3752.

Aron, A. R., Durston, S., Eagle, D. M., Logan, G. D., Stinear, C. M., and Stuphorn, V. (2007b). Converging evidence for a fronto-basal-ganglia network for inhibitory control of action and cognition. *J. Neurosci.* 27, 11860–11864.

Band, G. P. H., van der Molen, M. W., and Logan, G. D. (2003). Horserace model simulations of the stop-signal procedure. *Acta Psychol. (Amst.)* 112, 105–142.

Basso, M. A., and Wurtz, R. H. (1998). Modulation of neuronal activity in superior colliculus by changes in target probability. *J. Neurosci.* 18, 7519–7534.

Bogacz, R., Wagenmakers, E. J., Forstmann, B. U., and Nieuwenhuis, S. (2010). The neural basis of the speed-accuracy tradeoff. *Trends Neurosci.* 33, 10–16.

Boucher, L., Stuphorn, V., Logan, G. D., Schall, J. D., and Palmeri, T. J. (2007). Stopping eye and hand movements: are the processes independent? *Percept. Psychophys.* 69, 785–801.

Braver, T. S. (2012). The variable nature of cognitive control: a dual mechanisms framework. *Trends Cogn. Sci.* 16, 106–113.

Braver, T., Gray, J., and Burgess, G. (2007). "Explaining the many varieties of working memory variation: dual mechanisms of cognitive control," in *Variation in Working Memory*, eds A. Conway, C. Jarrold, M. Kane, A. Miyake, and J. Towse (Oxford: Oxford University Press), 76–106.

Brown, J. W., Hanes, D. P., Schall, J. D., and Stuphorn, V. (2008). Relation of frontal eye field activity to saccade initiation during a countermanding task. *Exp. Brain Res.* 190, 135–151.

Campos, M., Breznen, B., Bernheim, K., and Andersen, R. A. (2005). Supplementary motor area encodes reward expectancy in eye-movement tasks. *J. Neurophysiol.* 94, 1325–1335.

Carter, C. S., Barch, D. M., Gur, R., Gur, R., Pinkham, A., and Ochsner, K. (2009). CNTRICS final task selection: social cognitive and affective neuroscience-based measures. *Schizophr. Bull.* 35, 153–162.

Chen, X., Scangos, K. W., and Stuphorn, V. (2010). Supplementary motor area exerts proactive and reactive control of arm movements. *J. Neurosci.* 30, 14657–14675.

Contini, M., Baccarini, M., Borra, E., Gerbella, M., Rozzi, S., and Luppino, G. (2010). Thalamic projections to the macaque caudal ventrolateral prefrontal areas 45a and 45b. *Eur. J. Neurosci.* 32, 1337–1353.

Coxon, J. P., Stinear, C. M., and Byblow, W. D. (2006). Intracortical inhibition during volitional inhibition of prepared action. *J. Neurophysiol.* 95, 3371–3383.

Curtis, C. E., Cole, M. W., Rao, V. Y., and D'Esposito, M. (2005). Canceling planned action: an fmri study of countermanding saccades. *Cereb. Cortex* 15, 1281–1289.

De Jong, R., Coles, M. G., Logan, G. D., and Gratton, G. (1990). In search of the point of no return: the control of response processes. *J. Exp. Psychol. Hum. Percept. Perform.* 16, 164–182.

Deiber, M. P., Honda, M., Ibaez, V., Sadato, N., and Hallett, M. (1999). Mesial motor areas in self-initiated versus externally triggered movements examined with fmri: effect of movement type and rate. *J. Neurophysiol.* 81, 3065–3077.

Dorris, M. C., and Munoz, D. P. (1998). Saccadic probability influences motor preparation signals and time to saccadic initiation. *J. Neurosci.* 18, 7015–7026.

Eccles, J. C. (1982). The initiation of voluntary movements by the supplementarymotor area. *Arch. Psychiatr. Nervenkr.* 231, 423–441.

Emeric, E. E., Brown, J. W., Boucher, L., Carpenter, R. H. S., Hanes, D. P., Harris, R., Logan, G. D., Mashru, R. N., Paré, M., Pouget, P., Stuphorn, V., Taylor, T. L., and Schall, J. D. (2007). Influence of history on saccade countermanding performance in humans and

macaque monkeys. *Vis. Res.* 47, 35–49.

Emeric, E. E., Brown, J. W., Leslie, M., Pouget, P., Stuphorn, V., and Schall, J. D. (2008). Performance monitoring local field potentials in the medial frontal cortex of primates: anterior cingulate cortex. *J. Neurophysiol.* 99, 759–772.

Emeric, E. E., Leslie, M., Pouget, P., and Schall, J. D. (2010). Performance monitoring local field potentials in the medial frontal cortex of primates: supplementary eye field. *J. Neurophysiol.* 104, 1523–1537.

Everling, S., Par, M., Dorris, M. C., and Munoz, D. P. (1998). Comparison of the discharge characteristics of brain stem omnipause neurons and superior colliculus fixation neurons in monkey: implications for control of fixation and saccade behavior. *J. Neurophysiol.* 79, 511–528.

Floden, D., and Stuss, D. T. (2006). Inhibitory control is slowed in patients with right superior medial frontal damage. *J. Cogn. Neurosci.* 18, 1843–1849.

Forstmann, B. U., Dutilh, G., Brown, S., Neumann, J., von Cramon, D. Y., Ridderinkhof, K. R., and Wagenmakers, E. J. (2008). Striatum and preSMA facilitate decision-making under time pressure. *Proc. Natl. Acad. Sci. U.S.A.* 105, 17538–17542.

Fujii, N., Mushiake, H., and Tanji, J. (2002). Distribution of eye- and arm movement-related neuronal activity in the SEF and in the SMA and pre-SMA of monkeys. *J. Neurophysiol.* 87, 2158–2166.

Gerbella, M., Belmalih, A., Borra, E., Rozzi, S., and Luppino, G. (2010). Cortical connections of the macaque caudal ventrolateral prefrontal areas 45a and 45b. *Cereb. Cortex* 20, 141–168.

Geyer, S., Matelli, M., Luppino, G., and Zilles, K. (2000). Functional neuroanatomy of the primate isocortical motor system. *Anat. Embryol. (Berl.)* 202, 443–474.

Gilden, D. L. (2001). Cognitive emissions of 1/f noise. *Psychol. Rev.* 108, 33–56.

Godlove, D. C., Emeric, E. E., Segovis, C. M., Young, M. S., Schall, J. D., and Woodman, G. F. (2011). Event-related potentials elicited by errors during the stop-signal task. I. macaque monkeys. *J. Neurosci.* 31, 15640–15649.

Goldberg, G. (1985). Supplementary motor area structure and function: review and hypotheses. *Behav. Brain Sci.* 8, 567–588.

Haggard, P. (2008). Human volition: towards a neuroscience of will. *Nat. Rev. Neurosci.* 9, 934–946.

Hanes, D. P., and Carpenter, R. H. (1999). Countermanding saccades in humans. *Vis. Res.* 39, 2777–2791.

Hanes, D. P., and Schall, J. D. (1995). Countermanding saccades in macaque. *Vis. Neurosci.* 12, 929–937.

Hanes, D. P., and Schall, J. D. (1996). Neural control of voluntary movement initiation. *Science* 274, 427–430.

Hanes, D., Patterson, W., and Schall, J. (1998). Role of frontal eye fields in countermanding saccades: visual, movement, and fixation activity. *J. Neurophysiol.* 79, 817.

Hikosaka, O., Sakamoto, M., and Usui, S. (1989). Functional properties of monkey caudate neurons. III. Activities related to expectation of target and reward. *J. Neurophysiol.* 61, 814–832.

Hollerman, J. R., Tremblay, L., and Schultz, W. (1998). Influence of reward expectation on behavior-related neuronal activity in primate striatum. *J. Neurophysiol.* 80, 947–963.

Huerta, M. F., and Kaas, J. H. (1990). Supplementary eye field as defined by intracortical microstimulation: connections in macaques. *J. Comp. Neurol.* 293, 299–330.

Ikeda, A., Yazawa, S., Kunieda, T., Ohara, S., Terada, K., Mikuni, N., Nagamine, T., Taki, W., Kimura, J., and Shibasaki, H. (1999). Cognitive motor control in human pre-supplementary motor area studied by subdural recording of discrimination/selection-related potentials. *Brain* 122, 915–931.

Isoda, M., and Hikosaka, O. (2007). Switching from automatic to controlled action by monkey medial frontal cortex. *Nat. Neurosci.* 10, 240–248.

Isoda, M., and Hikosaka, O. (2008a). A neural correlate of motivational conflict in the superior colliculus of the macaque. *J. Neurophysiol.* 100, 1332–1342.

Isoda, M., and Hikosaka, O. (2008b). Role for subthalamic nucleus neurons in switching from automatic to controlled eye movement. *J. Neurosci.* 28, 7209–7218.

Ito, S., Stuphorn, V., Brown, J. W., and Schall, J. D. (2003). Performance monitoring by the anterior cingulate cortex during saccade countermanding. *Science* 302, 120–122.

Ivanoff, J., Branning, P., and Marois, R. (2008). Fmri evidence for a dual process account of the speed-accuracy tradeoff in decision-making. *PLoS ONE* 3:e2635. doi: 10.1371/journal.pone.0002635

Jacoby, L., Kelley, C., and Mcelree, B. (1999). "The role of cognitive control: early selection versus late correction," in *Dual Process Theories in Social Psychology*, eds S. Chaiken and Y. Trope (New York, NY: Guilford Press), 383–400.

Johansen-Berg, H., Behrens, T. E. J., Robson, M. D., Drobnjak, I., Rushworth, M. F. S., Brady, J. M., Smith, S. M., Higham, D. J., and Matthews, P. M. (2004). Changes in connectivity profiles define functionally distinct regions in human medial frontal cortex. *Proc. Natl. Acad. Sci. U.S.A.* 101, 13335–13340.

Kobayashi, S., Nomoto, K., Watanabe, M., Hikosaka, O., Schultz, W., and Sakagami, M. (2006). Influences of rewarding and aversive outcomes on activity in macaque lateral prefrontal cortex. *Neuron* 51, 861–870.

Kornhuber, H. H., and Deecke, L. (1965). Hirnpotentialägnderungen bei Willkürbewegungen und passiven Bewegungen des Menschen: Bereitschaftspotential und reafferente potentiale. *Pflügers Arch.* 284, 1–17.

Lang, W., Cheyne, D., Kristeva, R., Beisteiner, R., Lindinger, G., and Deecke, L. (1991). Three-dimensional localization of sma activity preceding voluntary movement. A study of electric and magnetic fields in a patient with infarction of the right supplementary motor area. *Exp. Brain Res.* 87, 688–695.

Lecas, J. C., Requin, J., Anger, C., and Vitton, N. (1986). Changes in neuronal activity of the monkey precentral cortex during preparation for movement. *J. Neurophysiol.* 56, 1680–1702.

Levy, R., and Dubois, B. (2006). Apathy and the functional anatomy of the prefrontal cortex-basal ganglia circuits. *Cereb. Cortex* 16, 916–928.

Li, C. S. R., Huang, C., Constable, R. T., and Sinha, R. (2006). Imaging response inhibition in a stop-signal task: neural correlates independent of signal monitoring and post-response processing. *J. Neurosci.* 26, 186–192.

Logan, G. (1981). "Attention, automaticity, and the ability to stop a speeded choice response," in *Attention and Performance IX*, eds J. Long and A. D. Baddeley (Hillsdale, NJ: Erlbaum), 205–222.

Logan, G. D. (1994). "On the abilty to inhibit thought and action: a user's guide to the stop signal paradigm," in *Inhibitory Processes in Attention, Memory, and Language*, eds D. Dagenbach and T. H. Carr (San Diego, CA, USA: Academic Press), 189–239.

Logan, G. D., and Burkell, J. (1986). Dependence and independence in responding to double stimulation: a comparison of stop, change, and dualtask paradigms. *J. Exp. Psychol. Hum. Percept. Perform.* 12, 549–563.

Logan, G. D., Cowan, W. B., and Davis, K. A. (1984). On the ability to inhibit simple and choice reaction time responses: a model and a method. *J. Exp. Psychol. Hum. Percept. Perform.* 10, 276–291.

Luce, R. D. (1986). *Response Times: Their Role in Inferring Elementary Mental Organization*. New York, NY: Oxford University Press.

Luppino, G., Matelli, M., Camarda, R. M., Gallese, V., and Rizzolatti, G. (1991). Multiple representations of body movements in mesial area 6 and the adjacent cingulate cortex: an intracortical microstimulation study in the macaque monkey. *J. Comp. Neurol.* 311, 463–482.

Miller, E. K., and Cohen, J. D. (2001). An integrative theory of prefrontal cortex function. *Annu. Rev. Neurosci.* 24, 167–202.

Mink, J. W. (1996). The basal ganglia: focused selection and inhibition of competing motor programs. *Prog. Neurobiol.* 50, 381–425.

Mirabella, G., Iaconelli, S., Romanelli, P., Modugno, N., Lena, F., Manfredi, M., and Cantore, G. (2012). Deep brain stimulation of subthalamic nuclei affects arm response inhibition in parkinson's patients. *Cereb. Cortex* 22, 1124–1132.

Mirabella, G., Pani, P., and Ferraina, S. (2008). Context influences on the preparation and execution of reaching movements. *Cogn. Neuropsychol.* 25, 996–1010.

Mirabella, G., Pani, P., and Ferraina, S. (2011). Neural correlates of cognitive control of reaching movements in the dorsal premotor cortex of rhesus monkeys. *J. Neurophysiol.* 106, 1454–1466.

Mirabella, G., Pani, P., Paré, M., and Ferraina, S. (2006). Inhibitory control of reaching movements in humans. *Exp. Brain Res.* 174, 240–255.

Mita, A., Mushiake, H., Shima, K., Matsuzaka, Y., and Tanji, J. (2009). Interval time coding by neurons in

the presupplementary and supplementary motor areas. *Nat. Neurosci.* 12, 502–507.

Monakow, K., Akert, K., and Künzle, H. (1978). Projections of the precentral motor cortex and other cortical areas of the frontal lobe to the subthalamic nucleus in the monkey. *Exp. Brain Res.* 33, 395–403.

Nambu, A. (2004). A new dynamic model of the cortico-basal ganglia loop. *Prog. Brain Res.* 143, 461–466.

Nambu, A., Takada, M., Inase, M., and Tokuno, H. (1996). Dual somatotopical representations in the primate subthalamic nucleus: evidence for ordered but reversed body-map transformations from the primary motor cortex and the supplementary motor area. *J. Neurosci.* 16, 2671–2683.

Nelson, M. J., Boucher, L., Logan, G. D., Palmeri, T. J., and Schall, J. D. (2010). Nonindependent and nonstationary response times in stopping and stepping saccade tasks. *Atten. Percept. Psychophys.* 72, 1913–1929.

Okano, K., and Tanji, J. (1987). Neuronal activities in the primate motor fields of the agranular frontal cortex preceding visually triggered and self-paced movement. *Exp. Brain Res.* 66, 155–166.

Padoa-Schioppa, C., and Assad, J. A. (2006). Neurons in the orbitofrontal cortex encode economic value. *Nature* 441, 223–226.

Papa, S. M., Artieda, J., and Obeso, J. A. (1991). Cortical activity preceding self-initiated and externally triggered voluntary movement. *Mov. Disord.* 6, 217–224.

Paré, M., and Hanes, D. P. (2003). Controlled movement processing: superior colliculus activity associated with countermanded saccades. *J. Neurosci.* 23, 6480–6489.

Petrides, M., and Pandya, D. N. (1999). Dorsolateral prefrontal cortex: comparative cytoarchitectonic analysis in the human and the macaque brain and corticocortical connection patterns. *Eur. J. Neurosci.* 11, 1011–1036.

Picton, T. W., Stuss, D. T., Alexander, M. P., Shallice, T., Binns, M. A., and Gillingham, S. (2007). Effects of focal frontal lesions on response inhibition. *Cereb. Cortex* 17, 826–838.

Ratcliff, R. (1978). A theory of memory retrieval. *Psychol. Rev.* 85, 59–108.

Reddi, B. A., and Carpenter, R. H. (2000). The influence of urgency on decision time. *Nat. Neurosci.* 3, 827–830.

Roesch, M. R., and Olson, C. R. (2003). Impact of expected reward on neuronal activity in prefrontal cortex, frontal and supplementary eye fields and premotor cortex. *J. Neurophysiol.* 90, 1766–1789.

Roesch, M. R., and Olson, C. R. (2004). Neuronal activity related to reward value and motivation in primate frontal cortex. *Science* 304, 307–310.

Romo, R., and Schultz, W. (1992). Role of primate basal ganglia and frontal cortex in the internal generation of movements. III. Neuronal activity in the supplementary motor area. *Exp. Brain Res.* 91, 396–407.

Sakagami, M., Tsutsui, Ki., Lauwereyns, J., Koizumi, M., Kobayashi, S., and Hikosaka, O. (2001). A code for behavioral inhibition on the basis of color, but not motion, in ventrolateral prefrontal cortex of macaque monkey. *J. Neurosci.* 21, 4801–4808.

Sakagami, M., and Watanabe, M. (2007). Integration of cognitive and motivational information in the primate lateral prefrontal cortex. *Ann. N.Y. Acad. Sci.* 1104, 89–107.

Sakai, K. (2008). Task set and prefrontal cortex. *Annu. Rev. Neurosci.* 31, 219–245.

Scangos, K. W., and Stuphorn, V. (2010). Medial frontal cortex motivates but does not control movement initiation in the countermanding task. *J. Neurosci.* 30, 1968–1982.

Schall, J. D. (1991a). Neuronal activity related to visually guided saccades in the frontal eye fields of rhesus monkeys: comparison with supplementary eye fields. *J. Neurophysiol.* 66, 559–579.

Schall, J. D. (1991b). Neuronal activity related to visually guided saccadic eye movements in the supplementary motor area of rhesus monkeys. *J. Neurophysiol.* 66, 530–558.

Schall, J. D. (1997). "Visuomotor areas of the frontal lobe," in *Cerebral Cortex*, Vol. 4, eds K. S. Rockland, A. Peters, and J. Kaas (New York, NY: Plenum), 527–638.

Schall, J. D., and Boucher, L. (2007). Executive control of gaze by the frontal lobes. *Cogn. Affect. Behav. Neurosci.* 7, 396–412.

Schlag, J., and Schlag-Rey, M. (1987). Evidence for a supplementary eye field. *J. Neurophysiol.* 57, 179–200.

Schmidt, L., d'Arc, B. F., Lafargue, G., Galanaud, D., Czernecki, V., Grabli, D., Schüpbach, M., Hartmann, A., Lévy, R., Dubois, B., and Pessiglione, M. (2008). Disconnecting force from money: effects of basal ganglia damage on incentive motivation. *Brain* 131, 1303–1310.

Segraves, M. A. (1992). Activity of monkey frontal eye field neurons projecting to oculomotor regions of the pons. *J. Neurophysiol.* 68, 1967–1985.

Segraves, M. A., and Goldberg, M. E. (1987). Functional properties of corticotectal neurons in the monkey's frontal eye field. *J. Neurophysiol.* 58, 1387–1419.

Sharp, D. J., Bonnelle, V., De Boissezon, X., Beckmann, C. F., James, S. G., Patel, M. C., and Mehta, M. A. (2010). Distinct frontal systems for response inhibition, attentional capture, and error processing. *Proc. Natl. Acad. Sci. U.S.A.* 107, 6106–6111.

So, N. Y., and Stuphorn, V. (2010). Supplementary eye field encodes option and action value for saccades with variable reward. *J. Neurophysiol.* 104, 2634–2653.

Sohn, J. W., and Lee, D. (2007). Order-dependent modulation of directional signals in the supplementary and presupplementary motor areas. *J. Neurosci.* 27, 13655–13666.

Sommer, M. A., and Wurtz, R. H. (2000). Composition and topographic organization of signals sent from the frontal eye field to the superior colliculus. *J. Neurophysiol.* 83, 1979–2001.

Stuphorn, V., and Schall, J. D. (2002). Neuronal control and monitoring of initiation of movements. *Muscle Nerve* 26, 326–339.

Stuphorn, V., and Schall, J. D. (2006). Executive control of countermanding saccades by the supplementary eye field. *Nat. Neurosci.* 9, 925–931.

Stuphorn, V., Brown, J. W., and Schall, J. D. (2010). Role of supplementary eye field in saccade initiation: executive, not direct, control. *J. Neurophysiol.* 103, 801–816.

Stuphorn, V., Taylor, T. L., and Schall, J. D. (2000). Performance monitoring by the supplementary eye field. *Nature* 408, 857–860.

Sumner, P., Nachev, P., Morris, P., Peters, A. M., Jackson, S. R., Kennard, C., and Husain, M. (2007). Human medial frontal cortex mediates unconscious inhibition of voluntary action. *Neuron* 54, 697–711.

Tanji, J. (1996). New concepts of the supplementary motor area. *Curr. Opin. Neurobiol.* 6, 782–787.

Thaler, D., Chen, Y.-C., Nixon, P. D., Stern, C. E., and Passingham, R. E. (1995). The functions of the medial premotor cortex. I. Simple learned movements. *Exp. Brain Res.* 102, 445–460.

Thaler, D. E., Rolls, E. T., and Passingham, R. E. (1988). Neuronal activity of the supplementary motor area (SMA) during internally and externally triggered wrist movements. *Neurosci. Lett.* 93, 264–269.

Tremblay, L., and Schultz, W. (1999). Relative reward preference in primate orbitofrontal cortex. *Nature* 398, 704–708.

Uchida, N., Kepecs, A., and Mainen, Z. F. (2006). Seeing at a glance, smelling in a whiff: rapid forms of perceptual decision making. *Nat. Rev. Neurosci.* 7, 485–491.

Verbruggen, F., and Logan, G. D. (2008). Response inhibition in the stopsignal paradigm. *Trends Cogn. Sci.* 12, 418–424.

Verbruggen, F., and Logan, G. D. (2009). Proactive adjustments of response strategies in the stop-signal paradigm. *J. Exp. Psychol. Hum. Percept. Perform.* 35, 835–854.

Verbruggen, F., Liefooghe, B., and Vandierendonck, A. (2004). The interaction between stop signal inhibition and distractor interference in the flanker and stroop task. *Acta Psychol. (Amst.)* 116, 21–37.

Verbruggen, F., Liefooghe, B., and Vandierendonck, A. (2006). The effect of interference in the early processing stages on response inhibition in the stop signal task. *Q. J. Exp. Psychol. (Hove)* 59, 190–203.

Wagenmakers, E.-J., Zeelenberg, R., Steyvers, M., Shiffrin, R., and Raaijmakers, J. (2004). Nonword repetition in lexical decision: support for two opposing processes. *Q. J. Exp. Psychol. A* 57, 1191–1210.

Wallis, J. D., and Miller, E. K. (2003). Neuronal activity in primate dorsolateral and orbital prefrontal cortex during performance of a reward preference task. *Eur. J. Neurosci.* 18, 2069–2081.

Yazawa, S., Ikeda, A., Kunieda, T., Ohara, S., Mima, T., Nagamine, T., Taki, W., Kimura, J., Hori, T., and Shibasaki, H. (2000). Human presupplementary motor area is active before voluntary movement: subdural recording of bereitschaftspotential from medial frontal cortex. *Exp. Brain Res.* 131, 165–177.

van Veen, V., Krug, M. K., and Carter, C. S. (2008). The neural and

computational basis of controlled speed-accuracy tradeoff during task performance. *J. Cogn. Neurosci.* 20, 1952–1965.

van den Wildenberg, W. P. M., van Boxtel, G. J. M., and van der Molen, M. W. (2003). The duration of response inhibition in the stop-signal paradigm varies with response force. *Acta Psychol. (Amst.)* 114, 115–129.

Conflict of Interest Statement: The authors declare that the research was conducted in the absence of any commercial or financial relationships that could be construed as a potential conflict of interest.

Received: 07 February 2012; paper pending published: 24 February 2012; accepted: 29 April 2012; published online: 19 June 2012.

*Citation: Stuphorn V and Emeric EE (2012) Proactive and reactive control by the medial frontal cortex. Front. Neuroeng. **5**:9. doi: 10.3389/fneng.2012.00009*

frontiers in
NEUROENGINEERING

ORIGINAL RESEARCH ARTICLE
published: 08 August 2012
doi: 10.3389/fneng.2012.00015

Decoding onset and direction of movements using Electrocorticographic (ECoG) signals in humans

Zuoguan Wang[1†], Aysegul Gunduz[2,3,4†], Peter Brunner[3,4], Anthony L. Ritaccio[4], Qiang Ji[1] and Gerwin Schalk[3,4]*

[1] *Department of ECSE, Rensselaer Polytechnic Institute, Troy, NY, USA*
[2] *J Crayton Pruitt Family Department of Biomed Engineering, University of Florida, Gainesville, FL, USA*
[3] *BCI R&D Program, Wadsworth Center, New York State Department of Health, Albany, NY, USA*
[4] *Department of Neurology, Albany Medical College, Albany, NY, USA*

Edited by:
Giovanni Mirabella, University of La Sapienza, Italy

Reviewed by:
Giovanni Mirabella, University of La Sapienza, Italy
Mikhail A. Lebedev, Duke University, USA

****Correspondence:***
Gerwin Schalk, Wadsworth Center, New York State Department of Health, C650 Empire State Plaza, Albany, NY, USA.
e-mail: schalk@wadsworth.org
† Co-first authors.

Communication of intent usually requires motor function. This requirement can be limiting when a person is engaged in a task, or prohibitive for some people suffering from neuromuscular disorders. Determining a person's intent, e.g., where and when to move, from brain signals rather than from muscles would have important applications in clinical or other domains. For example, detection of the onset and direction of intended movements may provide the basis for restoration of simple grasping function in people with chronic stroke, or could be used to optimize a user's interaction with the surrounding environment. Detecting the onset and direction of actual movements are a first step in this direction. In this study, we demonstrate that we can detect the onset of intended movements and their direction using electrocorticographic (ECoG) signals recorded from the surface of the cortex in humans. We also demonstrate in a simulation that the information encoded in ECoG about these movements may improve performance in a targeting task. In summary, the results in this paper suggest that detection of intended movement is possible, and may serve useful functions.

Keywords: brain computer interface, ECoG, movement direction prediction, movement onset prediction, neurorehabilitatation, performance augmentation

1. INTRODUCTION

Brain-computer interfaces (BCIs) aim to translate a person's intentions into meaningful computer commands using brain activity alone (Wolpaw et al., 2002; Mak and Wolpaw, 2009). In particular, determining when and where a person intends to move would have important clinical applications for those suffering from neuromuscular disorders (Sejnowski et al., 2007; Tan and Nijholt, 2010). For example, a BCI that detects intended movement onset in absence of actual movements could restore grasp function in people with chronic stroke (Buch et al., 2008; Daly and Wolpaw, 2008; Wisneski et al., 2008; Muralidharan et al., 2011; Yanagisawa et al., 2011). Also, a BCI that predicts intended movement onset prior to actual movements would have many practical applications in everyday life. For example, it may support faster braking during vehicle operation (Haufe et al., 2011) or more rapid targeting in military applications (Gunduz and Schalk, 2011).

The first step in this direction is to establish whether it is possible to detect the onset of actual movements from brain signals. Several previous studies have shown that intracortical activities recorded in primates over the premotor or parietal cortices are related to the onset of movements (Achtman et al., 2007; Lebedev et al., 2008; Hwang and Andersen, 2009; Hasan and Gan, 2011; Mirabella et al., 2011), but access to intracortical activity in humans has been scarce (e.g., Hochberg et al., 2006; Simeral et al., 2011). Other studies have investigated movement onset using electroencephalographic (EEG) signals in humans (Mason and Birch, 2000; Millan and Mouriño, 2003; Borisoff et al., 2004; Leeb et al., 2007; Bai et al., 2008; Hasan and Gan, 2011; Muralidharan et al., 2011), but accurately detecting the corresponding EEG signatures in single trials has proven difficult. Electrocorticographic (ECoG) signals are recorded directly from the surface of the cortex, and thus have a higher signal-to-noise ratio compared to EEG (Ball et al., 2009). They also readily support detection of certain physiological phenomena, such as high gamma activity (>70 Hz), that is largely inconspicuous on the scalp. The ability to detect high gamma activity is an important advantage, since many ECoG studies (e.g., Miller et al., 2007, 2009; Kubánek et al., 2009; Chao et al., 2010) demonstrated that spatially focused high gamma activity correlates closely with specific aspects of motor functions. Yet, no previous study comprehensively studied the possibility that movement onset can be detected using ECoG signals.

The second step in this direction is to determine whether ECoG also holds information about movement direction prior to the actual movement. Several studies (Schalk et al., 2007; Pistohl et al., 2008; Gunduz et al., 2009) showed that ECoG signals collected during movements hold information about two-dimensional trajectories of hand movements, and Leuthardt et al. (2004) and Schalk et al. (2008) demonstrated one- and two-dimensional real-time control of a computer cursor using ECoG, respectively. However, there has only been scarce evidence that

brain signals recorded in humans give information about movement direction prior to the movement (Leuthardt et al. (2004) using ECoG, Wang et al. (2010) using MEG), and that this information may be useful.

In this paper, we investigate whether ECoG holds information about the onset and direction of hand movements in a center-out task. Specifically, we use a support vector machine (SVM) classifier to determine, at each step in time, the probability that the subject initiated a hand movement at that particular time. We also characterize the ECoG features that hold the most information about movement onset. We then use a novel implementation of a time-varying dynamic Bayesian network (TVDBN), which was designed to take advantage of the spatio-temporal dynamics of ECoG features, to determine the direction of the intended movement using ECoG signals prior to the movement. Finally, we simulate a targeting application in which brain signals prior to the movement are combined with the actual movement signals. In this simulation, the time-to-target reduces by up to 150 ms when we use the directional information captured in ECoG signals. Overall, our results contribute to our understanding of the neural representation of intended movements and suggest that integrating information from brain signals and motor execution may eventually lead to systems that can improve a user's performance.

2. MATERIALS

2.1. HUMAN SUBJECTS

Five subjects participated in this study. The subjects were patients with intractable epilepsy who underwent temporary implantation of subdural electrode arrays for the localization of seizure foci prior to surgical resection. **Table 1** summarizes the subjects' clinical profiles. All of the subjects had normal cognitive capacity and were functionally independent. The study was approved by the Institutional Review Board of Albany Medical College as well as by the Human Research Protections Office of the US Army Medical Research and Materiel Command, and the subjects gave informed consent. The implanted electrode grids (Ad-Tech Medical Corp., Racine, WI) consisted of platinum-iridium electrodes that were 4 mm in diameter (2.3 mm exposed) and were configured with an inter-electrode distance of 1 cm. Subject E was implanted with a higher density (6 mm inter-electrode distance) grid with 68 contacts (PMT Corp., Chanhassen, MN) over the temporal lobe. Each subject had postoperative anterior-posterior and lateral radiographs (see **Figure A1**), as well as computer tomography (CT) scans to verify grid location. The number of implanted electrodes varied between 58 and 120 contacts across subjects (**Table 1**). We excluded data collected over the occipital strips (in Subjects A and B) from the analyses to minimize the potential impact of visual stimulation on the results.

2.2. CORTICAL MAPPING

We used Curry software (Compumedics, Charlotte, NC) to create subject-specific 3D cortical brain models from high resolution pre-op MRI scans. We co-registered the MRIs with post-op CTs and extracted the stereotactic coordinates of each grid electrode. We identified the cortical areas underneath each electrode using an automated Talairach Atlas (Lancaster et al., 2000) (http://www.talairach.org/daemon.html) for functional mapping. We also projected the electrodes onto the reconstructed brain models (see **Figure 1**) and generated activation maps using custom Matlab software to delimit the cortical areas involved in prediction of movement onset and direction.

2.3. DATA COLLECTION

We recorded ECoG signals at the bedside using eight 16-channel g.USBamp biosignal acquisition devices (g.tec, Graz, Austria) at a

Table 1 | Clinical profiles of the subjects that participated in the study.

Subject	Age	Sex	Handedness	Perf. IQ	Seizure focus	Grid/Strip location	# of Electrodes
A	29	F	R	136	Left temporal	Left fronto-parietal	64
						Left temporal	23
						Left temporal pole	3
						Left occipital	6
B	56	M	R	87	Left temporal	Left frontal	56
						Left temporal	35
						Left occipital	6
						Right posterior mesial	4
C	45	M	R	95	Left temporal	Left fronto-temporal	54
						Left temporal pole	4
D	49	F	L	99	Left temporal	Left fronto-temporal	61
						Left temporal mesial	4
						Left frontal	4
E	29	F	R	95	Left temporal	Left frontal	40
						Left temporal	68
						Left frontal	4
						Left inferior temporal	4
						Left parietal	4

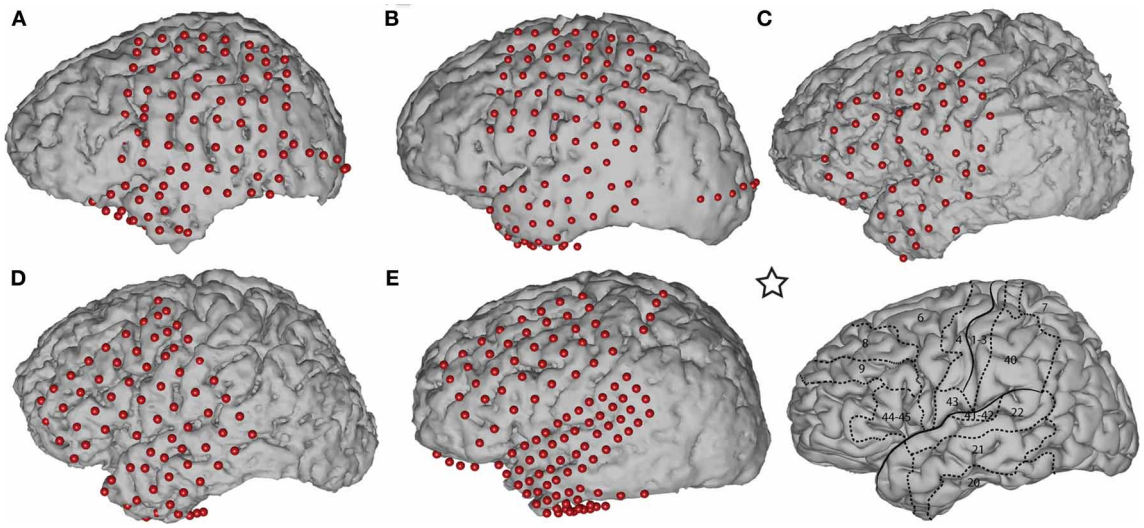

FIGURE 1 | Subject-specific brain models and projected electrode locations for Subjects A–E. The brain template on the bottom right, indicated with a star, depicts the location of the central sulcus, Sylvian fissure, and important Brodmann areas. The areas most relevant to our task are Brodmann areas 6 (premotor), 4 (primary motor), 1–3 (sensory motor), and 7 (posterior parietal cortex).

sampling rate of 1200 Hz. Electrode contacts distant from epileptic foci and areas of interest were used for reference and ground. In addition to recording brain activity, we also recorded the subjects' eye gaze using a monitor with a built-in eye tracking system (Tobii Tech., Stockholm, Sweden) positioned 54–60 cm in front of the subjects, and the movements of a joystick. The eye tracker was calibrated to each subject at the beginning of the experimental session using custom software that invoked standard calibration functions provided by Tobii. Data collection from the biosignal and behavioral acquisition devices (g.USBamp, eye tracker, and joystick, respectively), as well as control of the experimental paradigm and stimulus presentation, were accomplished simultaneously using BCI2000 software (Schalk et al., 2004; Schalk and Mellinger, 2010). BCI2000 provides a flexible general-purpose software platform that consists of modules that realize signal acquisition, signal processing, user feedback, and an operating protocol. BCI2000 facilitates the implementation of any BCI or related system, and is used in hundreds of laboratories for this purpose.

2.4. EXPERIMENTAL PARADIGM

ECoG signals were collected while the subjects performed an 8-target center-out cursor movement task (Georgopoulos et al., 1982) while fixating their eye gaze at a central fixation cross. Eye gaze fixation was enforced online by BCI2000: a trial was aborted if the subject looked away from the center for more than 5° for more than 500 msec. Each trial started with the presentation of a target in one of eight possible locations. A cursor appeared 1 s later at the center of the screen. The subjects' task was to use their hand contralateral to the implant(s) to control a joystick so as to move the cursor into the target. (Only Subject D used the non-dominant hand.) We positioned the subjects such that the joystick movements were mainly restricted to the wrist (see **Figure A2**). The subjects were instructed to make exaggerated movements and achieve maximal radial extension of the joystick to hit the targets. Once the target was hit, the next trial started after an inter-trial interval of 1 s. **Figure 2** gives a simple illustration of the stages of the task. Trials aborted by the eye tracker, trials in which joystick movement preceded the presentation of the cursor, and trials in which subjects failed to hit the correct target were omitted from further analyses. The total number of remaining valid trials were 394, 584, 258, 398, and 305 for Subjects A through E, respectively.

3. METHODS

The primary goal of this study was to determine whether ECoG may be used to detect the onset and direction of an intended movement, and whether this information could be useful to reduce the time-to-target in a simulated targeting application. In the following sections, we describe our methods for ECoG feature extraction, movement onset and direction prediction, and the simulation of the targeting application.

3.1. FEATURE EXTRACTION

We first re-referenced the raw ECoG signals (excluding occipital channels) using a common average reference (CAR) spatial filter to remove spatial noise (Kubánek et al., 2009). For each 100 ms time step and each channel, we converted 300 ms windows (i.e., 200 ms overlap) of ECoG time series into the frequency domain using an autoregressive model of order 25 (Marple, 1986). Using this model, we derived frequency amplitudes between 0 and 200 Hz in 1 Hz bins. **Figure 3** shows an example of ECoG activity at different frequencies during the preparation for and execution of the movement task with respect to rest averaged across trials. Spectral amplitudes were divided by an average spectrum of the rest condition. A normalized amplitude of 1 suggests no task-related modulations at a particular time and frequency, whereas a value of 2, for instance, suggests that the spectral amplitude of interest doubled during the task. ECoG features were attained

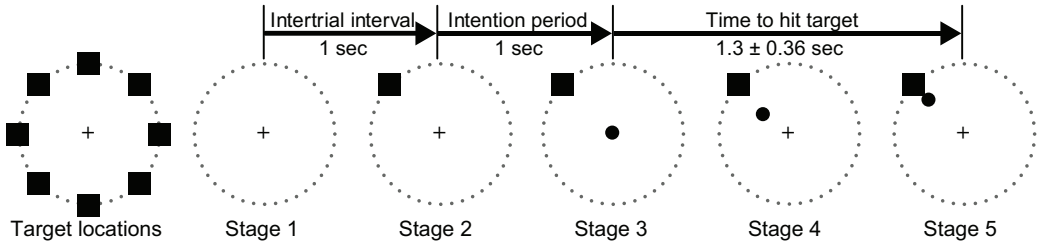

FIGURE 2 | Illustration of all eight possible target locations (left) and the five experimental stages.

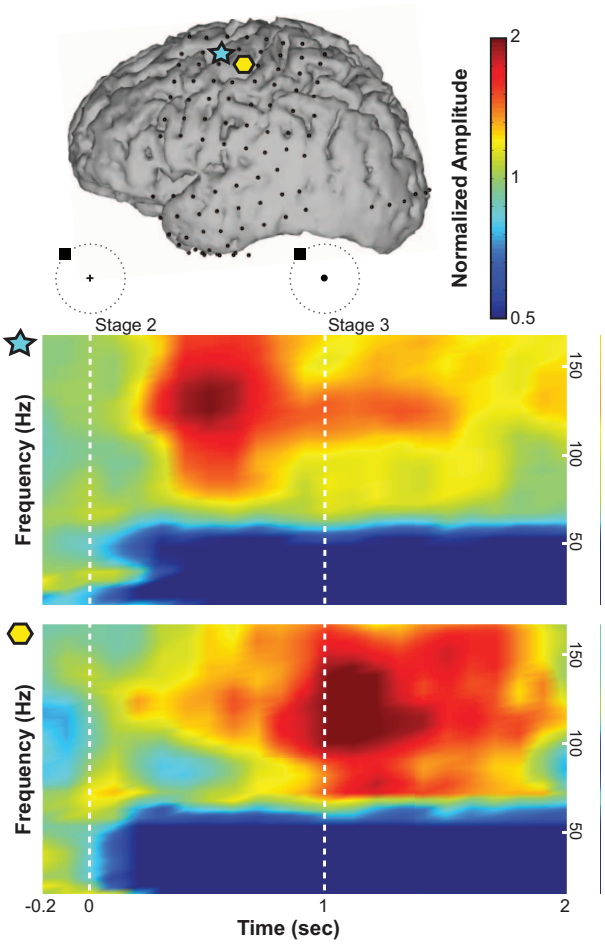

FIGURE 3 | Exemplary time-frequency plots from Subject B of normalized spectral amplitude (indicated with a linear colorscale) for an electrode over the premotor cortex (indicated by the blue star in the brain model on top) and an electrode over primary motor cortex (yellow hexagon). The horizontal axis gives time (the target was presented at time 0; the cursor was presented at 1 s). The vertical axis gives frequency.

by averaging these frequency amplitudes across three frequency bands: mu (8–12 Hz), beta (18–26 Hz), and high gamma activity (70–170 Hz). In addition to these three spectral features, we also calculated the local motor potential (LMP) (Schalk et al., 2007; Kubánek et al., 2009) by averaging the raw time-domain signal at each channel over each 300 ms time window (also 200 ms overlap). This process resulted in a total of four features from each ECoG channel at each (100 ms) time step.

To remove features unrelated to movement onset and direction prediction, we performed feature selection via forward search on five cross-validation folds (i.e., dividing the number of total trials into five and using four-folds for training and one-fold as the novel testing set, five times). The algorithm started with an empty feature set and, at every iteration, added a new feature to the set to generate best classification accuracy across each of the five testing folds. We chose the size of features as 20 for both movement onset prediction and movement direction prediction.

3.2. PREDICTION OF MOVEMENT ONSET

We downsampled the joystick data to 10 Hz using a moving average filter (300 ms window, 200 ms overlap) to align with the ECoG features. In each trial, we defined the actual movement onset as the time sample when the joystick was pushed beyond one eight of its maximum radial extension from its rest position. For each trial, there was a single onset sample and all time samples from the beginning of the trial up to this onset were labeled as not onset.

We then designed a detector that accumulated 1 s of ECoG features into a first-in-first-out (FIFO) buffer and determined from a full buffer whether the subsequent time step would be the onset of a movement. Each trial started with an empty buffer which was updated with new features every 100 ms. Once the buffer was full, a prediction was made every 100 ms via a weighted SVM (Huang and Du, 2005). We opted for a weighted SVM as it overcomes the classification bias that results from the unbalanced nature of the data (i.e., the class not onset' is much more likely than the class onset) by setting the ratio of penalties to the inverse ratio of the class sizes. We configured the weighted SVM to use a radial basis function as the kernel. The labeled joystick data was divided into 5-folds; four of these folds were used for training the weighted SVM, and one fold was allocated for testing. We repeated this process five times until each fold was used for testing [1].

[1] In ancillary analyses, we performed feature selection on 1/5th of the data, which were subsequently not used in the training and testing of the onset and direction predictors. The results of this more conservative analysis were very similar to the results reported in the paper.

The output of the weighted SVM classifier yielded the probability of an onset as a function of time. Time points were classified as movement onsets if their probability values were greater than an empirically determined threshold of 0.3. We chose the $F1$-score as our accuracy metric as it is preferable over percent accuracy or error rate for highly unbalanced classes (van Rijsbergen, 1979). $F1$-score is defined as:

$$F1 = \frac{2\text{TP}}{2\text{TP} + \text{FP} + \text{FN}} \tag{1}$$

where TP, FP, and FN are the occurrences of true positive, false positive, and false negative predictions. $F1$-score is particularly befitting for our onset predictor, as the metric is not influenced by true negative (TN) predictions. Given the imbalance of our two classes, any random classifier is likely to yield high TN rates. $F1$-scores take on values between 0 and 1, with the latter corresponding to a perfect classifier.

We computed the $F1$-scores of onset predictions for all subjects. We were also interested in determining the ECoG features (i.e., spectral bands and spatial locations) that were most predictive of movement onset. To do this, we calculated $F1$-scores separately for each ECoG feature using the methods described above. We ran the 5-fold cross validation 20 times; each time there was a random division of the folds. A series of high $F1$-scores suggests that the prediction was highly accurate, whereas ratios close to zero indicate a poor predictor. Hence, we tested whether the $F1$-scores in these 20-folds were significantly different than zero via a t-test. The corresponding p-values represent the significance of the $F1$-scores, and thus the accuracy of the classifier. We converted these p-values into indices of confidence [(i.e., $-log(p)$)], and mapped those confidence indices on the cortex models of the individual subjects.

3.3. PREDICTION OF DIRECTION OF INTENDED MOVEMENT

We predicted movement direction using all ECoG features from 1s prior to the actual movement onset (i.e., the same window used to predict the movement onset). Routinely in such multivariate prediction problems, multichannel time series are re-arranged into a vector to be used as input features to train a classifier, e.g., a neural network or SVM. However, the shortcoming of this approach is that it generally ignores the spatial and temporal structure of the multidimensional time series. Because we felt that such structure was likely important for directional classification, we opted to implement a novel modified time-varying dynamic Bayesian network (MTVDBN) that can capture the spatial and temporal dependency of the ECoG signals across both domains.

A Bayesian network is a probabilistic graphical model that represents a set of variables and their conditional dependencies via directed acyclic graphs, in which nodes represent random variables and edges represent conditional dependencies. A Bayesian network is an established method for modeling dependency structures in complex multivariate systems. An extension of Bayesian networks that models time series is called a dynamic Bayesian network (DBN). However, an important assumption underlying DBNs is that the time series are generated by a stationary process, which generally does not hold for neural signals. TVDBN (Song et al., 2009) introduced non-stationary temporal transitions, but did not describe spatial dependency between variables. In this paper, we extend the TVDBN to the modified TVDBN (MTVDBN) in which the non-stationary temporal and spatial dependencies of ECoG signals are modeled simultaneously. **Figure 4** depicts a block diagram of a MTVDBN in which (vertical) arrows within each time slice (i.e., across rows of a column) represent spatial dependencies, while (horizontal) arrows across time slices (i.e., across columns) describe the temporal dependencies. Regular TVDBNs lack the former spatial structure, i.e., the (vertical) arrows within each time slice.

Let $\mathbf{X}^t = (X_1^t, ..., X_M^t)^T$ be a vector representing the ECoG features (mu, beta, high gamma bands, and LMP) from all channels at time t (i.e., M is four times the number of channels for each subject). The joint likelihood of the time sequence of length T can be expressed as:

$$P(\mathbf{X}^1, ..., \mathbf{X}^T) = \prod_{t=1}^{T} \prod_{m=1}^{M} P(X_m^t | \mathbf{X}_{\pi_m}^{t-1}, \mathbf{X}_{\pi_m}^t), \tag{2}$$

where $\mathbf{X}_{\pi_m}^{t-1}$ and $\mathbf{X}_{\pi_m}^t$ denote the parents of input feature X_m^t at time $(t-1)$ and t, respectively (see **Figure 4**). Since we use 1 s of ECoG features, we are interested in a time sequence of length $T = 10$ samples. Note that the parent $\mathbf{X}_{\pi_m}^{t-1}$ represents temporal dependencies, where as parent $\mathbf{X}_{\pi_m}^t$ represents spatial dependencies. An equivalent form of representing $P(X_m^t | \mathbf{X}_{\pi_m}^{t-1}, \mathbf{X}_{\pi_m}^t)$ is the following linear model (Duda et al., 2008):

$$X_m^t = \mathbf{a}_m^{t-1} \mathbf{X}_{\pi_m}^{t-1} + \mathbf{a}_m^t \mathbf{X}_{\pi_m}^t + \varepsilon, \text{ where } \varepsilon \sim N(0, 1), \tag{3}$$

$\mathbf{a}_m^{t-1}$ and $\mathbf{a}_m^t$ are row vectors of the coefficients of parents of feature X_m^t at times $(t-1)$ and t, respectively, and the variable ε is Gaussian noise with mean zero and unit standard deviation. The coefficients $\mathbf{a}$ represent the structure of the network. The zero elements of $\mathbf{a}$ represent the missing links within the structure, whereas the non-zero elements stand for the dependence strength. The coefficients are learned through maximizing the likelihood of X_m^t across all training samples. To prevent overfitting and to encourage sparse structures, we learn $\mathbf{a}$ through an ℓ_1 penalty. Specifically, the coefficients $\mathbf{a}_m^{t-1}$ and $\mathbf{a}_m^t$ are learned by:

$$\min_{\mathbf{a}_m^{t-1}, \mathbf{a}_m^t} \frac{1}{N} \sum_{n=1}^{N} \left(X_m^{n,t} - \mathbf{a}_m^{t-1} \mathbf{X}_{\pi_m}^{n,t-1} - \mathbf{a}_m^t \mathbf{X}_{\pi_m}^{n,t} \right)^2 + \lambda (||\mathbf{a}_m^{t-1}||_1 + ||\mathbf{a}_m^t||_1), \tag{4}$$

where N is the size of training vector samples, $X_m^{n,t}$ represents the data at the feature m at time t in the n^{th} training vector. Similarly, $\mathbf{X}_{\pi_m}^{n,t}$ is the parent of $X_m^{n,t}$ at time t in the n^{th} training sample. Parameter λ is the penalty coefficient, which controls the sparsity of the structure and it is identified by cross validation. Equation (4) is solved by least angle regression and shrinkage (LARS) (Efron et al., 2004), which has a computational complexity of $O(N(2M-1)^3)$ time. Equation (4) was applied to each node to select the potential parents. However, this preprocessing

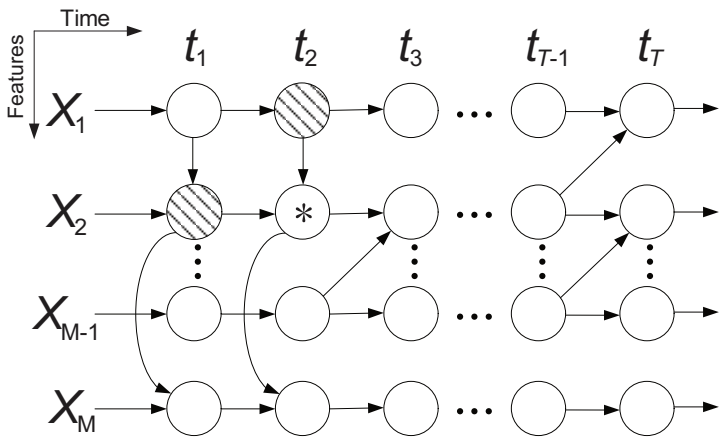

FIGURE 4 | Block diagram of a modified time-varying dynamic Bayesian network (MTVDBN). The shaded nodes are the parents of the node $*$.

does not automatically result in acyclic graphs at each time slice. A hill-climbing algorithm was then used to greedily construct an acyclic graph in which the edges were restricted by the selected potential parents (Schmidt et al., 2007).

We built a MTVDBN for each direction trained using only the trials toward that direction. For each direction $d = \{1, 2, ..., 8\}$, the set of parameters $\mathbf{a}^t_{d,m}$ for $m = \{1, 2, ..., M\}$ and $t = \{1, 2, ..., T\}$ were trained. Each MTVDBN thus learned the patterns of the input ECoG features associated with planning a movement in their assigned direction (Equation 3). After these model parameters were trained, given a test sample of ECoG features, the classification was done by:

$$d^* = \underset{d}{\operatorname{argmin}} \sum_{t=1}^{T} \sum_{m=1}^{M} -\log P(X^{*,t}_m | X^{*,t-1}_{\pi_m}, X^{*,t}_{\pi_m})$$

$$= \underset{d}{\operatorname{argmin}} \sum_{t=1}^{T} \sum_{m=1}^{M} (X^{*,t}_m - \mathbf{a}^{t-1}_{d,m} \mathbf{X}^{*,t-1}_{\pi_m} - \mathbf{a}^{t}_{d,m} \mathbf{X}^{*,t}_{\pi_m})^2. \quad (5)$$

In other words, every time an onset was detected, 1 s of input features (i.e., $T = 10$ samples) were fed into eight MTVDBNs. Each of these eight MTVDBNs yielded the joint likelihood of $\mathbf{X}^*$ for one particular direction, d. In each trial, we then chose the direction that yielded the highest likelihood (i.e., lowest negative log-likelihood) as the predicted direction.

3.4. INTEGRATION OF ECoG-BASED PREDICTIONS AND TASK

In additional offline analyses, we simulated the integration of the directional prediction using ECoG signals with the task. We placed the cursor in the predicted direction at a distance α from the center. In other words, if the directional prediction was accurate, the cursor would be placed closer to the target, resulting in a decreased time needed to hit the target. **Figure 5** gives a simple illustration of re-positioning the cursor toward the predicted target direction. In this figure, the black box is the target and the predicted direction is (somewhat inaccurately) towards the right. If the radius of the circle in **Figure 5** is R, to decrease movement

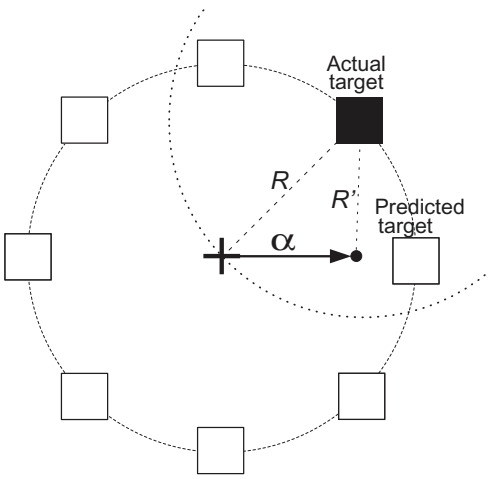

FIGURE 5 | An illustration of the simulated brain-assisted targeting system. The black box depicts the current target and the white boxes represent all other possible target locations. The arrow shows the incorrectly predicted direction. The dashed circle is the locus of all points at a distance R away from the target. When the cursor is re-positioned in this circle, the distance to the target is decreased, as $R' < R$.

time, the distance between the re-positioned cursor and the target should be less than R. The dashed circle is the locus of all points at a distance R to the target. Thus, to be closer to the target, after direction prediction the cursor should lie within the dashed circle. The area enclosed by the two circles is 39% of the area of the solid circle, implying that if we place the cursor in a random direction, then there would be a 61% chance that the cursor would be farther away from the target compared to if were left in the center of the circle. In other words, if we randomly placed the cursor within the solid circle, on average it would take the subject longer to hit the target. Conversely, if the output prediction is the correct target or at least one of its neighbors, this would bring the cursor closer to the target and may allow the user to reduce the time it would take to hit the target. The angle

between the imaginary line that passes through the center and the actual target and the imaginary line that passes through the center and one of the intersection points between the two circles is 60°. Hence, we have an error margin of ±60° to improve the performance.

4. RESULTS

4.1. PREDICTION OF MOVEMENT ONSET

As described in the Methods, we computed from ECoG signals (i.e., amplitudes in the mu, beta, and gamma band, as well as the LMP) the likelihood of an occurrence of a movement onset. **Figure 6** gives an exemplary resulting time course of the likelihood values of an onset over 20 s for Subject A, along with arrows that indicate the actual and predicted movement onsets. We observe that the likelihood curves exhibit sharp peaks around the actual movement onset, which demonstrates that the classifier can accurately detect movement onsets using ECoG signals. In each subject, we used these likelihood values to classify each time point t as "onset" if the likelihood value exceeded an empirically attained threshold value of 0.3. The confusion matrices, evaluated during actual movement, for all five subjects are shown in **Table 2** in percentages, along with the total number of events and the resulting $F1$-scores. Most of the false positives occur 200 ms around the movement onset (i.e., the peak of the probability function). The predictor yields high detection performance for Subjects A and B. The high occurrence of false negatives decreased the $F1$-score for Subjects D and E. The high number of false negatives and false positives led to reduced performance in Subject C.

Figure 7 shows the confidence indices of the ECoG features that are most predictive of the movement onset. (Note that a significance level of $p < 0.05$ corresponds to a confidence index of $-log(p) > 3$). The two larger brain models in the top row show the confidence indices for the high gamma band and LMP, the most predictive of the features, accumulated across all subjects. The bottom two rows show the results of the high gamma band and LMP for individual Subjects A–E. These results indicate that the brain areas yielding prediction of movement onset are centered on hand representations of motor cortical areas for the high gamma band and extend beyond the hand representations

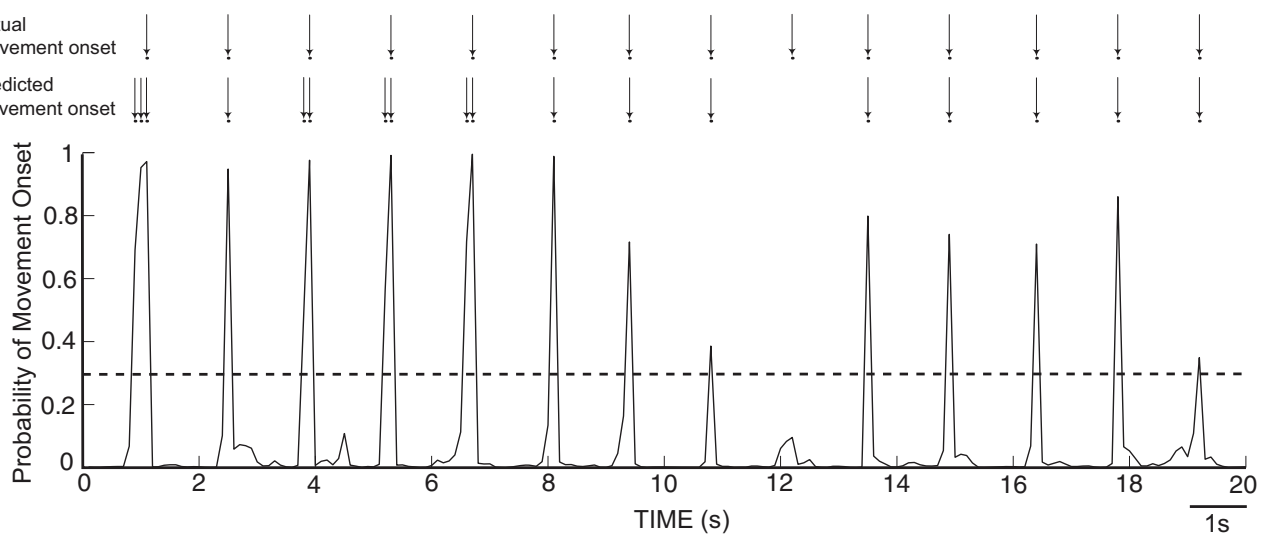

FIGURE 6 | Time course of likelihood of movement onset for Subject A. The dashed line represents a probability level of 0.3, which was used as a threshold to predict the movement onset.

Table 2 | Confusion matrices of movement onset prediction for Subjects A–E. The values shown in parentheses are the false positives that occur more than 200 ms away from the actual movement onset. The bottom row gives the *F*1-score.

	Subject A		Subject B		Subject C		Subject D		Subject E	
	Actual not onset	Actual onset	Actual not onset	Actual onset	Actual not onset	Actual onset	Actual not onset	Actual onset	Actual not onset	Actual onset
Predicted not onset	94%	27%	94%	36%	73%	74%	84%	65%	93%	66%
Predicted onset	6%(0.5%)	73%	6%(0.7%)	64%	27%(22%)	26%	16%(9%)	35%	7%(4%)	34%
Number of events	3991	316	4021	468	4537	205	3380	316	4640	320
*F*1-score	0.69		0.63		0.06		0.23		0.35	

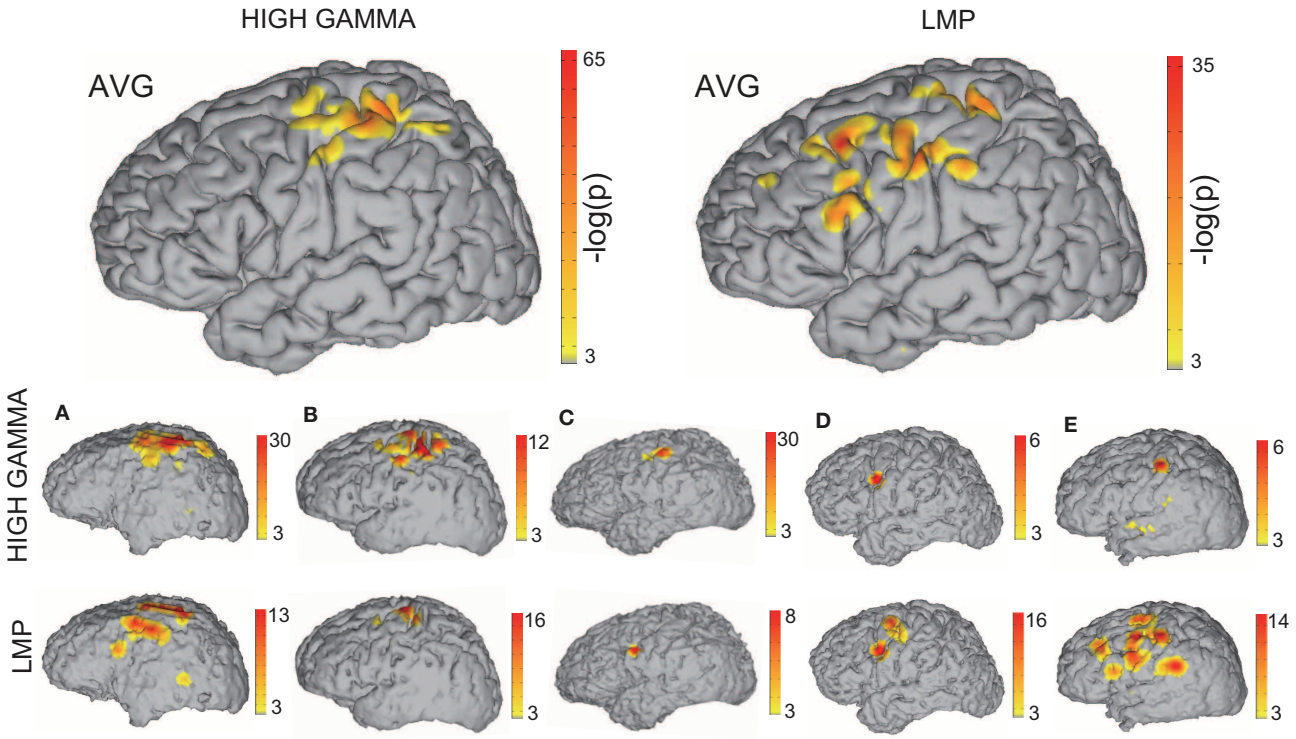

FIGURE 7 | Relationship of brain signals with movement onset. This figure shows the spatial distribution of accumulated confidence indices $-log(p)$ for the 70–170 Hz high gamma band (top left) or the LMP (top right) across all subjects. The spatial distribution of the confidence indices for each subject are depicted in the bottom rows.

for the LMP. This finding is in agreement with results from a previous report that investigated finger flexions (Kubánek et al., 2009). However, areas other than the sensorimotor cortex were used in the onset prediction as selected by the feature selection algorithm (see Methods). On the other hand, mu and beta bands did not yield statistically significant activations for prediction of movement onset. Although desynchronization of these bands has been posited to relate to local increases in high gamma amplitude in the motor cortex (i.e., as a gating mechanism) (Miller et al., 2009), the corresponding brain signals are known to be spatially widespread and slowly evolving, and thus may not be the best indicators for the exact timing of movement onset.

4.2. PREDICTION OF DIRECTION OF INTENDED MOVEMENT

We computed the absolute value of the angular error of the directional predictions obtained by the MTVDBNs for each trial and each subject, and calculated their mean and standard deviation across all trials. This yielded the following single-trial angular error statistics for Subjects A–E, respectively: $55.29° \pm 52.61°$, $46.28° \pm 57.80°$, $68.95° \pm 55.16°$, $70.55° \pm 53.78°$, and $87.8° \pm 57.9°$. A single-sided t-test revealed that the accuracy of our results was better than chance (i.e., $90.0 \pm 57.36°$) at a significance level of 5% ($p < 0.05$) for all subjects. Our method yielded single-trial angular errors that were smaller than 90° for all subjects, and as low as 46° in one subject. Given that the targets are separated by 45°, the results indicate that the classifier was able to infer the direction of intended movements within less than two targets in single trials.

4.3. INTEGRATION OF ECoG-BASED PREDICTIONS AND TASK

We further studied whether integrating information extracted from ECoG signals would improve performance in a simulated targeting task. Every time a movement onset and direction were predicted, we placed the cursor in the predicted direction. As described in the Methods, this stimulation will result in improved performance if the single-trial error of the predicted direction is less than 60°. **Figure 8** shows the positions of the cursor averaged across trials for each target for Subject A. It is clear that, after the re-positioning of the cursor based on the predicted directions, on average the subject would need to move a shorter distance to hit each target, and therefore should complete the task in less time assuming he/she would not have been distracted by the changing position of the cursor. After the cursor was placed closer to the decoded target, we simulated the cursor movement toward the target at each subject's average moving speed.

The distance α at which we place the cursor toward the predicted target is an important parameter that needs to be optimized. Note that α is a factor of the distance to the target (i.e., $\alpha = 0.5$ places the cursor halfway between the center and the predicted target) and thus $0 < \alpha \leq 1$. With either too small or too large of an α ($\alpha > 1$), we might not take full advantage of the prediction results. The time needed to hit the target as a

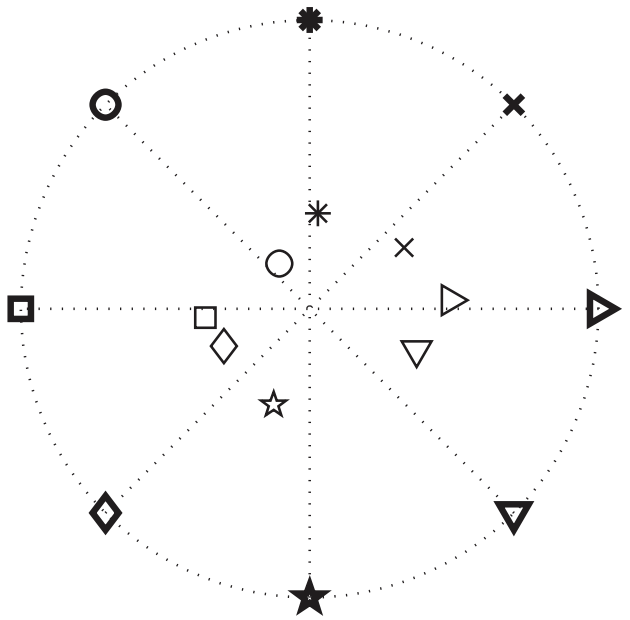

FIGURE 8 | Results for movement direction prediction results for Subject A. The symbols represent the eight different targets. The symbols in bold depict the actual positions of the targets and the thinner symbols show the averaged pre-movement positions of the cursor across all trials in each direction. (Note that these are average cursor positions. Values for single-trial angular errors are given in the text.)

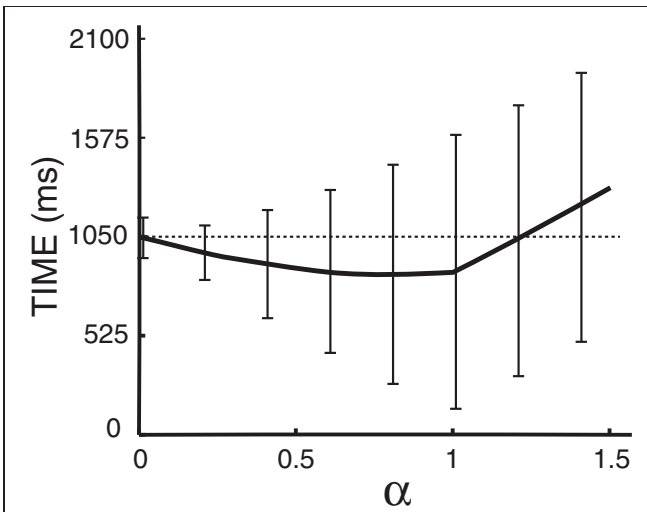

FIGURE 9 | Time to hit the target as a function of α for Subject A, where α is a scaling factor of the distance from the center to the targets. The dashed line gives the average time to hit the target without the assistance of ECoG signals. Error bars give the standard deviation of the mean. Note that predictions from the brain signals do not have any effect when α is zero.

function α is plotted in **Figure 9** for Subject A, which suggests an optimal value of 0.8 for α. The optimal α values for other subjects are listed in **Table 3**, which also compares the average movement time with and without the assistance of ECoG signals. The results in this table also demonstrate that the movement time of the majority of trials would have improved up to 150 ms. These encouraging results suggest that at least under certain assumptions[2], ECoG signals may improve a user's performance in a targeting task.

5. DISCUSSION

In this paper, we demonstrated that it is possible to use ECoG signals to detect the onset and the direction of an intended movement. We also demonstrate in a simulation that it may be possible to use these predictions to reduce the time to complete a targeting task by pre-positioning the cursor using ECoG signals acquired only prior to the movement. We achieved detection of movement onset by continually analyzing the incoming ECoG signals using a SVM classifier, and predicted the intended movement direction using a novel variant of a dynamic Bayesian network (i.e., the MTVDBN algorithm) that captures the spatial and temporal structure of the ECoG features.

5.1. OPTIMAL INTEGRATION OF BRAIN SIGNALS FOR IMPROVEMENT OF PERFORMANCE

The distance α from the center at which the cursor is repositioned affects the improvement in performance as shown in **Figure 9**. Moreover, we see in **Table 3** that the optimal α values ranges from 0.4 to 1.0 across subjects. It can also be observed that a higher α value is reflected in higher percentage of trials with improved movement time. This does not imply that a higher α value improves performance, which is not the case for Subjects D–E. Rather, it implies that if the directional classifier yields accurate outputs, we can take better advantage of the system (with a high α) for improving performance. Hence, improving classifier performance is crucial for the optimal integration of information from brain signals with external (e.g., joystick) control.

5.2. RELEVANCE FOR ASYNCHRONOUS BCIs

Synchronous BCIs restrict the user to communicate in predefined time frames. Asynchronous BCIs, which allow the user to communicate spontaneously, may support more powerful practical applications as they are self-initiated and self-paced systems. However, asynchronous BCIs require the detection of the event in addition to identifying the properties of the event. The results presented in this paper may prove useful as the basis for an asynchronous BCI. While data collection was achieved using cued external events, our decoder was ambivalent to these events and processed the incoming data asynchronously. That is, the only input to the decoder in our experiment was the ECoG time sequence. At each time *t*, the decoder detected whether the user was beginning to move the joystick, and also predicted the intended movement. Future research could explore similar capacities in completely uncued situations, and in people who attempt but do not actually execute movements, such as people with chronic stroke.

[2]One assumption here is that reduced distance-to-target will reduce movement time or at least will have other distinct benefits.

Table 3 | Statistics and parameters of the simulated performance: optimal α values, original average movement times, average simulated movement times achieved by integrating ECoG, percentage of trials with improved movement time, percentage of trials with degraded movement time, and the statistical significance of performance improvement (in trials with reduced movement time).

Optimal α	Subject A 0.6	Subject B 0.8	Subject C 0.6	Subject D 0.4	Subject E 0.4
Average movement time without ECoG (ms)	1050 ± 160	1067 ± 355	1710 ± 156	1635 ± 148	1507 ± 480
Average movement time with ECoG (ms)	882 ± 430	789 ± 469	1604 ± 494	1610 ± 687	1483 ± 733
Percentage of trials with improved movement time	61%	70%	54%	43%	53%
Percentage of trials with degraded movement time	39%	30%	46%	57%	47%
Significance (p-value) of improved movement time	7.3×10^{-9}	1.5×10^{-19}	2.7×10^{-4}	6.2×10^{-2}	7.4×10^{-3}

5.3. RELEVANCE FOR PERFORMANCE AUGMENTATION

We showed in a simulation that the time required to perform a directional motor task can be reduced by up to 150 ms. Such improvements in human performance should have a number of important applications. As an example, a reduction of the time to acquire a target may increase the probability to come out ahead in tactical combat. To investigate this possibility, the methods presented in this paper could be readily transferred to real-time testing. In this scenario, model parameters are estimated once initial training data are collected. The computational complexity of the MTVDBN directional classifier during the online testing session is $O(dTM^2)$, where d is the number of directions, T is the memory depth (i.e., input time samples), and M is the number of input features (i.e., spectral bands times the number of channels). This relatively modest computational requirement should readily support real-time testing once the MTVDBNs are trained. Nevertheless, real-time implementation and testing is necessary to determine whether the time to hit the target will also decrease in actual online experiments.

5.4. EXPERIMENTAL LIMITATIONS

While the signal characteristics of ECoG are attractive, the acquisition and study of ECoG have several important limitations. Foremost, to record cortical signals subdurally, a craniotomy and dural incision must be performed. Hence, the implantation of the grids is associated with infrequent, but serious risks, such as inflammation or death. Moreover, the extent of grid coverage and its placement is not standardized across subjects and is determined by the clinical needs of the patients. For instance, the subject with the smallest fraction of trials with improved movement time (i.e., Subject D) had grids implanted ipsilateral to her dominant (left) hand. Thus, she was asked to use her non-dominant hand (i.e., contralateral to her implants) during the experiment, which might have contributed to reduced information about movement direction, and hence the low percentage of trials with improved movement times. Next, the physical and cognitive condition and level of cooperation of each subject are variable. Moreover, ECoG experiments are for practical reasons performed in uncontrolled noisy environments (i.e., hospital rooms). Furthermore, the subjects in the study suffered from epilepsy, and thus may have some degree of functional or structural reorganization compared to healthy individuals. Despite these limitations, the results presented in this and other ECoG studies are usually consistent with expectations based on human neuroanatomy.

While we controlled for important variables in this study (such as eye gaze), the experimental setup in any ECoG study is necessarily somewhat less controlled than that in the typical animal or human neuroscientific study. However, real-world environments are typically very uncontrolled as well. This circumstance strengthens our claim that our results may translate into benefits in real-life scenarios.

In its present design, the onset predictor is based on ECoG signals from the previous 1s. In other words, at least 1s of data need to be available to make a prediction about movement onset. In addition, the directional classifier is designed for prediction of discrete directions at the time of movement onset. Moreover, it takes advantage of the $\pm 60^\circ$ error margin to bring the cursor closer to the target. Hence, it is unclear to what extent the information in ECoG would generalize to reliable predictions during continuous cursor control. Finally, real-time implementation of the proposed system (i.e., re-positioning of the cursor) is required for evaluating the proposed system, as unpredicted jumps in the cursor, whether closer to or farther from the target, might affect the performance of the user.

5.5. FUTURE DIRECTIONS

The work presented in this paper focused on detecting the onset and direction of movements using ECoG signals. The methodologies for initiation detection presented in this paper may also be extended to the detection of inhibition of a movement. Volitional inhibition is the process of adapting to sudden changes in the surrounding environment by stopping or modifying an action. Thus, future work may include testing countermanding of initiated motor responses, e.g.,using a stop-signal paradigm (Logan et al., 1984). Inhibiting a response has been suggested to recruit a fronto-basal ganglia-thalamic network, including the right inferior frontal gyrus (Aron et al., 2003, 2007; Rubia et al., 2003;

Chambers et al., 2006) and pre-supplementary motor cortical areas (Sumner et al., 2007; Chen et al., 2010; Scangos and Stuphorn, 2010). These areas are thought to influence the cortical areas underlying limb movement preparation and initiation, i.e., dorsal premotor (Mirabella et al., 2012) and primary motor cortices (Coxon et al., 2006; Swann et al., 2009), through the subthalamic nucleus (Aron and Poldrack, 2006; van den Wildenberg et al., 2006; Mirabella et al., 2011). Applying the methodological framework described in this study to ECoG signals collected over the right inferior gyrus, motor and pre-supplementary motor cortices during a countermanding task may thus allow for the detection of the onset of corresponding inhibitory processes. Using such an approach, it may be possible for stopping the cursor from moving in the wrong direction in cases when the directional classifier failed.

ACKNOWLEDGMENTS

This work was supported in part by grants from the US Army Research Office [W911NF-08-1-0216 (Gerwin Schalk) and W911NF-07-1-0415 (Gerwin Schalk) and the NIH EB006356 (Gerwin Schalk) and EB000856 (Gerwin Schalk)]. The authors would like to thank the subjects for their participation, the staff of AMC Epilepsy Monitoring Unit for their assistance, and Griffin Milsap for technical support.

REFERENCES

Achtman, N., Afshar, A., Santhanam, G., Yu, B. M., Ryu, S. I., and Shenoy, K. V. (2007). Free-paced high-performance brain-computer interfaces. *J. Neural Eng.* 4, 336–347.

Aron, A. R., Behrens, T. E., Smith, S., Frank, M. J., and Poldrack, R. A. (2007). Triangulating a cognitive control network using diffusion-weighted magnetic resonance imaging (MRI) and functional MRI. *J. Neurosci.* 27, 3743–3752.

Aron, A. R., Fletcher, P. C., Bullmore, E. T., Sahakian, B. J., and Robbins, T. W. (2003). Stop-signal inhibition disrupted by damage to right inferior frontal gyrus in humans. *Nat. Neurosci.* 6, 115–116.

Aron, A. R., and Poldrack, R. A. (2006). Cortical and subcortical contributions to Stop signal response inhibition: role of the subthalamic nucleus. *J. Neurosci.* 26, 2424–2433.

Bai, O., Lin, P., Vorbach, S., Floeter, M. K., Hattori, N., and Hallett, M. (2008). A high performance sensorimotor beta rhythm-based brain-computer interface aociated with human natural motor behavior. *J. Neural Eng.* 5, 24–35.

Ball, T., Kern, M., Mutschler, I., Aertsen, A., and Schulze-Bonhage, A. (2009). Signal quality of simultaneously recorded invasive and non-invasive EEG. *Neuroimage* 46, 708–716.

Borisoff, J. F., Mason, S. G., Bashashati, A., and Birch, G. E. (2004). Brain-computer interface design for asynchronous control applications: improvements to the LF-ASD asynchronous brain switch. *IEEE Trans. Biomed. Eng.* 51, 985–992.

Buch, E., Weber, C., Cohen, L. G., Braun, C., Dimyan, M. A., Ard, T., Mellinger, J., Caria, A., Soekadar, S., Fourkas, A., and Birbaumer, N. (2008). Think to move: a neuromagnetic brain-computer interface (BCI) system for chronic stroke. *Stroke* 39, 910.

Chambers, C. D., Bellgrove, M. A., Stokes, M. G., Henderson, T. R., Garavan, H., Robertson, I. H., Morris, A. P., and Mattingley, J. B. (2006). Executive "brake failure" following deactivation of human frontal lobe. *J. Cogn. Neurosci.* 18, 444–455.

Chao, Z. C., Nagasaka, Y., and Fujii, N. (2010). Long-term asynchronous decoding of arm motion using electrocorticographic signals in monkeys. *Front. Neuroeng.* 3:3. doi: 10.3389/fneng.2010.00003

Chen, X., Scangos, K. W., and Stuphorn, V. (2010). Supplementary motor area exerts proactive and reactive control of arm movements. *J. Neurosci.* 30, 14657–14675.

Coxon, J. P., Stinear, C. M., and Byblow, W. D. (2006). Intracortical inhibition during volitional inhibition of prepared action. *J. Neurophysiol.* 95, 3371–3383.

Daly, J. J., and Wolpaw, J. R. (2008). Brain-computer interfaces in neurological rehabilitation. *Lancet Neurol.* 7, 1032–1043.

Duda, R. O., Hart, P. E., and Stork, D. G. (2008). *Pattern Classification*. New York, NY: Wiley-Interscience.

Efron, B., Hastie, T., Johnstone, I., and Tibshirani, R. (2004). Least angle regression. *Ann. Stat.* 32, 407–499.

Georgopoulos, A. P., Kalaska, J. F., Caminiti, R., and Massey, J. T. (1982). On the relations between the direction of two-dimensional arm movements and cell discharge in primate motor cortex. *J. Neurosci.* 2, 1527–1537.

Gunduz, A., Sanchez, J. C., Carney, P. R., and Principe, J. C. (2009). Mapping broadband electrocorticographic recordings to two-dimensional hand trajectories in humans. *Neural Netw.* 22, 1257–1270.

Gunduz, A., and Schalk, G. (2011). "Defense-related insights and solutions from neuroscience and neuroengineering," in *Proceedings of SPIE, Volume 8058 of Independent Component Analyses, Wavelets, Neural Networks, Biosystems and Nanoengineering*, ed H. Szu (Orlando, FL, USA: International Society of Optics and Photonics).

Hasan, B. A. S., and Gan, J. Q. (2011). Temporal modeling of EEG during self-paced hand movement and its application in onset detection. *J. Neural Eng.* 8, 056015.

Haufe, S., Treder, M., Gugler, M., Sagebum, M., Curio, G., and Blankertz, B. (2011). EEG potentials predict upcoming emergency brakings during simulated driving. *J. Neural Eng.* 8, 056001.

Hochberg, L., Serruya, M., Friehs, G., Mukand, J., Saleh, M., Caplan, A., Branner, A., Chen, D., Penn, R., and Donoghue, J. (2006). Neuronal ensemble control of prosthetic devices by a human with tetraplegia. *Nature* 442, 164–171.

Huang, Y. M., and Du, S. X. (2005). "Weighted support vector machine for classification with uneven training class sizes," in *Proceedings of International Conference on Machine Learning and Cybernetics*, Vol. 7, (Guangzhou, China), 4365–4369.

Hwang, E. J., and Andersen, R. A. (2009). Brain control of movement execution onset using local field potentials in posterior parietal cortex. *J. Neurosci.* 29, 14363–14370.

Kubánek, J., Miller, K. J., Ojemann, J. G., Wolpaw, J. R., and Schalk, G. (2009). Decoding flexion of individual fingers using electrocorticographic signals in humans. *J. Neural Eng.* 6, 066001.

Lancaster, J. L., Woldorff, M. G., Parsons, L. M., Liotti, M., Freitas, C. S., Rainey, L., Kochunov, P. V., Nickerson, D., Mikiten, S. A., and Fox, P. T. (2000). Automated Talairach atlas labels for functional brain mapping. *Hum. Brain Mapp.* 10, 120–131.

Lebedev, M. A., O'Doherty, J. E., and Nicolelis, M. A. L. (2008). Decoding of temporal intervals from cortical ensemble activity. *J. Neurophysiol.* 99, 166–186.

Leeb, R., Friedman, D., Müller-Putz, G. R., Scherer, R., Slater, M., and Pfurtscheller, G. (2007). Self-paced (asynchronous) BCI control of a wheelchair in virtual environments: a case study with a tetraplegic. *Comput. Intell. Neurosci.* 2007, 7:1–7:12.

Leuthardt, E. C., Schalk, G., Wolpaw, J. R., Ojemann, J. G., and Moran, D. W. (2004). A brain-computer interface using electrocorticographic signals in humans. *J. Neural Eng.* 1, 63–71.

Logan, G. D., Cowan, W. B., and Davis, K. A. (1984). On the ability to inhibit simple and choice reaction time responses: a model and a method. *J. Exp. Psychol. Hum. Percept. Perform.* 10, 276–291.

Mak, J. N., and Wolpaw, J. R. (2009). Clinical applications of brain-computer interfaces: current state and future prospects. *IEEE Rev. Biomed. Eng.* 2, 187–199.

Marple, S. L. (1986). *Digital Spectral Analysis: With Applications*. Upper Saddle River, NJ: Prentice Hall.

Mason, S. G., and Birch, G. E. (2000). A brain-controlled switch for asynchronous control applications. *IEEE Trans. Biomed. Eng.* 47, 1297–1307.

Millan, J., and Mouriño, J. (2003). Asynchronous BCI and local neural classifiers: an overview of the adaptive brain interface project. *IEEE Trans. Neural Syst. Rehabil. Eng.* 11, 159–161.

Miller, K. J., Leuthardt, E. C., Schalk, G., Rao, R. P., Anderson, N. R., Moran, D. W., Miller, J. W., and Ojemann, J. G. (2007). Spectral changes in

cortical surface potentials during motor movement. *J. Neurosci.* 27, 2424–2432.

Miller, K. J., Zanos, S., Fetz, E. E., den Nijs, M., and Ojemann, J. G. (2009). Decoupling the cortical power spectrum reveals real-time representation of individual finger movements in humans. *J. Neurosci.* 29, 3132.

Mirabella, G., Iaconelli, S., Romanelli, P., Modugno, N., Lena, F., Manfredi, M., and Cantore, G. (2012). Deep brain stimulation of subthalamic nuclei affects arm response inhibition in Parkinson's patients. *Cereb. Cortex* 22, 1124–1132.

Mirabella, G., Pani, P., and Ferraina, S. (2011). Neural correlates of cognitive control of reaching movements in the dorsal premotor cortex of rhesus monkeys. *J. Neurophysiol.* 106, 1454–1466.

Muralidharan, A., Chae, J., and Taylor, D. M. (2011). Early detection of hand movements from electroencephalograms for stroke therapy applications. *J. Neural Eng.* 8, 046003.

Pistohl, T., Ball, T., Schulze-Bonhage, A., Aertsen, A., and Mehring, C. (2008). Prediction of arm movement trajectories from ECoG-recordings in humans. *J. Neurosci. Methods* 167, 105–114.

Rubia, K., Smith, A. B., Brammer, M. J., and Taylor, E. (2003). Right inferior prefrontal cortex mediates response inhibition while mesial prefrontal cortex is responsible for error detection. *Neuroimage* 20, 351–358.

Scangos, K. W., and Stuphorn, V. (2010). Medial frontal cortex motivates but does not control movement initiation in the countermanding task. *J. Neurosci.* 30, 1968–1982.

Schalk, G., Kubanek, J., Miller, K. J., Anderson, N. R., Leuthardt, E. C., Ojemann, J. G., Limbrick, D., Moran, D., Gerhardt, L. A., and Wolpaw, J. R. (2007). Decoding two-dimensional movement trajectories using electrocorticographic signals in humans. *J. Neural Eng.* 4, 264.

Schalk, G., McFarland, D. J., Hinterberger, T., Birbaumer, N., and Wolpaw, J. R. (2004). BCI2000: a general-purpose brain-computer interface (BCI) system. *IEEE Trans. Biomed. Eng.* 51, 1034–1043.

Schalk, G., and Mellinger, J., (2010). *A Practical Guide to Brain-Computer Interfacing with BCI(2000)*. New York, NY: Springer.

Schalk, G., Miller, K. J., Anderson, N. R., Wilson, J. A., Smyth, M. D., Ojemann, J. G., Moran, D. W., Wolpaw, J. R., and Leuthardt, E. C. (2008). Two-dimensional movement control using electrocorticographic signals in humans. *J. Neural Eng.* 5, 75–84.

Schmidt, M., Niculescu-Mizil, A., and Murphy, K. (2007). "Learning graphical model structure using L1-regularization paths," in *Proceedings of the 22nd National Conference on Artificial Intelligence*, Vol. 2, (AAAI Press), 1278–1283.

Sejnowski, T. J., Dornhege, G., del Millán, J. R., Hinterberger, T., McFarland, D. J., and Müller, K., (2007). *Toward Brain-Computer Interfacing (Neural Information Processing)*. Cambridge, MA: MIT Press.

Simeral, J. D., Kim, S.-P., Black, M. J., Donoghue, J. P., and Hochberg, L. R. (2011). Neural control of cursor trajectory and click by a human with tetraplegia 1000 days after implant of an intracortical microelectrode array. *J. Neural Eng.* 8, 025027.

Song, L., Kolar, M., and Xing, E. P. (2009). "Time-varying dynamic Bayesian networks," in *Proceedings of the 23rd Neural Information Processing Systems (NIPS)*, (Vancouver, Canada).

Sumner, P., Nachev, P., Morris, P., Peters, A. M., Jackson, S. R., Kennard, C., and Husain, M. (2007). Human medial frontal cortex mediates unconscious inhibition of voluntary action. *Neuron* 54, 697–711.

Swann, N., Tandon, N., Canolty, R., Ellmore, T. M., McEvoy, L. K., Dreyer, S., DiSano, M., and Aron, A. R. (2009). Intracranial EEG reveals a time- and frequency-specific role for the right inferior frontal gyrus and primary motor cortex in stopping initiated responses. *J. Neurosci.* 29, 12675–12685.

Tan, D. S., and Nijholt, A. (2010). *Brain-Computer Interfaces*. New York, NY: Springer Press.

van Rijsbergen, C. J. (1979). *Information Retrieval*. Cambridge, MA, USA: Butterworths.

van den Wildenberg, W. P. M., van Boxtel, G. J. M., van der Molen, M. W., Bosch, D. A., Speelman, J. D., and Brunia, C. H. (2006). Stimulation of the subthalamic region facilitates the selection and inhibition of motor responses in Parkinson's disease. *J. Cogn. Neurosci.* 18, 626–636.

Wang, W., Sudre, G. P., Xu, Y., Kass, R. E., Collinger, J. L., Degenhart, A. D., Bagic, A. I., and Weber, D. J. (2010). Decoding and cortical source localization for intended movement direction with MEG. *J. Neurophysiol.* 104, 2451–2461.

Wisneski, K. J., Anderson, N., Schalk, G., Smyth, M., Moran, D., and Leuthardt, E. C. (2008). Unique cortical physiology associated with ipsilateral hand movements and neuroprosthetic implications. *Stroke* 39, 3351.

Wolpaw, J. R., Birbaumer, N., McFarland, D. J., Pfurtscheller, G., and Vaughan, T. M. (2002). Brain-computer interfaces for communication and control. *Clin. Neurophysiol.* 113, 767–792.

Yanagisawa, T., Hirata, M., Saitoh, Y., Goto, T., Kishima, H., Fukuma, R., Yokoi, H., Kamitani, Y., and Yoshimine, T. (2011). Real-time control of a prosthetic hand using human electrocorticography signals. *J. Neurosurg.* 114, 1715–1722.

Conflict of Interest Statement: The authors declare that the research was conducted in the absence of any commercial or financial relationships that could be construed as a potential conflict of interest.

Received: 29 January 2012; paper pending published: 02 March 2012; accepted: 28 June 2012; published online: 08 August 2012.

*Citation: Wang Z, Gunduz A, Brunner P, Ritaccio AL, Ji Q and Schalk G (2012) Decoding onset and direction of movements using Electrocorticographic (ECoG) signals in humans. Front. Neuroeng. **5**:15. doi: 10.3389/fneng. 2012.00015*

APPENDIX

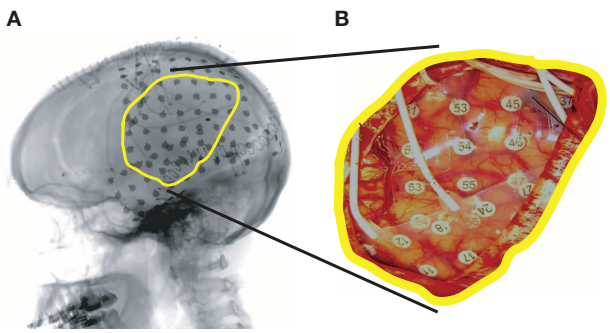

FIGURE A1 | Example of an implanted subdural grid (Subject A). **(A)** Lateral radiograph indicating grid position. **(B)** Subdural grid placed over left fronto-parietal and temporal lobes.

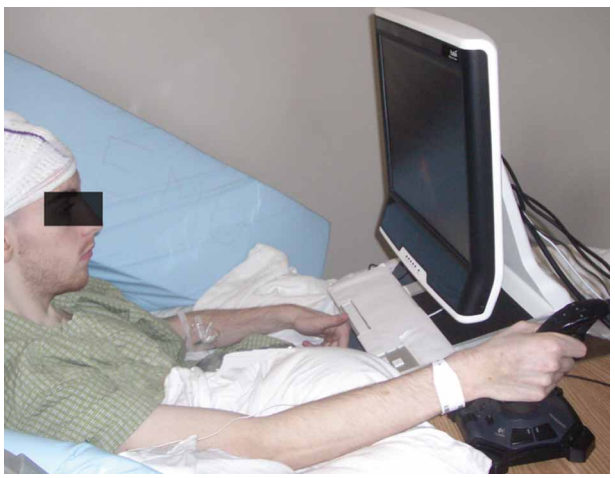

FIGURE A2 | The experimental setup at Albany Medical College. Joystick control mostly entailed wrist movements.

frontiers in
NEUROENGINEERING

ORIGINAL RESEARCH ARTICLE
published: 12 July 2012
doi: 10.3389/fneng.2012.00013

Detection of self-paced reaching movement intention from EEG signals

Eileen Lew[1], Ricardo Chavarriaga[1], Stefano Silvoni[2] and José del R. Millán[1]*

[1] *Defitech Chair in Non-Invasive Brain-Machine Interface, Center for Neuroprosthetics, School of Engineering, Ecole Polytechnique Fédérale de Lausanne, Switzerland*
[2] *Laboratory of Robotics and Kinematics, IRRCSS Camillo Hospital Foundation, Venice, Italy*

Edited by:
Giovanni Mirabella, University of La Sapienza, Italy

Reviewed by:
Hari S. Sharma, Uppsala University, Sweden
Vassiliy Tsytsarev, University of Maryland School of Medicine, USA
Peter J. Ifft, Duke University, USA

****Correspondence:***
José del R. Millán, Defitech Chair in Non-Invasive Brain-Machine Interface, Center for Neuroprosthetics, School of Engineering, Ecole Polytechnique Fédérale de Lausanne, Switzerland.
e-mail: jose.millan@epfl.ch

Future neuroprosthetic devices, in particular upper limb, will require decoding and executing not only the user's intended movement type, but also *when* the user intends to execute the movement. This work investigates the potential use of brain signals recorded non-invasively for detecting the time before a self-paced reaching movement is initiated which could contribute to the design of practical upper limb neuroprosthetics. In particular, we show the detection of self-paced reaching movement intention in single trials using the readiness potential, an electroencephalography (EEG) slow cortical potential (SCP) computed in a narrow frequency range (0.1–1 Hz). Our experiments with 12 human volunteers, two of them stroke subjects, yield high detection rates prior to the movement onset and low detection rates during the non-movement intention period. With the proposed approach, movement intention was detected around 500 ms before actual onset, which clearly matches previous literature on readiness potentials. Interestingly, the result obtained with one of the stroke subjects is coherent with those achieved in healthy subjects, with single-trial performance of up to 92% for the paretic arm. These results suggest that, apart from contributing to our understanding of voluntary motor control for designing more advanced neuroprostheses, our work could also have a direct impact on advancing robot-assisted neurorehabilitation.

Keywords: BCI, EEG, rehabilitation, self-paced protocol, stroke, voluntary movements

1. INTRODUCTION

Human movements are usually volitional, where we spontaneously decide when to initiate it and commit to a particular course of action to accomplish a daily task (Haggard, 2008). This is the reason why uncovering the neural correlates of voluntary movement is important for implementing practical Brain Computer Interface (BCI) technology that people can use over long periods of time in a natural way. Current non-invasive BCI allows its user to deliver mental commands to a robot controller that transforms them into appropriate motor actions—e.g., left, right, and forward decoded from electroencephalography (EEG) signals while the user imagines different limb movements (Galán et al., 2008; Millán et al., 2009). However, most brain-actuated robots assume that the user wants to operate the neuroprosthesis in well-defined periods of time, in contrast to daily experiences of motor control, where movements are executed sporadically in a self-paced manner.

In this paper, we investigate the feasibility of detecting the intention to perform a reaching movement in single trials before actual execution from human EEG. Intention has been described as doing something purposefully (Schall, 2004). In this paper, we defined intention as the time of awareness of wanting to perform a reaching task. This definition is not to be confused with the work of Congedo et al. (2006), Gonzalez et al. (2006), and Bai et al. (2007) where movement intention was defined as the problem of classifying the intention to move the left hand or right hand. To study movement intention, we follow a self-paced paradigm where subjects can execute a reaching movement at any time they wish. This is a more natural and ecological experimental setup than the classical reaction task paradigm, where subjects perform movements in response to a cue.

A number of recent studies have found neural correlates of *when* subjects decide to initiate a movement. Through invasive methods, Fried et al. (2011) have reported progressive neuronal recruitment in the supplementary motor area (SMA) over 1500 ms before subjects made the decision to move. In another study with human electrocorticography (ECoG), Ball et al. (2009) reported the existence peri-movement activity as early as 200 ms before movement onset. With regard to non-invasive EEG studies, the earliest evidence of the neural correlates of voluntary movement intention was discovered by Kornhuber and Deecke (1965), who identified a slow, negative potential as early as 1.5 s before the execution of movement. This slow cortical potential (SCP) was initially named as Bereitschaftspotential. This readiness potential has two main components. The first one is a slow negative potential starting 1.5 s before voluntary movement. This negativity is more prominent over the central-medial scalp. The late component occurs 400 ms before movement, with a steeper slope over the contralateral primary motor area (Shibasaki and Hallett, 2006). The slow potentials originate in depolarizations of the apical dendritic tree in the upper cortical layers that are caused by synchronous firing, mainly from thalamocortical afferents,

showing local excitatory mobilization for negative slow potentials (Birbaumer, 1999). The presence of this readiness potential was further analyzed in a series of famous studies by Libet et al. (1982, 1983) who showed that there is an unconscious preparatory brain activity that begins 1 s or more before movement, preceding the conscious awareness to act. Similar negativity components have been observed in patients with brain lesions (Deecke et al., 1987).

Nevertheless, being a SCP close to DC, the presence of the readiness potential in single trials seems to be elusive. Another EEG correlate of movement preparation and execution is the event-related desynchronization (ERD; Pfurtscheller and Lopes da Silva, 1999), a decrease in mu and beta power (8–30 Hz) over the contralateral primary motor cortex. Bai et al. (2011) showed that self-paced wrist extension movement onset can be detected on average 0.62 ± 0.25 s before actual movement from the analysis of ERD. Finally, Awwad Shiekh Hasan and Gan (2010, 2011) studied the EEG activity in the mu, beta and lower gamma bands (8–45 Hz) to detect movement onset also during self-paced wrist extension movements. They achieved good results, but with a poor temporal resolution (from 2 s before to 2 s after the movement).

Here we show for the first time the detection of self-paced reaching movement intention in single trials from the analysis of the readiness potential in 12 human volunteers, two of them stroke subjects. In this study, we used EEG signals filtered in a narrow frequency range of [0.1–1] Hz, which is reported to better capture anticipatory-related SCPs (Garipelli et al., 2011). We explicitly focus on the readiness potential for two reasons. Firstly, as mentioned above, it is a well-known correlate of voluntary movement intention. Secondly, it is a promising non-invasive method for localization of motor control after hemispheric lesions (Green, 2003), which could be useful for understanding motor functional improvements following rehabilitation.

In this respect, apart from contributing to our understanding of voluntary motor control and to the design of more advanced neuroprostheses, our work could also have a direct impact on advancing robot-assisted neurorehabilitation (Riener et al., 2005; Johnson, 2006). Indeed, robot-assisted therapy for stroke patients with moderate-to-severe upper-limb deficits has shown promising results in terms of improving motor functional recovery compared to traditional therapy (Kwakkel et al., 2008; Masiero et al., 2009; Staubli et al., 2009; Lo et al., 2010; Hogan and Krebs, 2011). Still this kind of neurorehabilitation therapy could be improved, as earlier detection of movement intention can minimize the delays in device activation and, thus, allow tighter coupling between the initial formation of the motor plan in the cortex and its execution at the periphery through movement-assisted devices, thus better promoting brain plasticity after stroke (Muralidharan et al., 2011). It is for this reason that, in one of the experiments, we have involved stroke patients in order to carry out a first feasibility study.

Single-trial classification of SCP has already been used in BCI, most notably by Birbaumer et al. (1999). Recently, Bradberry et al. (2010) showed the possibility of decoding arm trajectories from SCPs. Garipelli et al. (2009) has also analyzed the SCP for studying and classifying anticipatory behavior. Bai et al. (2007) explored the use of SCP, computed with a low-pass filter at 10 Hz, for classifying a right vs. left hand movement. In this work, the focus is on identifying the intention to execute a self-paced reaching action before the movement starts, irrespective of the movement direction or laterality. It is also worth noting that the readiness potentials have a similar shape to SCP associated to anticipatory behavior, in particular the contingent negative variation (Walter et al., 1964). However, as discussed in Rektor (2003), while both kinds of SCP are readily confounded in scalp recordings, more invasive techniques (Ikeda et al., 1994; Lamarche et al., 1995) or clever experimental designs (Ruchkin et al., 1986; Brunia and Damen, 1988) demonstrate differences.

The experiments and the proposed methods are detailed in section 2. In section 3, we report the experimental results where, in particular, we compare the effect of using manually and automatically selected channels. We also report on the classification of movement onset using electromyograph (EMG) signals as well as on the classification of non-movement intention period. Finally, we discuss the implications of our results in section 4.

2. MATERIALS AND METHODS

2.1. EXPERIMENTAL PROTOCOLS

We have designed two experiments: (1) EEG recordings of free arm reaching movements to a target button from healthy subjects using only their dominant arms, and (2) EEG measurements of a high-precision arm reaching task from stroke patients and healthy subjects as a control group. The reason why, after the promising results achieved in the first experiment, we have run a second experiment with a small stroke cohort is to make a preliminary study on the feasibility to detect movement intention in single trials as a potential tool for rehabilitation. This experiment was done in a clinical setting. In this later experiment, subjects performed the task with both arms in order to analyze possible differences in performance between the paretic and healthy arms of patients.

2.1.1. Experiment 1

Eight subjects (three female, age 29.33 ± 2.06) participated in the experiment. They were informed about the experimental procedures and gave their consent. All subjects were healthy with no known history of neurological abnormalities or musculoskeletical disorders. Seven out of the eight subjects in this experiment were right-handed.

The experimental workspace consisted of four targets (up, down, left, and right), which correspond to buttons on the horizontal plane located with respect to the mid-sagittal plane of the subjects as shown in **Figure 1** (left). Despite the center-out reaching task, it is important to highlight that the decoding of reaching directions is not within the scope of this paper as, here, we are interested in studying the common initiation of movement, irrespective of the movement type. The dimension of the horizontal plane was 47.0×48.5 cm (length $\times$ width). The distance from the home position to each target positions was approximately 20 cm. The target and home position buttons were a disc with a diameter of 27 mm. The design of the targets and home position consisted of microswitch buttons with direct connection to the input trigger of the ActiveTwo (EEG recording device) USB2 receiver. The buttons act as the event marker for

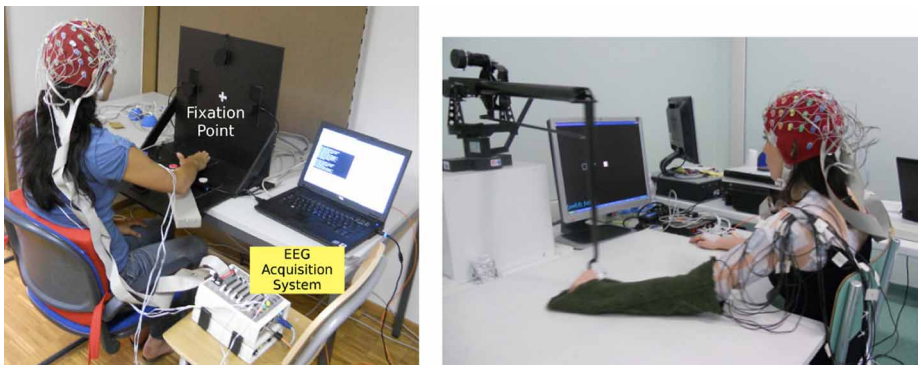

FIGURE 1 | Experimental setup for Experiment 1(left) and Experiment 2 (right).

the movement onset. This design provides a high temporal resolution in marking the movement onset events (releasing the buttons from the center rest position). The recordings were conducted in a normal office environment, with people working and speaking around, to mimic as close as possible a realistic scenario.

Subjects were instructed to perform natural self-paced center-out and center-in arm reaching tasks with their dominant arm. They were asked to fixate their eyes on a cross in the middle of the vertical plane as shown in **Figure 1** (left), thus minimizing eye movement-related artifacts in the recording. Each trial began with the subject placing their dominant hand on the center position. While at this position, subjects were asked to relax their hand, forearm, elbow, and arm in order not to induce any muscular tension which could possibly effect the outcome of the analysis. After 500 ms, an auditory cue informed the subject which target direction to reach. However, subjects were not supposed to react immediately (i.e., reaction task) or wait a fixed period of time (i.e., memory task) after the presentation of the cue. In contrast, they initiated the movement whenever they wish, but not before 2 s after the presentation of the auditory cue.

The role of the auditory cue was to ensure equal distribution of targets to be reached. There were a total of 200 trials recorded for each subject. Nevertheless, not all trials were kept for analysis. We discarded trials where the subject moved earlier than 2 s. We also removed trials if subjects reached to the wrong target. Finally, we discarded trials contaminated with strong artifacts or noise. After that, it remained an average of 188 trials across all subjects, where the average preparation time (T_{onset}) is 5.03 ± 1.77 s as shown in **Figure 2**.

The design of this experiment allows voluntary initiation of movement by the subjects, in contrast with most cue-based reaction time task experimental protocols where there is a *go* cue that instructs the subject when to start the movement. It has been shown that the brain areas involved in a spontaneous task differ from those of an instructed task (Thut et al., 2000). In particular, they found longer lasting activity in the SMA during the spontaneous task and in the premotor area (PMA) during the instructed condition. Lu et al. (2011) also reported different brain areas responsible for cued and self-initiated movements.

The reaching task in this study is a form of unconstrained, multi-degree of freedom movement. Therefore, besides EEG, we also recorded EMG signals from the *musculus biceps branchii* (selection of location through trial and error before experiment) to monitor that there is no muscular activity during the preparation period. This signal was also used to determine the time onset of muscular activation with respect to the movement onset given by the experimental apparatus (i.e., microswitch at center position).

Before the experiment starts, subjects were asked to perform a calibration session where they have to move their eyes toward the targets, and to perform a 1 min natural eye blinking (Schlögl et al., 2007). This session was used to measure the effects of eye movements on the EEG signals (see section 2.2.2).

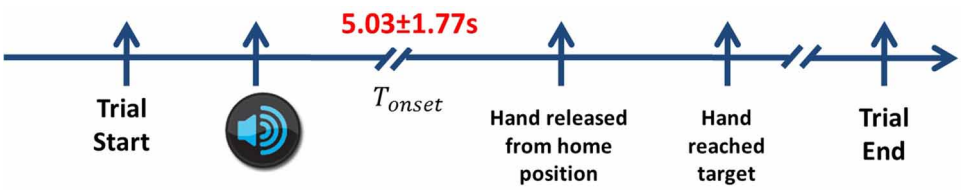

FIGURE 2 | The timeline of the experimental protocol. Each trial starts when the subject places their hand on the center button. Next, the auditory cue informs the subject which direction to reach. After a delayed period of more than 2 s, he releases his hands from the home position and reaches towards the target. In order to complete the movement, the subject returns back to the home position before starting the next trial. Only center-out reaching periods are considered. The average T_{onset} across all subjects in Experiment 1 is 5.03 ± 1.77 s.

2.1.2. Experiment 2

Four subjects, recorded at the San Camillo Hospital, Venice, Italy, participated in this experiment. There were two stroke patients and two healthy control subjects. All procedures were approved by the Ethics Committee of the San Camillo Hospital before experimentations. All subjects were informed about the experimental procedures and gave their consent.

Table 1 shows a summary of the subjects' particulars. All subjects were right-handed. Stroke subject **dpm** suffers from a left cerebellar hemorrhagic stroke, also commonly known as intracerebral bleed, where the ipsilateral body part is affected. Stroke subject **lg** suffers from a left nucleo-capsular stroke caused by lesion in a deeper brain structure, thus affecting the contralateral limb. **Table 1** also reports the Fugl-Meyer Motor Assessment score for upper extremity (FMA-UE)—maximum score of 66—for both stroke subjects. Both patients had preserved tactile and proprioceptive sensibility of the arm with normal cognitive abilities at the time of admission to the hospital.

The subject was seated in front of a computer screen holding on to a haptic manipulandum (PHANTOM Premium 3.0/6DOF, Sensable Technologies) with her arm resting on the table as shown in **Figure 1** (right). This experiment used a similar paradigm to the previous experiment. In contrast to the previous experiment, the reaching task was performed with both arms. The subjects were instructed to move a manipulandum that controls the position of a cursor (a green circle) on a computer screen. The rest position is the condition when the green circle remains inside the white box located in the middle of the screen. The task was to bring the cursor to one of the center-out target box. When the target was cued, the subject was asked to wait at least 2 s before initiating the movement. If he failed to do so, the subject had to move the cursor back to the rest position and wait for another 2 s before initiating the movement. The trial was discarded from analysis and repeated until the subject successfully fulfilled the requirement of 2 s delay period.

Subjects were asked to minimize their eye movements, in particular, before starting the arm movement. In this experiment, there was also a calibration session to record the baseline eye movement activity as in Experiment 1. The subject was asked to blink for 5 s, then, he had to look back and forth between the home position and the different targets as they appear on the screen where each target appeared five times. The recordings from the calibration session have been used for studying the effects of eye movements on the EEG channels (see section 2.2.2).

For each subject, we performed 3 recordings of 80 trials (targets are randomly cued), thus resulting in a total of 240 trials for each arm movement. After discarding early starts and artifacts, it remains an average of 229 trials for the left hand and 230 trials for the right hand across all subjects. For the stroke patients, the unaffected arm was tested first. The whole experiment lasted from 3 to 4 h, including the electrodes placement time. Each recording lasted from 6 to 15 min. Both stroke subjects were able to achieve the reaching task without much difficulty, but with longer average reaching time (as shown in **Table 1**) in comparison with the control subjects. Previous analysis with stroke subjects has reported that goal-directed arm movements are slower and more variable than healthy subjects' (Levin, 1996; Cirstea and Levin, 2000).

2.2. METHODS

2.2.1. EEG and EMG recordings

We acquired EEG potentials with a portable ActiveTwo measurement system from BioSemi (http://www.biosemi.com) using 64 electrodes arranged in the modified 10/20 International System. This system was also used to record the electrooculograph (EOG) signal. In Experiment 1, the Biosemi ActiveTwo measurement system was also used to record the EMG signals from the arm. As for the second experiment, the EMG signals were recorded with a Biopac System (http://www.biopac.com).

The signals were recorded at a sampling rate of 2048 Hz and downsampled to 256 Hz. To analyze EEG, we first applied the Common Average Referencing (CAR) procedure (Offner, 1950; Osselton, 1965), where, at each time step, the average potential over all the channels is subtracted from each channel. The re-referencing procedure removes the global background activity, keeping activity from local sources beneath the electrodes. The most intuitive implementation of a CAR is to use all the recorded channels (Bertrand et al., 1985). However, the EEG channels could be contaminated by noise, in particular by EOG and muscular artifacts, that may propagate to all other unaffected channels. In the next section we identify the EEG channels that are affected by EOG artifacts, which are the most prominent potential source of noise given the nature of the task and the frequency band to be analyzed. These channels are then removed from the analysis and, in particular, for computation of the CAR.

2.2.2. Ocular artifacts

EOG signals were acquired from three electrodes positioned above the nasion, and below the outer canthi of the eyes (Schlögl et al., 2007). The bipolar EOG channels in the *left-central* and *central-right* positions were able to capture both the horizontal and the vertical EOG components.

Table 1 | Details of subjects who participated in the Experiment 2.

Subject	Age	Medical condition	Paretic arm	Time since stroke	FMA-UE	Left hand MT	Right hand MT
cg	25	Healthy	–	–	–	0.61 ± 0.19	0.58 ± 0.15
gc	26	Healthy	–	–	–	0.70 ± 0.17	0.66 ± 0.16
dpm	50	Stroke	left	55 days	56/66	$\mathbf{3.53 \pm 1.63}$	1.67 ± 0.73
lg	61	Stroke	right	658 days	43/66	1.59 ± 0.35	$\mathbf{2.34 \pm 0.36}$

MT refers to the time needed to complete a reaching movement. Values in bold show the performance with the paretic arm.

Besides manual removal of noisy trials, we used a regression analysis method to assess the influence of EOG artifacts on each EEG channel (Schlögl et al., 2007). Briefly, channels having a large correlation with the EOG components are discarded from the montage before performing the CAR.

Figure 3 illustrates the regression coefficients of the horizontal and vertical EOG components with the EEG channels computed in the calibration session for one of the subjects. The EEG signals are re-referenced using CAR with all 64 channels recorded from the experiment. This figure illustrates high contributions of eye movement artifacts in the frontal and temporal electrodes.

We first remove the peripheral electrodes, filter the signals with CAR using the remaining 41 electrodes, and recomputed the coefficients. As shown in **Figure 4** (top panel), the effects of vertical EOG is still high on the frontal electrodes. We further remove electrodes for which the coefficients were above 0.3. Thus, re-referencing the signals with a total of 34 channels can minimize the effects of eye movements on the scalp EEG as shown in **Figure 4** (bottom).

Similar results were obtained for all other subjects in both experiments. Therefore, in this paper, we performed the analysis with only 34 channels as shown in **Figure 5**.

2.2.3. Pre-processing

The EEG signals were processed with a narrow band zero-phase non-causal IIR filter with cutoff frequencies of 0.1 and 1 Hz which has been reported to better capture anticipatory-related SCPs (Garipelli et al., 2011). The EOG signals were also preprocessed with the same method as the EEG signals.

EMG signals were acquired bipolarly over the *musculus biceps brachii* of the subject's arm, and high-pass-filtered with a Butterworth filter (8th order, cutoff of 50 Hz) to remove motion artifacts. The signals were then rectified, low-pass-filtered (8th order, cutoff of 20 Hz) and integrated over 25 ms to obtain envelopes of EMG activity (Cheung et al., 2009). The purpose of recording the EMG is to monitor that there is no muscular activity during the reaching preparation phase and to ensure that the movement intention detected is not due to the muscular activity of the arm through classification of the EMG activity (see section 3.3).

2.2.4. Channel selection

We compare the classification performance using manually and automatically selected channels. In the first case, channels were selected on the basis of the grand-average SCP. In the case of

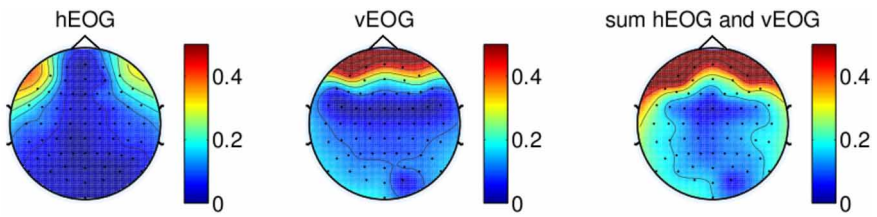

FIGURE 3 | Regression coefficients of EOG components plotted on a topographical map, showing the effect of eye movement on scalp electrodes using signal re-referenced with all 64-channels recorded from one of the subjects. The rightmost figure shows the sum of the contributions of both vertical EOG and horizontal EOG.

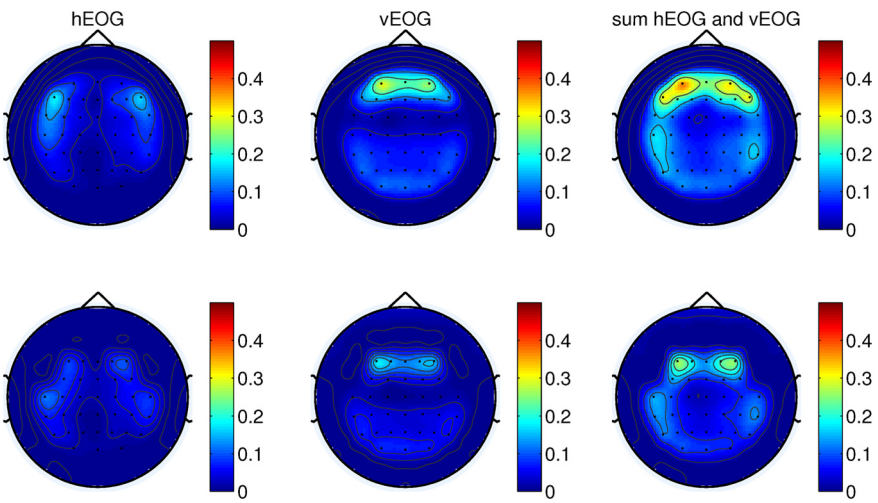

FIGURE 4 | (Top) The weights of EOG artifacts by re-referencing the signals with 41-channels and (bottom) 34-channels. This figure shows the EOG coefficients from the calibration session of one of the subjects participating in the experiments.

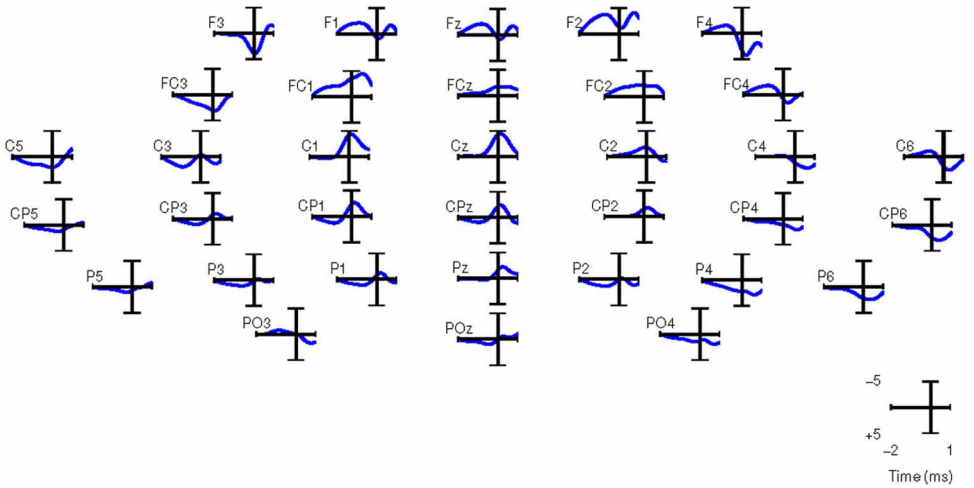

FIGURE 5 | Grand averages of SCPs for all the right-handed subjects participating in Experiment 1. EEG signals are filtered between 0.1 and 1 Hz. $t = 0$ corresponds to the movement onset.

automatic selection, the channels are ranked according to their discriminant power (DP; see below).

For computing the grand averages of SCPs, each epoch was baseline corrected with the average activity between [2 2.25] s before the movement onset. **Figure 5** shows the grand averages of SCPs over all right-handed subjects participating in Experiment 1 for each of the 34 channels. The SCPs in stroke subjects obtained from Experiment 2 exhibit a similar trend in the development of the negativity prior to the movement onset, as shown in **Figure 6**. However, the negativity peaked after 1 s of movement onset, when for control subjects the peak was roughly at movement onset (see also **Figure 5**). This is in agreement with Jankelowitz and Colebatch (2005), who recorded a larger and longer readiness potential when the stroke subjects moved the affected limb. The channels chosen manually for classification were C1, Cz, C2, CP1, CPz, CP2 as they exhibit prominent negative slopes in the grand average and are also consistent with previous literature (Kornhuber and Deecke, 1965; Libet et al., 1982).

Alternatively, we performed automatic channel selection using the Canonical Variant Analysis (CVA) (also commonly known as Multivariate Discriminant Analysis; Galán et al., 2007). This technique estimates the DP of each channel by comparing the movement preparation period to the non-movement related period. **Figure 7** shows the DP value of each channel in the form of a topographic map for EEG signals in the frequency range [0.1–1] Hz for all eight subjects in Experiment 1. It is observed that the channels with high DP for movement preparation are

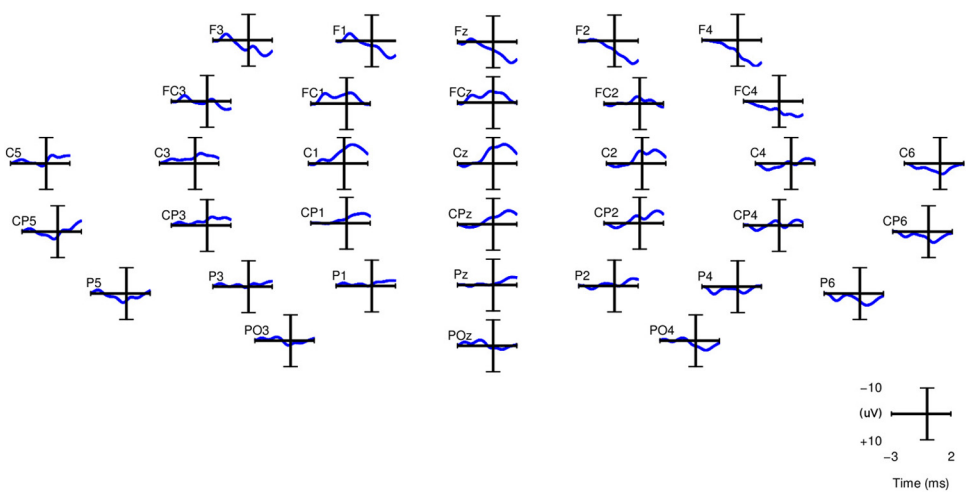

FIGURE 6 | Grand averages of SCPs, filtered between 0.1 and 1 Hz, for the paretic arm of stroke patient *lg* (right arm) from Experiment 2. $t = 0$ corresponds to the movement onset.

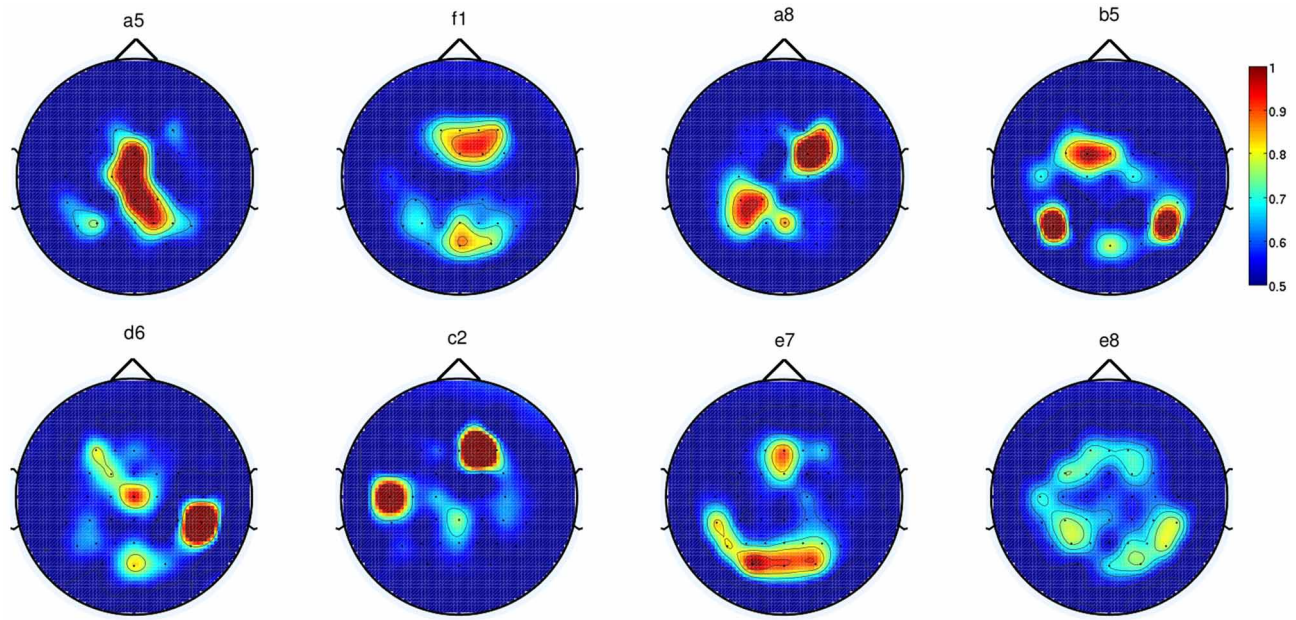

FIGURE 7 | Each topoplot shows the normalized discriminant power index of each channel for a single healthy subject in Experiment 1.

different for each subject, suggesting subject-specific brain patterns in preparing reaching movement. With the exception of subject **a5** (where four out of six of the predefined channels match the most discriminant channels selected by CVA), the topoplots for the rest of the subjects showed high DP index in the frontal and parietal regions. According to Andersen and Cui (2009), the posterior parietal and frontal cortical areas are responsible for planning and decision making of movement intent. In this respect, it has also been reported that the frontal and parietal cortex region of the human brain carried considerable information to predict the outcome of a motor decision the subject had not yet consciously made (Soon et al., 2008). For subjects **f1**, **b5**, **e7,** and **e8**, CVA did not show any similarity with the pre-defined channels. Finally, we can observe that the topographic map for subject **d6**, the only left-handed subject in this study, showed high DP on the contralateral channels (right hemisphere).

As for Experiment 2, **Figure 8** shows the DP value for each channel using the amplitudes of EEG signals filtered between [0.1–1] Hz for control subjects and stroke subjects (both left and right hand data). The regions showing the highest DP for healthy controls were similar to the observations in Experiment 1. Comparison between the pre-defined channels and the six most discriminant channels selected using the CVA method showed that four out of six channels were similar for stroke subject **lg** with data from both hands and for control subject **cg** only for the right hand. The topographic maps for stroke subject **lg** shows very consistent DP between left and right hand, and most importantly, the focus area is similar to the pre-defined channels set. As in Experiment 1, this central region is where the SCPs show high negativity prior to movement onset.

In section 3, we will show the performance differences between using pre-defined and CVA-selected channels.

2.2.5. Classification

To detect the movement intention, we categorized the signals into two different time periods, namely the baseline period (idle period) and the movement preparation (active period). During the *idle period*, we assume that there is no on-going movement preparation activity. This period was taken 500 ms before the auditory target cue at each trial. The second part is the movement preparation period, which we termed as the *active period*, defined at [–750 –250] ms before the movement onset. **Figure 9** depicts the selection of the EEG samples to train the movement intention classifier. Training data for the classifier consists of the baseline period (yellow box) as class *idle* and the movement preparation period (green box) as class *active*. As a classifier, we relied on Linear Discriminant Analysis (LDA), whose input was a vector with the EEG amplitude of the selected channels in a 500 ms window to capture the negative slope occurring 400 ms before start of movement. The EEG signals were subsampled from 256 to 8 Hz (four data points per window) before classification, resulting in a total of 24 features. To test the performance of our classifier, we used 500 ms windows shifted every 10 ms starting from 2500 ms before movement onset until 1000 ms after movement onset. We report below the results of a fivefold cross-validation. It is worth noting that the data used for feature selection is only based on the training data. Furthermore, we employed a cross-validation method which maintain the chronological order of the data (Millán, 2004; Bourdaud et al., 2008) which yields a better, and less optimistic, estimation of accuracy in comparison with the traditional method.

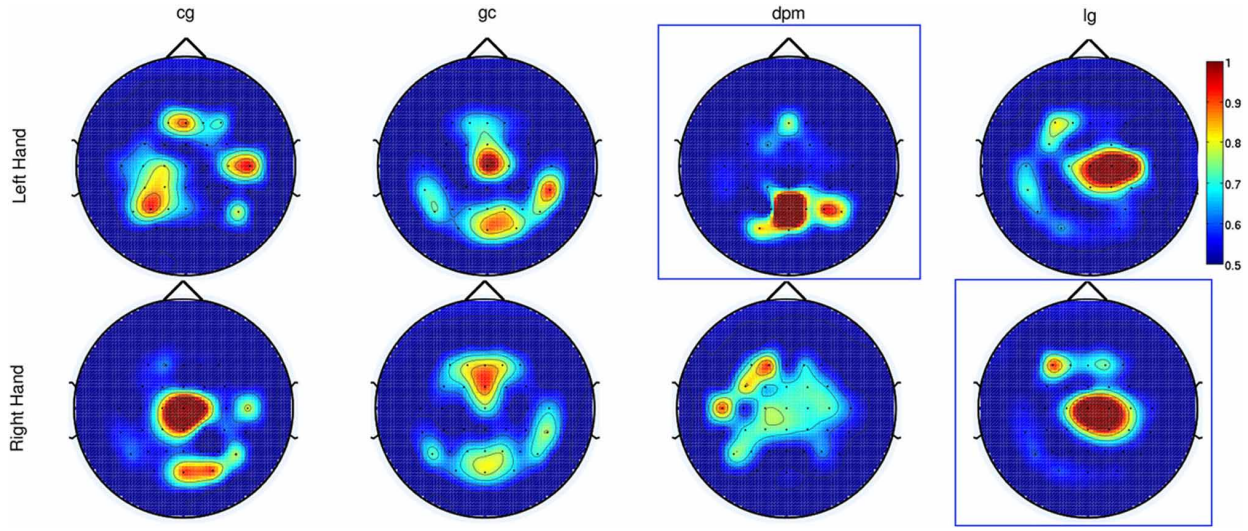

FIGURE 8 | The topographic maps show the normalized discriminant power index of each channel for the left and right hand for the control subjects (*cg* and *gc*) and the stroke subjects (*dpm* and *lg*). Plots highlighted with a blue frame refers to the paretic arm of the patients.

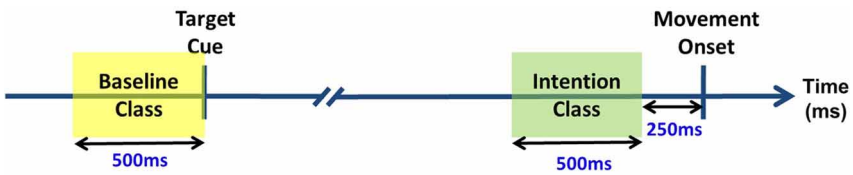

FIGURE 9 | Selected EEG samples to build the training set of the movement intention classifier.

3. RESULTS

3.1. EXPERIMENT 1

Figure 10 shows the results of movement intention detection where each plot represents the performance of a single subject in Experiment 1. Each plot reports the average *sensitivity* rate, or True Positive Rate (TPR), across the five test folds in the time window $[-2, 1]$ s with respect to the actual movement onset. This can also be interpreted as the percentage of trials being detected as movement intention at time t. This time in the plot (X-axis) corresponds to the last sample of the analysis window analyzed by the classifier. The shaded region bounding the average TPR illustrates the standard deviation at each point. The magenta line refers to the onset of *biceps branchii* muscular activation. This is defined as the time when the EMG activity exceeds a threshold equal to $\mu + 3\sigma$, where μ and σ are the mean and standard deviation of EMG signals of a one-second window after the target cue (Abbink et al., 1998). On average, all subjects exhibit an early arm muscular activity at 263 ± 40 ms. Similar EMG timing has been observed by Flanders (1991) and Hong et al. (1994) who studied the temporal patterns of muscles activation for unconstrained arm reaching movement in three dimensional space. The chance level line (in red) was calculated by shuffling the labels of the training data and performing 10 times fivefold cross validation. To test whether the sensitivity rate is significantly above the chance level with 95% confidence interval, we used the Wilcoxon rank sum test. The line in green depicts the first time a group of five consecutive samples has a true positive rate significantly above chance level ($p < 0.05$).

Movement intention can be detected above chance level across healthy subjects on average at 460 ± 85 ms before actual onset. The detection of movement intention is before arm muscular activation with the exception of subject **b5**. As reported in **Table 2**, the average maximum TPR was 0.76 ± 0.07, peaking on average 167 ms before movement onset. As we will see in section 3.3, although this peak performance is achieved slightly after EMG onset, using only EMG is a less reliable predictor for movement intention.

As described in section 2.2.4, we performed another analysis using the six best selected channels yielded by the CVA method. **Figure 11** shows an earlier detection of movement intention with the features selected automatically, except for subject **a5**, **b5**, and **e7**. Unsurprisingly, for subject **a5** time differences are only 50 ms, since the CVA-selected channels highly overlap with the pre-selected set. The left-handed subject, **d6**, with high discriminability on the right lateral brain area, showed an earlier detection time of 360 ms using channels selected with CVA feature selection method. All subjects showed TPR above 70%, except for subject **e8** whose DP topographic map did not show a strong discriminative area.

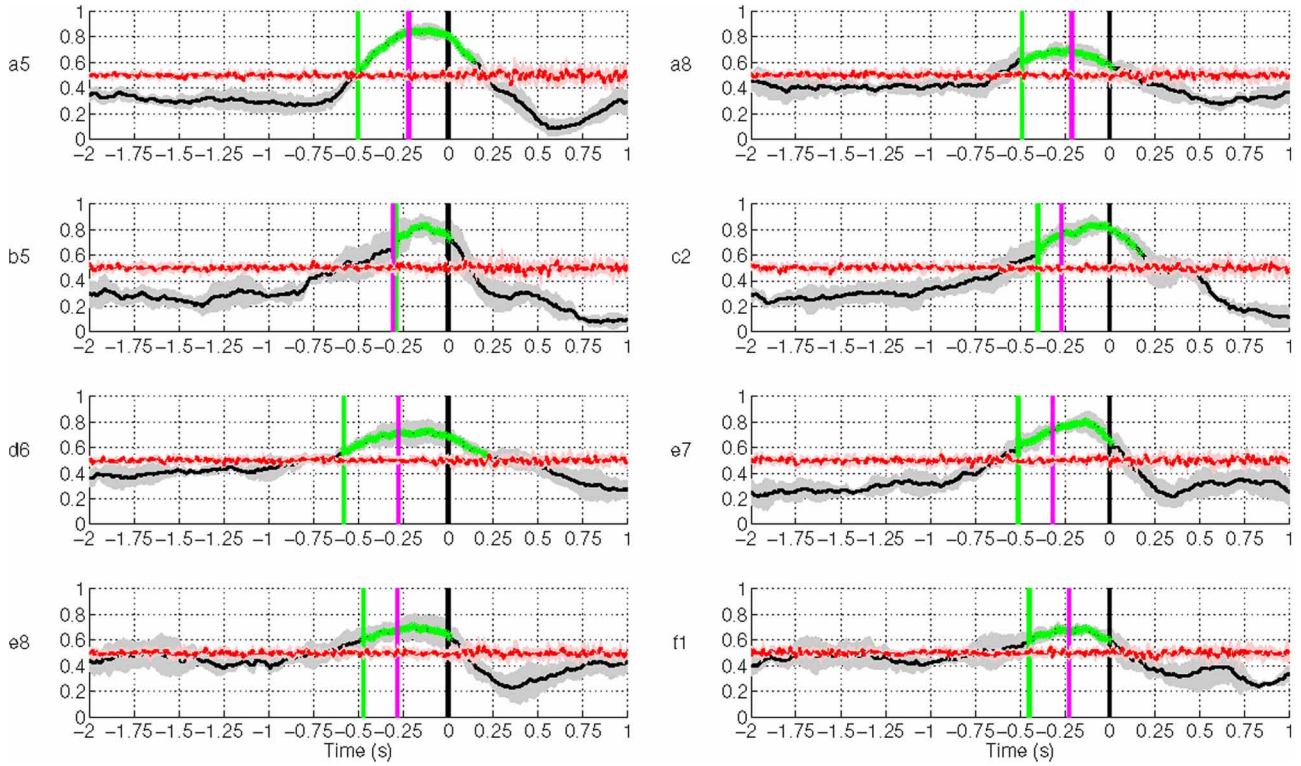

FIGURE 10 | Single trial performances of movement intention detection for all subjects in Experiment 1 using SCPs in the frequency range [0.1–1] Hz during the time interval (−2, 1) s with respect to the actual movement onset. Y-axis of the plots represents the movement intention detection rate. The magenta line depicts the onset from arm muscular activation (−263 ± 40 ms on average across all subjects). The green line depicts the first time a group of five consecutive samples has a TPR significantly above chance level ($p < 0.05$), which is shown as a red line. The gray and red shaded regions bounding the performance curves indicates their standard deviation at each point. Note that the variance of the random performance is so small that the red shaded area is barely visible.

Table 2 | Maximum TPR for each subject and the time point (in ms) when this value is reached.

Subject ID	TPR	Time (ms)
a5	0.85	−110
a8	0.70	−240
b5	0.83	−150
c2	0.84	−100
d6	0.72	−120
e7	0.80	−140
e8	0.71	−190
f1	0.69	−290
Average ± std	**0.76 ± 0.07**	**−167 ± 68**

3.2. EXPERIMENT 2

Figure 12 shows the results of movement intention detection for both the left and right hand reaching movement of all subjects (the upper graphs correspond to the healthy control subjects, followed by the two stroke patients). For all subjects, movement intention can be detected more than 400 ms before the recorded onset with their left hand and right hand. Movement intention can also be detected before the onset of EMG activity (magenta line, see previous section for details) for all subjects and conditions, except the non-paretic arm (right) of stroke subject **dpm**. The false positive rate prior to the detection of movement intention was also low (between 0.1 and 0.2 for both hands) for all subjects except stroke subject **dpm**. It is worthy to note that stroke subject **dpm** was a recent stroke patient (see **Table 1**) and, probably, the neural reorganization processes were still ongoing at the time of the experiment, which took place only 1.5 month after the stroke.

The result for stroke subject **lg** in **Figure 12** (last row) exhibits a different performance curve as compared with the results of healthy controls. In particular, a high detection rate sustained up to 1 s after onset of movement. This difference could be due to the slower speed of reaching (c.f. **Table 1**) of stroke subject **lg** is 2.34 ± 0.36 s using his paretic arm compared to a faster speed of 0.5–0.6 s for healthy controls. The longer sustained high performance could also be due to the fact that the readiness potential of the affected limb in stroke subjects has higher amplitude over a longer period of time (Jankelowitz and Colebatch, 2005).

As reported in **Table 3**, the average maximum TPR obtained in this experiment was 0.81 for the left hand, peaking on average 140 ms before movement onset, while for the right hand the average maximum TPR is 0.79 at 162 ms before movement onset. It is interesting to note that for the two conditions where the peak

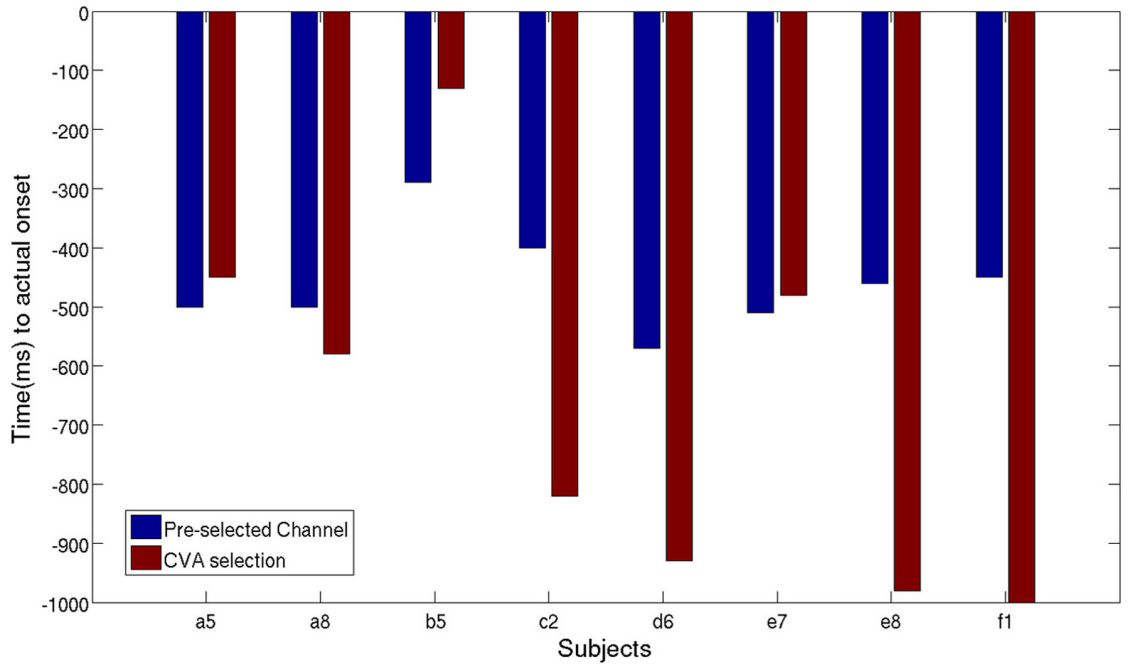

FIGURE 11 | Time of movement intention detection comparison between pre-selected channels set and best selected channel using CVA techniques.

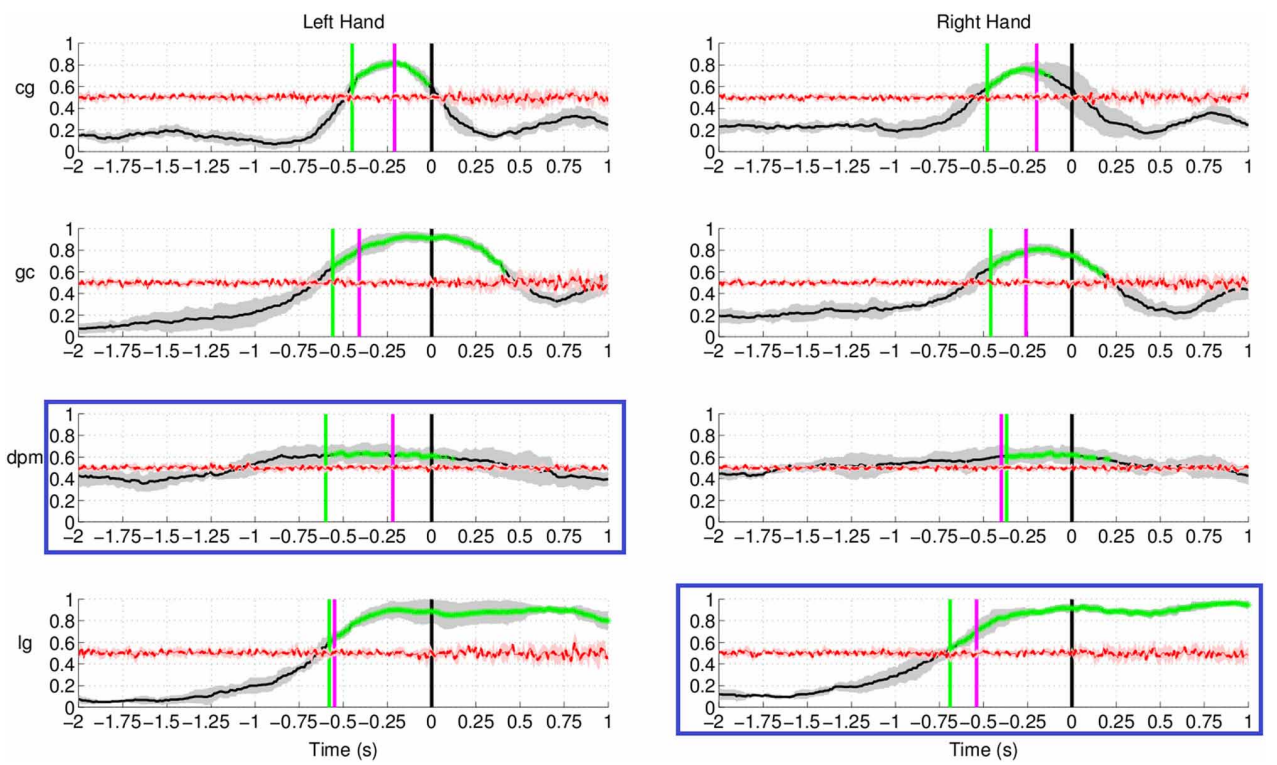

FIGURE 12 | Single trial performances of movement intention detection for all subjects in Experiment 2 (both left and right arm reaching movement) using SCPs in the frequency range [0.1–1] Hz during the time interval (−2, 1) s with respect to the actual movement onset. This figure has a similar format to **Figure 10**. Plots highlighted with a blue frame refers to the paretic arm of the stroke subjects.

Table 3 | Maximum TPR for each subject and hand, and the time point (in ms) when the TPR reaches maximum value.

Subject ID	Left hand		Right hand	
	TPR	Time (ms)	TPR	Time (ms)
cg	0.84	−200	0.79	−310
gc	0.90	−30	0.80	−140
dpm	0.66	−100	0.63	−140
lg	0.85	−230	0.92	−60
Average ± std	**0.81 ± 0.11**	**−140 ± 92**	**0.79 ± 0.12**	**−162 ± 105**

performance is closer to movement onset (left hand of healthy subject **gc** and right hand of stroke subject **dpm**), performance stabilizes soon after EMG onset (in between −300 and −200 ms before movement onset) and slowly reaches its maximum value, which is 0.9 or higher. Altogether, these results are in agreement with those of Experiment 1 carried out with a larger set of subjects.

We also compared the earliest time of onset detection using either the pre-selected channels or the channels chosen with the CVA data driven approach. Stroke subject **dpm** was excluded from the comparison because of the random results, to avoid misleading conclusion from the earlier detected intention. **Figure 13** shows the earliest time when movement intention was detected for the two control subjects and stroke subject **lg**. Differences in time and performance between the two approaches are not significant.

3.3. EFFECTS OF MUSCULAR ARTIFACTS

In this section, we are interested in studying how and when movement intention can be detected from the arm muscular activity. To model the movement class, we take the window ended at 0 s (between −500 and 0 ms) because the grand averages of EMG activity showed no movement on average 250 ms before the movement onset.

Figure 14 shows the EMG classification results using the same technique as in the case of EEG for the subjects in Experiment 1. The results show that movement intention can be detected from EMG activity at a time point close to the actual onset derived from the button release. Interestingly, the EMG classifier detects movement intention *after* the thresholding method (magenta line in **Figure 14**) and *significantly later* than the EEG classifier. We can thus conclude that detection of movement intention from EEG signals is not due to muscular artifacts.

Similarly, in Experiment 2 (**Figure 15**) movement intention can be detected significantly above chance level *only after* the time obtained from the thresholding method (magenta line in **Figure 15**) for the control subjects, which is in agreement with the results from Experiment 1. The EMG signal classification for both stroke patients, however, yielded random level classification, showing that these signals cannot be used to detect reliably movement intention or onset. Further analysis of other muscles, such as triceps and deltoid, yielded similar results. The reason for this is that, given the precision and spatial accuracy required in this task, agonist and antagonist muscles are activated synergistically to achieve a fine control of the forearm.

Altogether, these results show that detection of movement intention from EEG signals occurs before the muscular activation, showing high probability that preparation for movement happens before the peripheral system reacts and this information could be exploit for detecting the intent to move. This result is also in line with the behavioral study of Libet et al. (1983), where participants in the experiment reported the conscious intention to act 206 ms before the onset of muscle activity.

3.4. ANALYSIS OF THE NON-MOVEMENT INTENTION PERIOD

Up to now, we have studied the performance of the EEG classifier to detect movement intention during the preparation period. The results show a quite high *sensitivity* rate of the EEG decoder. In this section, we analyze the *specificity* of such an EEG classifier. To do so, we examine the performance of the proposed method during the non-movement intention period—i.e., the time where

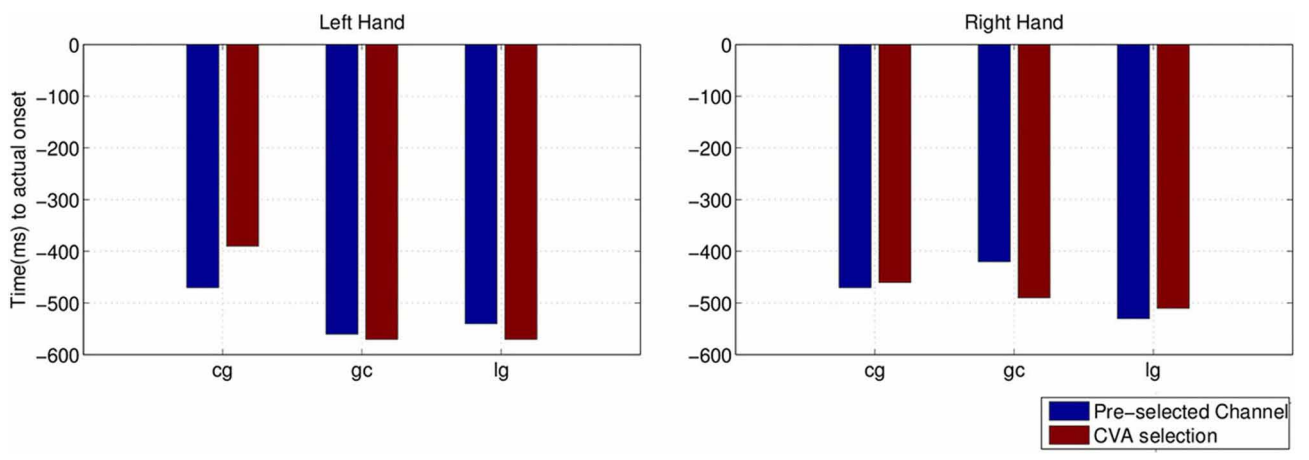

FIGURE 13 | Comparison of detected movement intention when TPR is above chance level ($p < 0.05$) between using pre-selected channel set and best selected channel from the data using CVA technique.

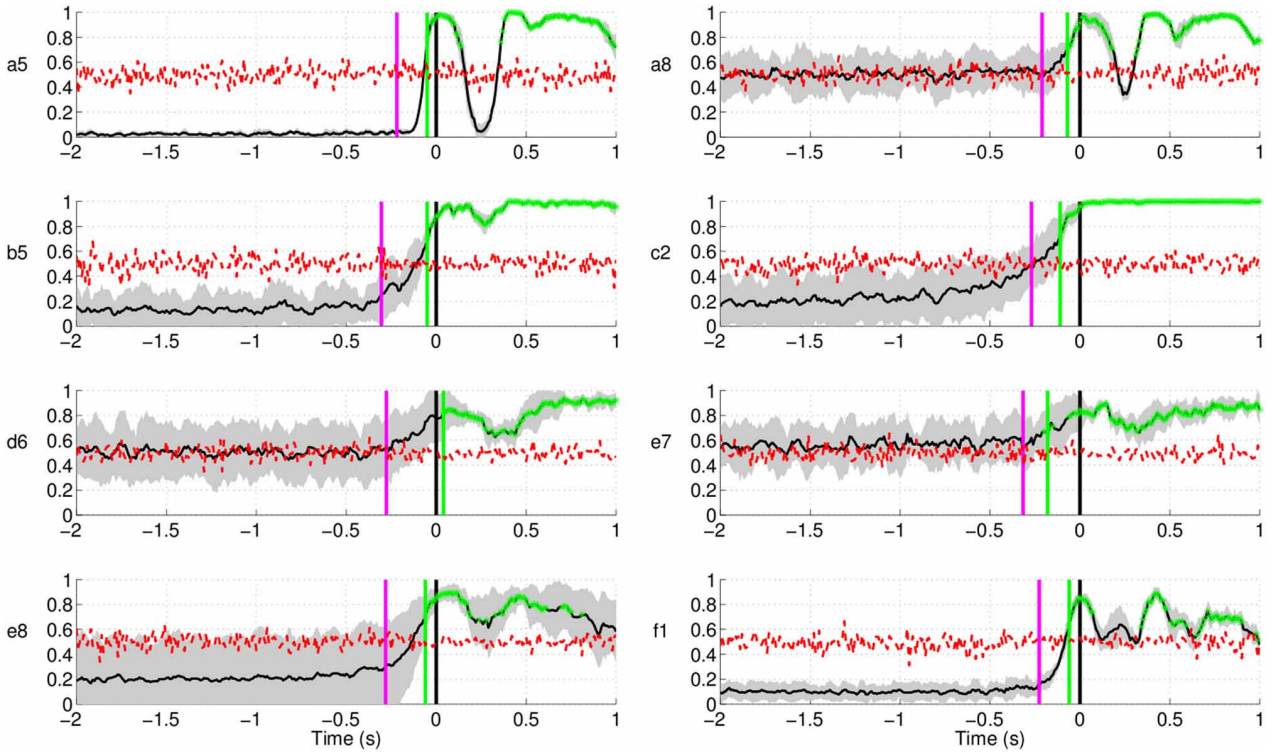

FIGURE 14 | Single trial detection of movement intention from EMG activity for all subjects in Experiment 1. Y-axis of the plots represents movement intention detection rate.

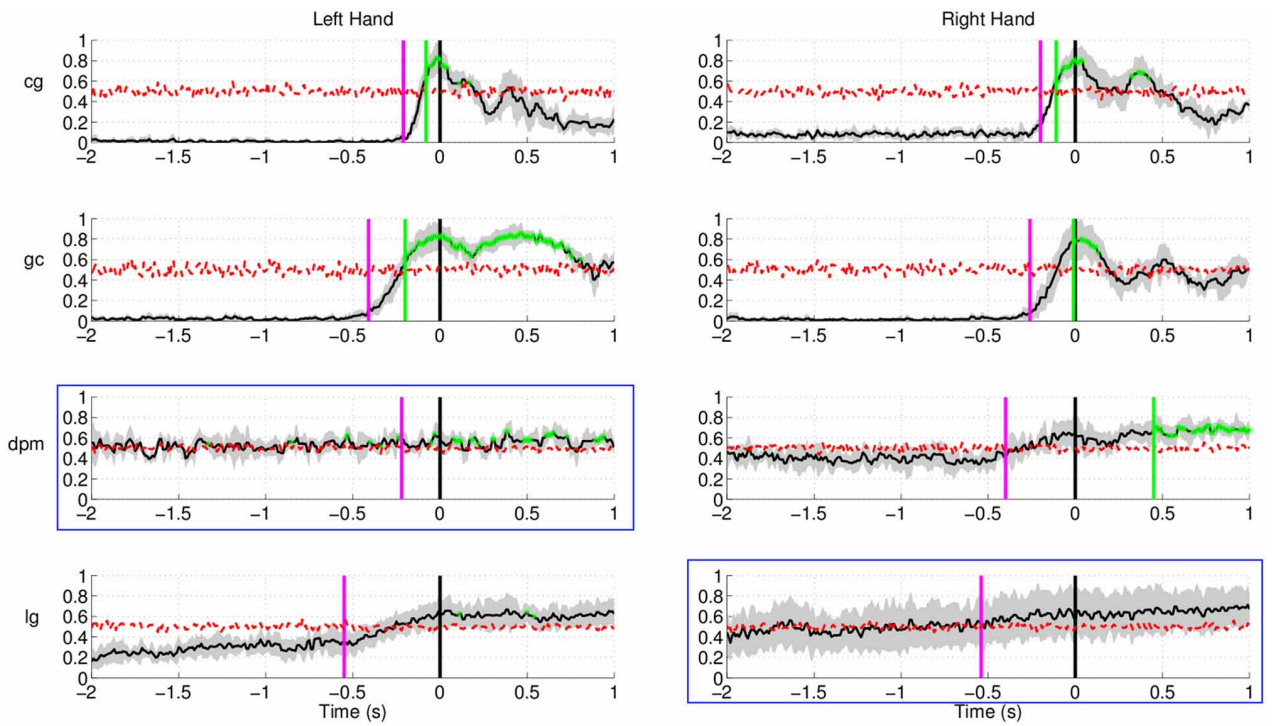

FIGURE 15 | Single trial detection of movement intention from EMG activity for all subjects and hands in Experiment 2. Plots highlighted with a blue frame refers to the paretic arm of the patients. Y-axis of the plots represents movement intention detection rate.

subjects should not engage in preparing the movement. **Figure 16** shows the rate of trials detected as movement intention during such a period lasting from –1000 ms before the auditory target cue until 2000 ms afterwards for all subjects in Experiment 1. Since windows for classification are 500 ms long, the first decision point is at −500 ms before the target cue. Interestingly, the detection of movement intention remains significantly below random level over the whole period preceding the target cue. And, remarkably, this is also the case during the first 2 s after the target cue (when the subjects should not move) for five out of eight subjects. The remaining three subjects (**b5**, **d6**, and **f1**) reached detection rates significantly above random, but only for a short period of time (less than 250 ms for all three subjects, starting at 750 ms after the target cue for **b5** and **d6**, and at 1000 ms for **f1**) before they decreased rapidly below chance level again. This may reflect some form of movement preparation after the subjects were informed of the target that they suppressed afterwards.

Regarding Experiment 2, **Figure 17** shows lower (false) detection rates, at approximately 10%, for both control subjects and one of the stroke subject, **lg**. Detection rates started rising approximately 1.5 s after the target cue, with the exception of stroke subject **dpm**, who showed constant random level performance throughout the entire period. A plausible explanation for this increase is that, in this experiment, subjects had a large number of trials where the movement onset was between 2 and 3 s after the target cue, in particular stroke subject **lg**.

As a conclusion, our approach demonstrates to have a high sensitivity and a reasonably good specificity (below random detection level during the non-movement period) to allow robust single trial detection of movement intention from human EEG.

4. DISCUSSION

Our experiments, involving healthy subjects and stroke subjects, demonstrate successful single-trial detection of movement intention from EEG prior to the actual movement in a self-paced reaching protocol. In particular, we show the detection of self-paced reaching movement intention in single trials from the analysis of the readiness potential, an EEG slow potentials that we compute in a narrow frequency range between 0.1 and 1 Hz. In these experiments, SCPs seem to carry most of the relevant information for the detection of movement intention as performance is higher than other frequency bands, as shown in **Figure 18**. In future work we will explore whether coherence among different EEG frequencies and channels, reflecting the rather complex brain network involved in this task, could offer further insight into the underlying mechanism of self-paced movement preparation and improve the performance of the detection.

Our SCP approach yields high detection rates close to the movement onset (sensitivity) and below random detection level during the non-movement period (specificity). Also, movement intention was detected around 500 ms before actual onset, in agreement with previous studies on readiness potentials using

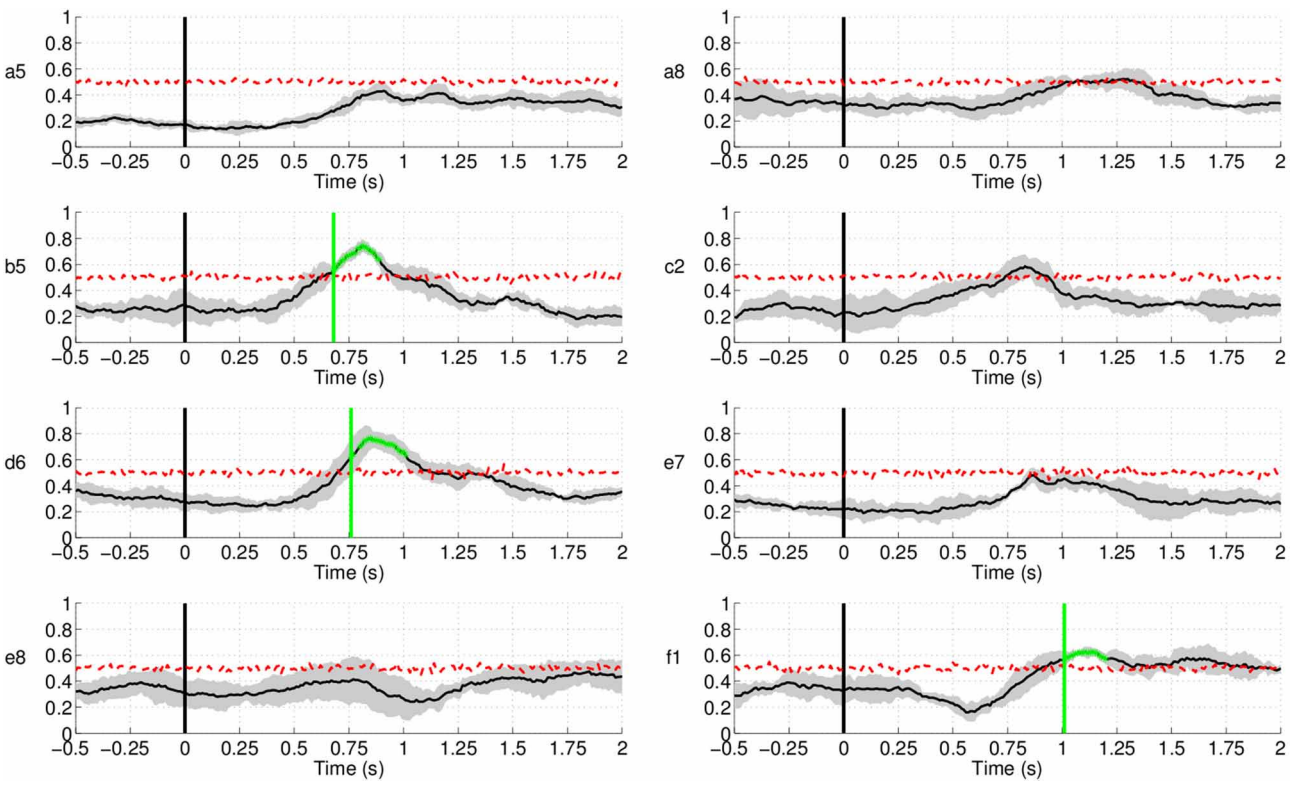

FIGURE 16 | Detection of movement intention during the non-movement intention period for all subjects in Experiment 1. Time 0 s refers to the delivery of the auditory target cue. Y-axis of the plots represents movement intention detection rate.

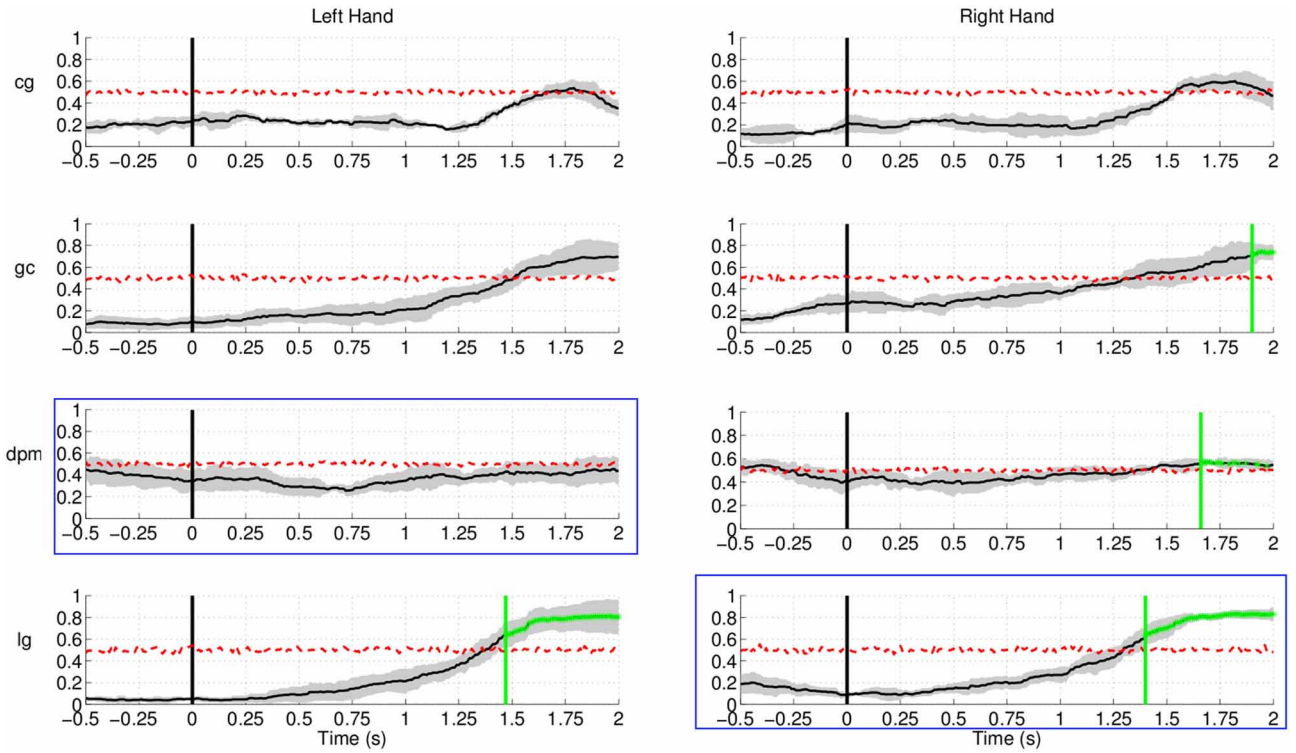

FIGURE 17 | Detection of movement intention during the non-movement intention period for all subjects and hands in Experiment 2. Time 0 s refers to the delivery of the visual target cue. Plots highlighted with a blue frame refers to the paretic arm of the patients. Y-axis of the plots represents movement intention detection rate.

grand average activity (Kornhuber and Deecke, 1965; Libet et al., 1982). To further increase the performance of our method, in particular its specificity, we could improve our experimental protocol in order to better model the non-movement intention period. It would suffice to incorporate null trials (i.e., no movement trials). We will also explore the use of an evidence accumulation framework (Perdikis et al., 2011) that have proven beneficial in BCI as it only issues commands with high probability of confidence levels.

Previous works on movement onset have focused on hand/wrist flexion only (Awwad Shiekh Hasan and Gan, 2010, 2011; Bai et al., 2011), without reaching to a definite goal. Cortical activity is different in both cases. Readiness potentials, and their associated topography, have been found to be modulated by the consequence of movement, complexity of the movement, level of skill, sequence of hand movements; as well as the part of the body performing the movement, force, speed, and precision of a movement (Lang, 2003). In particular, Simonetta et al. (1991) reported larger amplitudes of the readiness potential in sequential motor tasks than in simple movements. There is also a larger late BP in self-paced movement of the proximal than the distal part of the upper extremities (Jankelowitz and Colebatch, 2002). Finally, different studies have reported that the attentional level has an influence on the neural correlates of movement onset. Libet et al. (1982) showed differences in the shape of the readiness potential depending on subjects' strategies, either involvement of general preplanning to act in the near future or direct movement when subjects were aware of the need to move. The former showed earlier onset (about 1 s). Keller and Heckhausen (1990) compared the readiness potentials between consciously and unconsciously performed motor actions, and found larger amplitudes in Cz, FCz, and Fz with consciously performed movements.

A previous study with four stroke subjects (Muralidharan et al., 2011) reported that attempted finger extension could be detected in stroke subjects with accuracy rates varying across subjects with a maximum true positive rate of 70% through combinations of PSD in the range of [2–30] Hz. These results, however, were obtained in a reaction task paradigm where subjects performed the movement or relaxed in response to a cue. In our study, the average maximum true positive rate was 0.81 ± 0.11 across both groups, controls and stroke subjects. The performance for one of the stroke subjects, **dpm**, was slightly above random, with maximum TPR of 0.66, while for another stroke subject, **lg**, the maximum TPR was 0.92 for reaching trials executed with his paretic hand. Although promising, the results achieved with stroke patients can only be taken as a preliminary feasibility study because of the limited number of subjects involved in the study. Nevertheless, it is worth noting that one of the patients achieved similar performance to the healthy subjects with the paretic arm.

In this work we have explored the use of EEG readiness potentials to decode a key aspect of voluntary movement behavior,

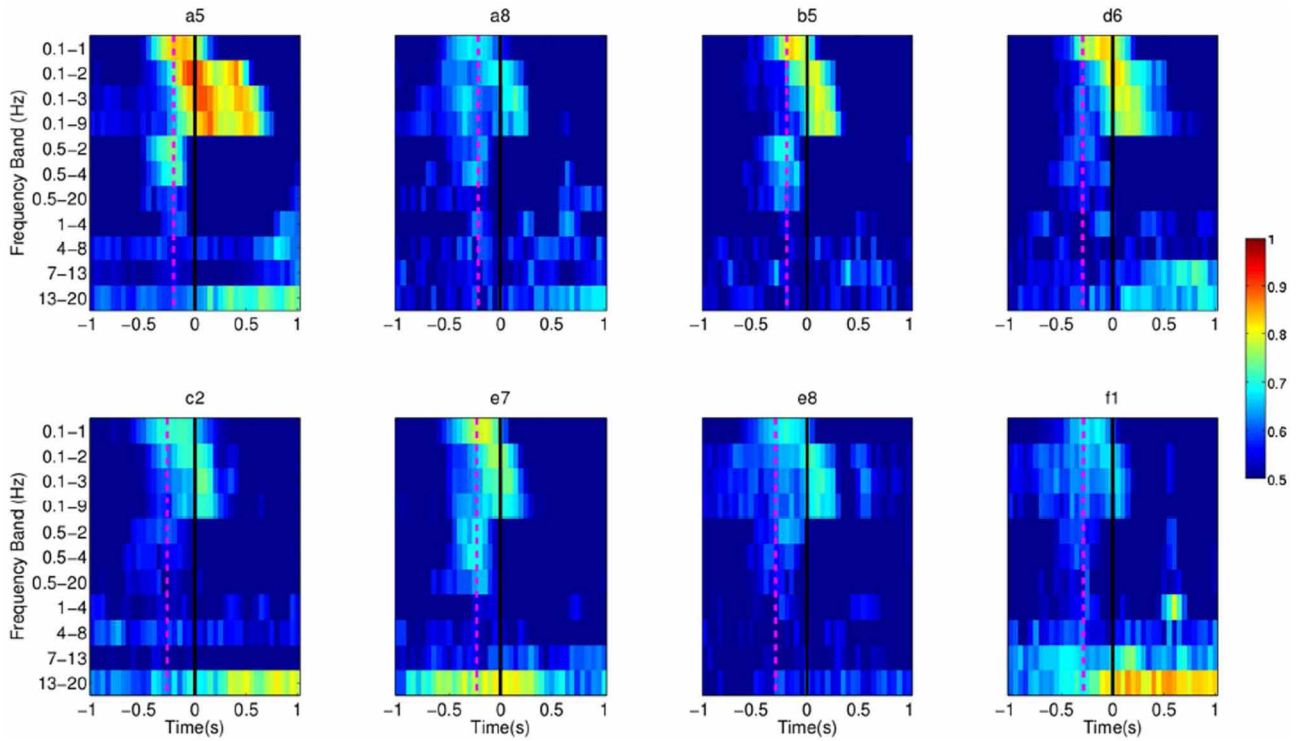

FIGURE 18 | Each pixel refers to the single trial performance of movement intention detection for all subjects in Experiment 1 using signals filtered in various frequency ranges (Y-axis). The dotted line in magenta refers to the EMG activation for each subject.

namely self-paced onset. But it could also be related to another critical aspects of voluntary behavior, in particular volitional inhibition—stopping or changing a planned motor action that is not any more appropriate to the current context. In fact, Chen et al. (2010) have found that SMA is involved in both, movement preparation and movement inhibition. It would be interesting to detect the onset of an inhibitory process in a reaching version of the countermanding paradigm proposed by Mirabella et al. (2006, 2008, 2011). In particular, Mirabella et al. (2011) shows the existence of neurons in the dorsal premotor cortex exhibiting a pattern of activity compatible with the control of reaching arm movement initiation and suppression, thus suggesting that motor cortices are the final target of the inhibitory command elaborated elsewhere. The identification of the inhibitory process onset, in conjunction with detection of voluntary self-paced movement onset, may lead to more efficient and natural neuroprosthetics as well as more effective post-stroke motor rehabilitation training.

Detection of voluntary movement intention prior to its actual execution is a new capability that may advance the current state of the art in BCI and neurorehabilitation. For motor recovery, triggering the robotic-assistive device before EMG activation can largely improve the outcome of therapy (Muralidharan et al., 2011). In this case, decoding readiness potentials suits naturally in the design of goal-directed protocols where patients need to execute purposeful actions, which have been shown to produce significantly smoother, faster, and more forceful movement than repetitive routine movement (Trombly and Wu, 1999). In the case of motor substitution, it will provide a natural signal to enable usual brain control of wheelchairs and upper limb neuroprostheses while blocking their operation until the subject wishes to do so. The results reported here are certainly encouraging and can be extended in a couple of ways for its practical application in a neuroprosthesis. Future work will be devoted to test the proposed method in an online implementation and perform the analysis with more disabled users. In particular, subjects could learn to control a robotic arm. It will be interesting to analyze the learning effects and the stability of the signals during such closed-loop real-time control applications. Regarding neurorehabilitation, as discussed in the Introduction, it would be extremely exciting to try our approach in combination with rehabilitation robotics for motor recovery of spinal cord injury and stroke patients.

ACKNOWLEDGMENTS

Authors warmly thank G. Garipelli for useful discussions and insights on the analysis of slow cortical potentials, as well as S. Degallier, L. Tonin, G. Cisotto, and C. Genna for their precious help with recordings. This work is supported by the European ICT Programme Project FP7-224631, Swiss NCCR "Robotics", S. Camillo Hospital Foundation, and Italian Ministry of Health. This paper only reflects the authors' views and funding agencies are not liable for any use that may be made of the information contained herein.

REFERENCES

Abbink, J. H., van der Bilt, A., and van der Glas, H. W. (1998). Detection of onset and termination of muscle activity in surface electromyograms. *J. Oral Rehabil.* 25, 365–369.

Andersen, R. A., and Cui, H. (2009). Intention, action planning, and decision making in parietal-frontal circuits. *Neuron* 63, 568–583.

Awwad Shiekh Hasan, B., and Gan, J. Q. (2010). Unsupervised movement onset detection from EEG recorded during self-paced real hand movement. *Med. Biol. Eng. Comput.* 48, 245–253.

Awwad Shiekh Hasan, B., and Gan, J. Q. (2011). Temporal modeling of EEG during self-paced hand movement and its application in onset detection. *J. Neural Eng.* 8, 1–8.

Bai, O., Lin, P., Vorbach, S., Li, J., Furlani, S., and Hallett, M. (2007). Exploration of computational methods for classification of movement intention during human voluntary movement from single trial EEG. *Clin. Neurophysiol.* 118, 2637–2655.

Bai, O., Rathi, V., Lin, P., Huang, D., Battapady, H., Fei, D. Y., Schneider, L., Houdayer, E., Chen, X., and Hallett, M. (2011). Prediction of human voluntary movement before it occurs. *Clin. Neurophysiol.* 122, 364–372.

Ball, T., Schulze-Bonhage, A., Aertsen, A., and Mehring, C. (2009). Differential representation of arm movement direction in relation to cortical anatomy and function. *J. Neural Eng.* 6, 016006.

Bertrand, O., Perrin, F., and Pernier, J. (1985). A theoretical justification of the average reference in topographic evoked potential studies. *Electroencephalogr. Clin. Neurophysiol.* 62, 462–464.

Birbaumer, N. (1999). Slow cortical potentials: plasticity, operant control, and behavioral effects. *Neuroscientist* 5, 74–78.

Birbaumer, N., Ghanayim, N., Hinterberger, T., Iversen, I., Kotchoubey, B., Kübler, A., Perelmouter, J., Taub, E., and Flor, H. (1999). A spelling device for the paralysed. *Nature* 398, 297–298.

Bourdaud, N., Chavarriaga, N., Galán, F., and Millán, J. d. R. (2008). Characterizing the EEG correlates of exploratory behavior. *IEEE Trans. Neural Syst. Rehabil. Eng.* 16, 549–556.

Bradberry, T. J., Gentili, R. J., and Contreras-Vidal, J. L. (2010). Reconstructing three-dimensional hand movements from noninvasive electroencephalographic signals. *J. Neurosci.* 30, 3432–3437.

Brunia, C. H., and Damen, E. J. (1988). Distribution of slow brain potentials related to motor preparation and stimulus anticipation in a time estimation task. *Electroencephalogr. Clin. Neurophysiol.* 69, 234–243.

Chen, X., Scangos, K. W., and Stuphorn, V. (2010). Supplementary motor area exerts proactive and reactive control of arm movements. *J. Neurosci.* 30, 14657–14675.

Cheung, V. C. K., Piron, L., Agostini, M., Silvoni, S., Turolla, A., and Bizzi, E. (2009). Stability of muscle synergies for voluntary actions after cortical stroke in humans. *Proc. Natl. Acad. Sci. U.S.A.* 106, 19563–19568.

Cirstea, M. C., and Levin, M. F. (2000). Compensatory strategies for reaching in stroke. *Brain* 123, 940–953.

Congedo, M., Lotte, F., and Lécuyer, A. (2006). Classification of movement intention by spatially filtered electromagnetic inverse solutions. *Phys. Med. Biol.* 51, 1971–1989.

Deecke, L., Lang, W., Heller, H. J., Hufnagl, M., and Kornhuber, H. H. (1987). Bereitschaftspotential in patients with unilateral lesions of the supplementary motor area. *J. Neurol. Neurosurg. Psychiatry* 50, 1430–1434.

Flanders, M. (1991). Temporal patterns of muscle activation for arm movements in three-dimensional space. *J. Neurosci.* 11, 2680–2693.

Fried, I., Mukamel, R., and Kreiman, G. (2011). Internally generated preactivation of single neurons in human medial frontal cortex predicts volition. *Neuron* 69, 548–562.

Galán, F., Ferrez, P. W., Oliva, F., Guárdia, J., and Millán, J. d. R. (2007). "Feature extraction for multi-class BCI using canonical variates analysis," in *IEEE International Symposium on Intelligent Signal Processing,* (Alcala de Henares, Spain).

Galán, F., Nuttin, M., Lew, E., Ferrez, P. W., Vanacker, G., Philips, J., and Millán, J. d. R. (2008). A brain-actuated wheelchair: asynchronous and non-invasive brain-computer interfaces for continuous control of robots. *Clin. Neurophysiol.* 119, 2159–2169.

Garipelli, G., Chavarriaga, R., and Millán, J. d. R. (2009). "Anticipation based brain-computer interfacing (aBCI)," in *Fourth International IEEE EMBS Conference on Neural Engineering,* (Antalya, Turkey).

Garipelli, G., Chavarriaga, R., and Millán, J. d. R. (2011). "Single trial recognition of anticipatory slow cortical potentials: the role of spatio-spectral filtering," in *Fifth International Conference on Neural Engineering,* (Cancun, Mexico).

Gonzalez, S. L., Grave de Peralta, R., Thut, G., Millán, J. d. R., Morier, P., and Landis, T. (2006). Very high frequency oscillations (VHFO) as a predictor of movement intentions. *Neuroimage* 32, 170–179.

Green, J. B. (2003). Brain reorganization after stroke. *Top. Stroke Rehabil.* 10, 1–20.

Haggard, P. (2008). Human volition: towards a neuroscience of will. *Nat. Rev. Neurosci.* 9, 934–946.

Hogan, N., and Krebs, H. I. (2011). Physically interactive robotic technology for neuromotor rehabilitation. *Prog. Brain Res.* 192, 59–68.

Hong, D. A., Corcos, D. M., and Gottlieb, G. L. (1994). Task dependent patterns of muscle activation at the shoulder and elbow for unconstrained arm movements. *J. Neurophysiol.* 71, 1261–1265.

Ikeda, A., Shibasaki, H., Nagamine, T., Terada, K., Kaji, R., Fukuyama, H., and Kimura, J. (1994). Dissociation between contingent negative variation and Bereitschaftspotential in a patient with cerebellar efferent lesion. *Electroencephalogr. Clin. Neurophysiol.* 90, 359–364.

Jankelowitz, S. K., and Colebatch, J. G. (2002). Movement-related potentials associated with self-paced, cued and imagined arm movements. *Exp. Brain Res.* 147, 98–107.

Jankelowitz, S. K., and Colebatch, J. G. (2005). Movement related potentials in acutely induced weakness and stroke. *Exp. Brain Res.* 161, 104–113.

Johnson, M. (2006). Recent trends in robot-assisted therapy environments to improve real-life functional performance after stroke. *J. Neuroeng. Rehabil.* 3, 29.

Keller, I., and Heckhausen, H. (1990). Readiness potentials preceding spontaneous motor acts: voluntary vs. involuntary control. *Electroencephalogr. Clin. Neurophysiol.* 76, 351–361.

Kornhuber, H. H., and Deecke, L. (1965). Changes in the brain potential in voluntary movements and passive movements in man: readiness potentials and reafferent potentials. *Pflugers Arch. Gesamte Physiol. Menschen Tiere* 284, 1–17.

Kwakkel, G., Kollen, B. J., and Krebs, H. I. (2008). Effects of robot-assisted therapy on upper limb recovery after stroke: a systematic review. *Neurorehabil. Neural Repair* 22, 111–121.

Lamarche, M., Louvel, J., Buser, P., and Rektor, I. (1995). Intracerebral recordings of slow potentials in a contingent negative variation paradigm: an exploration in epileptic patients. *Electroencephalogr. Clin. Neurophysiol.* 95, 268–276.

Lang, W. (2003). "Surface recordings of the Bereitschaftspotential in normals," in *The Bereitschaftspotential: Movement-Related Cortical Potentials,* eds M. Hallett and M. Jahanshahi (New York, NY: Kluwer Academic/Plenum Publisher), 17–34.

Levin, M. F. (1996). Interjoint coordination during pointing movements is disrupted in spastic hemiparesis. *Brain* 119, 281–293.

Libet, B., Gleason, C. A., Wright, E. W., and Pearl, D. K. (1983). Time of conscious intention to act in relation to onset of cerebral activity (readiness-potential). *Brain* 106, 623–642.

Libet, B., Wright, E. W., and Gleason, C. A. (1982). Readiness-potentials preceding unrestricted spontaneous' vs. pre-planned voluntary acts. *Electroencephalogr. Clin. Neurophysiol.* 54, 322–335.

Lo, A. C., Guarino, P. D., Richards, L. G., Haselkorn, J. K., Wittenberg, G. F., Federman, D. G., Ringer, R. J., Wagner, T. H., Krebs, H. I., Volpe, V. T., Bever, C. T., Bravata, D. M., Duncan, P. W., Corn, B. H., Maffucci, A. D., Nadeau, S. E., Conroy, S. S., Powell, J. M., Huang, G. D., and Peduzzi, P. (2010). Robot-assisted therapy for long-term upper-limb impairment after stroke. *N. Engl. J. Med.* 362, 1772–1783.

Lu, M. K., Arai, N., Tsai, C. H., and Ziemann, U. (2011). Movement related cortical potentials of cued versus self-initiated movements: double dissociated modulation by dorsal premotor cortex versus supplementary motor area rTMS. *Hum. Brain Mapp.* 33, 824–839.

Masiero, S., Rosati, G., Valarini, S., and Rossi, A. (2009). Post-stroke robotic training of the upper limb in the early rehabilitation phase. *Funct. Neurol.* 24, 203–206.

Millán, J. d. R. (2004). "On the need for on-line learning in brain-computer interfaces," in *International Joint Conference on Neural Networks,* (Budapest, Hungary).

Millán, J. d. R., Galán, F., Vanhooydonck, D., Lew, E.,

Philips, J., and Nuttin, M. (2009). "Asynchronous non-invasive brain-actuated control of an intelligent wheelchair," in *31st Annual International Conference of the IEEE Engineering in Medicine and Biology Society,* (Minneapolis, USA).

Mirabella, G., Pani, P., and Ferraina, S. (2008). Context influences on the preparation and execution of reaching movements. *Cogn. Neuropsychol.* 25, 996–1010.

Mirabella, G., Pani, P., and Ferraina, S. (2011). Neural correlates of cognitive control of reaching movements in the dorsal premotor cortex of rhesus monkeys. *J. Neurophysiol.* 106, 1454–1466.

Mirabella, G., Pani, P., Paré, M., and Ferraina, S. (2006). Inhibitory control of reaching movements in humans. *Exp. Brain Res.* 174, 240–255.

Muralidharan, A., Chae, J., and Taylor, D. M. (2011). Extracting attempted hand movements from EEGs in people with complete hand paralysis following stroke. *Front. Neurosci.* 5:39. doi: 10.3389/fnins.2011.00039

Offner, F. F. (1950). The EEG as potential mapping: the value of the average monopolar reference. *Electroencephalogr. Clin. Neurophysiol.* 2, 213–214.

Osselton, J. W. (1965). Acquisition of EEG data by bipolar unipolar and average reference methods: a theoretical comparison. *Electroencephalogr. Clin. Neurophysiol.* 19, 527–528.

Perdikis, S., Bayati, H., Leeb, R., and Millán, J. d. R. (2011). Evidence accumulation in asynchronous BCI. *Int. J. Bioelectromagnetism* 13, 131–132.

Pfurtscheller, G., and Lopes da Silva, F. H. (1999). Event-related EEG/MEG synchronization and desynchronization: basic principles. *Electroencephalogr. Clin. Neurophysiol.* 110, 1842–1857.

Rektor, I. (2003). "Intracerebral recordings of the bereitschaftspotential and related potentials in cortical and subcortical structures in human subjects," in *The Bereitschaftspotentials – Movement Related Cortical Potentials,* eds M. Jahanshani and M. Hallett (New York, NY: Kluwer Academic/Plenum Publishers), 61–77.

Riener, R., Nef, T., and Colombo, G. (2005). Robot-aided neurorehabilitation of the upper extremities. *Med. Biol. Eng. Comput.* 43, 2–10.

Ruchkin, D. S., Sutton, S., Mahaffey, D., and Glaser, J. (1986). Terminal CNV in the absence of motor response. *Electroencephalogr. Clin. Neurophysiol.* 63, 445–463.

Schall, J. D. (2004). On building a bridge between brain and behavior. *Annu. Rev. Psychol.* 55, 23–50.

Schlögl, A., Keinrath, C., Zimmermann, D., Scherer, R., Leeb, R., and Pfurtscheller, G. (2007). A fully automated correction method of EOG artifacts in EEG recordings. *Clin. Neurophysiol.* 118, 98–104.

Shibasaki, H., and Hallett, M. (2006). What is the Bereitschaftspotential? *Clin. Neurophysiol.* 117, 2341–2356.

Simonetta, M., Clanet, M., and Rascol, O. (1991). Bereitschaftspotential in a simple movement or in a motor sequence starting with the same simple movement. *Electroencephalogr. Clin. Neurophysiol.* 81, 129–134.

Soon, C. S., Brass, M., Heinze, H. J., and Haynes, J. D. (2008). Unconscious determinants of free decisions in the human brain. *Nat. Neurosci.* 11, 543–545.

Staubli, P., Nef, T., Klamroth-Marganska, V., and Riener, R. (2009). Effects of intensive arm training with the rehabilitation robot ARMin II in chronic stroke patients: four single-cases. *J. Neuroeng. Rehabil.* 6, 46.

Thut, G., Hauert, C.-A., Viviani, P., Morand, S., Spinelli, L., Blanke, O., Landis, T., and Michel, C. (2000). Internally driven vs. externally cued movement selection: a study on the timing of brain activity. *Brain Res. Cogn. Brain Res.* 9, 261–269.

Trombly, C. A., and Wu, C. (1999). Effect of rehabilitation tasks on organization of movement after stroke. *Am. J. Occup. Ther.* 53, 333–344.

Walter, W. G., Cooper, R., Aldridge, V. J., McCallum, W. C., and Winter, A. L. (1964). Contingent negative variation: an electric sign of sensorimotor association and expectancy in the human brain. *Nature* 203, 380–384.

Conflict of Interest Statement: The authors declare that the research was conducted in the absence of any commercial or financial relationships that could be construed as a potential conflict of interest.

Received: 05 March 2012; paper pending published: 23 April 2012; accepted: 20 June 2012; published online: 12 July 2012.

*Citation: Lew E, Chavarriaga R, Silvoni S and Millán JdR (2012) Detection of self-paced reaching movement intention from EEG signals. Front. Neuroeng. **5**:13. doi: 10.3389/fneng.2012.00013*

frontiers in
NEUROENGINEERING

ORIGINAL RESEARCH ARTICLE
published: 18 July 2012
doi: 10.3389/fneng.2012.00016

Reprogramming movements: extraction of motor intentions from cortical ensemble activity when movement goals change

***Peter J. Ifft*[1,2]*, *Mikhail A. Lebedev*[2,3] *and Miguel A. L. Nicolelis*[1,2,3,4,5]**

[1] *Department of Biomedical Engineering, Duke University, Durham, NC, USA*
[2] *Center for Neuroengineering, Duke University, Durham, NC, USA*
[3] *Department of Neurobiology, Duke University, Durham, NC, USA*
[4] *Department of Psychology and Neurosciences, Duke University, Durham, NC, USA*
[5] *Edmond and Lily Safra International Institute of Neurosciences of Natal, Natal, Brazil*

Edited by:
Giovanni Mirabella, University of La Sapienza, Italy

Reviewed by:
Ricardo Chavarriaga, Ecole Polytechnique Fédérale de Lausanne, Switzerland
Jonathan R. Wolpaw, New York State Department of Health, USA

***Correspondence:**
Peter J. Ifft, Department of Biomedical Engineering, Duke University Center for Neuroengineering, Duke University, 136 Hudson Hall, Box 90281, Durham, NC 27708, USA.
e-mail: peter.ifft@duke.edu

The ability to inhibit unwanted movements and change motor plans is essential for behaviors of advanced organisms. The neural mechanisms by which the primate motor system rejects undesired actions have received much attention during the last decade, but it is not well understood how this neural function could be utilized to improve the efficiency of brain-machine interfaces (BMIs). Here we employed linear discriminant analysis (LDA) and a Wiener filter to extract motor plan transitions from the activity of ensembles of sensorimotor cortex neurons. Two rhesus monkeys, chronically implanted with multielectrode arrays in primary motor (M1) and primary sensory (S1) cortices, were overtrained to produce reaching movements with a joystick toward visual targets upon their presentation. Then, the behavioral task was modified to include a distracting target that flashed for 50, 150, or 250 ms (25% of trials each) followed by the true target that appeared at a different screen location. In the remaining 25% of trials, the initial target stayed on the screen and was the target to be approached. M1 and S1 neuronal activity represented both the true and distracting targets, even for the shortest duration of the distracting event. This dual representation persisted both when the monkey initiated movements toward the distracting target and then made corrections and when they moved directly toward the second, true target. The Wiener filter effectively decoded the location of the true target, whereas the LDA classifier extracted the location of both targets from ensembles of 50–250 neurons. Based on these results, we suggest developing real-time BMIs that inhibit unwanted movements represented by brain activity while enacting the desired motor outcome concomitantly.

Keywords: motor cortex, sensorimotor transformation, volitional inhibition, neurophysiology, decision making, brain-machine interfaces, neuroprosthetics, monkey

INTRODUCTION

Neurophysiological studies conducted during the last two decades have revealed a complex representation of spatial information in the brain, including the representation of multiple motor targets (Cisek and Kalaska, 2002, 2005), sequences (Mushiake et al., 1990; Isoda and Tanji, 2004), spatial attention (Lebedev and Wise, 2001; Lebedev et al., 2004; Ikkai and Curtis, 2011), and gaze (Boussaoud et al., 1993; Baker et al., 1999; Boussaoud and Bremmer, 1999; Balan and Ferrera, 2003)—all in different reference frames, depending from which brain area neural activity was sampled (Lacquaniti and Caminiti, 1998; Cohen and Andersen, 2002; McGuire and Sabes, 2009). These representations underlie rich behavioral repertoires of advanced organisms, primates in particular, that can flexibly control their attention and motor processing to meet demanding challenges of their environments (Wise et al., 1996; Wise and Murray, 2000; Lebedev and Wise, 2002). In particular, advanced organisms can inhibit and reprogram movements once the corresponding neural planning or even the movement itself have been initiated (Matsuzaka and Tanji, 1996; Band and van Boxtel, 1999; Schall et al., 2002; Mostofsky and Simmonds, 2008; Verbruggen and Logan, 2008; Stinear et al., 2009; Mirabella et al., 2011).

An adaptive neural framework can enable the planning stages of potential movements to begin in parallel with preparations for an alternative motor plan (Resulaj et al., 2009; Cisek and Kalaska, 2010). As a result, neural representations of distinct motor plans may compete prior to movement onset in behavioral tasks with several potential targets of movement (Cisek and Kalaska, 2005; Rickert et al., 2009; Mirabella et al., 2011). Studies of reaching movements have identified populations of neurons that represent multiple potential motor plans throughout the dorsal premotor (Cisek and Kalaska, 2005; Pesaran et al., 2008; Mirabella et al., 2011), supplementary motor (Chen et al., 2010), and posterior parietal cortices (Snyder et al., 1998; Scherberger and Andersen,

2007). A bounded-accumulation model (Resulaj et al., 2009) proposes that when multiple motor outcomes are presented, neural networks prepare for the most likely upcoming movement. The network accumulates noisy evidence over time until a bound threshold is reached, at which point an initial decision is reached, which is then either reversed or reaffirmed.

In the present study, we investigated the representation of multiple potential movement targets and the specification of a change in motor plan by neuronal ensembles simultaneously recorded in primary motor (M1) and sensory (S1) cortical areas. We approached neural representation of motor plan transitions from a brain-machine interface (BMI) perspective. BMIs extract motor commands from the brain and convert them into movements of external actuators, such as computer cursors and robotic devices (Andersen et al., 2004; Lebedev and Nicolelis, 2006; Fetz, 2007; Birbaumer et al., 2008; Nicolelis and Lebedev, 2009; Chase and Schwartz, 2011; Lebedev and Nicolelis, 2011; Lebedev et al., 2011). At the current stage of the BMI field, up to several hundred neurons in the brain can be recorded simultaneously by chronically implanted multielectrode arrays (Nicolelis et al., 2003; Chapin, 2004; Churchland et al., 2007; Miller and Wilson, 2008; Lebedev and Nicolelis, 2011; Lebedev et al., 2011; Stevenson and Kording, 2011). Recording from large neuronal populations is essential because the range of information extracted from neural activity and accuracy of extraction improves with the number of recorded neurons (Wessberg et al., 2000; Carmena et al., 2003; Lebedev et al., 2005; Lebedev and Nicolelis, 2006; Fitzsimmons et al., 2009; Nicolelis and Lebedev, 2009). Notwithstanding the successes of the BMI field, signals extracted from the brain are typically noisy (Lebedev and Nicolelis, 2006; Tonet et al., 2008). BMI algorithms are usually trained to reproduce one particular behavior and do not generalize well when a transition to a new set of rules and conditions is needed (Santucci et al., 2005; Fitzsimmons et al., 2009). This is why many improvements are needed: from a significant increase of the number of simultaneously recorded neurons to the development of better extraction algorithms capable of approximating natural behaviors.

Although some work has been done on the extraction of behavioral parameters during delay intervals, during which monkeys prepare movements but withhold their execution (Musallam et al., 2004; Lebedev et al., 2008; Afshar et al., 2011), the problem of motor plan transitions has not yet been fully investigated from a BMI perspective. We examined cortical representation of motor programming in a reaction-time task in which monkeys had to rapidly reprogram their center-out reaching movements. The monkeys had been previously overtrained to move a hand-held joystick toward computer screen targets. In this study, we introduced distracting targets that flashed on the screen for a short period (50–250 ms) and triggered motor preparation on 75% of the trials. This motor preparation had to be canceled when a true target appeared at a new screen location. Both the distracting and the true targets were represented by neuronal ensemble activity recorded in the M1 and S1 cortices. We used ensemble modulations to extract target locations using a linear discriminant analysis (LDA) classifier. In addition, a Wiener filter was used to make continuous extractions offline.

METHODS

CORTICAL IMPLANTS

All studies were conducted with approved protocols from the Duke University Institutional Animal Care and Use Committee and were in accordance with the NIH guidelines for the Care and Use of Laboratory Animals (National Research Council et al., 2011).

Two rhesus monkeys (one male and one female, monkeys M and N, respectively) were chronically implanted with multielectrode arrays in M1 and S1 of both right and left hemispheres using previously described surgical methods (Nicolelis et al., 2003). Within each hemisphere, two 96 channel microelectrode arrays were placed in cortical areas corresponding to cortical representations of the arm and leg (**Figure 1B**), but in this study, neural activity was recorded only in the arm representation area of right hemisphere M1 (in both monkeys) and S1 (only in monkey M). Each array consisted of two 4 by 4 grids of independently movable electrode triplets. Triplets were comprised of electrodes of different lengths, in 0.3 mm intervals, which allowed us to sample neuronal activity from different depths in the cortical tissue. Recorded signals were amplified, digitized, and filtered by a multichannel recording system (Plexon Inc, Dallas, TX, USA). Neuronal spikes were sorted using waveform template matching algorithm built into the real-time spike-sorting software.

BEHAVIORAL TASK

Each monkey was trained to move a hand-held joystick to control the two-dimensional location of a computer cursor on a screen (**Figure 1A**). X(left-right) and Y(forward-backward) position of the joystick were translated to X(left-right) and Y(up-down) cursor position on the screen. The joystick was affixed to the chair at the waist level of the monkey on the side of the working hand (left hand in both monkeys). During the task, the display screen was positioned in front of the monkey, at 45 cm from the monkey's eyes. The cursor diameter was 0.5 cm.

To begin each trial, the monkey placed its left hand on the top of the joystick, causing a cursor to appear on the screen. A trial was immediately canceled if the monkey removed its hand from the joystick at any time. Next, a 5 cm diameter circle appeared at the center of the screen. The monkey moved the cursor inside this circle and held it for a random interval between 1 and 2 s. After this hold period, the center target disappeared and a single peripheral target became visible. The peripheral target appeared as a thickened 40° arc on a thin boundary circle aligned on the center of the screen (**Figure 1C**). Reaching the target required the cursor to pass over the thickened arc from the inside of the circle, moving outwards (**Figure 1D**). If the cursor crossed the circle, but missed the target, trial was terminated without reward delivery. Both monkeys had been previously overtrained to perform center-out movements toward the targets, triggered by target appearance and characterized by reaction times (RTs) of 0.49 ± 0.17 s (mean $\pm$ standard deviation) in monkey M and 0.44 ± 0.18 s in monkey N (Ifft et al., 2011).

In this study we introduced target switches to produce dual target representation in the sensorimotor cortex. This design was to

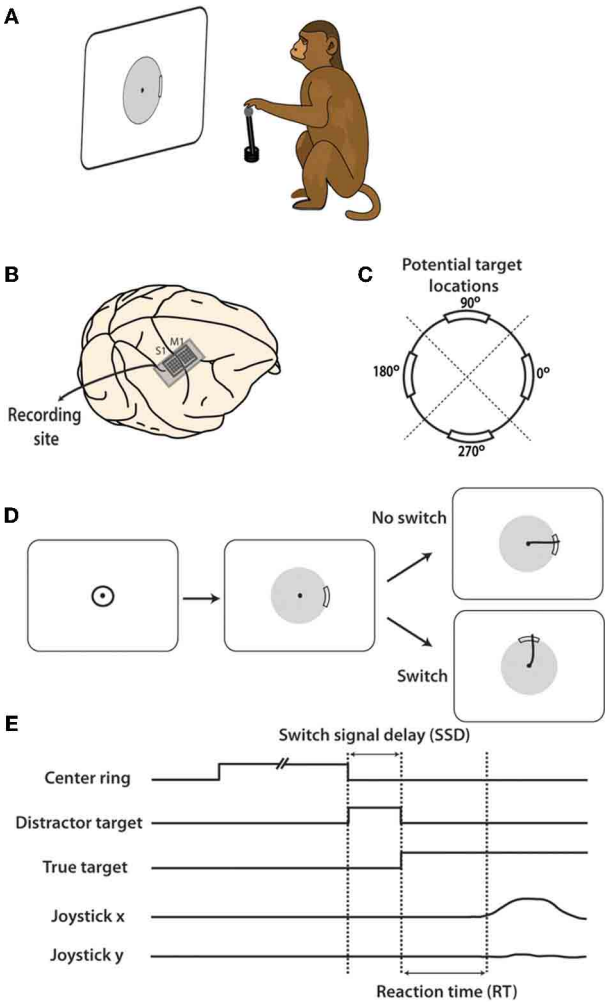

FIGURE 1 | Experiment and location of neural recordings. (A) Rhesus monkey controlled joystick with left hand which translated to movements on computer screen. **(B)** Electrode arrays in arm representation regions of M1 and S1 cortex were implanted prior to data collection. **(C)** During task, peripheral targets appeared at one of four potential locations on the screen: 0, 90, 180, 270°. Workspace was divided into four quadrants, centered on each target location as divided by dashed diagonal lines. **(D)** Typical task sequence begins with cursor inside central target. After a random hold time, the target appears an as an arc on the gray boundary circle. On 25% of trials, this target persists and the cursor must be move through the target for reward. On the remaining trials, the target moves after a brief delay and the cursor must be move toward the new target to obtain a reward. **(E)** Shown are timelines of the presence of each target and joystick position. SSD is defined to be the time between when the first target appears and when the target is switched to the second location.

mimic the momentary preparations followed by changes in motor plans. In switch trials, initial targets served as distractors. They appeared on the screen and were then replaced by a second target at different locations after a short interval, termed the switch signal delay (SSD). A similar switching task was previously reported (Georgopoulos et al., 1981, 1983) with a difference that monkeys were overtrained in those studies and M1 neurons were recorded serially. Our distracting and true targets always appeared at one of four locations on the screen, at angles 0, 90, 180, or 270° relative to the center of the screen (**Figure 1C**). Initial targets switched in 75% of trials. The SSD for a given trial was either 50, 150, or 250 ms, with each occurring with equal probability. When the distracting target disappeared, a second target appeared at one of the remaining three potential locations. We call this second target the true target because a juice reward was obtained only by moving the cursor through this target. In the remaining 25% of trials, the first target remained on the screen throughout the trial and a reward was obtained by passing the cursor through this target location. Once the true target appeared, the monkey had 2.5 s to complete each trial before timing out. The experiment was repeated over two daily recording sessions in both monkey M and monkey N.

Single trial trajectories were categorized depending on the degree of deviation made toward the distracting target. For switch trials, a threshold distance was set at 1.5 cm along the axis between the center target and the distractor. Joystick movements which surpassed this threshold in the direction of the distractor were categorized as distracted trials. Remaining trials were categorized as direct if, in addition to not moving toward the distractor, the path to the true target deviated less than 1.5 cm in the direction orthogonal to the ideal trajectory. Strict criteria were enforced for direct trials to ensure that the only movement made was to the true target, isolating the role of movements with a singular goal from the onset. Direct trials could, however, be unrewarded if they were near misses and the cursor did not move toward the distractor. Violation of these criteria on a given trial resulted into classification as a distracted trial and later analyses evaluated these two trial groupings separately. Furthermore, trials where the initial center target was held but no movement was made to any target (beyond the 1.5 cm threshold distance) were not considered in the present analysis. Trial movement onset was computed using a previously implemented algorithm where movement initiation was detected based on the analysis of specific patterns in velocity and acceleration (Ifft et al., 2011). To perform statistical testing on performance accuracy measured as proportion of trials, such as fraction direct trials (**Figure 2C**) or fraction correct for different target location, trials were subdivided into groups of 15 trials. Number of outcomes of each type per 15 trials was computed for each group, and their statistical sample for all groups was entered in an appropriate statistical test (e.g., unpaired t-test that could be used either directly to compare two outcomes, or *post-hoc* following analysis of variance for comparing several outcomes).

RT was defined as the time from either the distractor or true target onset until movement onset. The RT measured from distractor onset was elongated by the SSD during which an initial, false, target was presented. At the same time, it could be additionally shortened for some SSDs because the distractor primed the appearance of the true target. That is, when the true target was presented, a shorter response latency could indicate that the transient distractor presence expedited pre-movement processes with respect to the true target. For the RT measured from true target onset (**Figure 1E**), the priming effect of the distractor is more clearly demonstrated. Each definition yields its own interpretation thus we included both in our analysis.

POPULATION RESPONSES

All neural analyses were performed using recordings from Monkey M M1 and S1 neurons, and Monkey N M1 neurons. Population-level analyses were conducted separately for each of these three cortical areas. Neural activity was analyzed using peri-event time histograms (PETHs) (Awiszus, 1997) aligned on distractor target onset. Recorded timestamps of action potentials were counted in bins of 50 ms width. The PETH from 0.5 s before to 1.0 s after distractor target onset (true target onset in the case of no-switch trials) for each neuron was computed separately for each combination of distractor and true target location (four no-switch combinations and 12 switch combinations), for each of the four SSD conditions. For single neuron analysis (**Figures 4**, **5**), single trial spike rasters were constructed over the same 1.5 s epoch aligned on distractor onset. Corresponding PETHs represent the bin counts of total spikes that occurred within each of the 50 ms bins, summed across trials in the same SSD category as well as matching the same combination of distractor and true target locations. Bin counts were then divided by the fixed 50 ms bin width to represent firing rate in units of spikes/second.

To analyze population-level modulations, the average modulation profile for each neuron was normalized by subtracting the mean bin count of the neuron (over all conditions) and dividing by the standard deviation of the neuron's bin count. This normalized quantity represented modulations as a fraction of the overall modulations, or statistically, the *z*-score. The directional tuning of each neuron was computed from normalized PETH data on trials where there was no switching of the peripheral target. The mean normalized firing rate was computed within the 750 ms window following target onset for each target direction. The four directions were then ranked from most preferred to least preferred in subsequent analyses reflecting the directional preference of the each neuron (**Figure 6A**). Next the mean PETH over the entire population of neurons was computed for each of the sixteen distractor/true target configurations and for each of the three SSD groups (**Figure 6B**).

To further understand the neural representation of the distractor target and the true target, the population mean firing rate (MFR) was computed during different epochs for each of the 12 distractor-true target combinations, and four no-switch trial categories (**Figure 7**). Furthermore, we separated the trials by SSD to elucidate the effect of an elongated distractor presence (**Figures 7A–C**). For each neuron, the MFR was computed for each of the 16 positions on a 4×4 grid, with rows representing preference ranking of the true target location (ranks 1 through 4) and columns representing the preference ranking of the distractor target (ranks 1 through 4). The layout is clarified in **Figure 7D**. Firing rate was normalized and the directional preferences of each neuron were determined from most to least preferred direction as in **Figure 6**. Population MFR was obtained by averaging the MFR across all neurons in the given area. This procedure was repeated for six temporal epochs: the epoch when the distractor was present, and five consecutive 100 ms epochs following true target appearance. To evaluate the specific contribution of the distractor and true target neural representations on MFR, we fit MFR as a linear function of the preference ranking of each target preference combination (1–4) for each 4×4 grid, show in Equation 1 (Lebedev and Wise, 2001; Lebedev et al., 2004):

$$\mathrm{MFR} = A \cdot PD_{\mathrm{true}} + B \cdot PD_{\mathrm{distractor}} + C \tag{1}$$

Coefficients A and B represent the contribution of the true target and the distractor target, respectively.

We also separated trials depending on whether the monkey correctly switched to the true target (**Figure 8**). In this analysis, trials were separated into two groups depending on the monkey behavior: (1) trials where the true target was reached (rewarded trials) and (2) trials where the monkey was distracted (as defined earlier) and failed to reach the true target. Trials outside of these two categories were not included in the **Figure 8** analysis.

To evaluate the variation in neural activity profile between the different SSD groups, single neuron normalized PETH data from each of the 12 switch conditions were subtracted from the PETH data from the corresponding no-switch condition and this value was squared. The mean of the 12 difference-squared terms was computed over the -0.5 to 1 s trial epoch for each neuron and for each SSD group, and the square root of this value was computed, yielding a root-mean-square (RMS) difference, shown by Equation 2:

$$\mathrm{RMS}_{\mathrm{cell}} = \sqrt{\mathrm{mean}\left\{\sum_{i \neq j} \left(\mathrm{PETH}_{jj} - \mathrm{PETH}_{ij}\right)^2\right\}} \tag{2}$$

where PETH_{ij} represents the normalized neural activity profile for a single neuron when the distractor is at position i and the true target is at position j. PETH_{jj} represents the normalized activity profile of the same neuron on a no-switch trial. Both i and j have four possible values resulting in 12 differences to be computed for each neuron. This procedure was repeated for data collected in each of the four SSD groups.

The difference profile across the population was thus computed by taking the mean difference across neurons, while maintaining temporal information (**Figure 9A**). Lastly, the population average for each of the SSD groups was compared to identify the relevant interval during the trial where modulations reflect the transient distractor representation (**Figure 9B**).

To assure that the differences arose as a result of the distractor, and not due to increased variance during elevated neural activity during movement, trials were shuffled amongst distractor location groups and the analysis was repeated, however, the SSD categorization remained intact. Once shuffled, the single neuron and population RMS differences were computed in the exact method as performed for the unshuffled data. The shuffled RMS difference profile for each SSD was generated five times and the average of these profiles was subtracted from the unshuffled population RMS difference profile, thus reflecting the true difference accounted for by the distractor presence.

CLASSIFIER

To extract the location of both the first (distractor) target location and the second (true) target locations, LDA (Fisher, 1936)

was used to decode neural activity offline and make categorical predictions of each target location (**Figures 9–11**) (Ifft et al., 2011). In no-switch trials, the locations of the distractor and true targets were considered the same. Neural activity aligned on distractor onset was used to train the classifier on 60% of randomly selected trials. Training data for each time point was provided by neural discharges within a 150 ms window slid across the task interval from 0.5 s before to 1 s after distractor target onset. Predictions of both target locations were made using sample data from the remaining 40% of trials. The same 150 ms sliding window was used to obtain predictions. For each session, sliding LDA predictions were computed five times, each with randomly redrawn training and sample subsets. Overall reported predictions represent the average of these five runs per session. Neural activity used to train the decoder was separated into exclusively M1 or S1 recorded neurons in the case of monkey M, and just M1 neurons in monkey N. LDA predictions were also made with shuffled data; that is, when the group information is randomly permutated prior to training the LDA classifier. For each LDA figure (**Figures 10–12**), we computed the fraction correct prediction of each parameter minus fraction correct of the LDA predictions from shuffled data. The chance level performance (0.25 because of four potential targets) was then added to this amount to again return to the conventional [0, 1] scale. The *y*-axis thus becomes fraction correct with unrelated modulations removed. For each analysis, confidence intervals were computed using the 1-proportion *z*-test from Equation 3:

$$z = \frac{\hat{p} - p_0}{\sqrt{p_0(1 - p_0)}}\sqrt{n} \tag{3}$$

where p_0 is 0.25 (four potential targets) and n is the number of trials used for testing (40% of total trials). All confidence intervals were constructed at $\alpha = 0.05$.

Trial types were then divided according whether the movement was direct to the true target or revealed a deviation toward the distractor (see Behavioral Task section above) as a way to test whether the transient representation of the distractor target is explained by motor movements. LDA was trained on both trial types combined and was then utilized to make predictions of the first and second target location separately for each trial type (**Figure 11**).

A separate analysis was performed using LDA to decode the presence of the switching of target location (**Figure 12A**). Again, a 150 ms sliding window of neural activity trained the decoder. At each time step, LDA made a prediction of whether the trial was a switch or no-switch trial. Data were again aligned on the time of distractor onset and all switch-trials were grouped together. First target in this case means distractor target in the case of switch trials, or true target (only target) in the case of no-switch trials. The 150 ms sliding window was incremented along the time axis in 25 ms steps from 0.5 s before to 1 s after first target onset. The fraction of correct predictions was computed at each time step as described for previous sliding window LDA analyses. As this analysis involves a binary classification procedure, a second metric was used to quantify extraction of event information from neural activity (**Figure 12B**). The Matthews correlation coefficient (MCC) is a common measure of classifiers for binary outcomes (Matthews, 1975; Baldi et al., 2000). MCC is computed as shown in Equation 4:

$$\mathrm{MCC} = \frac{\mathrm{TP} \times \mathrm{TN} - \mathrm{FP} \times \mathrm{FN}}{\sqrt{(\mathrm{TP} + \mathrm{FN})(\mathrm{TP} + \mathrm{FP})(\mathrm{TN} + \mathrm{FP})(\mathrm{TN} + \mathrm{FN})}} \tag{4}$$

where TP is the count for true positives predictions, TN for true negatives, FP for false positives, and FN for false negatives. Similar to the conventional correlation coefficient, the values of MCC range from −1 to 1 depending on the strength and directionality of the prediction. At each shift, the MCC was computed five times as a result of randomly redrawing the training and sample data, as was done in each LDA analysis. With two sessions per monkey, MCC at each time step of the sliding window represents the mean of 10 values.

Concurrent to prediction of trial type (switch or no-switch) at each time step, location of the first and second targets was also decoded. Although the training data included both switch and no-switch trials, LDA performance in terms of fraction correct locations only included prediction data from switch trials. This was necessary because if the no-switch target was identified as the distractor, the LDA predictions may have been artificially improved due to the prolonged presence of that target on the screen. If it was identified as the true target, the prediction may have also been improved because of the absence of interference from a distractor.

CONTINUOUS OFFLINE PREDICTIONS USING WIENER FILTER

To mimic continuous, real-time BMI predictions, we used a simple Wiener filter with six 100 ms taps of neural data to predict cursor X and Y coordinates, and true target X and Y coordinates at a 10 Hz output rate (**Figure 13**). For monkey M, both M1 and S1 neurons were used to improve predictions of these parameters (**Figures 13A–E**). To reject noisy neurons and reduce overfitting, we computed weights that reflected each neuron's contribution toward kinematic predictions. We selected the 80% of all neurons which had the highest weights.

The Wiener filter weights were fit using 60% of the session length and predictions were made using the remaining 40%. Due to variable durations of all targets in the session, we inflated the true target duration to 1000 ms to ensure targets could be represented despite a low 10 Hz rate of prediction. To reduce the effect of noisy predictions, the predicted radius of movement, r, was computed at each time as shown in Equation 5:

$$r = \sqrt{X_p^2 + Y_p^2} \tag{5}$$

where X_p and Y_p are the predicted X and Y position of the cursor at a given time (**Figure 13B**). A threshold for r was chosen at 5 cm (screen coordinates) such that when r surpassed this threshold, a reach had been predicted. Time of threshold crossing was thus recorded and predictions of target locations relative to this time were made. At each time from when r exceeded $r_{\mathrm{threshold}}$, predictions of cursor and true target position were made and compared to actual. To quantify performance in terms of fraction correct, the screen was divided into four (90°) quadrants surrounding

each target (see **Figure 1C**). For example, quadrant 1 would occur from −45° to 45° relative to the center of the screen. A prediction of cursor X and Y was correct if the Wiener prediction was in the correct quadrant as the actual cursor (X, Y). True target location predictions were evaluated in the same way. Predicted true target quadrant was compared with the target locations. The fraction correct was computed at each time step beginning at threshold crossing until 800 ms after threshold crossing, during all threshold crossings in the last 40% of each session. If during this 800 ms window, r became less than $r_{\text{threshold}}$, predictions were no longer made. If r was greater than $r_{\text{threshold}}$, but the true target was not on the screen (with all durations fixed at 1 s, as stated before), this was counted as incorrect.

RESULTS

BEHAVIOR

While the monkeys had been previously overtrained in the single target task, no prior training was performed in the task with switching targets. We chose to avoid excessive training on the two target sequence because we wanted to obtain the maximum effect of the switching target and avoid the monkeys developing alternative behavioral strategies, such as timing their responses in a way such that the initially presented target is wholly ignored. We suppose that previous overtraining in reaction-time responses toward single targets helped to enhance the representation of the distractor target because that was the target toward which monkeys were accustomed to moving in a RT manner. However, neither the contribution of prior training nor the effect of continued training with switching targets were examined in this study.

As it would be expected, the introduction of switching targets resulted in erroneous responses on a portion of trials (**Figure 2**), more so for monkey N. We consider reaching movements that crossed into the true target to be correct trials. Incorrect trials consisted of movements that crossed distracting targets, movements that missed both targets, canceled and time-out trials (**Figure 2B**). The overall proportion of correct trials was higher in monkey M than in monkey N: 88% in monkey M and only 27% in monkey N ($p < 0.001$; Wilcoxon rank sum test) (**Figures 2B,C**). Monkey N compensated for this inaccuracy by making many more trials per recording session (1519 and 1072 in each of two sessions, respectively) than monkey M (594 and 418 trials). This difference in accuracy is seen in the example trajectories for a particular target configuration (**Figure 2A**). Monkey M produced straight and carefully targeted reaching trajectories, whereas monkey N's trajectories were less accurately directed and often missed the target. Monkey M made errors only for the longest, 250 ms, SSD (**Figure 2C**). Another observation was that 90° switch trials were less frequently direct, compared to 180° switch trials (78.4% vs. 90.3% of trials for monkey M and 55.9% vs. 70.2% of trials for monkey N, $p < 0.01$, unpaired t-test). In other words, the distractor had a stronger effect on the cursor trajectory when it was closer to the true target.

To separate accurate and inaccurate reaches toward the true target, trials were divided into two groups consisting of direct trials and distracted trials. Classification of trials is described in detail within Methods. In the separation of all monkey M's trials, 505 trials were classified as direct, 145 classified as distracted, compared against a total of 214 no-switch trials. Joystick trajectories for these types of trials are shown in **Figure 3** for monkey M. Trials are grouped by target configuration: with 90° separation between the initial and true targets (left panels), and with 180° separation (right panels). Our data show reach trajectories that deviate toward the distractor on the infrequent distracted trials. Inaccurately performed trials for long presentations of distracting targets can be also seen in the examples of **Figure 2A**. The trial-averaged traces reveal the largest deviation during the longest, 250 ms, SSD (**Figure 3E**). In both monkeys, the fraction of trials categorized as "direct" decreased with longer SSDs (**Figure 2C**, $P < 0.001$, Kruskal–Wallis test). More precisely, there was a decrease in fraction direct trials for 150 ms and 250 ms durations for monkey N ($p < 0.05$; *post-hoc* unpaired t-test) and for 250 ms duration for monkey M ($p < 0.05$) in comparison with no-switch trials. Previous studies of an overtrained switching task reported mostly distracted trials where monkeys initiated movements toward the distractor and then curved the trajectory toward the true target (Georgopoulos et al., 1981, 1983).

The effect of SSD on RT was dependent on how RT was defined (see Methods). When defined from distractor target appearance until movement onset, longer SSDs caused a lengthening in RT in both monkeys ($p < 0.001$, One-Way Kruskal–Wallis test). This is somewhat expected because with longer SSDs, the longer the monkey must wait for the true target, thus inflating the RT. However, when RT was defined relative to true target appearance (**Figure 2D**), longer SSD caused shorter RTs ($p < 0.001$, One-Way Kruskal–Wallis test). Thus, the appearance of the distractor on the screen primed the response to the true target, even though the directional information that it provided was incorrect. *Post-hoc* analysis revealed significant differences from no-switch trial RT among both the 150 and 250 ms SSD groups for monkey N ($p < 0.001$; Wilcoxon rank sum test) and among all three SSD groups in monkey M ($p < 0.001$). Mean RTs for monkey N (0.52 ± 0.24 s; mean ± sd) were significantly longer than the RTs for the single target task (0.44 ± 0.18 s; $p < 0.001$; Wilcoxon rank sum test), however, monkey M performance was similar in both experiments (two-target sequence RT: 0.46 ± 0.10 s; single target task 0.49 ± 0.17 s for monkey M). Overall, monkey N behavior was more erratic in the present experiment, as evidence by cursor trajectories (**Figure 2A**) and RT standard deviation more than twice that of monkey M. In the previously overtrained reaches to single targets both monkeys performed well (e.g., 84% and 74% correctly performed trials in monkeys M and N, respectively) (Ifft et al., 2011). Note that data from the previous study represents center-out movements to a target less than half the size of the target used in the present study.

NEURONAL RESPONSES

The initial distracting targets were represented by M1 and S1 modulations even when they appeared for a brief 50 ms interval. This representation became more pronounced with longer presentations of distracting targets.

Figure 4 shows a representative M1 neuron recorded in monkey M that had a clear directional preference for the 90° and 180° target location and was modulated in response to both the

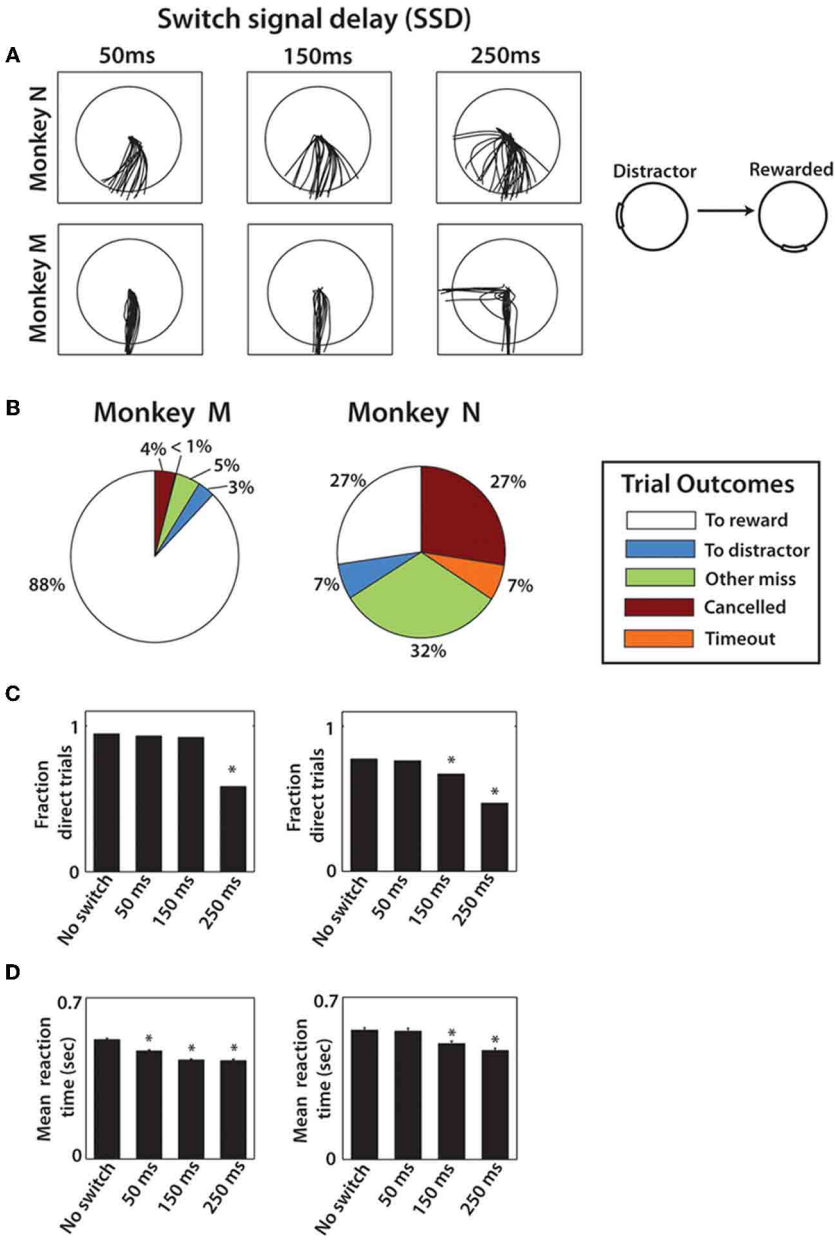

FIGURE 2 | Behavioral results from both monkeys. (A) Typical movement traces from one combination of distractor and true target locations. The columns show different cursor trajectories on trials with different SSDs. The first row is data from monkey N and the second row from monkey M. **(B)** Pie chart shows the breakdown in trial outcomes by monkey. **(C)** The fraction of direct trials shown for each SSD group in both monkey M (left) and N (right). One-Way Kruskal–Wallis test followed by *post-hoc* unpaired *t*-tests were performed. *denotes $p < 0.001$ relative to no-switch group. **(D)** Mean reaction time shown for both monkeys for each SSD group with error bars that represent standard error. Reaction time is defined as the time from true target appearance to movement onset. Same statistical procedure as **(C)**.

distractor and true targets. Data are arranged in a 4 by 4 matrix representation (Lebedev and Wise, 2001; Lebedev et al., 2004) where columns of panels correspond to the distractor target location and rows correspond to the true target location. The panels on the diagonal (shaded in gray) correspond to trials where the first target did not disappear and was the true target to which the monkey had to move. Modulations reflecting the distractor location can be appreciated from the comparison of the responses within the same rows of panels, but for different columns. Modulations reflecting the true target location are seen within the same columns, but for different rows. With the exception of the diagonals, which are identical in both **Figures 4A** and **B**, **Figure 4A** shows data for the 50 ms duration of the distractor, and **Figure 4B** shows data for the 150 ms duration. The responses to the distractor target are mostly clear in **Figure 4B** where bursts of activity are seen in response to that target appearing at the

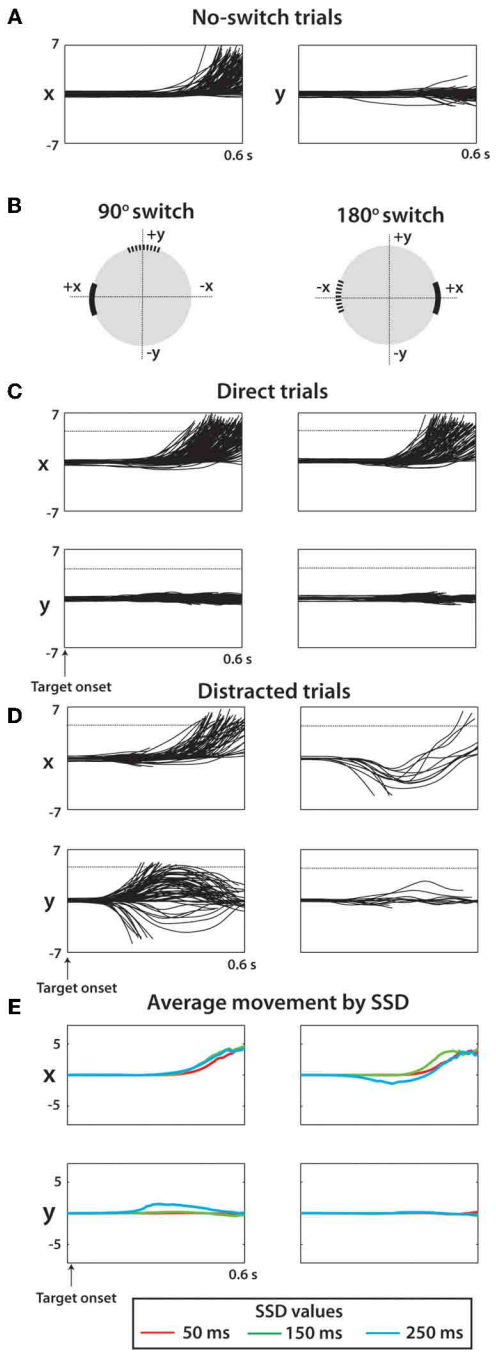

FIGURE 3 | Raw cursor trajectories for two sessions (1018 total trials) from monkey M. (A) X and Y position of cursor versus time during no-switch trials. Offline, all targets were moved to (X,Y) position (5,0) and the associated coordinate transform was made to all kinematic data. Y indicates movement orthogonal to the ideal trajectory. **(B)** For switch trials, two categories of trials shown separately for clarity: trials with a 90° switch (left) and trials with a 180° switch (right). The coordinate systems for a given trial were rotated such that the true target was in the positive X direction and the Y direction was orthogonal to this axis. **(C)** X and Y cursor positions versus time for direct trials among 90° switch (left) trials and 180° switch trials (right). **(D)** Same as **(C)** except looking at only distracted trials. **(E)** Average X and Y trajectory of cursor separated by SSD (see Legend) and by switch angle (columns same as **C,D**).

preferred location (90°, less clear for 180°). Responses to the distractor target are not as clear in **Figure 4A**, but it still can be noticed that this neuron's rate was higher following the distractor target appearance at the preferred locations (90° and 180°) compared to the non-preferred locations (0° and 270°).

Figure 5 illustrates, using the same neuron as shown in **Figure 4**, that the distractor target influenced neuronal patterns even when the monkey moved directly to the true target (**Figures 5B,C**, left panels) as it did in the no-switch trials (**Figure 5A**).

Figure 6 shows neuronal activity patterns for the entire population of M1 neurons recorded in monkey M. The format is similar to **Figure 4** with the difference being that target locations were ranked for each neuron according to the firing rate exhibited for each location. Trials without distracting targets (no-switch trials) were used to rank directions into the first preferred direction (Pref 1), second preferred direction (Pref 2) and so on for each neuron. As in **Figure 4**, no-switch trials are shown on the diagonal (denoted by gray boxes). The off-diagonal panels show the switch trials with 250 ms SSDs. **Figure 6B** shows average PETHs for each SSD. Population PETHs (**Figure 6A**) and their averages (**Figure 6B**) indicate that M1 firing rates reflected both the distractor (modulations for different columns of panels with the same row) and the true (different rows within the same column) target locations. It can be also seen that each configuration of the distractor and true target locations was associated with a unique pattern of population activity. Here, as in **Figure 4**, the initial component of the response is modulated across panel columns (i.e., representation of the distractor target), and the late component is modulated across panel rows (representation of the true target). Average PETHs of **Figure 6B** indicate that the duration of the distractor was clearly reflected by the population activity—both as the average PETH shape and (e.g., bottom row of panels) and its amplitude (e.g., top row of panels). One can also notice the location of the true target was clearly reflected as average PETH amplitude for all conditions, and the location of the true target was better reflected by average PETHs for longer SSDs—both as PETH shape and amplitude. Because of these differences between PETHs for different conditions, we were able to extract information about target locations from neuronal ensemble activity using a discrete classifier.

The results from **Figure 6** are additionally clarified in **Figure 7** that shows the evolution of neuronal rates using 4×4 diagrams. In the diagrams, vertical and horizontal bands correspond to neuronal tuning to the distractor and true target location, respectively. The diagrams are shown for different time with respect to true target onset (left to right) and for different SSDs (**Figures 7A–C**). The most prominent result seen in all SSD groups is the emergence of the true target location (bottom horizontal band of the 4×4 grid) as the strongest modulator of population MFR. The effect of the distractor is weaker. Early in the trial, most clearly in the 0 to 200 ms epochs, the distractor location is the primary modulator of neural activity. This is especially prominent when following a long SSD (**Figure 7C**). Notably, the effect of the distractor continues well into the true target presentation epoch. This is clear from the regression coefficients shown above each panel indicating the strength of the role

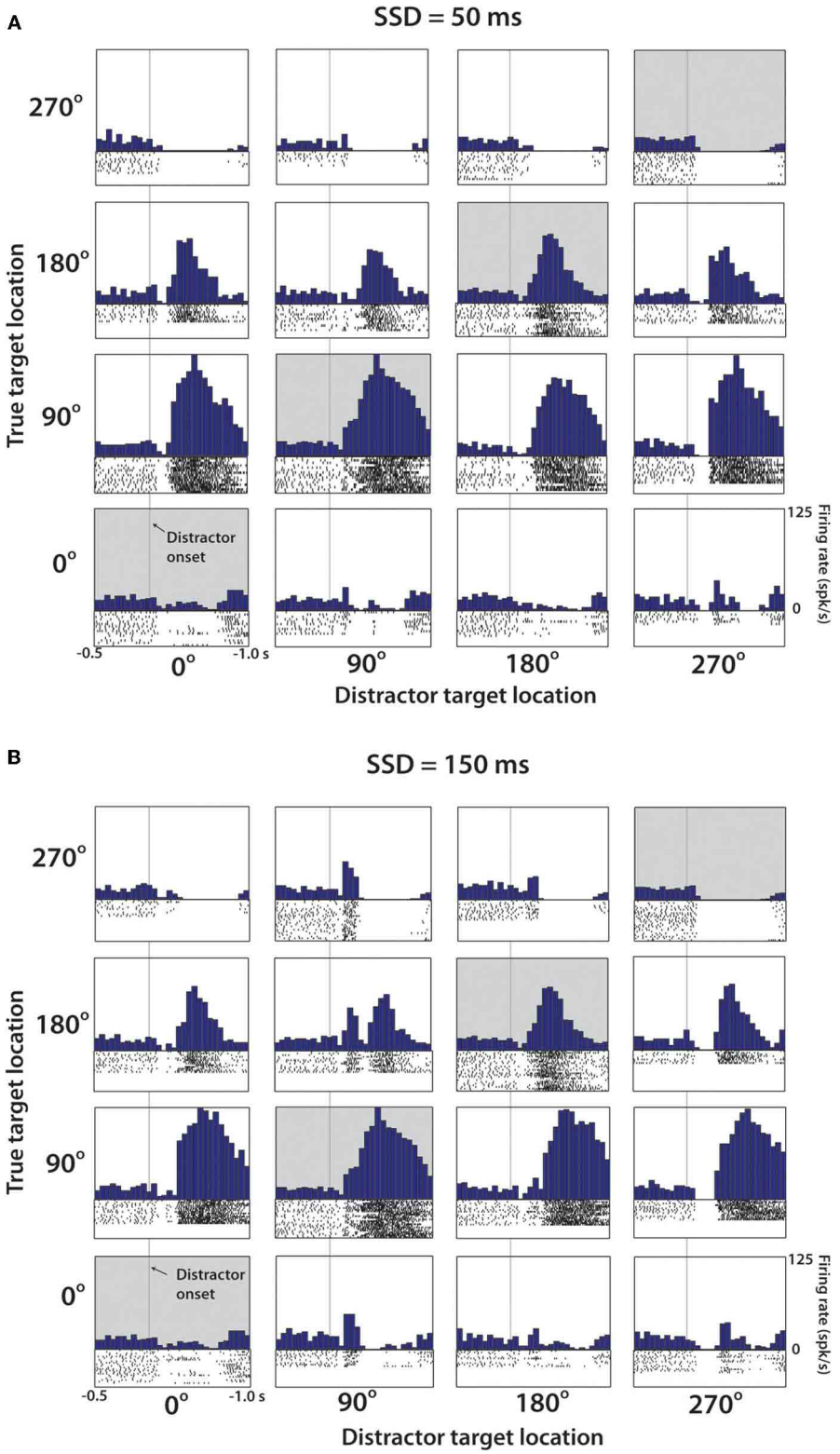

FIGURE 4 | Representative M1 neuron from Monkey M. (A) PETH aligned on distractor target onset from trials with SSD of 50 ms. Position within the 4 × 4 grid determined by the position of the distractor and true target. Along the diagonal (shaded), these PETHs are generated from no-switch trials. Units are in terms of firing rate, where the bin count is divided by the bin width (50 ms in each case). Spike rasters below each histogram indicate time stamps of spikes from all trials of this particular combination. **(B)** Same cell and analysis as **(A)**, with only difference being that data collected from trials with SSD of 150 ms.

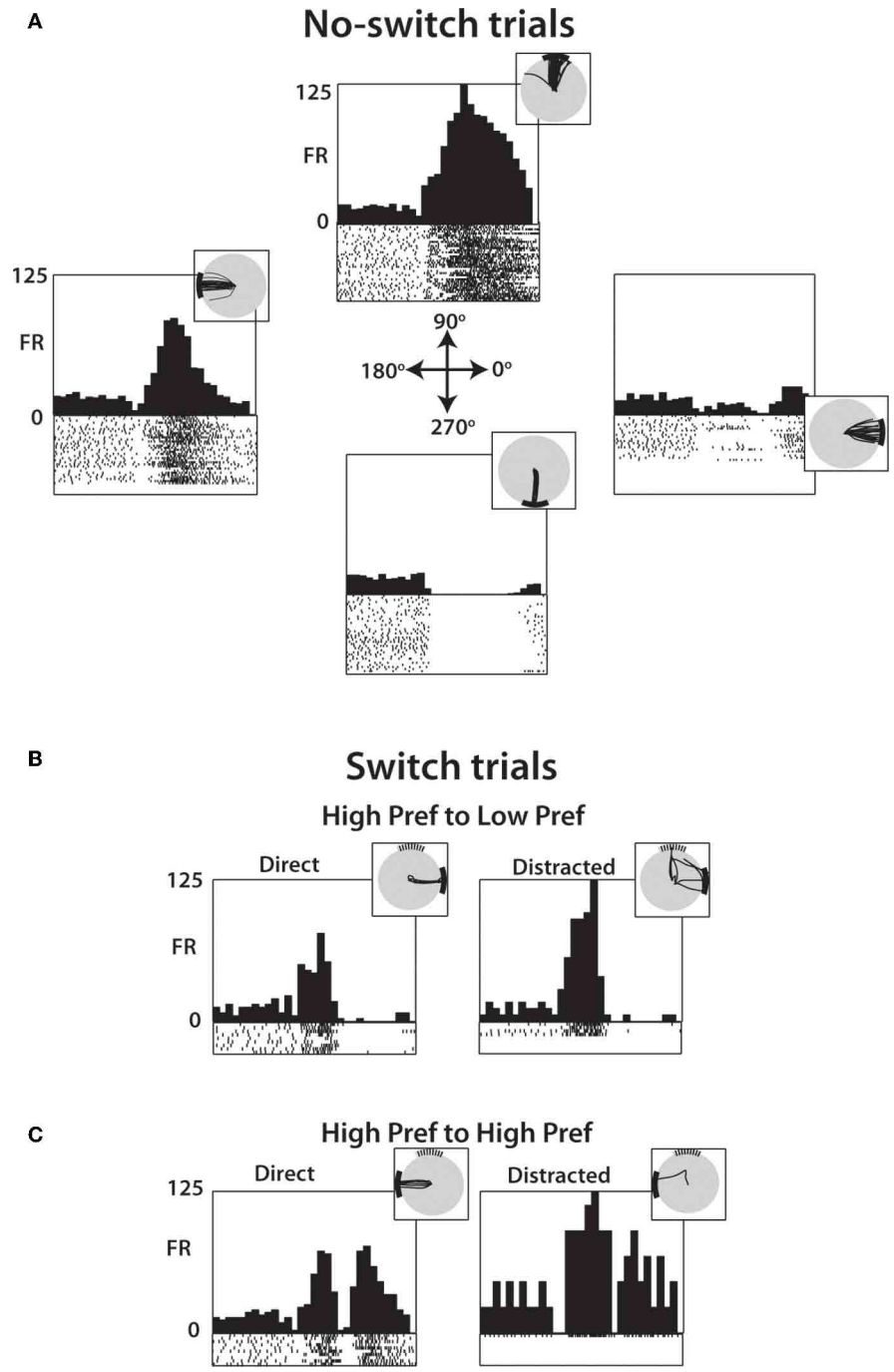

FIGURE 5 | PETH of a single M1 neuron during specific transitions after 250 ms SSD. (A) Neural activity from no-switch trials separated by target location shows directional preferences with PETH and single-trial raster plots (below PETH) aligned on distractor target onset. Inset shows cursor trajectory from trials to the specified target. **(B)** Among switch trials, PETH and raster plots generated from trials with distractor in one of the neuron's preferred direction (90°) and the true target in a non-preferred direction (0°). Data from both direct (left) and distracted (right) shown, with inset showing cursor traces. **(C)** Same as **(B)** except data drawn from trials where both the distractor and true target are in preferred directions (90° and 180°, respectively).

of true target and distractor target preference ranking on MFR (see Methods). At short SSDs (**Figure 7A**), the distractor coefficient never reaches the level of significance ($p > 0.05$), however, the true target is strongly represented. At both 150 ms and 250 ms SSDs (**Figures 7B,C**), the distractor contributes a smaller, but still significant amount to the MFR. The MFR, even 400 ms after the distractor disappears, is still influenced by both targets as seen by the lower left corner triangle seen in the 400–500 ms epoch in

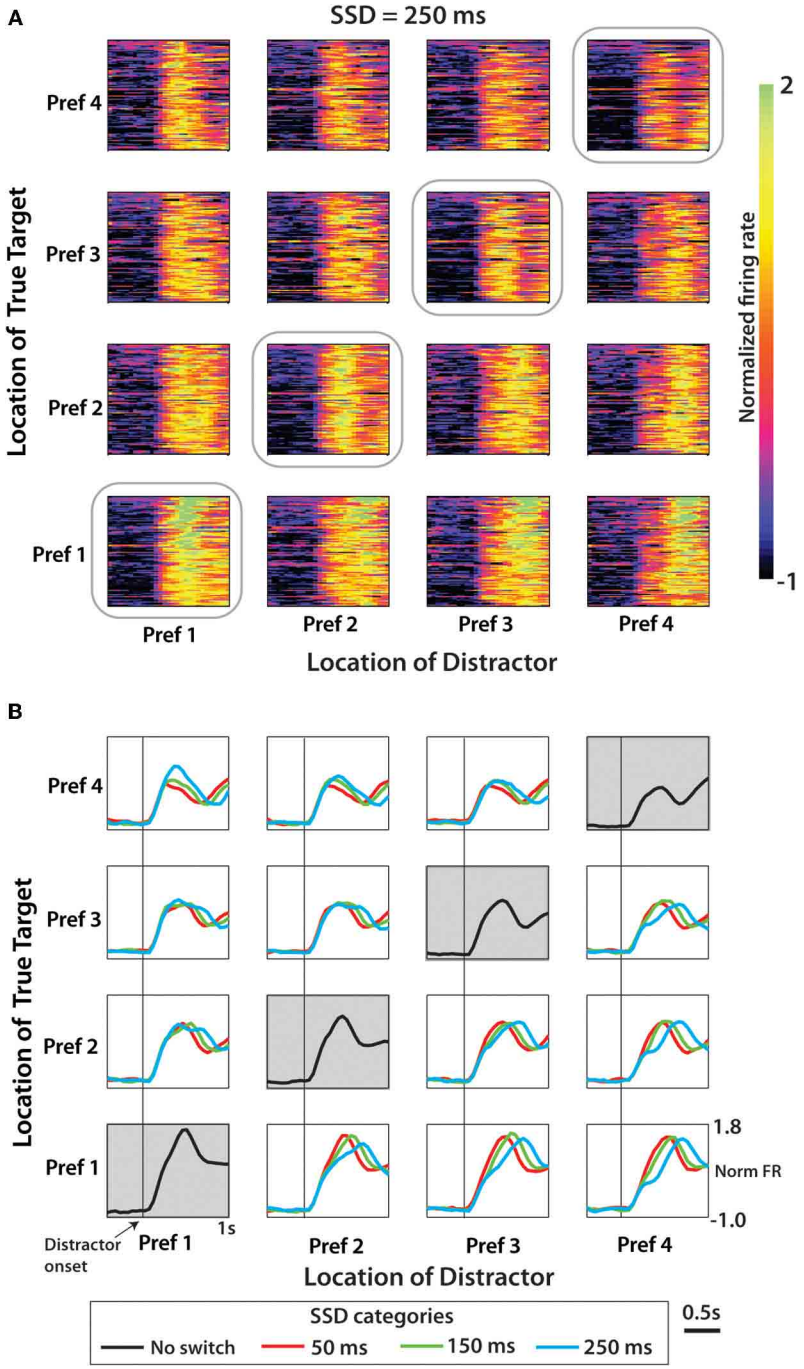

FIGURE 6 | Population activity from M1 neurons in Monkey M aligned on distractor target onset. (A) Normalized firing rate for each cell and each pairwise combination of distractor and true targets shown for the SSD of 250 ms condition. Amplitude of firing shown by color scale (on right) interpreted as the *z*-score. Position within the 4 × 4 grid for each cell determined separately according to directional preference order. Data along the diagonal is from no-switch trials. **(B)** Population mean PETH for each of the three SSD conditions. Time-series data averaged across neurons within a specific condition (within one box on the 4 × 4 grid) organized by neuron directional preference ranking. Along the diagonal is mean population PETH for no-switch trials.

Figures 7B,C. More generally, a transition occurs from distractor representation to true target representation.

Average PETHs were also used to analyze the difference in neuronal patterns between correctly and incorrectly performed switch trials. The strategy for separating trials into these two groups is described in the Methods. Average PETHs were calculated in the following steps. First, PETHs for each neuron were computed for each of 12 possible combinations of distractor and

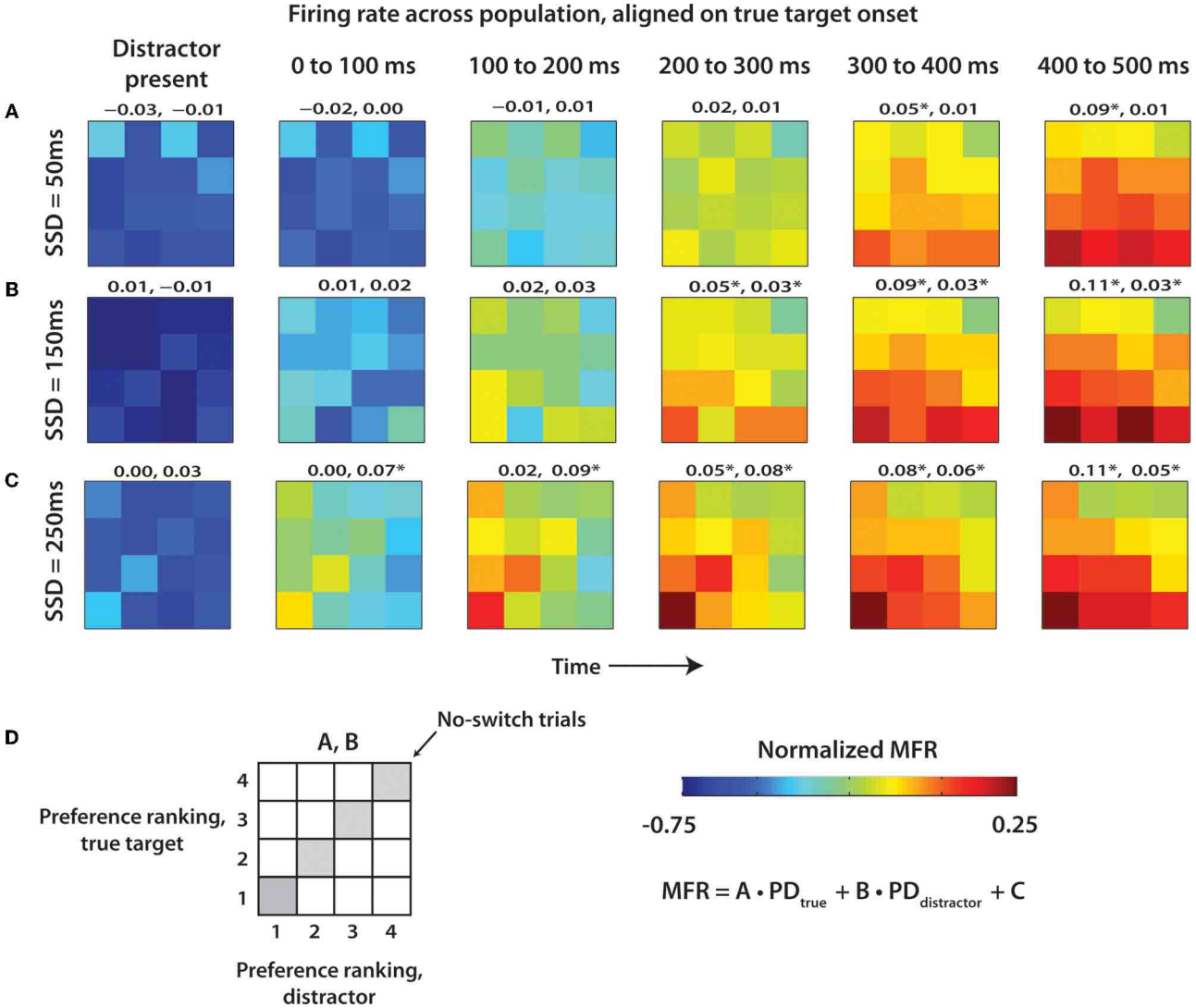

FIGURE 7 | Mean population firing rate as a function of distractor and true target locations. 4 × 4 grids showing population MFR for each target combination. Targets for each cell were ranked in terms of preferred direction as shown in **Figure 6**. 4 × 4 grids were computed for epochs throughout the trial, beginning with presence of the distractor. Six epochs are reflected by six time columns proceeding from left to right. Data from each of the SSD conditions was shown separately for 50 ms **(A)**, 150 ms **(B)**, and 250 ms **(C)**. MFR within each 4 × 4 grid was fit by a linear function of true and distractor preference ranking. Coefficients for true target and distractor target, respectively, are shown above each panel. **(D)** Layout of 4 × 4 grid, color scale, and linear regression equation.

true target locations. This computation was performed separately for correctly and incorrectly performed trials. Then, PETHs for correct trials were grouped together for all combinations and all neurons, and an overall average PETH was calculated. An average PETH for incorrect trials was calculated, as well. This computation assured that the averages were not biased by the proportions of correct and incorrect trials for different conditions. We chose to average across all conditions because the differences for such averages were not specific to certain combinations of target directions. As seen in **Figure 8**, the average PETHs differed depending on whether the monkeys successfully switched to the true target. More specifically, trials where the monkeys switched to the true target had lower initial slopes of firing rates than trials where the monkeys failed to reach to the true target. This effect was observed in both monkeys, both in M1 and S1 neurons. In monkey M, the neural activity in both M1 and S1 clearly rose before the target switch and more steeply in trials where the monkey failed to switch to the true target. In monkey N, the difference in FR slopes was more subtle and occurred later than in monkey M, which was likely related to the more variable behavior of that monkey (**Figure 2**).

Among rewarded trials, we analyzed neuronal representation of the target switch (**Figure 9**). To do this, the trial-averaged PETH for switch trials was directly compared with the PETH of no-switch trials (see Methods). As the metric for the neuronal representation of the switch, we used RMS differences between

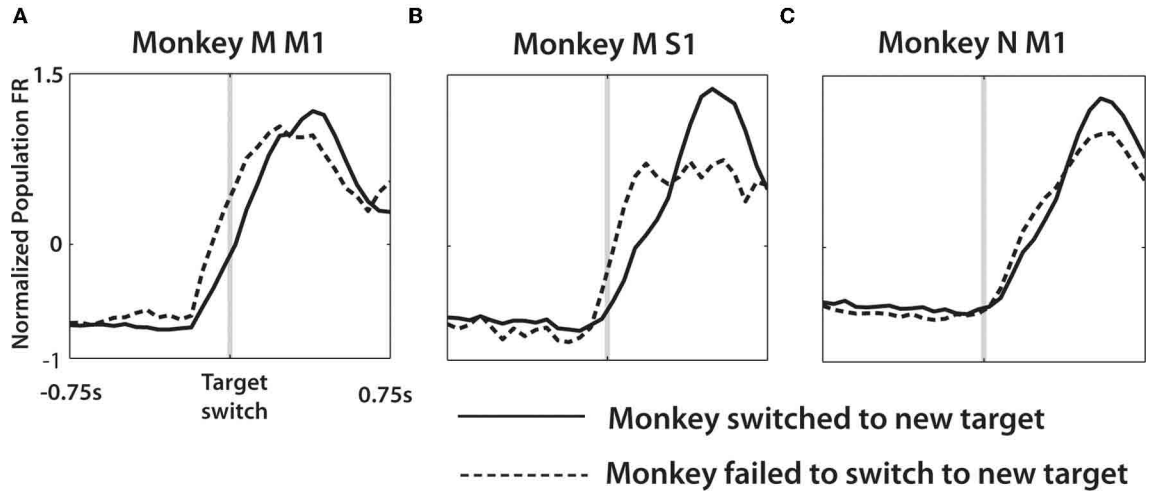

FIGURE 8 | Average population PETH differs depending on whether a switch is successfully made. Single neuron activity was averaged across all trials where the distractor was presented. Each such trial was categorized as either a successful switch (solid line), where the true target was reached, or unsuccessful (dashed line) when the monkey failed to reach the target and the trial was categorized as distracted (see Methods). Single neuron PETHs aligned on the true target onset, for both behavioral categories were then normalized to *z*-score and averaged across the population of monkey M M1 **(A)**, monkey M S1 **(B)**, and monkey N M1 **(C)**.

PETHs for the trials with no target switches (diagonal data in **Figures 4** and **6**) and the trials with target switches. **Figure 9A** shows RMS differences averaged across all possible locations of the distractor and true targets for each individual neuron, and **Figure 9B** shows the result of additional averaging across neurons in particular cortical areas. These averages depict the intervals when neuronal activity started to reflect the target switch from its initial position.

It is clear from **Figures 9A** and **B** that neurons represented target switch in M1 and S1 of both monkeys. Monkey M M1 population represented the timing of target switch for all tested SSDs, as evident from the latencies of the average curves (**Figure 9B**, left). S1 population of monkey M resolved the timing of the switch at 250 ms from the switches at 50 and 150 ms. The difference in switch timing was less clear in monkey N. Because of these representations of both the distracting and true targets by M1 and S1 neurons, we were able to extract target information from neuronal population activity.

EXTRACTION OF TARGET POSITION WITH LDA CLASSIFIER

An LDA classifier extracted the position of distractor (**Figure 10A**) and true (**Figure 10B**) targets from ensemble activity of M1 and S1 neurons. In the analysis depicted in **Figure 10**, predictions of target position were obtained from a short (150 ms) window slid along the task epoch. Behavioral trials were aligned on the distractor target onset in this analysis, and the LDA classifier was trained anew for each window position. Prediction accuracy was calculated as a fraction of correctly predicted target locations. The analysis was performed separately for 50, 150, 250 ms SSDs (red, green, and cyan traces, respectively) and no-switch trials (black trace). The LDA classifier revealed the changes in the representation of the distractor and true target locations as a function time. Note that the true target could be decoded with high accuracy despite the appearance of a distracting target. This accuracy approached 90% correct in monkey M and could be decoded nearly as fast with a distractor as without a distractor (**Figure 10B**). With longer SSDs, the ability to decode the true target remained similar but occurred at a longer latency. Such good decoding of the true target is not surprising given that the monkeys' overt behavior consisted of reaching movements to the true target. Future work should probe this decoding under real-time BMI control without overt behavior. The LDA model used for **Figure 10** included training data from all SSD conditions, as described in the Methods. We found that limiting training data to only no-switch trials reduced the fraction correct over all SSD groups and predicted parameters in monkey M M1 by 19.9% ($p < 0.01$, paired t-test), monkey M S1 by 6.8% ($p < 0.01$), and monkey N M1 by 4.2% ($p < 0.01$).

Consistent with the results of **Figure 7**, we observed that the representations of both the distractor and true targets outlasted the duration of target presence on the screen. In particular, the representation of the distractor lasted much longer than SSD (**Figure 10A**). Monkey M M1 ensemble provided the best predictions of the distractor target location, as it detected SSDs as short as 50 ms. SSDs of 150 and 250 ms were clearly represented by the M1 and S1 ensembles in monkey M and the M1 ensemble in monkey N. The duration of the distractor location representation increased with the increased SSD, and for all SSDs it extended well into the true target epoch when the distractor target was turned off. The onset of the representation of the true target matched the true target onset, and the prediction accuracy was higher for the true target than for the distractor target in all cases. The peak LDA predictions for distractor location from the monkey M M1 ensemble were 20.2% more accurate than those for monkey N M1 and 34.3% more accurate when predicting the true target.

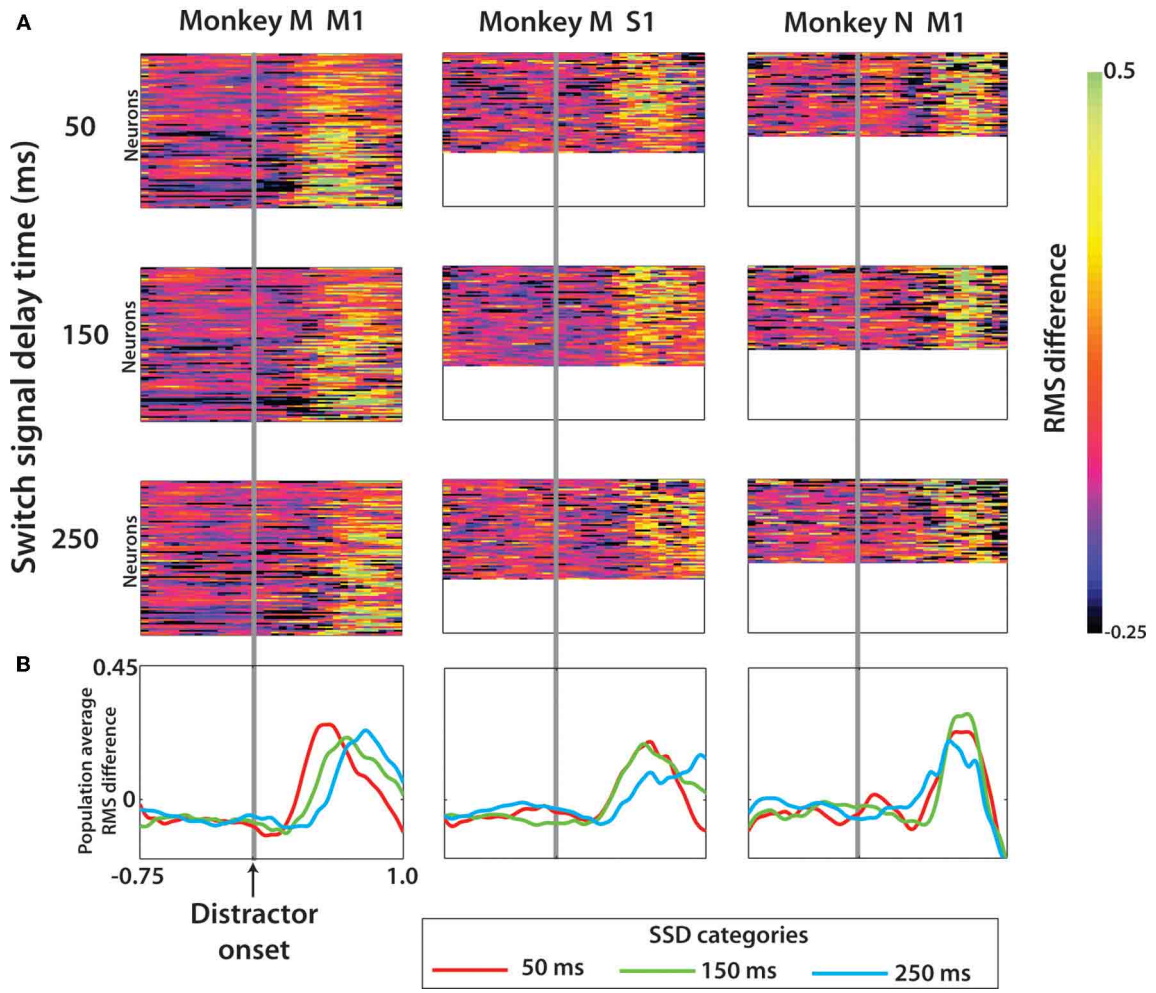

FIGURE 9 | Effect of a target switch on the firing rate in each of the three neuronal populations. (A) RMS difference computed for each cell (see Methods) at each time step from 0.75 s before to 1.0 s after distractor target onset. Data shown separately for three SSD groups, with rows 1–3 the cell RMS difference for trials SSD of 50, 150, and 250 ms, respectively. Within each panel, the rows of the color plot indicate one single cell and the row height was fixed in all three cell groups (the three columns). The panel size is thus a reflection of the number of neurons in this population. **(B)** The population average RMS difference was computed from each panel in **(A)**.

To clarify whether this was the effect of different ensemble sizes, we repeated the analysis of **Figures 10A,B** for monkey M and N M1 populations using equally-sized subsets of each ($n = 35$ neurons; not shown in figure). We found that the prediction performance disparity in **Figure 10A** between the two monkeys became less pronounced (monkey M M1 now only 9.9% more accurate in predicting distractor location), but still existed, when using $n = 35$ neurons for both. The difference between the two groups in **Figure 10B** remained approximately the same (monkey M M1 now 33.1% more accurate than monkey N M1 in predicting true target location). From this we conclude that the size of the neuronal population was one contributing factor to LDA performance, but there were other factors as well, such as more erratic performance of monkey N and characteristics of recorded neuronal populations.

Since the predictions of the distractor target location by M1 and S1 ensembles could simply reflect the fact that in a portion of trials monkeys initiated movements to that target, we separately analyzed the trials in which the monkeys moved directly toward the true target (direct trials; **Figures 11A,C,D**) and those in which the presence of the distractor affected the movement trajectory (distracted trials; **Figures 11B,E,F**). After the direct trials were separated, the predictions remained similar to those shown in **Figure 10**, indicating that cortical populations represented the distractor target even when the monkey did not produce movements toward that target. Curiously, monkey M M1 and S1 ensembles predicted the distractor target location even better when that monkey made straight movements to the true target. This was likely related to the predominance of such direct trials in the training data, resulting in a better prediction model. An opposite effect was observed for monkey N, presumably because it produced less direct movements. The predictions of the true target were similar for direct and distracted trials, and similar to the predictions shown in **Figure 10**. Note that the predictions of

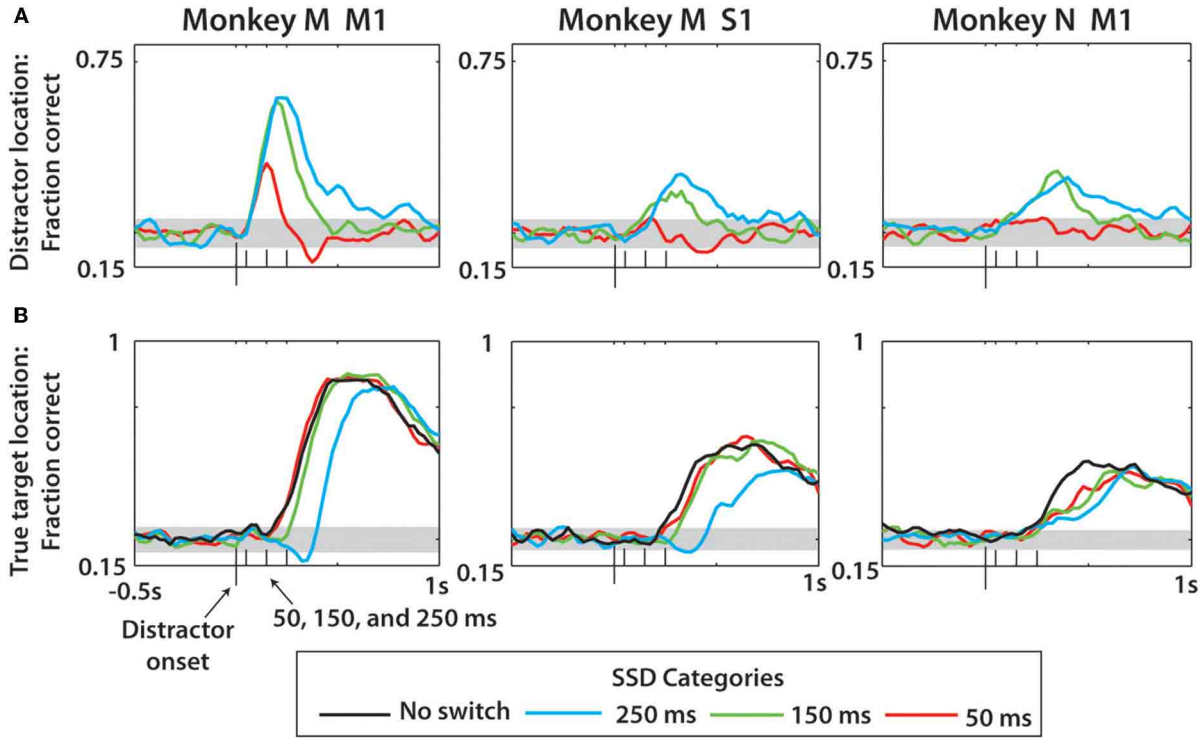

FIGURE 10 | Prediction of distractor and true target locations using neural activity and LDA classification over all trials. (A) Prediction of distractor location for each of the three neuronal populations (columns). Within each panel, fraction correct data represents LDA fraction correct minus the same predictions with the trial data shuffled, then again adding chance level performance (0.25) (see Methods). **(B)** Prediction of true target location, which is the second target in the case of switch trials but the first in no-switch trials. In addition to three SSD groups, the no-switch prediction is shown for comparison. Gray horizontal bands indicate the 95% confidence intervals as determined by the 1-proportion *z*-test. On *x*-axis are four ticks representing the distractor onset (largest tick) and the three SSDs (50, 150, 250 ms).

the distractor location for the shortest, 50 ms, SSD were much less accurate compared to the difference plots of **Figure 9**. This was because the LDA training data, unlike the **Figure 9** data, included all possible SSDs, as well as no-switch trials. The model had to generalize to all these conditions, which led to less accurate predictions for less represented cases. When 50 ms SSDs were analyzed separately by an LDA, the predictions improved (not shown).

In addition to the distractor and true target location, we trained an LDA classifier to predict the target switch signal as a binary variable (**Figure 12**). Along the task interval, predictions of the distractor and true target locations were made concurrently to serve as a temporal reference. As shown in **Figure 12A**, the strongest predictions made by LDA were for the true target in each case. Both monkey N and M M1 populations represented the distracting target with approximately equal facility relative to the true target representation. Overall, the predictions were less robust that those predicted when separated by SSD (**Figure 10**) and behavior (**Figure 11**). This was a result of computing the fraction correct of all three SSD groups collectively, rather than separately. This caused the less strongly predicted 50 ms SSD trials to reduce the classifier performance overall. As shown in **Figure 9**, the temporal profile of neural activity is strongly dependent on the SSD of a given trial. Target switch was moderately decoded in all three populations, each time with the peak occurring in the span between distractor and true target representations. The exact timing of the switch signal representation is dependent on the SSD and thus the peaks that are present in **Figure 12** represent approximate event epochs. The variation on when the target switch occurs relative to the distractor onset—the time which all data is aligned to—is likely a contributing factor to the low fraction correct. If a single SSD were to be used, the switch event detection would likely occur in the SSD-dependent windows found in **Figure 9B**. The strongest representation of both the distractor and the switch event (note the scale difference) were obtained from monkey M M1 neurons. This is consistent with our previous data and strongly correlates with the higher number of quality recorded neural units in the Monkey M M1 population. Furthermore, the binary classification of switch vs. no-switch trial was evaluated in terms of the MCC (**Figure 12B**). In all three neuronal populations, the peak MCC for the switch detection occurred within 700 ms of the distractor onset, although MCC begins to rise as early as 300 ms in monkey M M1. The performance of detecting the switch event was strongest among M1 cells, with peak MCC of 0.19 (monkey M) and 0.23 (monkey N), respectively. Thus, the neural basis for motor plan switching can itself be decoded from ensembles of M1 and S1 neurons.

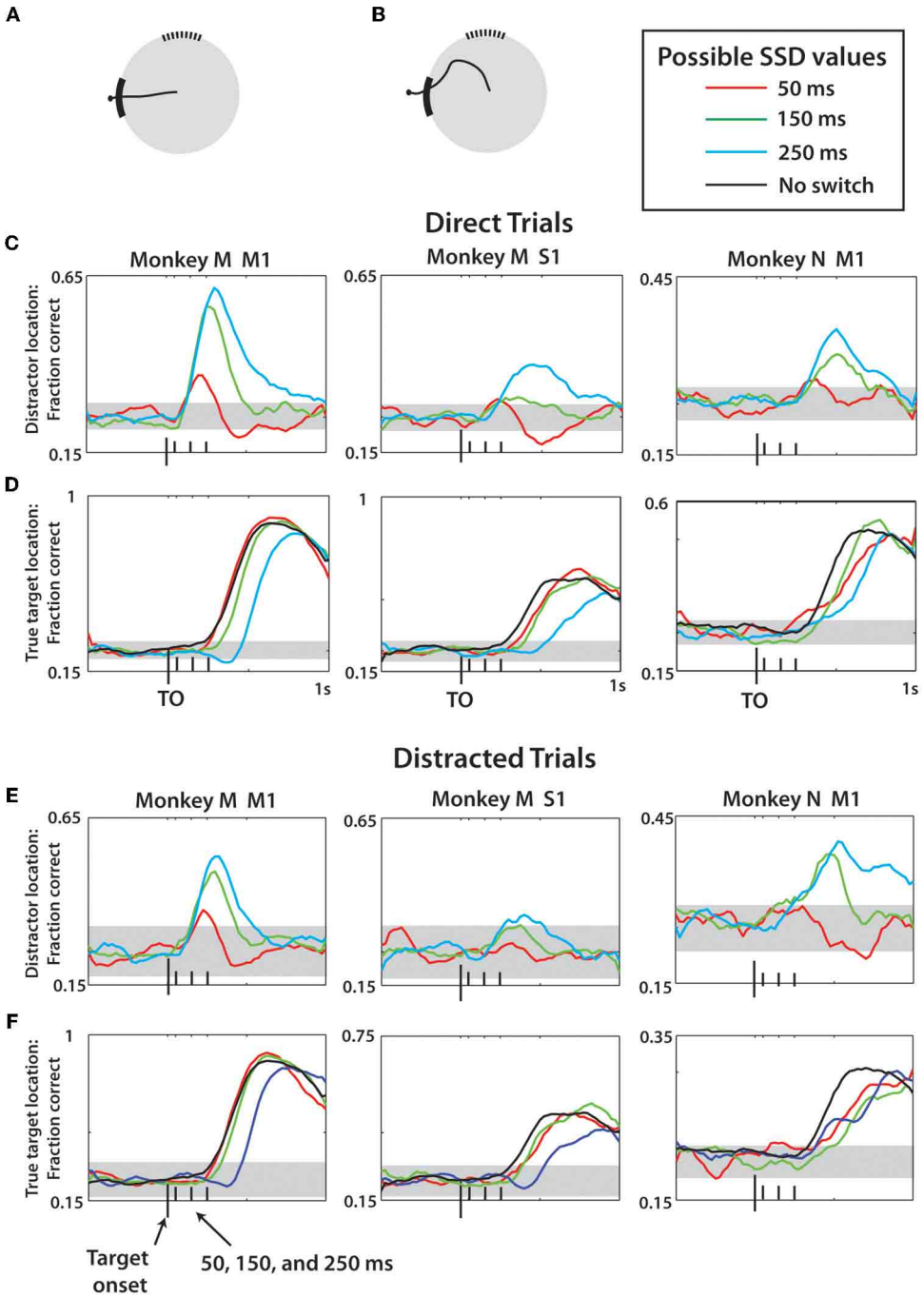

FIGURE 11 | LDA prediction of distractor and true target separated by movement type. (A) Example of a direct trial. **(B)** Example of a distracted trial—see Methods for more details. For **(C–F)**, the prediction methods and display are the same as **Figure 10**. All reported data is actual fraction correct minus fraction correct from shuffled data, plus chance level fraction correct (0.25). **(C,D)** Predictions of distractor **(C)** and true **(D)** target location made using data only drawn from direct trials for monkey M M1, monkey M S1, and monkey N M1 (left to right). Different SSD groups denoted by colors, see Legend. **(E,F)** Same as **(C,D)** except data reflects only predictions made for distracted trials. Horizontal gray bands indicate 95% confidence intervals generated by 1-proportion *z*-test.

DECODING OF CURSOR AND TARGET POSITION USING WIENER FILTER

We next utilized a continuous linear decoding algorithm, the Wiener filter, to predict cursor and true target position at a 10 Hz output rate throughout the session (**Figure 13**). A representative 25 s window of predicted parameters, along with actual parameter values is shown in **Figures 13A–D** for Monkey M. Cursor X and Y were predicted with high correlation to actual movements in monkey M (X: R = 0.84; Y: R = 0.86) and moderate correlation

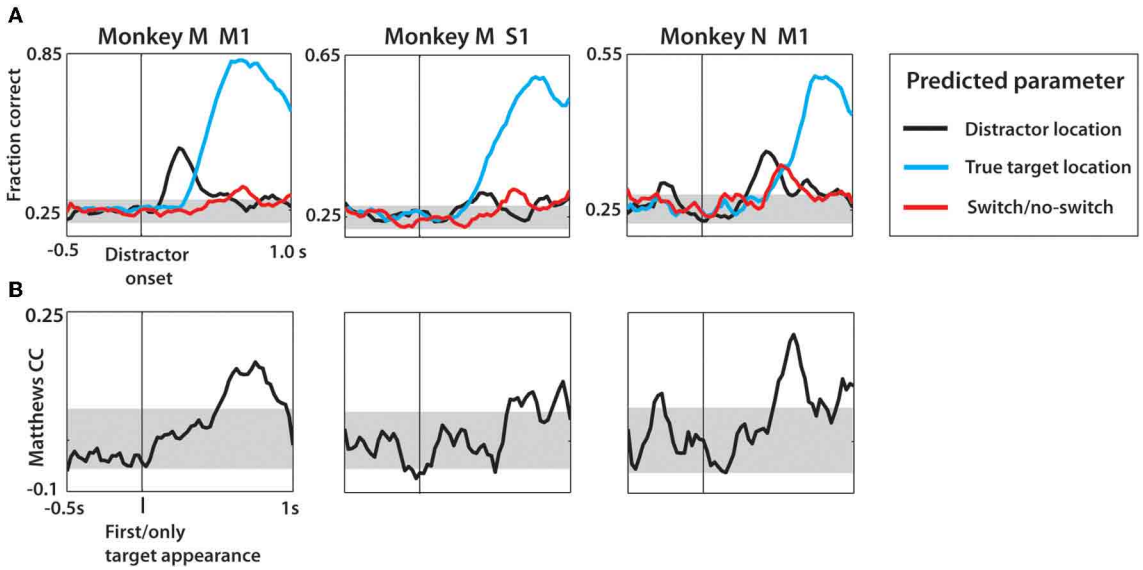

FIGURE 12 | Decoding of target location and switch/no-switch occurrence from neural activity during task interval, not separated by SSD. (A) Linear discriminant analysis predictions of location of distractor target (black) and second target (cyan) as well as switch/no-switch (red). Data aligned on distractor onset shown with vertical black line. Values shown are fraction correct prediction at each time step of the sliding window. Gray horizontal band is the 95% confidence interval generated using the 1 proportion *z*-test. **(B)** Matthews correlation coefficient shown over the task interval. Data are aligned on the distractor appearance. Confidence interval generated from mean ± 2 standard deviations obtained from distribution of MCC from data with shuffled group information prior to LDA predictions.

in monkey N (X: R = 0.49; Y: R = 0.33). Computing the predicted radial movement, *r*, resulted in clear peaks indicating predicted reach events (**Figure 13B**). True target location was decoded very effectively (**Figure 13C**). To quantify this, predictions aligned on threshold crossing of *r* were made (see Methods). We found that the threshold crossing event occurred often within 700 ms after the true target appeared in both monkeys (**Figures 13D,E**). Performance of cursor and true target location predictions remained consistent for approximately 500 ms after threshold crossing, before declining. (**Figures 13D,E**, insets). In both monkeys, the cursor position was predicted highly effectively (up to 99%, monkey M; 59% monkey N). Prediction of true target position was strong from Monkey M (up to 59%), but was much weaker for monkey N (up to 26%). Chance level prediction in this case was 20% due to four potential target locations and one condition where the target was not on the screen. The results from this continuous approach agree with the findings using a discrete LDA classifier. Furthermore, the analysis of **Figure 13** provides evidence that the results of this study could be implemented into BMI systems to continuously extract intended reach locations.

DISCUSSION

In this study we examined M1 and S1 ensemble activity recorded in a motor task that required reprogramming of center-out reaching movements to visual targets. This was achieved by changing the target location in the midst of the RT period (Georgopoulos et al., 1981, 1983). We hypothesized that BMI decoding algorithms could dissociate representations of potential and selected motor targets from the activity of sensorimotor cortex ensembles. We found that locations of distracting targets presented shortly before the true targets of movements were indeed represented by M1 and S1 ensembles and could be extracted by an LDA classifier. The LDA results were recapitulated using a continuous Wiener filter which extracted cursor and target location. These results suggest that real-time BMI decoders could be implemented in the future to decode motor programming and decision making under the conditions of multiple potential choices.

Despite the behavioral differences between the two monkeys in this study, as is common in primate studies, both helped to elucidate behavioral responses and the neural basis for transient distractors. In our previous study (Ifft et al., 2011) we overtrained these monkeys to perform center-out movements with high accuracy when no distractor was used. In monkey N, the distractor markedly changed movement trajectories. Thus the distractor and true target locations were represented by both the overt behavior and cortical modulations. Monkey M was less distracted and the cortical effect of a change in motor plan could be studied, even when movements to the first target were wholly absent.

SENSORIMOTOR CORTEX AND REPROGRAMMING MOVEMENTS

Neural processes of motor program selection and cancellation has received much attention during the last two decades of research. The summary of this body of work suggests that different aspects of sensorimotor transformations that involve multiple potential choices are processed by multiple cortical and subcortical areas (Crammond and Kalaska, 1994; Shen and Alexander, 1997; Lee and Assad, 2003). Here we recorded ensemble activity in M1

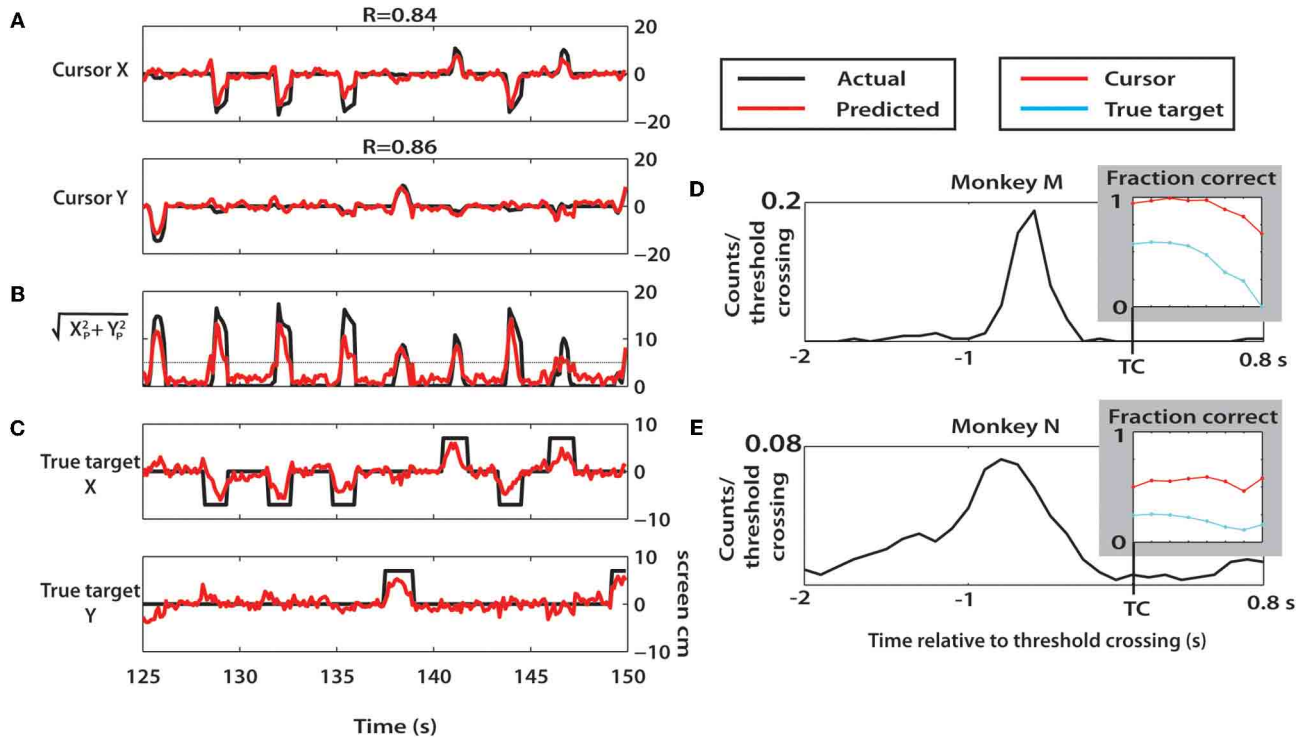

FIGURE 13 | Offline Wiener filter predictions of cursor and target locations. (A–D) A 25 s epoch of trials during a session with monkey M. **(A)** Cursor X and Y positions (black) and corresponding Wiener predictions (red) during selected epoch. **(B)** The radial distance of the predicted cursor location was computed and plotted versus time. Reach threshold level of 5 cm is shown as horizontal gray line. **(C)** True target X and Y position during selected epoch (black) and Wiener predictions (red). **(D,E)** Probability distribution of the time of true target onset relative to threshold crossings from monkey M **(D)** and monkey N **(E)**. Inset: fraction correct predictions of cursor and true target location during the 0 to 0.8 s epoch beginning with threshold crossing.

and S1—the areas most closely reflecting the final motor output that results from decision making. Consistent with previous work (Alexander and Crutcher, 1990) we observed M1 activity that represented potential motor targets even when no movement was initiated toward those targets. This representation persisted well beyond distractor disappearance and the termination of this encoding coincided with the onset of the robust second (true) target representation. Somewhat surprisingly, we observed moderate movement and pre-movement modulation in S1—an area whose primary function is commonly assumed to be related with sensory processing, but also known to be activated in advance of movements (Soso and Fetz, 1980; Nelson et al., 1991; Lebedev et al., 1994) and encode information about potential reach targets (Ifft et al., 2011).

Here we cannot resolve whether representation of potential targets that we observed in M1 and S1 merely reflected inputs from associative areas that were the primary players in target selection (Thaler and Goodale, 2011) or M1 and S1 constituted an integral part of a distributed network with less clearly defined hierarchy (Shen and Alexander, 1997; Hernandez et al., 2010). Visuomotor information has been shown to be encoded by cortial visual processing networks in parietal (Kertzman et al., 1997; Wise et al., 1997; Baumann et al., 2009), premotor (Crammond and Kalaska, 1994; Lebedev and Wise, 2000; Cisek and Kalaska, 2002), and prefrontal (Genovesio et al., 2005; Lebedev et al., 2005) areas. These associative areas could act as filters of sensory information that is subsequently signaled to M1 output areas. The exact mechanisms of interactions between non-primary and primary areas will have to be elucidated by future investigations.

Our previous unpublished observations indicate that certain initial stages of target selection for a movement goal have to take place for target information to start to be represented in M1 and S1. In that experiment, animals had to deal with two targets that appeared on the screen simultaneously instead of in rapid succession. One of the targets was large, and the other was small. The monkeys would be rewarded for reaching to either of the targets, but they typically selected the larger target because it was easier to hit with the cursor. In contrast to the results from our distractor experiments reported here, in the unpublished study M1 and S1 neurons represented the non-chosen target in a much more subtle way, with less than 10% of recorded cells exhibiting any significant directional tuning to its location. This observation, in the context of the results of the present study, suggests that M1 and S1 representation of movement direction is much stronger when the motor goal is chosen, even if only for several hundred milliseconds.

Serial activation of M1 during motor sequences has been well-studied (Fu et al., 1995; Tanji, 2001) and the results of our study suggest that the manifestation of change-of-decision in the motor

cortex is a sequential, but somewhat overlapped representation of distinct motor plans. In other words, sensorimotor cortex represents selected motor targets, but movements to those targets can still be canceled. Such movement cannot be canceled if M1 activity is already elevated and has reached a certain motor initiation threshold (**Figure 8**) (Hanes and Schall, 1996; Wong-Lin et al., 2010).

A prominent model to describe the change-of-decision is a bounded form of the accumulator model (Vickers and Smith, 1985), drift-diffusion model, or race model with criterion boundaries for both initial decision and change of decision events (Resulaj et al., 2009). Applying this model to neurophysiology of sensorimotor neurons, one hypothesis would be that the firing rate of a single neuron or entire neuronal populations would encode the degree of commitment to the specific motor plan. Lower levels of activity would elongate the decision window while additional evidence is accumulated, even if a different movement had been initiated. To address this hypothesis our study compared population activity between a subset of trials where the true target was successfully reached versus trials where an error in behavioral outcome was caused by the transient distractor presence. Whether this lower population activity is causal to the behavioral differences is beyond the scope of this study. However, our results reinforce this model by showing lower initial population activity and more gradual FR slope between distractor target presentation and movement initiation on trials where the switch was successfully made (**Figure 8**). Such differences in population activity may provide intuitive understanding for the ability to detect the switch/no-switch event using neural activity from single trials (**Figure 12B**) with high fidelity.

DECODING MOTOR REPROGRAMMING

Here we used a rather simple LDA decoder that extracted target and target switch information from both cortical activity and the timing of the distractor target onset. This decoder was useful to describe the representation of targets by neuronal activity as a function of time. A practical decoder will have to extract target onset, as well. Our BMI approach added an interesting twist to our experiments because information extracted from different parts of sensorimotor hierarchy could be used to retrain brain circuitry. For instance, learning a BMI task that involves extraction of target information may result in an enhanced representation of such information in M1. Additionally, non-primary areas should be considered as sources of information about multiple potentials targets (Snyder et al., 1998; Cisek and Kalaska, 2002, 2005) for a practical real-time decoder. With the current approach, we were able to extract the location of distractor targets from the primary sensorimotor cortical activity even if those targets were presented for a brief period of time (as short as 50 ms) and if no movement was initiated to that target. It is important to emphasize that under this same condition, the true target to which the monkeys moved was also decoded very accurately.

As the BMI field advances, practical, versatile neuroprosthetics based on BMI technology become a real possibility (Lebedev and Nicolelis, 2006; Nicolelis and Lebedev, 2009; Gilja et al., 2011; Jackson and Fetz, 2011; Lebedev et al., 2011). The need for practical clinical applications that provide higher degree of freedom control (Velliste et al., 2008) and expanded decoding strategies (Zacksenhouse and Nemets, 2008) will drive BMI research to expand into more complex motor programs. Naturally enacted movements require the flexibility to rapidly modify upcoming motor plans. Such a behavior capability was reflected in the neuronal data we collected in the present study. The ability to decode such changes has critical implications for not only accuracy but also safety in the execution of everyday movements by a prosthetic device controlled by brain activity.

Our present experimental approach, based on a discrete rather than continuous decoder, adds to previous literature where similar ideas were evaluated under the framework of a potential cognitive neuroprosthetic (Musallam et al., 2004; Pesaran et al., 2006). A cognitive neuroprosthetic extracts from brain activity information that is different from motor execution signals and utilizes it to improve the performance. For example, a high-performance BMI proposed by Santhanam et al. (2006) extracted target location from delay-period activity recorded in dorsal premotor cortex and thereby obtained information transfer rate of up to 6.5 bits per second. Additional improvements may come from hybrid BMI designs that utilize both single-unit recordings and local field potentials (LFPs). Thus, Hwang and Andersen (Hwang and Andersen, 2009) decoded movement onset from LFPs while decoding movement direction from single-unit activity.

Hasegawa et al. (Hasegawa et al., 2006, 2009) implemented decoding algorithms that served a similar purpose that we describe here. They decoded go/no go decisions from the activity of 2–5 neurons recorded in monkey superior colliculus and were able to extract multidimensional decisions (e.g., go/no go for two potential movement directions). The information was accessed approximately 150 ms after cue onset, which is consistent with our present results and the results of Santhanam et al. (2006). Given a high interest to neurophysiological mechanisms of response inhibition (Hanes and Schall, 1995; Pare and Hanes, 2003; Chen et al., 2010; Scangos and Stuphorn, 2010; Mirabella et al., 2011), it is reasonable to expect that BMIs that extract response inhibition and response reprogramming information will continue to develop.

VERSATILE BMIs OF THE FUTURE

The original conception of BMI systems strive to mimic normal functions of the brain as closely as possible (Nicolelis, 2001). The approach that we propose here can be generally characterized as a BMI with impulsivity control. Impulsivity is a person's inability to inhibit unwanted actions (Basar et al., 2010; Kim and Lee, 2011). Prefrontal mechanisms are normally responsible for such inhibition in primates (Miller, 2000; Krawczyk, 2002; Kim and Lee, 2011). It is conceivable that practical BMIs of the future will need an inhibition control module to operate properly. Moreover, such a module may become one of the essential elements of the design. It may not only examine potential actions and select those that fit the context and are wanted by the user, but also set the limits to volitional control. In the past, we have already

proposed that such an optimal design may be based on a shared-control BMI, i.e., one that gives the user control over higher-order goals and delegates lower-order controls to the robotic controller (Kim et al., 2006). A prominent role of prefrontal cortex is executive function, such as the one required for inhibition of potential actions. Future work could seek to exploit the multiple levels of control within the brain to not only recreate naturalistic movements, but at the same time streamline the transitions and selections from the many possible behavioral outcomes. Certainly this goal is challenging, but we remain optimistic in light of recent developments in the fast growing field of neuroprosthetics.

ACKNOWLEDGMENTS

We are grateful for the work of Gary Lehew in the building of the experimental setup and the multielectrode arrays; Dragan Dimitrov and Laura Oliveira for conducting neurosurgeries; Tamara Phillips for experimental support; Susan Halkiotis for administrative support. This work was supported by R01NS073952, R01NS073125, and RC1HD063390 to Miguel A. L. Nicolelis and Award Number DP1OD006798 from the Office of the Director, National Institutes of Health to Miguel A. L. Nicolelis. The content is solely the responsibility of the authors and does not necessarily represent the official views of the Office of the Director or NIH.

REFERENCES

Afshar, A., Santhanam, G., Yu, B. M., Ryu, S. I., Sahani, M., and Shenoy, K. V. (2011). Single-trial neural correlates of arm movement preparation. *Neuron* 71, 555–564.

Alexander, G. E., and Crutcher, M. D. (1990). Neural representations of the target (goal) of visually guided arm movements in three motor areas of the monkey. *J. Neurophysiol.* 64, 164–178.

Andersen, R. A., Musallam, S., and Pesaran, B. (2004). Selecting the signals for a brain-machine interface. *Curr. Opin. Neurobiol.* 14, 720–726.

Awiszus, F. (1997). Spike train analysis. *J. Neurosci. Methods* 74, 155–166.

Baker, J. T., Donoghue, J. P., and Sanes, J. N. (1999). Gaze direction modulates finger movement activation patterns in human cerebral cortex. *J. Neurosci.* 19, 10044–10052.

Balan, P. F., and Ferrera, V. P. (2003). Effects of gaze shifts on maintenance of spatial memory in macaque frontal eye field. *J. Neurosci.* 23, 5446–5454.

Baldi, P., Brunak, S., Chauvin, Y., Andersen, C. A., and Nielsen, H. (2000). Assessing the accuracy of prediction algorithms for classification: an overview. *Bioinformatics* 16, 412–424.

Band, G. P., and van Boxtel, G. J. (1999). Inhibitory motor control in stop paradigms: review and reinterpretation of neural mechanisms. *Acta Psychol. (Amst.)* 101, 179–211.

Basar, K., Sesia, T., Groenewegen, H., Steinbusch, H. W., Visser-Vandewalle, V., and Temel, Y. (2010). Nucleus accumbens and impulsivity. *Prog. Neurobiol.* 92, 533–557.

Baumann, M. A., Fluet, M. C., and Scherberger, H. (2009). Context-specific grasp movement representation in the macaque anterior intraparietal area. *J. Neurosci.* 29, 6436–6448.

Birbaumer, N., Murguialday, A. R., and Cohen, L. (2008). Brain-computer interface in paralysis. *Curr. Opin. Neurol.* 21, 634–638.

Boussaoud, D., Barth, T. M., and Wise, S. P. (1993). Effects of gaze on apparent visual responses of frontal cortex neurons. *Exp. Brain Res.* 93, 423–434.

Boussaoud, D., and Bremmer, F. (1999). Gaze effects in the cerebral cortex: reference frames for space coding and action. *Exp. Brain Res.* 128, 170–180.

Carmena, J. M., Lebedev, M. A., Crist, R. E., O'Doherty, J. E., Santucci, D. M., Dimitrov, D. F., Patil, P. G., Henriquez, C. S., and Nicolelis, M. A. (2003). Learning to control a brain-machine interface for reaching and grasping by primates. *PLoS Biol.* 1:E42. doi: 10.1371/journal.pbio.0000042

Chapin, J. K. (2004). Using multi-neuron population recordings for neural prosthetics. *Nat. Neurosci.* 7, 452–455.

Chase, S. M., and Schwartz, A. B. (2011). Inference from populations: going beyond models. *Prog. Brain Res.* 192, 103–112.

Chen, X., Scangos, K. W., and Stuphorn, V. (2010). Supplementary motor area exerts proactive and reactive control of arm movements. *J. Neurosci.* 30, 14657–14675.

Churchland, M. M., Yu, B. M., Sahani, M., and Shenoy, K. V. (2007). Techniques for extracting single-trial activity patterns from large-scale neural recordings. *Curr. Opin. Neurobiol.* 17, 609–618.

Cisek, P., and Kalaska, J. F. (2002). Simultaneous encoding of multiple potential reach directions in dorsal premotor cortex. *J. Neurophysiol.* 87, 1149–1154.

Cisek, P., and Kalaska, J. F. (2005). Neural correlates of reaching decisions in dorsal premotor cortex: specification of multiple direction choices and final selection of action. *Neuron* 45, 801–814.

Cisek, P., and Kalaska, J. F. (2010). Neural mechanisms for interacting with a world full of action choices. *Annu. Rev. Neurosci.* 33, 269–298.

Cohen, Y. E., and Andersen, R. A. (2002). A common reference frame for movement plans in the posterior parietal cortex. *Nat. Rev. Neurosci.* 3, 553–562.

Crammond, D. J., and Kalaska, J. F. (1994). Modulation of preparatory neuronal activity in dorsal premotor cortex due to stimulus-response compatibility. *J. Neurophysiol.* 71, 1281–1284.

Fetz, E. E. (2007). Volitional control of neural activity: implications for brain-computer interfaces. *J. Physiol.* 579, 571–579.

Fisher, R. A. (1936). *Statistical Methods for Research Workers.* Edinburgh, London: Oliver and Boyd.

Fitzsimmons, N. A., Lebedev, M. A., Peikon, I. D., and Nicolelis, M. A. (2009). Extracting kinematic parameters for monkey bipedal walking from cortical neuronal ensemble activity. *Front. Integr. Neurosci.* 3:3. doi: 10.3389/neuro.07.003.2009

Fu, Q. G., Flament, D., Coltz, J. D., and Ebner, T. J. (1995). Temporal encoding of movement kinematics in the discharge of primate primary motor and premotor neurons. *J. Neurophysiol.* 73, 836–854.

Genovesio, A., Brasted, P. J., Mitz, A. R., and Wise, S. P. (2005). Prefrontal cortex activity related to abstract response strategies. *Neuron* 47, 307–320.

Georgopoulos, A. P., Kalaska, J. F., Caminiti, R., and Massey, J. T. (1983). Interruption of motor cortical discharge subserving aimed arm movements. *Exp. Brain Res.* 49, 327–340.

Georgopoulos, A. P., Kalaska, J. F., and Massey, J. T. (1981). Spatial trajectories and reaction times of aimed movements: effects of practice, uncertainty, and change in target location. *J. Neurophysiol.* 46, 725–743.

Gilja, V., Chestek, C. A., Diester, I., Henderson, J. M., Deisseroth, K., and Shenoy, K. V. (2011). Challenges and opportunities for next-generation intracortically based neural prostheses. *IEEE Trans. Biomed. Eng.* 58, 1891–1899.

Hanes, D. P., and Schall, J. D. (1995). Countermanding saccades in macaque. *Vis. Neurosci.* 12, 929–937.

Hanes, D. P., and Schall, J. D. (1996). Neural control of voluntary movement initiation. *Science* 274, 427–430.

Hasegawa, R. P., Hasegawa, Y. T., and Segraves, M. A. (2006). Single trial-based prediction of a go/no-go decision in monkey superior colliculus. *Neural Netw.* 19, 1223–1232.

Hasegawa, R. P., Hasegawa, Y. T., and Segraves, M. A. (2009). Neural mind reading of multi-dimensional decisions by monkey mid-brain activity. *Neural Netw.* 22, 1247–1256.

Hernandez, A., Nacher, V., Luna, R., Zainos, A., Lemus, L., Alvarez, M., Vazquez, Y., Camarillo, L., and Romo, R. (2010). Decoding a perceptual decision process across cortex. *Neuron* 66, 300–314.

Hwang, E. J., and Andersen, R. A. (2009). Brain control of movement execution onset using local field potentials in posterior parietal cortex. *J. Neurosci.* 29, 14363–14370.

Ifft, P. J., Lebedev, M. A., and Nicolelis, M. A. (2011). Cortical correlates of fitts' law. *Front. Integr. Neurosci.* 5:85. doi: 10.3389/fnint.2011.00085

Ikkai, A., and Curtis, C. E. (2011). Common neural mechanisms supporting spatial working memory, attention and motor intention. *Neuropsychologia* 49, 1428–1434.

Isoda, M., and Tanji, J. (2004). Participation of the primate pre-supplementary motor area in

sequencing multiple saccades. *J. Neurophysiol.* 92, 653–659.
Jackson, A., and Fetz, E. E. (2011). Interfacing with the computational brain. *IEEE Trans. Neural Syst. Rehabil. Eng.* 19, 534–541.
Kertzman, C., Schwarz, U., Zeffiro, T. A., and Hallett, M. (1997). The role of posterior parietal cortex in visually guided reaching movements in humans. *Exp. Brain Res.* 114, 170–183.
Kim, H. K., Biggs, S. J., Schloerb, D. W., Carmena, J. M., Lebedev, M. A., Nicolelis, M. A., and Srinivasan, M. A. (2006). Continuous shared control for stabilizing reaching and grasping with brain-machine interfaces. *IEEE Trans. Biomed. Eng.* 53, 1164–1173.
Kim, S., and Lee, D. (2011). Prefrontal cortex and impulsive decision making. *Biol. Psychiatry* 69, 1140–1146.
Krawczyk, D. C. (2002). Contributions of the prefrontal cortex to the neural basis of human decision making. *Neurosci. Biobehav. Rev.* 26, 631–664.
Lacquaniti, F., and Caminiti, R. (1998). Visuo-motor transformations for arm reaching. *Eur. J. Neurosci.* 10, 195–203.
Lebedev, M. A., Carmena, J. M., O'doherty, J. E., Zacksenhouse, M., Henriquez, C. S., Principe, J. C., and Nicolelis, M. A. (2005). Cortical ensemble adaptation to represent velocity of an artificial actuator controlled by a brain-machine interface. *J. Neurosci.* 25, 4681–4693.
Lebedev, M. A., Denton, J. M., and Nelson, R. J. (1994). Vibration-entrained and premovement activity in monkey primary somatosensory cortex. *J. Neurophysiol.* 72, 1654–1673.
Lebedev, M. A., Messinger, A., Kralik, J. D., and Wise, S. P. (2004). Representation of attended versus remembered locations in prefrontal cortex. *PLoS Biol.* 2:e365. doi: 10.1371/journal.pbio.0020365
Lebedev, M. A., and Nicolelis, M. A. (2006). Brain-machine interfaces: past, present and future. *Trends Neurosci.* 29, 536–546.
Lebedev, M. A., and Nicolelis, M. A. (2011). Toward a whole-body neuroprosthetic. *Prog. Brain Res.* 194, 47–60.
Lebedev, M. A., O'doherty, J. E., and Nicolelis, M. A. (2008). Decoding of temporal intervals from cortical ensemble activity. *J. Neurophysiol.* 99, 166–186.
Lebedev, M. A., Tate, A. J., Hanson, T. L., Li, Z., O'doherty, J. E., Winans, J. A., Ifft, P. J., Zhuang, K. Z., Fitzsimmons, N. A., Schwarz, D. A., Fuller, A. M., An, J. H., and Nicolelis, M. A. (2011). Future developments in brain-machine interface research. *Clinics (Sao Paulo)* 66(Suppl. 1), 25–32.
Lebedev, M. A., and Wise, S. P. (2000). Oscillations in the premotor cortex: single-unit activity from awake, behaving monkeys. *Exp. Brain Res.* 130, 195–215.
Lebedev, M. A., and Wise, S. P. (2001). Tuning for the orientation of spatial attention in dorsal premotor cortex. *Eur. J. Neurosci.* 13, 1002–1008.
Lebedev, M. A., and Wise, S. P. (2002). Insights into seeing and grasping: distinguishing the neural correlates of perception and action. *Behav. Cogn. Neurosci. Rev.* 1, 108–129.
Lee, I. H., and Assad, J. A. (2003). Putaminal activity for simple reactions or self-timed movements. *J. Neurophysiol.* 89, 2528–2537.
Matsuzaka, Y., and Tanji, J. (1996). Changing directions of forthcoming arm movements: neuronal activity in the presupplementary and supplementary motor area of monkey cerebral cortex. *J. Neurophysiol.* 76, 2327–2342.
Matthews, B. W. (1975). Comparison of the predicted and observed secondary structure of T4 phage lysozyme. *Biochim. Biophys. Acta* 405, 442–451.
McGuire, L. M., and Sabes, P. N. (2009). Sensory transformations and the use of multiple reference frames for reach planning. *Nat. Neurosci.* 12, 1056–1061.
Miller, E. K. (2000). The prefrontal cortex and cognitive control. *Nat. Rev. Neurosci.* 1, 59–65.
Miller, E. K., and Wilson, M. A. (2008). All my circuits: using multiple electrodes to understand functioning neural networks. *Neuron* 60, 483–488.
Mirabella, G., Pani, P., and Ferraina, S. (2011). Neural correlates of cognitive control of reaching movements in the dorsal premotor cortex of rhesus monkeys. *J. Neurophysiol.* 106, 1454–1466.
Mostofsky, S. H., and Simmonds, D. J. (2008). Response inhibition and response selection: two sides of the same coin. *J. Cogn. Neurosci.* 20, 751–761.
Musallam, S., Corneil, B. D., Greger, B., Scherberger, H., and Andersen, R. A. (2004). Cognitive control signals for neural prosthetics. *Science* 305, 258–262.
Mushiake, H., Inase, M., and Tanji, J. (1990). Selective coding of motor sequence in the supplementary motor area of the monkey cerebral cortex. *Exp. Brain Res.* 82, 208–210.
National Research Council (US), Committee for the Update of the Guide for the Care, and Use of Laboratory Animals, Institute for Laboratory Animal Research (US), and National Academies Press (US). (2011). *Guide for the Care and Use of Laboratory Animals*, 8th Edn. Washington, DC: National Academies Press.
Nelson, R. J., Smith, B. N., and Douglas, V. D. (1991). Relationships between sensory responsiveness and premovement activity of quickly adapting neurons in areas 3b and 1 of monkey primary somatosensory cortex. *Exp. Brain Res.* 84, 75–90.
Nicolelis, M. A. (2001). Actions from thoughts. *Nature* 409, 403–407.
Nicolelis, M. A., Dimitrov, D., Carmena, J. M., Crist, R., Lehew, G., Kralik, J. D., and Wise, S. P. (2003). Chronic, multisite, multielectrode recordings in macaque monkeys. *Proc. Natl. Acad. Sci. U.S.A.* 100, 11041–11046.
Nicolelis, M. A., and Lebedev, M. A. (2009). Principles of neural ensemble physiology underlying the operation of brain-machine interfaces. *Nat. Rev. Neurosci.* 10, 530–540.
Pare, M., and Hanes, D. P. (2003). Controlled movement processing: superior colliculus activity associated with countermanded saccades. *J. Neurosci.* 23, 6480–6489.
Pesaran, B., Musallam, S., and Andersen, R. A. (2006). Cognitive neural prosthetics. *Curr. Biol.* 16, R77–R80.
Pesaran, B., Nelson, M. J., and Andersen, R. A. (2008). Free choice activates a decision circuit between frontal and parietal cortex. *Nature* 453, 406–409.
Resulaj, A., Kiani, R., Wolpert, D. M., and Shadlen, M. N. (2009). Changes of mind in decision-making. *Nature* 461, 263–266.
Rickert, J., Riehle, A., Aertsen, A., Rotter, S., and Nawrot, M. P. (2009). Dynamic encoding of movement direction in motor cortical neurons. *J. Neurosci.* 29, 13870–13882.
Santhanam, G., Ryu, S. I., Yu, B. M., Afshar, A., and Shenoy, K. V. (2006). A high-performance brain-computer interface. *Nature* 442, 195–198.
Santucci, D. M., Kralik, J. D., Lebedev, M. A., and Nicolelis, M. A. (2005). Frontal and parietal cortical ensembles predict single-trial muscle activity during reaching movements in primates. *Eur. J. Neurosci.* 22, 1529–1540.
Scangos, K. W., and Stuphorn, V. (2010). Medial frontal cortex motivates but does not control movement initiation in the countermanding task. *J. Neurosci.* 30, 1968–1982.
Schall, J. D., Stuphorn, V., and Brown, J. W. (2002). Monitoring and control of action by the frontal lobes. *Neuron* 36, 309–322.
Scherberger, H., and Andersen, R. A. (2007). Target selection signals for arm reaching in the posterior parietal cortex. *J. Neurosci.* 27, 2001–2012.
Shen, L., and Alexander, G. E. (1997). Neural correlates of a spatial sensory-to-motor transformation in primary motor cortex. *J. Neurophysiol.* 77, 1171–1194.
Snyder, L. H., Batista, A. P., and Andersen, R. A. (1998). Change in motor plan, without a change in the spatial locus of attention, modulates activity in posterior parietal cortex. *J. Neurophysiol.* 79, 2814–2819.
Soso, M. J., and Fetz, E. E. (1980). Responses of identified cells in postcentral cortex of awake monkeys during comparable active and passive joint movements. *J. Neurophysiol.* 43, 1090–1110.
Stevenson, I. H., and Kording, K. P. (2011). How advances in neural recording affect data analysis. *Nat. Neurosci.* 14, 139–142.
Stinear, C. M., Coxon, J. P., and Byblow, W. D. (2009). Primary motor cortex and movement prevention: where Stop meets Go. *Neurosci. Biobehav. Rev.* 33, 662–673.
Tanji, J. (2001). Sequential organization of multiple movements: involvement of cortical motor areas. *Annu. Rev. Neurosci.* 24, 631–651.
Thaler, L., and Goodale, M. A. (2011). Neural substrates of visual spatial coding and visual feedback control for hand movements in allocentric and target-directed tasks. *Front. Hum. Neurosci.* 5:92. doi: 10.3389/fnhum.2011.00092
Tonet, O., Marinelli, M., Citi, L., Rossini, P. M., Rossini, L., Megali, G., and Dario, P. (2008). Defining brain-machine interface applications by matching interface performance with device requirements. *J. Neurosci. Methods* 167, 91–104.
Velliste, M., Perel, S., Spalding, M. C., Whitford, A. S., and Schwartz, A. B. (2008). Cortical control of a prosthetic arm for self-feeding. *Nature* 453, 1098–1101.
Verbruggen, F., and Logan, G. D. (2008). Response inhibition in the stop-signal paradigm. *Trends Cogn. Sci.* 12, 418–424.
Vickers, D., and Smith, P. (1985). Accumulator and random-walk

models of psychophysical discrimination: a counter-evaluation. *Perception* 14, 471–497.

Wessberg, J., Stambaugh, C. R., Kralik, J. D., Beck, P. D., Laubach, M., Chapin, J. K., Kim, J., Biggs, S. J., Srinivasan, M. A., and Nicolelis, M. A. (2000). Real-time prediction of hand trajectory by ensembles of cortical neurons in primates. *Nature* 408, 361–365.

Wise, S. P., Boussaoud, D., Johnson, P. B., and Caminiti, R. (1997). Premotor and parietal cortex: corticocortical connectivity and combinatorial computations. *Annu. Rev. Neurosci.* 20, 25–42.

Wise, S. P., Di Pellegrino, G., and Boussaoud, D. (1996). The premotor cortex and nonstandard sensorimotor mapping. *Can. J. Physiol. Pharmacol.* 74, 469–482.

Wise, S. P., and Murray, E. A. (2000). Arbitrary associations between antecedents and actions. *Trends Neurosci.* 23, 271–276.

Wong-Lin, K., Eckhoff, P., Holmes, P., and Cohen, J. D. (2010). Optimal performance in a countermanding saccade task. *Brain Res.* 1318, 178–187.

Zacksenhouse, M., and Nemets, S. (2008). "Strategies for neural ensemble data analysis for brain-machine interface (BMI) applications," in *Methods for Neural Ensemble Recordings*, 2nd Edn. ed M. A. L. Nicolelis (Boca Raton, FL), 57–80.

Conflict of Interest Statement: The authors declare that the research was conducted in the absence of any commercial or financial relationships that could be construed as a potential conflict of interest.

Received: 09 March 2012; paper pending published: 07 May 2012; accepted: 02 July 2012; published online: 18 July 2012.

Citation: Ifft PJ, Lebedev MA and Nicolelis MAL (2012) Reprogramming movements: extraction of motor intentions from cortical ensemble activity when movement goals change. Front. Neuroeng. ***5****:16. doi: 10.3389/fneng. 2012.00016*

frontiers in
NEUROENGINEERING

ORIGINAL RESEARCH ARTICLE
published: 11 June 2012
doi: 10.3389/fneng.2012.00010

Adaptive proactive inhibitory control for embedded real-time applications

Shufan Yang *, T. Martin McGinnity and KongFatt Wong-Lin

Intelligent Systems Research Centre, University of Ulster, Derry, Northern Ireland, UK

Edited by:
Giovanni Mirabella, University of La Sapienza, Italy

Reviewed by:
Hari S. Sharma, Uppsala University, Sweden
Simeon A. Bamford, L'Istituto Superiore di Sanità, Italy

****Correspondence:***
Shufan Yang, Intelligent Systems Research Centre, Magee Campus, University of Ulster, Derry, Northern Ireland BT48 7JL, UK.
e-mail: s.yang@ulster.ac.uk

Psychologists have studied the inhibitory control of voluntary movement for many years. In particular, the countermanding of an impending action has been extensively studied. In this work, we propose a neural mechanism for adaptive inhibitory control in a firing-rate type model based on current findings in animal electrophysiological and human psychophysical experiments. We then implement this model on a field-programmable gate array (FPGA) prototyping system, using dedicated real-time hardware circuitry. Our results show that the FPGA-based implementation can run in real-time while achieving behavioral performance qualitatively suggestive of the animal experiments. Implementing such biological inhibitory control in an embedded device can lead to the development of control systems that may be used in more realistic cognitive robotics or in neural prosthetic systems aiding human movement control.

Keywords: countermanding saccade, frontal eye fields, adaptive inhibitory control, FPGA, neural network model

INTRODUCTION

Psychological research reveals that humans can adapt to dynamic environments using inhibitory control (Logan and Cowan, 1984; Logan and Gordon, 2001; Emeric et al., 2007). In cognitive models of behavior, proactive inhibition can be understood as the suppression of previously activated or planned cognitive processes. This type of inhibition is a vital part of human behavior because it allows flexible adaptation to changing environments or rules. Inhibitory control in countermanding tasks is studied in the motor system, since it requires the suppression of motor outputs. In humans, evidence of neural correlates of inhibitory control can be revealed from neuroimaging (e.g., functional magnetic resonance imaging; Curtis et al., 2005; Chikazoe et al., 2009). However, studies such as these often do not provide sufficient temporal or spatial information to reveal the possibly rapid neural mechanisms underlying inhibitory behavior such as stopping an impending (saccadic) eye movement. During the last decade, animal electrophysiologists have begun to employ behavioral task paradigms in psychology, such as the saccade countermanding tasks to search for the neuronal correlates of inhibitory control behavior (Hanes et al., 1998; Murthy et al., 2001; Sato and Schall, 2003; Schall, 2004; Schall et al., 2004, 2011; Cohen et al., 2007; Pouget et al., 2011).

This series of electrophysiological work on behaving non-human primates has shown that there are neurons in the frontal eye fields (FEFs) and superior colliculus that correlate with an impending saccadic eye movement (classified as "movement" neurons) or inhibition (classified as "fixation" neurons), while neurons in other brain regions (e.g., supplementary eye fields) seem to correlate with monitoring and/or controlling voluntary movements. These findings have inspired various computational neural models (Boucher et al., 2007; Lo et al., 2009; Wong-Lin et al., 2010), which provide good accounts of how the interaction between go and stop processes can be reconciled with the observation at the neuronal and behavioral levels. More recently, Pouget et al. (2011) interestingly shows that movement neurons can temporally shift their activation onset times based on whether the previous trials have a stop-signal or not, thus allowing longer term adaptation in the inhibitory control system. This phenomenon has not been accounted for in previous computational models.

Modern neural computational models can provide powerful ideas to be used in neural prosthetics and robotic development. Specifically, implementations of these models in hardware may give (especially transfemoral) prosthetics users or cognitive/mobile robots an enhanced capability of controlling their pre-movement acts related to the decision of whether to move, and also the possibility of adapting to dynamically changing environments (Farwell and Donchin, 1988; Schwartz, 2004; Chestek et al., 2009; Perrin et al., 2010). However, while many attempts to implement neuronal models in hardware have been made, neural computational models for a countermanding task are currently coded in software and used to account for experimental findings. They have not, as yet, been implemented in a real-time embedded field-programmable gate array (FPGA) system for more practical applications.

In this paper, we build on our previous computational inhibitory control model for countermanding saccadic eye movements and propose an adaptive inhibitory control mechanism inspired by Pouget et al. (2011). We then implement the proactive adaptive inhibitory control exploring a synthesizable HDL coding approach. The proposed framework has been evaluated on an FPGA (Xilinx Virtex-6 LX240) platform (Xilinx Inc., 2011a). The implementation in digital hardware provides the possibility of creating a realistic motor control system in embedded portable devices and is anticipated to integrate into existing neuronal prosthetics and robotic systems.

MATERIALS AND METHODS

As a first step toward prototyping, we shall focus only on a firing-rate type model modified from Wong et al. (2007), Wong-Lin et al. (2010). The model was designed in a way similar to the saccade countermanding task in animal experiments to account for the experimental data (Hanes et al., 1998; Boucher et al., 2007).

EXPERIMENTAL MOTIVATION

The countermanding stop-signal task is a common procedure for investigating the control of thought and action by probing the subjects' ability to withhold a planned movement in response to an unanticipated countermanding signal (Logan, 1981; Logan and Cowan, 1984). This task has been used to study executive control and flexibility in behavior, since the performance of this task demonstrates an empirical model of self-control (Lappin and Eriksen, 1966; Logan, 1981; Akerfelt et al., 2005; Boucher et al., 2007; Bissett and Logan, 2011).

In the countermanding task experiment, two types of trials (no-stop-signal trial and stop-signal trial) were designed, as shown in **Figures 1A,B**. Trials with or without the stop signal are referred to as stop-signal trials or no-stop-signal trials, respectively. As shown in **Figure 1A**, in a typical experimental trial, the task started with a black screen. In Hanes et al. (1998) a fixation point (stop signal) was on after 1 s. Then the fixation point was then turned off while a peripheral target (go signal) was turned on at the same time after 500 ms. The subject is instructed to make a saccadic eye movement to this target. However, a fraction of the trials include a stop signal (e.g., in the form of a reappearance of the fixation point) shortly after target onset (**Figure 1B**). The subject is instructed to withhold their gaze at the fixation point whenever a stop signal appears. The ability of the subject to withhold his or her gaze at the fixation point depends on the delay between the go signal and stop signal onset times, termed the stop signal delay (SSD); the shorter the SSD, the easier to withhold the gaze. Thus, stop-signal trials can be further categorized into (successfully) canceled trials and non-canceled trials (also known as "signal inhibit" and "signal respond" respectively, in the literature; Logan and Cowan, 1984). A trial will end after another 700 ms has elapsed.

An inhibition function describes the probability of stopping across a range of SSD values can be easily gathered from the

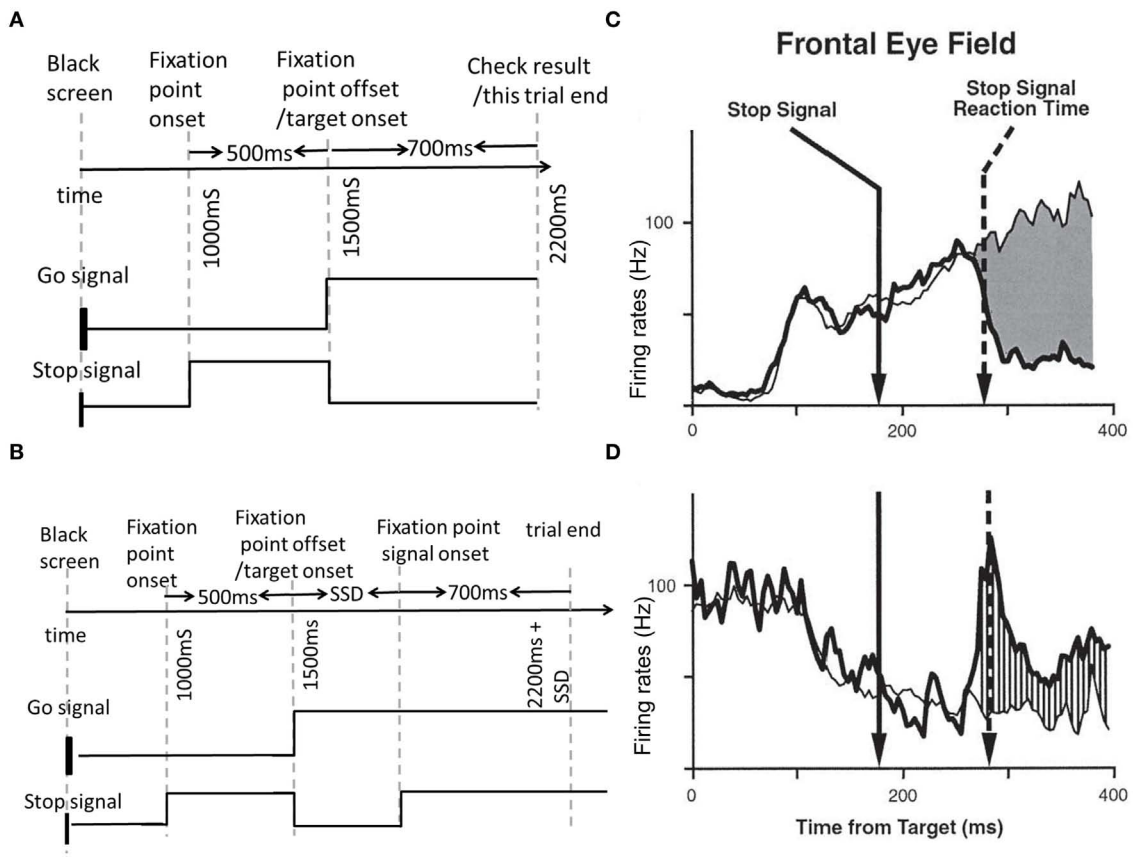

FIGURE 1 | Schematic and neural activities in a saccade countermanding task. (A,B) Schematic representation of a no-stop-signal trial type **(A)**, and a stop-signal trial type **(B)**. These two trial types are randomly interleaved in a block of trials. In both trials, a central fixation signal (also the stop signal) is presented for a period of time, and then the peripheral target for a saccade (go signal) turns on. In a stop-signal trial, briefly after the go signal onset, a stop signal appears (i.e., fixation point reappears). This time interval is labeled as the stop-signal delay (SSD). **(C,D)** Neural firing rates of movement **(C)** and fixation **(D)** neurons in the frontal eye fields (FEFs) during the task. Saccades are correlated with the movement neuronal activities reaching a certain firing rate threshold level; successful cancelations correlated with simultaneous reactivation of fixation neuronal activities and suppression of movement neuronal activities (bold lines) before reaching some motor response threshold. **(C,D)** Adapted from Schall et al., 2002; with permission).

behavioral response. We would expect the probability of responding in a stop-signal trial to increase with SSD. The change in reaction time distribution with different SSDs can also be used to estimate the length of time needed to cancel the planned movement. This time length is also called the stop signal reaction time (SSRT). We would expect only the faster responses not to be inhibited when SSD is short. Therefore, a subject's ability to inhibit the motor response will depend on the individual's SSRT and the experimentally controlled SSD.

Previously, the inhibition function and the SSRT were the only means to deduce an individual's responsiveness and cognitive control abilities. However, more recent neurophysiological experiments using implanted electrodes in non-human primates have allowed measurements with better spatial and temporal resolution, prior to a movement or no movement (Schall et al., 2002). The behavioral and neuronal data in the classic experiments of Hanes et al. (1998) were collected from monkeys, who were trained to allocate their gaze to spot on the screen. One of the most interesting findings in these experiments was that unlike previous cognitive models such as the race model (Logan, 1981; Logan and Cowan, 1984), the movement and stopping processes could interact. That is, neurons that encode the impeding movement ramp up their firing rates over time after a go signal onset and suppressed to baseline level during successful saccade or fixation cancelation. These movement neurons were anti-correlated with the drop and rise in firing rate of another group of neurons – the fixation neurons (as illustrated in **Figures 1C,D**).

Both response time and probability of responding can also be influenced by previous trials, depending upon whether the former have stop signals, and less so on whether the stop trials were successfully canceled (Emeric et al., 2007; Bissett and Logan, 2011; Pouget et al., 2011). Variations in the fraction of stop-signal trials can also influence the countermanding performance (Schall et al., 2002). Chikazoe et al. (2009) introduced a concept of prepared inhibition, in which inhibition is prepared in anticipation of an upcoming stop cue. A more recent research finding suggests that if the previous trials are (canceled) stop trials, the movement neurons show a delay in the onset time of their stereotypical ramping up activities (Pouget et al., 2011; **Figure 5B**). This is also correlated with behavioral performance changes. For example, Bissett and Logan, 2011 suggests that there is a small slowing after signal-inhibit (canceled stop trial) and signal-respond trials (non-canceled stop trial). Those results provide new insights into the adaptive mechanisms of inhibitory control.

NEURAL NETWORK MODEL OF THE FEF

Our neural control circuit adopts the basic firing-rate type model of Wong-Lin et al. (2010) that can perform the countermanding task. The proposed neural network model includes two main units: a FEF network module, and an adaptive control module.

As shown in **Figure 2A**, the inhibitory dynamics of the interneurons is implicitly modeled by an effective direct mutual inhibition. This is justified if the excitatory timescale is much slower than its inhibitory counterpart (Wong and Wang, 2006; Wong-Lin et al., 2010). In a no-stop-signal trial or unsuccessfully canceled trial, the movement neurons successfully crossed a prescribed movement threshold in order to make a motor (saccadic eye) movement. However, in a stop-signal trial, the fixation neurons can be reactivated in time to suppress the movement neurons from crossing the movement threshold via a highly potent lateral inhibition, which can successfully prevent a motor movement.

The neural activity of movement neurons (r_{MN}) and the neural activity of fixation neurons (r_{FN}) can be described by Eqs 1 and 2, respectively.

$$dr_{MN} = \left(-r_{MN} + \left[\beta_{\mathrm{MN}} r_{FN} + I_{go}\right]_{+}\right)\frac{dt}{\tau_E} + \sigma\sqrt{\frac{dt}{\tau_E}}\gamma \tag{1}$$

$$dr_{\mathrm{FN}} = \left(-r_{\mathrm{FN}} + \left[\beta_{\mathrm{FN}} r_{\mathrm{MN}} + I_{\mathrm{stop}}\right]_{+}\right)\frac{dt}{\tau_E} + \sigma\sqrt{\frac{dt}{\tau_E}}\gamma \tag{2}$$

Here, r_{MN} and r_{FN} represent population firing rates of movement and fixation neurons respectively; β_{MN} and β_{FN} are the effective inhibitory synaptic strengths from fixation to movement neurons and from movement to fixation neurons; σ is the magnitude of additive noise and γ is a random Gaussian variable with zero mean and standard deviation of 1. $[x]_+$ denotes a threshold-linear function which is equal to x if $x > 0$, and 0 otherwise. I_{go} and I_{stop} are the input currents in the presence of the go and stop signals, respectively. During the appearance of the fixation point prior to target onset, an input current is applied to the fixation neural population to allow a high firing rate of about 80 Hz (Hanes et al., 1998).

A NEURAL NETWORK MODEL OF FEF WITH AN ADAPTIVE CONTROL MODEL

Previous studies have demonstrated the presence of behavioral monitoring and control in the supplementary eye field and the anterior cingulate cortex of macaque monkeys and their possible influence on behavioral psychophysics over trials (Chen et al., 2010; Stuphorn et al., 2010). In particular, such studies have shown that the onset of movement neuronal activities upon a go signal onset can be delayed and the reaction times in the no-stop-signal trials can be slowed down, if the immediately preceding trials are stop-signal trials, thus, affecting the overall countermanding performance (Emeric et al., 2007; Pouget et al., 2011).

Compared to the neural network model of FEF (Wong-Lin et al., 2010), we have included an input-output/gating function of adaptive inhibitory control module to account for an excitatory control on the movement neurons. This control can be adjusted based on whether the previous history is a stop-signal trial or not. As the input from the control module to the movement neural population is a non-linear threshold function, it takes a longer time to activate the movement neurons when the control module has a lower activation level compared to when the previous trial is a no-stop-signal trial.

We propose a simple adaptive inhibitory control module to gate the flow of the control signal input into the movement neural population (**Figure 2**), depending on whether the previous trial is a stop-signal trial or not. The neural activity of fixation neurons

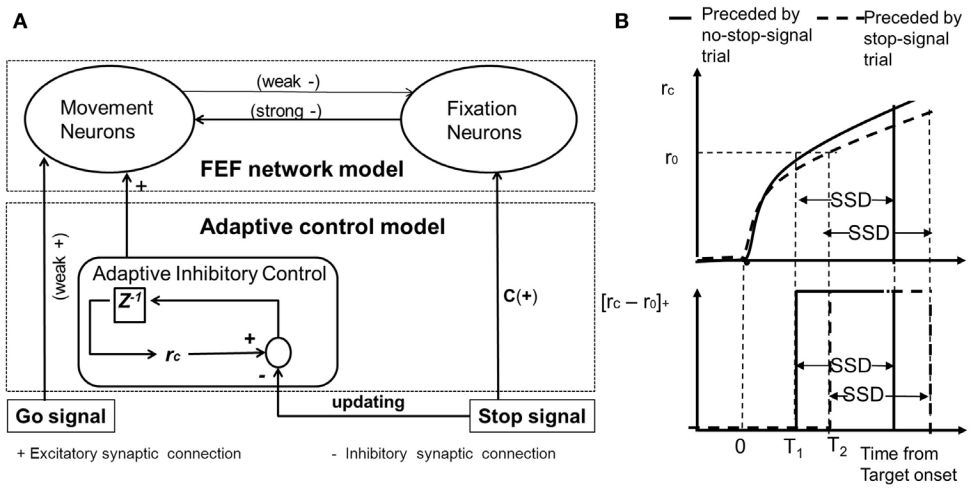

FIGURE 2 | (A) The proposed neural network model of inhibitory control for the countermanding task. The schematic model architecture consists of a population of movement neurons, a population of fixation neurons, and a population of neurons for adaptive control. Z^{-1} corresponds to the delay. C is a fixation stimulus input to set the fixation neurons to be at a high firing rate prior to the target onset. **(B)** The schematic mechanism of delaying the onset of control signal. Top: when a trial is preceded by a no-stop-signal trial (as compared to a stop-signal trial), it takes a shorter time to reach threshold (r0), due to a larger p value. T_1 denotes threshold-crossing time when the current trial is preceded by a no-stop-signal trial. T2 denotes the threshold-crossing time when the current trial is preceded by a stop-signal trial. Bottom: The corresponding afferent inputs into the movement neural population are delayed. Gain is turned off upon stop-signal onset at time T_1/T_2 plus SSD (for current stop-signal trial) or T_1/T_2 plus decision time (for current no-stop-signal trial; not shown), i.e., upon crossing saccadic/decision threshold.

(r_{FN}) can be described by Eq. 2. The neural activity of movement neurons (r_{FN}) can be described by Eq. 3.

$$dr_{MN} = \left(-r_{MN} + \left[\beta_{MN} r_{FN} + I_{go} + [r_c - r_0]_+\right]_+\right)\frac{dt}{\tau_E} + \sigma\sqrt{\frac{dt}{\tau_E}}\gamma \quad (3)$$

Where a threshold-linear function (denoted by $[]_+$) gates an afferent input into the movement neural population. r_c is the control activity of the control neural population and is assumed to follow leaky integrating dynamics with a steady state value of P that depends on the previous trial (as described in Eq. 4). r_0 is the fixed threshold for gating the afferent input. The output from the control neural population sends a delayed excitatory input to the movement neurons upon receipt of a go signal onset. The specific temporal delay can be controlled by the value of P, related to heightened urgency to respond. The neural activity of the control neural population can be described by Eq. 4:

$$\tau_c \frac{dr_c}{dt} = -r_c + P \quad (4)$$

P adopts a higher value if the previous trial is a no-stop-signal trial compared to a stop-signal trial (**Table 1**). Intuitively, the control activity can relate a higher sense of urgency signal (that increases over time) when the previous trial is a no-stop-signal trial. Thus a subject may anticipate the current trial to also be a no-stop-signal trial (Bissett and Logan (2011)). This urgency-gating signal can be related to previous work in response time tasks in perceptual decision-making (Cisek et al., 2009; Gao et al., 2009; Standage et al., 2011). However, when the previous trial is an occasional stop-signal trial, the urgency to respond is lowered, and the current trial is anticipated to be a stop-signal trial, and a more cautious response is required. The control (r_c) is turned off upon stop-signal onset during a current stop-signal trial or upon decision threshold (for saccadic eye movement) during a current no-stop-signal trial (**Figure 2B**). The dynamical time constant for the control neural population is assumed to be that of the NMDA-mediated synapses (which is prevalent in brain areas associated with higher-order cognition and cognitive control, e.g., prefrontal cortex; Wang, 2001).

Table 1 | Parameter values for the models.

Parameter	Note	Value
Threshold of r_{MN}	Fit neuronal data of Hanes et al. (1998)	90 Hz
β_{MN}	Fit behavioral data of Hanes et al. (1998)	0.69
β_{FN}	Fit behavioral data of Hanes et al. (1998)	0.08
I_{go}	Fit neuronal data of Hanes et al. (1998)	1.4
I_{stop}	Fit neuronal data of Hanes et al. (1998)	2.7
σ	Fit behavioral data of Hanes et al. (1998)	7.09
τ_c	Synaptic decay time constant	50 ms
r_0	Critical threshold for afferent input. Fit Pouget et al. (2011)	50 Hz
P	Updating currents. Fit Pouget et al. (2011)	1.8(*preceded by stop− signal trial*) 2.4(*preceded by no − stop− signal trial*)

As shown in **Figure 2B**, we can see that the control activity is generally higher if the previous trial is a no-stop-signal trial as compared to a stop-signal trial. In both cases, the control activity increases. As the input from the control module to the movement neural population is a threshold-linear function, it will take a longer time to activate the movement neurons when the control module has a lower activation level compared to when the previous trial is a stop-signal trial. Consequently, the onset of the movement neural activities due to the target signal is delayed, as observed in Pouget et al. (2011).

The model and related behavioral data parameters were selected to be consistent with experiment data of Hanes et al. (1998) and Boucher et al. (2007). For instance, we choose the time constant to be 50 ms (assumed mediated by slow receptors such as those mediated by NMDA). The FEF network model has asymmetrical mutual inhibitory couplings with β_{MN} is $0.69 \ll \beta_{FN} = 0.08$, which fit the data of Hanes et al. (1998). White Gaussian noise is included in the model, which provides overall fluctuations in the network, and thus creating a distribution of reaction times, and also allows non-zero spontaneous firing rate in the network. Further details of the model parameters are given in **Table 1**. Following the neuronal activities in Hanes et al. (1998), movement neurons are assumed to respond to a go signal onset after a delay of 100 ms and fixation neurons respond 80 ms after the stop-signal appears. In this modeling simulation, the inter-trial interval of 1 s is assumed.

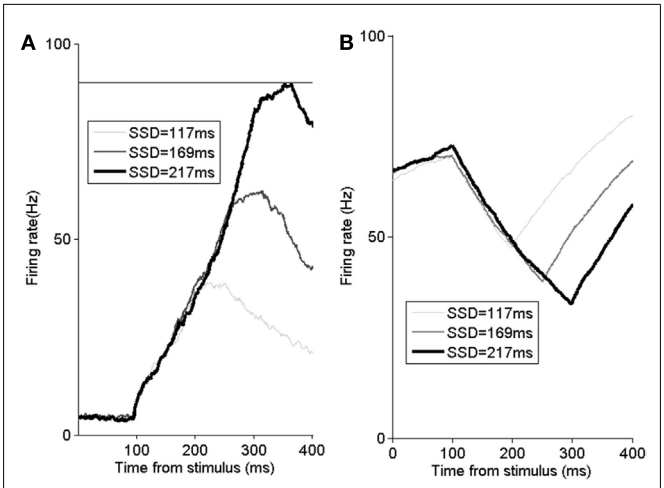

FIGURE 3 | The FEF model's neural activity time-course simulated with the FPGA platform. (A) Time course of trial-averaged activities of successfully canceled trials for movement neurons with various SSDs. All data are averaged over 5000 trials. Horizontal line: decision to saccade threshold (90 Hz). **(B)** Time course of trial-averaged activities of successfully canceled trials for fixation neurons with various SSDs. SSDs of 117 ms (light gray), 169 ms (dark gray), and 217 ms (thick black). To be compared with Boucher et al. (2007) and Wong-Lin et al. (2010). All data are averaged over 5000 trials.

RESULTS

In this experiment, we use a rapid prototyping flow on an FPGA-based embedded system. Parameterized electronic design entries are defined and used as inputs to the parameterized System Generator models (.mdl files; Xilinx Inc., 2011b). These models provide a library of pre-designed circuit blocks that can be converted into a hardware description language for seamless integration with the Xilinx FPGA design flow. After a successful synthesis process, an FPGA bit stream file is generated using the ISE synthesis tools. Following this, the simulation is executed in real-time using the FPGA resource, working in conjunction with a host PC. All simulation results can be imported into Matlab for visualization (Mathworks Inc., 2011). More FPGA implementation details are described in the Appendix.

In this section, we shall first reproduce the essential neural and behavioral data in the experiments. We then demonstrate that the model can also exhibit trial-history (sequential) effects on the movement neural activity and behavioral performance.

BEHAVIOR OF THE FEF NETWORK MODEL

The observed neural activities from FPGA simulation are shown in **Figure 3**. When there is a stop-signal presented, this ramping activity may be suppressed in time to inhibit the impending saccade (as shown in **Figure 3A**). Neural activity of the fixation neural population ramps back up when there is a stop-signal (as shown in **Figure 3B**). This anti-correlation of activities between the two neural populations is a manifestation of the mutual inhibitory couplings in the FEF network.

As previously discussed, a subject's ability to stop a pre-planned saccade can be evaluated through the inhibition function and reaction time distribution SSRT with various SSD. The proportion of canceled trials at each delay is referred to as the "inhibition function." To investigate the efficiency of an inhibitory process, the probability of stop-signal trials with signal-response trials as a function of SSD is plotted. As SSD increases, the probability of non-canceled trials increases (**Figure 4A**). In **Figure 4A**, the model demonstrates that it can capture the inhibition function rather well (compared with Boucher et al., 2007). It should be noted that the probability of a canceled stop trial is very low when SSD is 69 ms (the data used in the study of Boucher et al., 2007) and is thus not included in this study. **Figure 4B** shows the signal-respond reaction time cumulative probability distribution from non-canceled stop-signal trials. We can see that when SSD is short (e.g., 117 ms), only the faster responses are not inhibited. The distribution is very similar to in the experiments in Boucher et al. (2007). These results confirm that our model implemented in hardware can replicate both the essential neurophysiological and behavioral findings in the experiments (Hanes et al., 1998).

NEURAL ACTIVITY AND BEHAVIORAL MODULATION BY THE ADAPTIVE CONTROL SYSTEM

An important part of this study is to implement the sequential effects due to adaptive adjustment based on the trial history. We have proposed a simple mechanism that depends on whether the previous trial is a stop-signal trial type. This modulation can affect the gating onset of incoming neural signal due to the no-stop-signal trial stimulus.

To study the effects on the dynamics of the adaptive control system and movement neural activity, we simulated 5000 trials randomly mixed with equal number of stop-signal trials and no-stop-signal trials. The simulation was carried out using FPGA-based embedded system platform (see Appendix for more details).

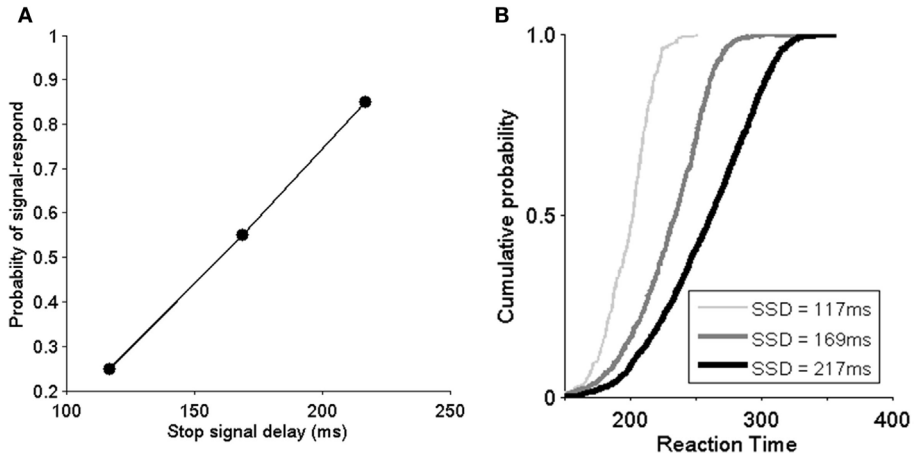

FIGURE 4 | Model implemented in hardware replicates the behavioral data of the monkey experiments (Hanes et al., 1998; Boucher et al., 2007). (A) Inhibition function shows the probability of non-canceled (signal response) in stop-signal trials as a function of stop-signal delay (SSD). SSD: 117, 169, and 217 ms. **(B)** Cumulative distribution of reaction times from non-canceled stop-signal trials for different SSDs. To be compared with Boucher et al. (2007).

The results are recorded in FPGA on-board SDRAM and read back into Matlab. We subsampled the activation of the fixation and movement neurons in a manner comparable to the sampling of neural activity in the physiology experiments via the following procedure. We simulated the model with 10–12 trials at each SSD to mimic the number of trials typically obtained in the physiology experiments. In this simulation, we mix 25% of stop-signal trials and 75% of no-stop-signal trials randomly.

In particular, **Figure 5A** shows that the model produces a rightward shift in the reaction time distribution for no-stop-signal trials if the previous trial is a stop-signal trial type, very similar to that as in the experimental data (**Figure 5B**).This rightward shift in the movement neural activity onset due to a previous stop-signal trial can result in longer reaction times, and allows a better chance of inhibiting a respond. **Figure 6** confirms these predictions in our model.

Intuitively, we can understand that the occurrence of a previous stop-signal trial triggers the need for subsequent caution, and resulting in prolonged response time. This adaptive adjustment has been regarded as the "goal priority hypothesis" in cognitive psychology (Bissett and Logan, 2011), which suggests that stimuli that occur on stop trials become associated with stopping. If the stimuli do not repeat, they do not retrieve associations with stopping to slow RT. Thus the memory hypothesis predicts greater post-stop-signal slowing when stimuli repeat after stop trials than when stimuli do not repeat.

DISCUSSION

In this work, we have implemented in hardware a computational neural model of the FEF with proactive inhibitory control for the saccade countermanding task. Inspired by recent experimental findings (Emeric et al., 2007; Pouget et al., 2011), we have proposed a simple adaptive neural inhibitory control module to gate the flow of the go signal input into the movement neural population, depending on whether the previous trial is a stop-signal trial or not. Our hardware implementation is based on a FPGA prototyping system using dedicated real-time hardware circuitry.

HARDWARE IMPLEMENTATION OF A COMPUTATIONAL MODEL OF INHIBITORY CONTROL

The main goal of this work is to implement an adaptive proactive inhibitory control model for voluntary movement on an FPGA platform. Emulating biological signal processing on an FPGA platform is an economical option for complex systems modeling, prior to proceeding to fully integrated circuit design and fabrication. This work is an important step toward the eventual goal of incorporating into hardware a sufficiently biologically realistic FEF model potentially for neural prosthetic or robotic devices. We have demonstrated that a hardware implementation is feasible using currently available technology.

Field-programmable gate arrays have been less commonly used in bionic creativity engineering, with several exceptions. Protein (Armstrong et al., 2007) and DNA sequencing search (Knodel et al., 2011) are using FPGAs to reduce processing time. Real-time processing, registration and fMRI image analyses are enabled by FPGAs (Koo et al., 2009). Most modeling applications on FPGAs have been limited to studying neural dynamics in low-level simulations. Recently we have made several implementation of spiking neural network models which include integrate-and-fire neuronal models and conductance-based neural models (Maguire et al., 2007; Glackin et al., 2009; Ghani et al., 2011; Yang and McGinnity, 2011). However, each of these designs consists of a relatively small number of neurons, and do not typically link to behavioral data. This paper extends previous work of firing-rate type neural models and cognitive neural models in countermanding impending actions by providing fast prototyping architecture for current software-based cognitive neural modeling into FPGA-based embedded system. Building on this work, we should be more confident that we will be able to build a fast inhibitory control system that deals with more realistic neuronal spike coding (Lo et al.,

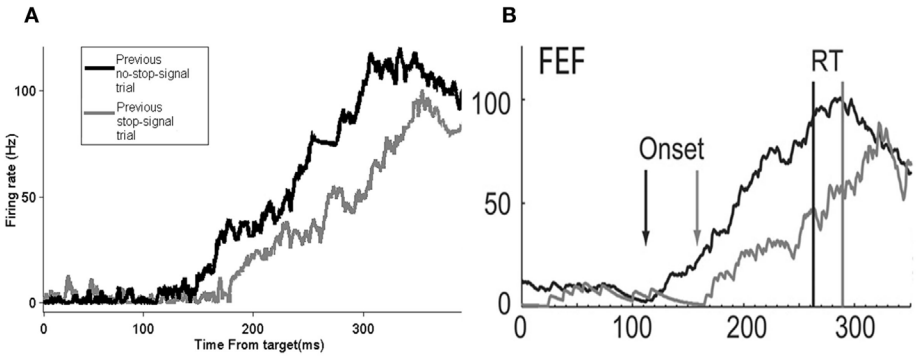

FIGURE 5 | The model's neural activity time course is similar to that of the experimental data. The time course of average firing rates activity of movement neurons response time for no-stop-signal trials preceded by either a no-stop-signal trial or a stop-signal trial for data collected in 25% stop-signal trials session experiment in the model with 5000 trials **(A)** and in the experiment **(B)**. **(B)** Adapted from Pouget et al., 2011; with permission).

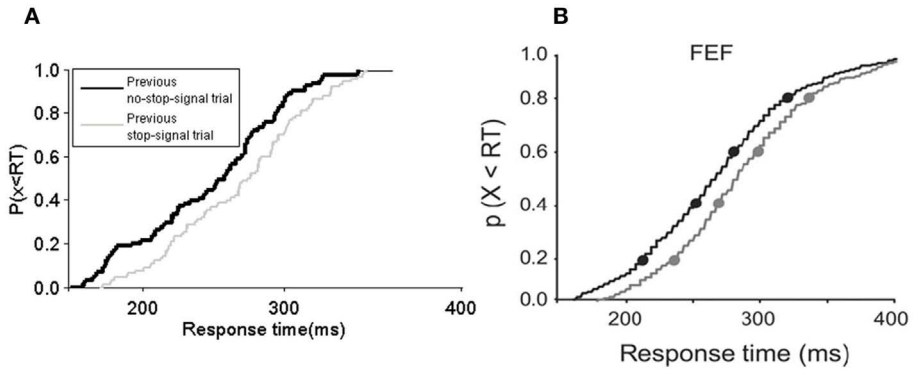

FIGURE 6 | Cumulative frequency distribution of response time in the model and experiment. (A) The cumulative frequency distribution of response time in the model and **(B)** in the experiment of Pouget et al. (2011). **(A,B)** Both using a 25% stop-signal trials session experiment with SSD of 217 ms. Black: Preceded by no-stop-signal trial. Gray: stop-signal trial [canceled trial in **(B)**]. **(B)** Adapted from Pouget et al., 2011; with permission).

2009). In fact, we should expect the FPGA-based system to greatly enhance the computational speed of the model in Lo et al. (2009).

The research presented in this work has shown that our fast prototyping platform with hardware evaluation framework reproduced qualitatively the data from Pouget et al. (2011). The disadvantage of our FPGA model is that once the algorithm is synthesized and programmed into the FPGA the parameters cannot be changed without another synthesis. The design cycle is longer than software implementation, but much shorter than for a full-Application Specific Integrated Circuit (ASIC) design. For fabricating a chip to be used in neural prosthetic devices, more work for design optimization is necessary. Firstly, an efficient way to save power consumption could be achieved using a low frequency clock. Secondly, balancing between high precision and silicon area is a key issue for implementation in a small die area. Thirdly, the analog-to-digital converters should be integrated for sensor inputs/control outputs. Finally, as shown in **Figures A1** and **A2**, in Appendix, the overall logic usage for the proactive control design is just over 4% of that available, which is very promising for future extensions, since it suggests that there is plenty of scope left to add new embedded features.

ADAPTIVE INHIBITORY CONTROL MECHANISM

In this work, we have proposed a mechanism for implementing an inhibitory control system that can adapt to previous trial type and performance. Specifically, we have implemented a neural transit delay mechanism of the inhibitory control unit that depends on whether the previous trial is a stop-signal trial or no-stop-signal trial type. This may allow the system to autonomously track the statistics in noisy, dynamic environments (e.g., there is a stop-signal in 25% of the time) better in order to respond more appropriately (Sugrue et al., 2004; Wong et al., 2007; Shenoy et al., 2010). This is an extension of our previous computational model; the results are qualitatively suggestive of the neural and behavioral data in Hanes et al. (1998), Boucher et al. (2007), and Pouget et al. (2011).

Our simple adaptive control mechanism has the interesting features of incorporating previous neural mechanisms in simple decision-making tasks; namely, the integration of the urgency-gating mechanism (Cisek et al., 2009; Niyogi and Wong-Lin, 2010; Standage et al., 2011) and sequential effects (Fecteau and Munoz, 2003; Gao et al., 2009). In the model, we have assumed that the memory of the previous trial affects the current trial differently,

depending on the previous trial type. Bissett and Logan (2011) has shown that when the frequency of stop-signal trials increases, the post-stop-signal slowing is greater. This can be implemented easily in our model either by having the parameter P as a monotonically increasing function of the frequency of stop-signal trial or with slightly longer memory trace (e.g., memory of two trials back instead of one). This memory-based hypothesis may perhaps be tested by slightly modifying the present task. For example, by presenting a distractor stimulus during the inter-trial intervals, the memory of the previous trials may be reduced (i.e., the P values due to the two different previous trial types are closer). As a consequence, the difference of the movement neural activity accumulating onset times and reaction times between a previously stop-signal and no-stop-signal trial may also be reduced. In the future, it would also be interesting to study quantitatively how this history-dependent mechanism is related to more optimal performance in action countermanding in a dynamic environment, e.g., in the form of maximizing overall reward rates (Shenoy et al., 2010; Wong-Lin et al., 2010; Shenoy and Yu, 2011).

Although we have explored other control mechanisms which include more realistic transient activation of the control unit via inhibitory feedback mechanism, similar neural and behavioral results can be obtained (not shown).Our simple adaptive control mechanism with minimal biological features is sufficient to readily account for both neural and behavioral data from the experiments. Before we embark on a fully fledged biological implementation of the adaptive control mechanism, it may be worth identifying more extensive neuronal recording brain areas responsible for such adaptive control/adjustment and also performance monitoring. These regions may include the supplementary eye fields, the inferior frontal gyrus and the dorsal lateral prefrontal cortex, and the anterior cingulate cortical areas (Schall, 2004). Good temporal resolution will be needed since this control module may operate transiently within a timescale of tens of milliseconds. Thus, techniques such as fMRI may ultimately not be appropriate. However, in terms of its practical applications (e.g., in neural prosthetics), our simple autonomous history-based adjustment mechanism may be able to circumvent the need to search for sources of inhibitory controls or performance monitoring; our efficient artificial control system mimic the real biological system fairly well. This may also reduce the amount of extensive surgery to be performed on motor-impaired patients, e.g., one in FEF for eye movement (or supplementary motor area for finger movement) and another in the area(s) for monitoring, control, and adjustment (e.g., prefrontal cortex).

GENERALIZABILITY

Although we have focused only on modeling the FEF, our model may be generalized to other brain areas that are part of the oculomotor system such as the superior colliculus (e.g., Paré and Hanes, 2003) as their organization is quite similar. We further speculate that our model may be useful in task-switching paradigms when to switch rapidly between different tasks (due to context or rule changes), subjects typically have to first inhibit the previous "task set" through active inhibitory control of the previous motor plan or action before implementing the new one (Stuphorn et al., 2010). However, there is a limit to generalizing our current model to inhibitory control for arm movement as there is evidence that shows distinctive differences between countermanding saccadic and arm movements (Mirabella et al., 2009, 2011). In the future, it would be interesting to compare among multiple modalities (e.g. finger and saccadic eye movement) and search for common brain regions for cognitive monitoring and control in the countermanding task paradigm.

REFERENCES

Akerfelt, A., Colonius, H., and Diederich, A. (2005). Visual-tactile saccadic inhibition. *Exp. Brain Res.* 169, 554–563.

Armstrong, N. B., Lopes, H. S., and Erig Lima, R. C. (2007). "Reconfigurable computing for accelerating protein folding simulations," in *Proceedings of the 3rd International Conference on Reconfigurable Computing: Architectures, Tools and Applications (ARC'07)*, Berlin, 314–325.

Bissett, P. G., and Logan, G. D. (2011). Balancing cognitive demands: control adjustments in the stop-signal paradigm. *J. Exp. Psychol. Learn. Mem. Cogn.* 37, 392–404.

Boucher, L., Palmeri, T. J., Logan, G. D., and Schall, J. D. (2007). Inhibitory control in mind and brain: an interactive race model of countermanding saccades. *Psychol. Rev.* 114, 376–397.

Chen, X., Scangos, K. W., and Stuphorn, V. (2010). Supplementary motor area exerts proactive and reactive control of arm movements. *J. Neurosci.* 30, 14657–14675.

Chestek, C. A., Gilja, V., Nuyujukian, P., Kier, R. J., Solzbacher, F., Ryu, S. I., Harrison, R. R., and Shenoy, K. V. (2009). HermesC: low-power wireless neural recording system for freely moving primates. *IEEE Trans. Neural Syst. Rehabil. Eng.* 17, 330–338.

Chikazoe, J., Jimura, K., Hirose, S., Yamashita, K., Miyashita, Y., and Konishi, S. (2009). Preparation to inhibit a response complements response inhibition during performance of a stopsignal task. *J. Neurosci.* 29, 15870–15877.

Cisek, P., Puskas, G. A., and El-Murr, S. (2009). Decisions in changing conditions: the urgency-gating model. *J. Neurosci.* 29, 11560–11571.

Cohen, J. Y., Pouget, P., Woodman, G. F., Subraveti, C. R., Schall, J. D., and Rossi, A. F. (2007). Difficulty of visual search modulates neuronal interactions and response variability in the frontal eye field. *J. Neurophysiol.* 98, 2580–2587.

Curtis, C. E., Cole, M. W., Rao, V. Y., and D'Esposito, M. (2005). Canceling planned action: an FMRI study of countermanding saccades. *Cereb. Cortex* 15, 1281–1289.

Emeric, E. E., Brown, J. W., Boucher, L., Carpenter, R. H., and Hanes, D. P. (2007). Influence of history on saccadecountermanding performance in humans and macaque monkeys. *Vision Res.* 47, 35–49.

Farwell, L. A., and Donchin, E. (1988). Talking off the top of your head: toward a mental prosthesis utilizing event-related brain potentials. *Electroencephalogr. Clin. Neurophysiol.* 70, 510–523.

Fecteau, J. H., and Munoz, D. P. (2003). Exploring the consequences of the previous trial. *Nat. Rev. Neurosci.* 4, 435–443.

Gao, J., Wong-Lin, K., Holmes, P., Simen, P., and Cohen, J. D. (2009). Sequential effects in two-choice reaction time tasks: decomposition and synthesis of mechanisms. *Neural. Comput.* 21, 2407–2436.

Ghani, A., McDaid, L., Belatreche, A., Kelly, P., Hall, S., Dowrick, T., Huang, H., Marsland, J., and Smith, A. (2011). "Evaluating the training dynamics of a CMOS based synapse," in *International Joint Conference on Neural Networks*, San Jose, 1–7.

Glackin, B., Harkin, J., McGinnity, T. M., and Maguire, L. P. (2009). "A hardware accelerated simulation environment for spiking neural networks, ARC '09," in *Proceedings of the 5th International Workshop on Reconfigurable Computing: Architectures, Tools and Applications*, Karlsruhe, 336–341.

Hanes, D. P., Patterson, W. F., and Schall, J. D. (1998). The role of frontal eye field in countermanding saccades: visual, movement and fixation activity. *J. Neurophysiol.* 79, 817–834.

Knodel, O., Preusser, T. B., and Spallek, R. G. (2011). "Next-generation massively parallel short-read mapping on FPGAs 2011," in *IEEE International Conference on Application-Specific Systems, Architectures and Processors (ASAP)*, Santa Monica, 195–201.

Koo, J. J., Evans, A. C., and Gross, W. J. (2009). 3-D Brain MRI tissue classification on FPGAs. *IEEE Trans. Image Process* 18, 2735–2746.

Lappin, J. S., and Eriksen, C. W. (1966). Use of a delayed signal to stop a visual reaction-time response. *J. Exp. Psychol.* 72, 803–811.

Lo, C. C., Boucher, L., Paré, M., Schall, J. D., and Wang, X. J. (2009). Proactive inhibitory control and attractor dynamics in countermanding action: a spiking neural circuit model. *J. Neurosci.* 29, 9059–9071.

Logan, G. D. (1981). "Attention, automaticity, and the ability to stop a speeded choice response," in *Attention and Performance IX*, eds J. Long and A. Baddeley (Hillsdale, NJ: Erlbaum), 205–222.

Logan, G. D., and Cowan, W. B. (1984). On the ability to inhibit thought and action. A theory of an act of control. *Psychol. Rev.* 91, 295–327.

Logan, G. D., and Gordon, R. D. (2001). Executive control of visual attention in dual-task situations. *Psychol. Rev.* 108, 393–434.

Maguire, L. P., McGinnity, T. M., Glackin, B., Ghani, A., Belatreche, A., and Harkin, J. (2007). Challenges for large-scale implementations of spiking neural networks on FPGAs. *Neurocomputing* 71, 13–29.

Mathworks Inc. (2011). *MATLAB Version 7.12.0*. Natick, MA: The MathWorks Inc.

Mirabella, G., Pani, P., and Ferraina, S. (2009). The presence of visual gap affects the duration of stopping process. *Exp. Brain Res.* 192, 199–209.

Mirabella, G., Pani, P., and Ferraina, S. (2011). Neural correlates of cognitive control of reaching movements in the dorsal premotor cortex of rhesus monkeys. *J. Neurophysiol.* 106, 1454–1466.

Murthy, A., Thompson, K. G., and Schall, J. D. (2001). Dynamic dissociation of visual selection from saccade programming in frontal eye field. *J. Neurophysiol.* 86, 2634–2637.

Niyogi, R., and Wong-Lin, K. F. (2010). "Time-varying gain modulation on neural circuit dynamics and performance in perceptual decisions, Abstract #246," in *Computational and Systems Neuroscience 2010*, Salt Lake City, UT.

Paré, M., and Hanes, D. P. (2003). Controlled movement processing: superior colliculus activity associated with countermanded saccades. *J. Neurosci.* 23, 6480–6489.

Perrin, X., Chavarriaga, R., Colas, F., Siegwart, R., and Millán, J. R. (2010). Brain-coupled interaction for semi-autonomous navigation of an assistive robot. *Rob. Auton. Syst.* 58, 1246–1255.

Pouget, P., Logan, G. D., Palmeri, T. J., Boucher, L., Pare, M., and Schall, J. D. (2011). Neural basis of adaptive response time adjustment during saccade countermanding. *J. Neurosci.* 31, 12604–12612.

Sato, T., and Schall, J. D. (2003). Effects of stimulus-response compatibility on neural selection in frontal eye field. *Neuron* 38, 637–648.

Schall, J. D. (2004). On building a bridge between brain and behaviour. *Annu. Rev. Psychol.* 55, 23–50.

Schall, J. D., Purcell, B. A., Heitz, R. P., Logan, G. D., and Palmeri, T. J. (2011). Neural mechanisms of saccade target selection: gated accumulator model of the visual–motor cascade. *Eur. J. Neurosci.* 33, 1991–2002.

Schall, J. D., Sato, T. R., Thompson, K. G., Vaughn, A. A., and Juan, C. H. (2004). Effects of search efficiency on surround suppression during visual selection in frontal eye field. *J. Neurophysiol.* 91, 2765–2769.

Schall, J. D., Stuphorn, V., and Brown, J. W. (2002). Monitoring and control of action by the frontal lobes. *Neuron* 36, 309–322.

Schwartz, A. B. (2004). Cortical neural prosthetics. *Annu. Rev. Neurosci.* 27, 487–507.

Shenoy, P., Rao, R., and Yu, A. J. (2010). "A rational decision making framework for inhibitory control," in *Advances in Neural Information Processing Systems*, Vol. 23 (Cambridge: MIT Press), 2146–2154.

Shenoy, P., and Yu, A. J. (2011). Rational decision-making in inhibitory control. *Front. Hum. Neurosci.* 5:48. doi:10.3389/fnhum.2011.00048

Standage, D., You, H., Wang, D. H., and Dorris, M. C. (2011). Gain modulation by an urgency signal controls the speed-accuracy trade-off in a network model of a cortical decision circuit. *Front. Comput. Neurosci.* 5:7. doi:10.3389/fncom.2011.00007

Stuphorn, V., Brown, J. W., and Schall, J. D. (2010). Role of supplementary eye field in saccade initiation: executive, not direct, control. *J. Neurophysiol.* 103, 801–816.

Sugrue, L. P., Corrado, G. S., and Newsome, W. T. (2004). Matching behavior and the representation of value in the parietal cortex. *Science* 304, 1782–1787.

Wang, X.-J. (2001). Synaptic reverberation underlying mnemonic persistent activity. *Trends Neurosci.* 24, 455–463.

Wong, K.-F., Eckhoff, P., Holmes, P., and Cohen, J. D. (2007). Analysis of a biologically realistic model for saccade-countermanding tasks. *Soc. Neurosci.*, abstr. 719.

Wong, K.-F., and Wang, X.-J. (2006). A recurrent network mechanism of time integration in perceptual decisions. *J. Neurosci.* 26, 1314–1328.

Wong-Lin, K., Eckhoff, P., Holmes, P., and Cohen, J. D. (2010). Optimal performance in a countermanding saccade task. *Brain Res.* 1318, 178–187.

Xilinx Inc. (2011a). *Getting Started with the Xilinx Virtex-6 FPGA ML605 Evaluation Kit UG533 (V. 1.5)*, San Jose. Available at: http://www.Xilinx.com

Xilinx Inc. (2011b). *System Generator for DSP User Guide UG640 (V. 13.1)*, San Jose. Available at: http://www.Xilinx.com

Xilinx Inc. (2011c). *ML605 Reference Design User Guide UG535 (V. 1.0)*, San Jose. Available at: http://www.Xilinx.com

Yang, S., and McGinnity, T. M. (2011). "A biologically plausible real-time spiking neuron simulation environment based on a multiple-FPGA platform," in *ACM SIGARTH Computer Architecture News*, London, 39, 78–81.

Conflict of Interest Statement: The authors declare that the research was conducted in the absence of any commercial or financial relationships that could be construed as a potential conflict of interest.

Received: 01 February 2012; accepted: 16 May 2012; published online: 11 June 2012.

Citation: Yang S, McGinnity TM and Wong-Lin K (2012) Adaptive proactive inhibitory control for embedded real-time applications. Front. Neuroeng. ***5****:10. doi: 10.3389/fneng.2012.00010*

APPENDIX

The system generator diagrams for implementing the FEF module and the control module are shown in **Figure A1**.

The following describes our architecture using a Xilinx ML605 evaluation board equipped with an XC6VLX240T FPGA with speedgrade-1 and package FF1156 (Xilinx Inc., 2011c).

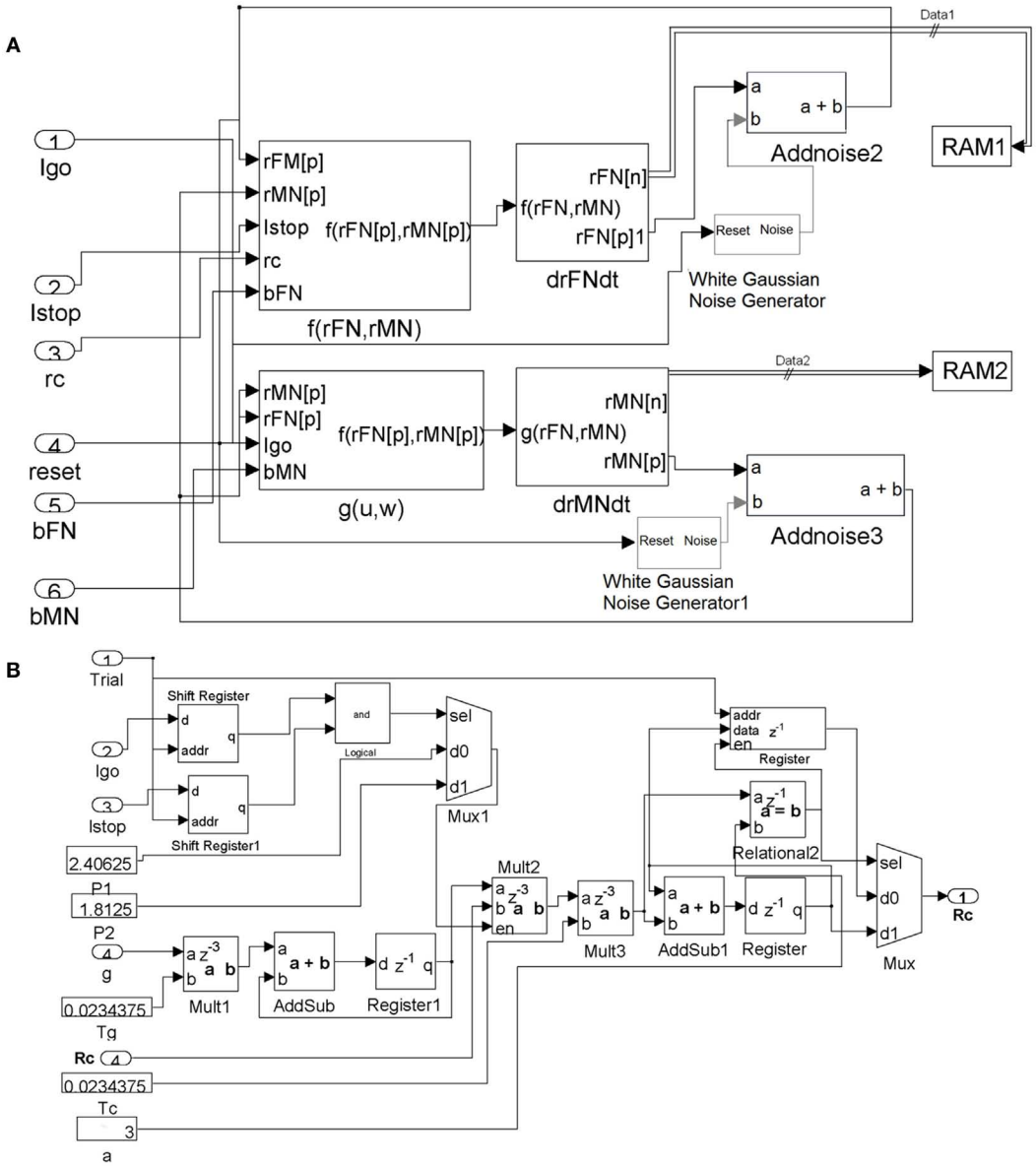

FIGURE A1 | (A) System Generator diagram of the FEF module. Data ports for the subsystems are the numbered oval blocks. Delays through the system are expressed in the z domain where the superscript is the latency in cycles from output back to input. The resulting data (rFM and rMN) are continuously stored back in RAM, via the RAM1 and RAM2 connections. **(B)** System Generator diagram of the adaptive control module.

A

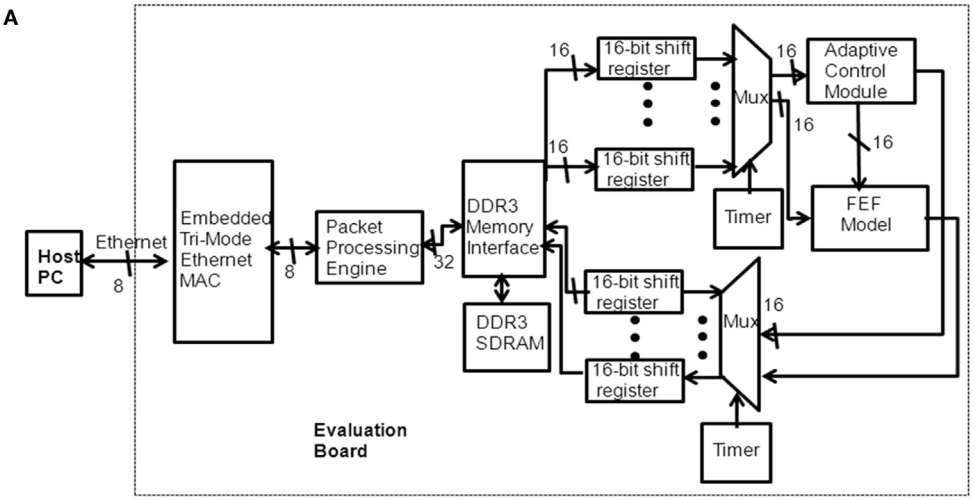

B

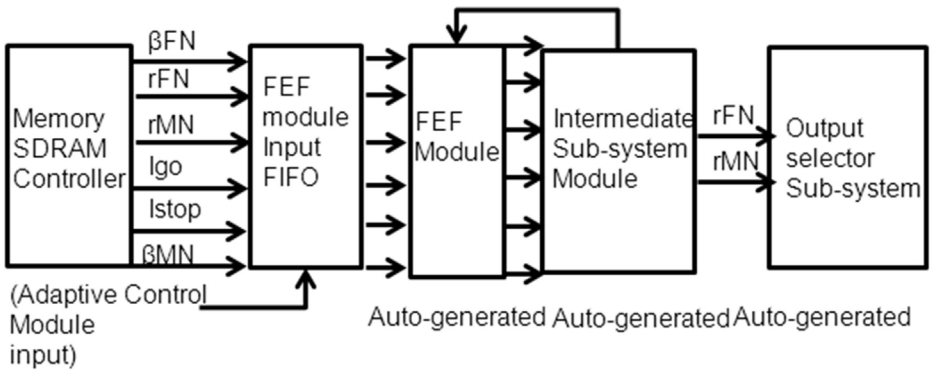

C

Resource Type	Module		
	FEF network model	Adaptive control module	Total (%)
Flip-Flop	8,896	3,459	12,355 (4%)
Lookup Tables	7,069	1,963	9,032(5.9%)
I/Os	400	250	750(12%)
Block RAM(36kb)	80	18	98(1.2%)
DSP48	18	0	18(2%)

FIGURE A2 | (A) illustrates a top-level structure of the inhibitory control prototyping system. Our prototype design includes common functions for Ethernet interface, external memory interface, adaptive control, and FEF module. The Ethernet interface includes an on-chip MAC module and a packet processing engine. Every packet is sent or received using the packet processing engine. A DDR3 memory block is used to store both the simulation setup (stimuli) and simulation results locally on a FPGA device. The stored stimuli are read from DDR3 SDRAM. The outputs are stored back into a DDR3 memory bank. The control activity (rc) is an input from the adaptive control subsystem module. With the programmable timer, all the tasks in a trial are guaranteed to complete before the next trial starts. **(B)** Illustrates a top-layer diagram of the FPGA design of the FEF module. After circuit reset, the data are read from SDRAM into the FEF module's input FIFO. The design of movement and fixation neural populations in the FEF module is generated by System Generator. The circuitry to implement the adaptive control model includes the memory interface (using similar modules to the FEF module design) and the adaptive function (as descripted in Eqs 4 and 5). **(C)** Summarizes the resource usage for the whole design. We divided the design into two modules in order to analysis the adaptive control resource usage, which will be useful for considering a potential future Application Specific Integrated Circuit (ASIC) design. The first column shows the type of hardware resources. The second column shows the number of the specified logical resource used. The third column shows the total number of logical resource usage and utilization. The extra usage of DSP is due to the small amount of arithmetic logic utilized.